Design, synthesis and evaluation of 3-hydroxypyridin-4-ones as inhibitors of catechol-O-methyltransferase

J. de Beer

22155600

Dissertation submitted in fulfilment of the requirements for the degree *Magister Scientiae* in Pharmaceutical Chemistry at the Potchefstroom Campus of the North-West University

Supervisor: Prof. A. Petzer

Co-Supervisor: Dr. A.C.U. Lourens

Co-Supervisor: Prof. J.P. Petzer

November 2015

The financial assistance of the National Research Foundation (NRF) towards this research is hereby acknowledged. Opinions expressed and conclusions arrived at, are those of the author and are not necessarily to be attributed to the NRF.

TABLE OF CONTENTS

LIST OF ABBREVIATIONS

Abbreviation	*Description*
A	
AADC	Aromatic-L-amino acid decarboxylase
ALDH	Aldehyde dehydrogenase
APCI	Atmospheric-pressure chemical ionization
Asn	Asparagine
Asp	Aspartic acid
ATP13A2	Adenosine triphosphatase type 13A2
C	
^{13}C-NMR	Carbon nuclear magnetic resonance
COMT	Catechol-*O*-methyltransferase
COSY	^{1}H-^{1}H Correlation spectroscopy
CV	Coefficient of variation
D	
3,5-DNC	3,5-Dinitrocatechol
DDC	Dopa decarboxylase
DEPT	Distortionless enhancement by polarisation transfer
DJ-1	A protein mutated in autosomal recessive early onset Parkinson's disease
DMSO	Dimethylsulfoxide
DMSO-*d6*	Deuterated dimethylsulfoxide
DNA	Deoxyribonucleic acid
DOPAC	3,4-Dihydroxyphenylacetic acid
DTT	Dithiothreitol
F	
6-FD	6-[^{18}F]-fluorodopa
FT-IR	Fourier Transform Infrared
G	
GABA	γ-Aminobutyric acid
GBA	Glucocerebrosidase
GBMV	Generalised Born approximation with Molecular Volume
Glu	Glucine

H	
^{1}H-NMR	Proton nuclear magnetic resonance
HMBC	Heteronuclear multi-bond correlation spectroscopy
HPLC	High-performance liquid chromatography
HRMS	High resolution mass spectra
HSQC	Heteronuclear single-quantum correlation spectroscopy
HVA	Homovanillic acid / 3-methoxy-4-hydroxyphenylacetic acid
I	
IC_{50}	Inhibitor concentration at 50% inhibition
IR	Infrared
K	
K_i	Enzyme-inhibitor dissociation constant
K_m	Substrate concentration when v_i is one-half of V_{max} / Michaelis constant
L	
Leu	Leucine
LLRK-2	Leucine rich repeat kinase 2
LNAA	Large neutral amino acid
LogP	Octanol-water partition coefficient
Lys	Lysine
M	
3-MT	3-Methoxytyramine
MAO	Monoamine oxidase
MAO-B	Selective type B monamine oxidase
MB-COMT	Membrane bound catechol-*O*-methyltransferase
Met	Methionine
mp	Melting point / melting points (mps)
MPP^{+}	1-Methyl-4-phenylpyridinium
MPTP	1-Methyl-4-phenyl-1,2,3,6-tetrahydropyridine
mRNA	Messenger ribonucleic acid
MS	Mass spectrometry
N	
NE	(-)-Norepinephrine
NMDA	N-methyl-D-aspartate

NMN	Normetanephrine
NMR	Nuclear magnetic resonance
NR4A2	Nuclear receptor subfamily 4 group A member 2
O	
3-OMD	3-O-methyldopa
3-OMFD	3-Methyl-6-[^{18}F]-fluorodopa
P	
PARK1	Alpha-nuclein
PARK2	Parkin
PDB	Protein Data Bank
PET	Positron Emission Tomography
PINK1	PTEN-induced putative kinase 1
Pro	Proline
R	
RMSD	Root-mean-square deviation
RNS	Reactive nitrogen species
ROS	Reactive oxygen species
S	
[S]	Substrate concentration
SAH	S-adenosylhomocysteine
SAMe/SAM	S-adenosyl-L-methionine
SARs	Structure-activity relationships
S-COMT	Soluble catechol-*O*-methyltransferase
SD	Standard deviation
SNPs	Single nucleotide polymorphisms
T	
TLC	Thin Layer Chromatography
Trp	Tryptophan
Tyr	Tyrosine
U	
U-0521	3,4-Dihydroxy-2-methylpropiophenone
UCHL1	Ubiquitin carboxy terminal hydrolase-L1
UV	Ultraviolet
V	

V	Velocity
Val	Valine
v_i	Initial velocity
V_{max}	Maximum velocity

NMR:

δ	Delta scale indicating chemical shift
br d	Broad doublet
br s	Broad singlet
br t	Broad triplet
d	Doublet
ddd	Doublet of doublet of doublets
J	Coupling constant
m	Multiplet
ppm	Parts per million
s	Singlet
t	Triplet
p	Pentet

LIST OF FIGURES

LIST OF TABLES

ABSTRACT

Keywords: 3-Hydroxypyridin-4-ones, catechol-*O*-methyltransferase inhibitors, Parkinson's disease.

Parkinson's disease is a bradykinetic disorder that is the result of the death of dopaminergic neurons in the basal ganglia of the brain. This, in turn, leads to the depletion of dopamine in the striatum, which is responsible for the characteristic motor symptoms of the disease. The most effective treatment for restoring central dopamine levels is levodopa, the metabolic precursor of dopamine. However, due to extensive peripheral enzymatic metabolism by dopa decarboxylase (DDC) and *O*-methylation by catechol-*O*-methyltransferase (COMT), less than 1% of levodopa reaches the brain unchanged. Thus, by preventing levodopa metabolism and increasing the availability of levodopa for uptake into the brain, the inhibition of COMT would be beneficial in Parkinson's disease. COMT serves as a catalyst in the methyl transmission from S-adenosyl-L-methionine (SAMe/SAM) to a hydroxy group of a catechol substrate. Nitrocatechol COMT inhibitors, such as tolcapone and entacapone, have been used in the treatment of Parkinson's disease. Poor bioavailability and undesirable side-effect profiles sometimes limit the clinical use of nitrocatechol COMT inhibitors. The aim of this study therefore was to discover new non-nitrocatechol COMT inhibitors for the treatment of Parkinson's disease. In the present study, the 3-hydroxypyridin-4-one scaffold was selected for the design of non-nitrocatechol COMT inhibitors since the COMT inhibitory potential of this class has been illustrated. 3-Hydroxypyridin-4-ones are isosteric to the catechol ring, but are not *O*-methylated by the enzyme themselves. Further, it has been illustrated that non-nitrocatechol COMT inhibitors can be MB-COMT (membrane bound COMT) specific, which may be beneficial when considering peripheral side-effects.

The present study thus reports the synthesis of new members of the 3-hydroxypyridin-4-one class of compounds, which may act as COMT inhibitors. Such compounds may represent useful agents for the treatment of Parkinson's disease with improved safety profiles compared to nitrocatechol COMT inhibitors. Different structural aspects of the nitrogen substituent that were explored included simple

aromatic and aliphatic substitution (JDB1, JDB10 and JDB11), chain elongation and increasing flexibility (JDB3, JDB4, JDB5 and JDB9), as well as halogen and methyl substitution of the side chain phenyl ring (JDB12, JDB13 and JDB14). Molecular modelling studies (Discovery Studio 3.1, Accelrys) were conducted in a preliminary attempt to predict the inhibition activities of the proposed 3-hydroxypyridin-4-one derivatives. All the derivatives fitted within the catechol binding site of COMT and formed productive interactions with the residues of the enzyme. Therefore the potential inhibition activities of these compounds were confirmed. The compounds were synthesised by reacting maltol with a suitable primary amine in an acidic environment, with ethanol serving as co-solvent. Nuclear magnetic resonance spectroscopy (NMR), infrared spectroscopy (IR) and mass spectrometry (MS) were used to characterise the structures. The purities of the compounds were estimated by high-performance liquid chromatography (HPLC) analysis.

COMT obtained from porcine liver was used as enzyme source to evaluate the *in vitro* COMT inhibitory properties of the synthesised 3-hydroxypyridin-4-ones. A HPLC method with fluorescence detection was validated and employed to measure COMT activity. The natural COMT substrate, (-)-norepinephrine (NE), was incubated with COMT in the presence of various concentrations of the test inhibitors. The formation of normetanephrine (NMN), the *O*-methylated product of NE metabolism, was measured by the validated HPLC system. From the inhibition data IC_{50} (inhibitor concentration at 50% inhibition) values for the inhibition of COMT were calculated. The synthesised 3-hydroxypyridin-4-ones were found to be inhibitors of COMT with IC_{50} values ranging from 4.55 to 19.79 µM. Compared to the reference COMT inhibitors, entacapone (IC_{50} = 0.00047 µM) and tolcapone (IC_{50} = 0.00675 µM), the 3-hydroxypyridin-4-ones were significantly lower potency COMT inhibitors. 1-Benzyl-3-hydroxy-2-methylpyridin-4-one (JDB3) was the most potent compound with an IC_{50} value of 4.55 µM. Some preliminary structure-activity relationships (SARs) were derived, for example, benzyl substitution of the 3-hydroxypyridin-4-one moiety yielded the most potent COMT inhibitors of the series. Phenylethyl, phenylpropyl and phenylbutyl substitution yielded lower potency inhibitors. This shows that chain elongation of the substituent reduces COMT inhibition potency.

In conclusion, several 3-hydroxypyridin-4-one derivatives were synthesised and their COMT inhibitory activities were determined. Although these compounds are not highly potent inhibitors, they may act as leads for the development of non-nitrocatechol COMT inhibitors with possibly better safety profiles. Such compounds would be appropriate for the treatment of Parkinson's disease.

UITTREKSEL

Kernwoorde: 3-Hidroksipiridien-4-one, katesjol-*O*-metieltransferase inhibeerders, Parkinson se siekte.

Parkinson se siekte is 'n bradikinetiese siekte wat veroorsaak word deur die afsterwe van dopaminergiese neurone in die basale ganglia van die brein. Dit lei tot die uitputting van dopamien in die striatum wat verantwoordelik is vir die karakteristieke motorsimptome van die siekte. Die mees doeltreffendste behandeling wat tans vir Parkinson se siekte beskikbaar is, behels die aanvulling van sentrale dopamienvlakke met levodopa, die metaboliese voorloper van dopamien. 'n Hoë mate van perifere metabolisme deur aromatiese-L-aminosuur dekarboksilase (AADK) en *O*-metilering deur katesjol-*O*-metieltransferase (KOMT) veroorsaak egter dat minder as 1% van levodopa onveranderd in die brein opgeneem word. Inhibering van KOMT mag dus voordelig wees deur die afbraak van levodopa te verminder en gevolglik die beskikbaarheid van levodopa vir opname in die brein te verhoog. KOMT tree op as 'n katalis vir die oordrag van 'n metielgroep vanaf S-adenosiel-L-metionien (SAMe/SAM) na 'n hidroksiel groep van 'n katesjol substraat. Tolkapoon en entakapoon is nitrokatesjol inhibeeders van KOMT wat tans gebruik word vir die behandeling van Parkinson se siekte. Weens swak biobeskikbaarheid en newe-effekte wat met nitrokatesjol

KOMT-inhibeerders geassosieer word, is die kliniese gebruik van hierdie inhibeerders soms ingeperk. Die doel van hierdie studie was om nuwe KOMT-inhibeerders te ontdek vir die behandeling van Parkinson se siekte. Die 3-hidroksipiridien-4-oon klas is tydens die huidige studie gekies met die doel om nitrokatesjol KOMT-inhibeerders te ontwerp, aangesien die KOMT-inhibisie potensiaal van hierdie klas verbindings voorheen geïllustreer was. Die KOMT-inhibisie potensiaal van 3-hidroksipiridien-4-one kan daaraan toegeskryf word dat hulle isosteries met die katesjolring is, maar self nie *O*-metilering deur die KOMT ensiem ondergaan nie. Verder is dit voorheen bewys dat 3-hidroksipiridien-4-one spesifiek MB-KOMT (membraangebonde KOMT) inhibeer. Hierdie eienskap mag die perifere newe-effekte wat met KOMT-inhibisie geassosieer is, verminder.

Hierdie studie vermeld die sintese van nuwe 3-hidroksipiridien-4-one, verbindings wat as KOMT-inhibeerders mag optree. Hierdie verbindings kan aangewend word vir die behandeling van Parkinson se siekte en kan moontlik ook beter veiligheidsprofiele besit as nitrokatesjol KOMT-inhibeerders. Verskeie strukturele aspekte van die 3-hidroksipiridien-4-oon stikstofsubstituent was ondersoek, onder andere eenvoudige aromatiese en alifatiese substitusie (JDB1, JDB10 en JDB11), kettingverlenging en buigsaamheid (JDB3, JDB4, JDB5 en JDB9), sowel as halogeen- en metielsubstitusie van die fenielring in die syketting (JDB12, JDB13 en JDB14). Molekulêre modelleringstudies (Discovery Studio 3.1, Accelrys) was uitgevoer in 'n poging om die inhibisiesaktiwiteite van die voorgestelde 3-hidroksipiridien-4-oon derivate te voorspel. Al die derivate het in die katesjol bindingsetel van KOMT gepas en het produktiewe interaksies met die ensiem ondergaan. Dus was die potensiële inhibisiesaktiwiteite van hierdie klas verbindings bevestig. Die verbindings was gesintetiseer deur maltol met 'n geskikte primêre amien te reageer in 'n suuromgewing. Etanol het as oplosmiddel gedien. Kern magnetiese resonans spektroskopie, infrarooi spektroskopie en massaspektrometrie was gebruik om die strukture te karakteriseer. Die suiwerhede van die verbindings was beraam deur van hoëdrukvloeistof-chromatografiese analises gebruik te maak.

Varklewer KOMT is gebruik as ensiembron om die *in vitro* KOMT-inhibisie eienskappe van die gesintetiseerde 3-hidroksipiridien-4-oon derivate te evalueer. 'n HPLC metode met fluorosensie deteksie was gevalideer en is gebruik om KOMT-aktiwiteit te meet. 'n Natuurlike substraat van KOMT, (-)-norepinefrien (NE), was in die teenwoordigheid van KOMT en verskeie konsentrasies van die toetsinhibeerders geïnkubeer. Die vorming van die *O*-metiel produk van NE metabolisme, normetanefrien (NMN), was sodoende gemeet met die gevalideerde HPLC sisteem. Dit was gevind dat die gesintetiseerde 3-hidroksipiridien-4-oon derivate wel inhibeerders van KOMT is met IC_{50}-waardes (inhiberende konsentrasie waardes by 50% van die inhibeerder) wat wissel tussen 4.55 en 19.79 µM. Die gesintetiseerde verbindings was aansienlik minder potent as die verwysingsinhibeerders, entakapoon (IC_{50} = 0.00047 µM) en tolkapoon (IC_{50} = 0.00675 µM). 1-Bensiel-3-hidroksie-2-metielpiridien-4-oon (JDB3) was die mees potente verbinding met 'n IC_{50}-waarde van 4.55 µM. Sommige voorlopige struktuuraktiwiteitsverwantskappe is uit die studie afgelei. Daar is onder andere bevind dat bensiel-substitusie van die 3-hidroksipiridien-4-oon kern lei tot die

mees potente KOMT-inhibeerders van die reeks. Fenieletiel-, fenielpropiel- en fenielbutielsubstitusie het egter minder potente inhibeerders opgelewer. Dus veroorsaak kettingverlenging van die substituent dat die KOMT-inhibisie potensie van hierdie klas verbindings verlaag.

In samevatting, verskeie 3-hidroksipiridien-4-oon derivate is in hierdie studie gesintetiseer en hul KOMT-inhibisie aktiwiteite is bepaal. Al is hierdie verbindings nie hoogs potente inhibeerders nie, mag hulle optree as leidraadverbindings vir die ontwikkeling van nuwe KOMT-inhibeerders met moontlik beter veiligheidsprofiele. Sulke verbindings sal gepas wees vir die behandeling van Parkinson se siekte.

ACKNOWLEDGEMENTS

I would like to thank the following people:

- First, I would like to thank my supervisor, Prof. Anél Petzer, and my co-supervisors, Dr. Arina Lourens and Prof. Jacques Petzer, for the great amount of help and support they have given me in completing a Master's study. You are an inspiration to me for your love of science.
- This dissertation would not have been possible without the financial assistance of the NRF and NWU.
- Dr. Johan Jordaan and Mr. André Joubert for recording the MS and NMR spectra.
- Prof. Jan du Preez for his assistance with the HPLC analyses.
- Miss. Monique Smit for assistance with the biological assays.
- Special thanks to my family and friends who believed that I would be able to pursue postgraduate studies, and who have supported me during this time.
- Finally, I am eternally grateful and blessed for the opportunity the Lord has given me to walk the extra mile. Without His grace this Master degree would not have been possible.

CHAPTER 1

INTRODUCTION

The following chapter will serve as an introduction towards Parkinson's disease and the reasoning behind COMT (catechol-*O*-methyltransferase) inhibitors being useful agents in treatment of the disease. The rationale of the present study will be discussed, including the hypothesis, aims and objectives of the study.

1.1 BACKGROUND

1.1.1 Parkinson's disease

Parkinson's disease is a neurodegenerative disorder characterised by the death of dopaminergic neurons in the basal ganglia of the brain (Standaert & Roberson, 2011). It is described by Garbayo *et al*. (2013) as the difficulty to perform coordinated movements, with bradykinesia, resting tremor and rigidity as the core clinical features. The exact cause of Parkinson's disease is unknown and the progression of the disease seems to worsen over time and cannot be treated (Tugwell, 2008). The only pharmacotherapy currently available includes symptomatic treatment and promoting quality of life (Tugwell, 2008). It is estimated to be the second most common neurodegenerative disorder of the ageing brain (Garbayo *et al*., 2013). Approximately 1.5% of people over the age of 65 are globally affected by the disease (Garbayo *et al*., 2013) and the number of individuals afflicted by the disease is expected to increase. The motor symptoms of Parkinson's disease are the result of the loss of nigrostriatal dopamine (Lees, 2009). Levodopa, the metabolic precursor of dopamine, remains the most effective treatment for restoring dopamine levels in the parkinsonian brain (Standaert & Roberson, 2011). However, due to extensive peripheral enzymatic metabolism by dopa decarboxylase (DDC) and O-methylation by COMT, only a small fraction of the levodopa dose reaches the brain (Kaakkola, 2000).

1.1.2 Catechol-*O*-methyltransferase (COMT)

COMT was first defined in 1958 by Julius Axelrod and is responsible for eliminating biologically active or toxic substances that contain a catechol structure, such as levodopa (Kaakkola, 2000; Männistö & Kaakkola, 1999). COMT also methylates other hydroxylated metabolites (Kaakkola, 2000). COMT is widely distributed throughout the body with the liver containing the highest COMT activity (Männistö & Kaakkola, 1999). MB-COMT (membrane bound COMT) and the soluble isoform of COMT, S-COMT, are the two major isoforms for the enzyme (Robinson *et al*., 2011). S-COMT is dominant in the peripheral tissue and MB-COMT is mainly found in the brain (Tubridge, 2010). COMT is responsible for the transmission of a methyl group from SAMe (S-adenosyl-L-methionine, also referred to as SAM) to a hydroxyl group of a catechol substrate in the presence of magnesium (Männistö & Kaakkola, 1999).

Thus, inhibition of the *O*-methylation of levodopa increases the availability of levodopa for uptake into the brain, which explains the significance of COMT inhibitors in the treatment of Parkinson's disease (Bonifácio *et al*., 2007). Early COMT inhibitors had poor oral bioavailability profiles which made them unsuitable for routine clinical use (Bonifati & Meco, 1999). New generation COMT inhibitors, such as the nitrocatechol COMT inhibitors, have successfully been used in the treatment of Parkinson's disease, but are subject to some limitations (Robinson *et al*., 2012). Other drug classes used in the treatment of Parkinson's disease include DDC inhibitors, monoamine oxidase (MAO) inhibitors, anticholinergic agents as well as dopamine agonists (Standaert & Roberson, 2011).

Hatano *et al*. (2009) conducted a study on the unmet needs of patients suffering from Parkinson's disease. With 264 participants it became evident that despite symptomatic treatments, patients still require better treatment of the motor symptoms (Hatano *et al*., 2009). This study will attempt to discover novel COMT inhibitors with improved safety profiles compared to the COMT inhibitors currently used in the clinic. The 3-hydroxypyridin-4-one scaffold was selected for the synthetic part of this study since the COMT inhibitory potential of several of these compounds have been illustrated (Mannisto & Kaakola, 1999; Robinson *et al*., 2012; Borchardt, 1973). By

inhibiting the metabolism of levodopa by COMT, therapeutic outcomes for the treatment of Parkinson's disease may be improved.

1.2 RATIONALE OF THE PRESENT STUDY

COMT inhibitors contribute to the sustained release of levodopa into the central nervous system during the treatment of Parkinson's disease (Bonifati & Meco, 1999). This leads to improved pharmacotherapeutic outcomes and reduces disability in early stages of Parkinson's disease. In addition, COMT inhibitors reduce motor fluctuations in advanced stages of Parkinson's disease (Bonifati & Meco, 1999). The current COMT inhibitors, tolcapone and entacapone (Figure 1.1), contain a nitrocatechol moiety and as a result suffer from poor bioavailability and toxicity (Robinson *et al*., 2012). Identifying and designing non-nitrocatechol COMT inhibitors may be a possible solution for addressing these shortcomings.

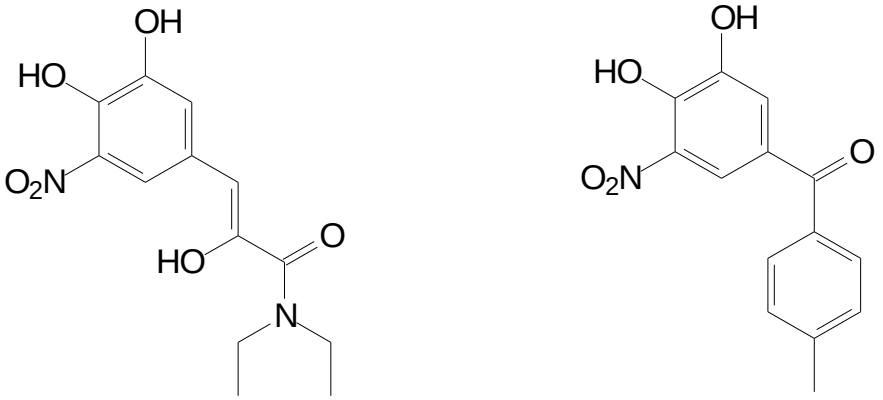

Entacapone Tolcapone

Figure 1.1: The nitrocatechol COMT inhibitors, entacapone and tolcapone (Männistö & Kaakkola, 1999).

COMT inhibitory potential has been illustrated by several compounds that possesses the 3-hydroxypyridin-4-one moiety (Figure 1.2) (Borchardt, 1973; Guldberg & Marsden, 1975; Mannisto & Kaakola, 1999; Robinson *et al.*, 2012). These derivatives have either very small substituents at R^1, or contain large rigid bicyclic aromatic substituents (Borchardt, 1973; Rai *et al*., 1999). It is important to note that a free

hydroxy group is essential for COMT inhibition as found in a study done by Borchardt (1973). These compounds possess good affinities for COMT since they are isosteric to the catechol ring (Figure 1.2), but are not *O*-methylated themselves (Borchardt, 1973). The structure-activity relationships (SARs) of the 3-hydroxypyridone scaffold have not been comprehensively explored for COMT inhibition, and it is to this regard that this study would contribute.

Catechol 3-Hydroxypyridin-4-one

Figure 1.2: The structures of catechol and the general structure of 3-hydroxypyridin-4-ones (Guldberg & Marsden, 1975; Rai *et al*., 1999).

3-Hydroxypyridin-4-ones exhibit three advantages: (1) Several derivatives have been shown to be orally active compounds that are efficiently absorbed from the gastrointestinal tract (Rai *et al*., 1999); (2) due to the presence of excessive iron deposits in the basal ganglia of the brain that are associated with Parkinson's disease (Ward *et al*., 1995), it is of clinical benefit that 3-hydroxypyridin-4-ones display iron chelating activity (Rai *et al*., 1999) as this can reduce oxidative stress (Ward *et al*., 1995); and (3) analgesic effects of certain 3-hydroxypyridin-4-ones have further been illustrated in previous studies, indicating similar activity compared to aspirin, and similar anti-inflammatory activity compared to indomethacin (Öztürk *et al*., 2001). This is beneficial for neuroinflammation that is believed to accompany Parkinson's disease (Ramsey & Tansey, 2014).

Taking into consideration that some 3-hydroxypyridin-4-ones, such as deferipone (Figure 1.3), have been proven to be iron chelators, it is important for the iron chelator to be able to penetrate the blood-brain barrier and not to adversely intrude with other vital systems, including the enzymes, dopamine synthase and ribonuclease reductase, that requires iron for their functions (Ward *et al*., 1995). Unfortunately, it has been reported that some pyridone derivatives inhibit tyrosine (Tyr) hydroxylase,

which may interfere with dopamine synthesis (Männistö & Kaakkola, 1999; Ward *et al*., 1995; Liu *et al*., 2001).

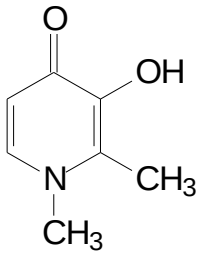

Deferipone

Figure 1.3: The structure of deferipone, currently marketed as an iron chelator for clinical use (Liu *et al*., 2001).

Liu *et al*. (2001), however, found that hydrophilic 3-hydroxypyridin-4-one iron chelators [with an octanol-water partition coefficient (logP) of ≤ -1.0] are relatively weak Tyr hydroxylase inhibitors. Hydrophilic 3-hydroxypyridin-4-ones exhibit a reduced degree of membrane penetration, which lowers access to the brain as well as entrance into tissues, such as the liver, where metabolism of pyridones takes place (Rai *et al*., 1999). Reduced metabolism may lead to a more prolonged action of the chelators (Rai *et al*., 1999). Unfortunately, in addition to reduced liver extraction, absorption from the gastrointestinal tract is also decreased with hydrophilic compounds. Reduced liver extraction may lead to insufficient biliary iron-excretion that is essential for treatment of an iron overload (Rai *et al*., 1999). Rai *et al*. (1999) showed that hydrophobic prodrugs can overcome most of these barriers and should be considered in the design of novel non-catechol COMT inhibitors.

For the design of COMT inhibitors, it should be kept in mind that more than one COMT isoform exist. MB-COMT specific inhibitors are particularly relevant to the treatment of Parkinson's disease since MB-COMT is the predominant isoform in the brain (Robinson *et al*., 2011). Robinson *et al*. (2011) conducted a study on non-nitrocatechol MB-COMT specific inhibitors with therapeutic potential (Figure 1.4) and concluded that future exploratory work is urgently required in this regard. Based on the analysis above, the present study will attempt to discover novel 3-hydroxypyridin-4-one derived COMT inhibitors. The structures of proposed derivatives with different hydrophobic

nitrogen substituents are given in Table 1.1. Hydrophobicity is explored in the current study as this will improve brain penetration, liver extraction and absorption of the derivatives, which are important properties should future *in vivo* studies be undertaken.

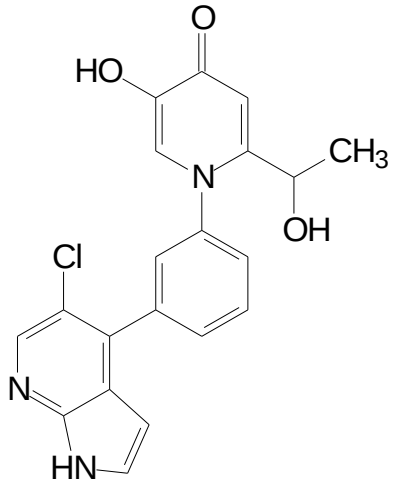

Figure 1.4: The structure of a human MB-COMT inhibitor described by Robinson *et al*. (2011) [Inhibitor concentration at 50% inhibition (IC_{50}) = 39.6 nM].

Table 1.1: The proposed 3-hydroxypyridin-4-one derivatives for the inhibition of COMT.

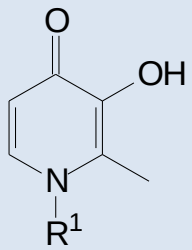

Compound	*R^1*
JDB1	$–C_6H_5$
JDB3	$–CH_2C_6H_5$
JDB4	$–(CH_2)_2C_6H_5$
JDB5	$–(CH_2)_3C_6H_5$
JDB9	$–(CH_2)_4C_6H_5$
JDB10	$–C_6H_{11}$
JDB11	$–C_5H_9$
JDB12	$–(C_6H_4)$-3′-Cl
JDB13	$–(C_6H_4)$-4′-Cl
JDB14	$–CH_2(C_6H_4)$-4′-CH_3

1.3 HYPOTHESIS

Because the 3-hydroxypyridin-4-one scaffold has been shown to be appropriate for COMT inhibition (Mannisto & Kaakola, 1999), it is postulated that, with the appropriate structural modification, highly potent COMT inhibitors in this class may be discovered compared to nitrocatechol COMT inhibitors.

1.4 AIMS AND OBJECTIVES

The aims of this study are:

- To design and synthesise novel 3-hydroxypyridin-4-one derivatives as possible non-catechol COMT inhibitors.
- To use molecular modelling software to determine provisional binding energies and orientations of the 3-hydroxypyridin-4-one structures in the COMT binding site.
- To evaluate the synthesised compounds as inhibitors of COMT, and compare the inhibition potencies to those of current clinical relevant COMT inhibitors.

The objectives of the study will include:

- The synthesis of ten 3-hydroxypyridin-4-one derivatives with different nitrogen substituents will be achieved by making use of a general synthetic route:

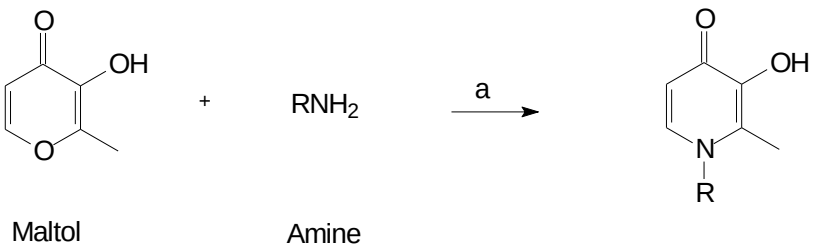

Figure 1.5: General synthetic route for the preparation 3-hydroxypyridin-4-one derivatives *via* a single step synthetic pathway. (a) HCl, H_2O, ethanol, 72 h, 110 °C (Fassihi *et al*., 2009).

- Docking of the synthesised 3-hydroxypyridin-4-one structures into the reported crystal structure of the COMT enzyme will be achieved by making use of Discovery Studio 3.1 (Accelrys®). This will assist the prediction of inhibition activity by investigating the binding of the synthesised compounds to the COMT protein.
- The inhibition properties of the synthesised 3-hydroxypyridin-4-ones will be determined by using the literature method described by Aoyama *et al*. (2005). The principle of this method is based on the formation of the metabolite that forms when NE [(-)-norepinephrine] is *O*-methylated by COMT, which is NMN (normetanephrine) (Figure 1.6). The use of reversed-phase HPLC (high-performance liquid chromatography) separation with florescence detection will be used to quantify the NMN that forms when the *O*-methylation reaction illustrated in Figure 1.6 is inhibited by the test inhibitors (Table 1.1) and the reference COMT inhibitors, entacapone and tolcapone (Figure 1.1).

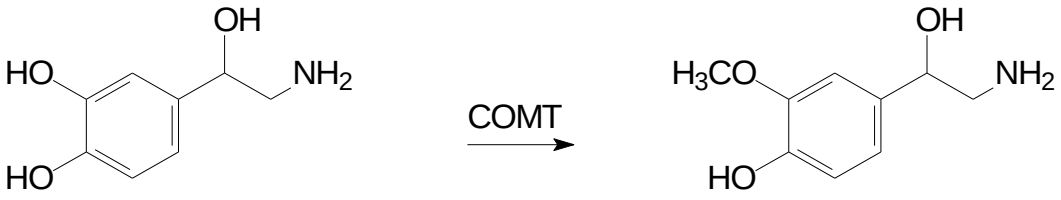

(-)-Norepinephrine Normetanephrine

Figure 1.6: *O*-Methylation of NE [(-)-norepinephrine] by COMT.

CHAPTER 2

LITERATURE OVERVIEW

This chapter provides a brief overview of Parkinson's disease, referring to the aetiology, pathogenesis and treatment of the disease. Special focus will be provided on the role of COMT inhibitors in Parkinson's disease with a short discussion included at the end of the chapter on enzyme kinetics.

2.1. PARKINSON'S DISEASE

2.1.1 Background

In 1817, James Parkinson defined the clinical features of idiopathic Parkinson's disease for the first time (Standaert & Roberson, 2011). Parkinson's disease is a bradykinetic disorder that consists of four typical clinical features: Resting tremor, abnormal slowness of movement, muscle rigidity and instability of postural balance (Chen & Swope, 2007). This form of parkinsonism was first described as *paralysis agitans*, or the "shaking palsy" (Standaert & Roberson, 2011). Non-motor symptoms also seem to accompany the disease, such as sleep disorders, neuropsychiatric issues and cognitive dysfunction (Garbayo *et al*., 2013).

Death of dopaminergic neurons, located in the substantia nigra of the brain, is the primary pathological feature of Parkinson's disease (Dauer & Przedborski, 2003). The cause remains a mystery (Lees *et al*., 2009), but several environmental and genetic factors have been identified as contributors to Parkinson's disease (Silva & Schapira, 2001). The most effective therapy for Parkinson's disease is a combination of levodopa and a DDC inhibitor (Lees *et al*., 2009). Dopamine agonists, MAO-inhibitors, amantadine, anticholinergic drugs as well as COMT-inhibitors can serve as adjunctive or alternative treatments in Parkinson's disease (Standaert & Roberson, 2011). Therapy becomes more challenging as the disease progresses (Tugwell, 2008). Symptoms become more severe and levodopa-associated motor complications later interfere with pharmacotherapy (Tugwell, 2008).

2.1.2 Pathophysiology

Dopaminergic neuron loss and the presence of Lewy bodies in the substantia nigra pars compacta are the two pathological hallmark features of Parkinson's disease (Wells, 2009). In the brain, the substantia nigra innervates the striatum (Standaert & Roberson, 2011). The striatum, globus pallidus, substantia nigra and subthalamic nucleus form part of the subcortical nuclei in the basal ganglia, which control voluntary movement (Tugwell, 2008). When presynaptic nigrostriatal dopamine neurons are depleted, there is a reduced stimulation of dopamine-1 and dopamine-2 receptors leading to inhibition of thalamic and motor cortex activity (Wells, 2009). Any deficiency in striatal dopamine can lead to a syndrome of resting tremor, decreased voluntary movement, instability, freezing and rigidity (Dauer & Przedborski, 2003). This syndrome is called "parkinsonism" (Dauer & Przedborski, 2003). By the time symptoms occur, 50-70% of striatal dopamine activity has been lost (Silva & Schapira, 2001).

The dopaminergic pathway from the substantia nigra maintains the balance between excitatory glutamate and inhibitory γ-aminobutyric acid (GABA) pathways in the motor cortex and motor thalamus (Tugwell, 2008). A decrease in dopamine results in an overactivity of GABA, which induces inhibition in the striatopallidal pathway (Tugwell, 2008). Subsequent inhibition of the thalamus results in reduced stimulation of the motor cortex (Tugwell, 2008). Contributing to the tremor that is experienced during Parkinson's disease, is the increase of striatal cholinergic activity that occurs when nigrostriatal dopamine is inhibited or lost (Wells, 2009).

2.1.2.1 Lewy bodies

Intracellular inclusions, called Lewy bodies, appear together with the dopaminergic nerve cell loss (Standaert & Roberson, 2011). They occur mostly in the brainstem, but are also found in the peripheral autonomic nuclei that may affect some autonomic features that form part of Parkinson's disease (Tugwell, 2008). Lewy bodies can be classified as classical Lewy bodies, cortical Lewy bodies, pale bodies, and Lewy neurites (Lees *et al.*, 2009). According to Tugwell (2008), it remains unclear whether they are a result of Parkinson's disease or part of the aetiology. Lewy bodies steadily

increases with age, which correlates with the age-related progress in neurodegeneration in Parkinson's disease (Tugwell, 2008).

2.1.3 Aetiology

The exact cause of Parkinson's disease has not yet been identified (Tugwell, 2008). Only knowledge of neuronal pathways and brain areas affected have been established (Tugwell, 2008). Silva and Schapira (2001) explains that multiple factors may contribute to idiopathic Parkinson's disease. Factors that contribute to the disease include genetic susceptibility and certain environmental factors (Silva & Schapira, 2001).

2.1.3.1 Environmental factors

Exposures to certain environmental toxins may cause Parkinson's disease (Tugwell, 2008). People, who are exposed to pesticides, for example farmers, have an increased risk of developing parkinsonism (Tugwell, 2008). Quick developing and severe parkinsonism can be created by the proneurotoxin, MPTP (1-methyl-4-phenyl-1,2,3,6-tetrahydropyridine) (Tugwell, 2008). MPTP is used to create animal models of Parkinson's disease in the laboratory (Tugwell, 2008).

2.1.3.2 Genetic factors

According to Lees *et al.* (2009), several genetic mutations can be responsible for a more benign course of parkinsonism. These include mutations in the genes of leucine (Leu) rich repeat kinase 2 (LLRK-2), α-synuclein, glucocerebrosidase (GBA), parkin (PARK2), DJ-1, PTEN-induced putative kinase 1 (PINK1) and ATP13A2 (adenosine triphosphatase type 13A2) (Lees *et al*., 2009). Tugwell (2008) also mentions that mutations in the genes alpha-nuclein (PARK1), ubiquitin carboxy terminal hydrolase-L1 (UCHL1) and nuclear receptor subfamily 4 group A member 2 (NR4A2) have been identified in Parkinson's disease.

The intracytoplasmic Lewy bodies that occur along with neuron loss, contains ubiquitin (Silva & Schapira, 2001) and an abnormal aggregated form of α-synuclein (Lees *et al.*,

2009). Mutated α-synuclein was the first association to be made with inherited Parkinson's disease (Tugwell, 2008). According to Tugwell (2008), the risk rises from 2% to 6% to develop inherited Parkinson's disease when mutations in α-synuclein are present. Mutations in the gene of parkin are associated with young-onset Parkinson's disease (Tugwell, 2008).

2.1.3.3 Risk factors

Ageing remains a major risk factor for developing Parkinson's disease (Lees *et al*., 2009). People who never smoke and who consume low quantities of caffeine have a twofold higher chance to develop Parkinson's disease (Lees *et al*., 2009). This may be related to the dopaminergic reward pathways that are stimulated by caffeine's and nicotine's ability to increase striatal dopamine release (Lees *et al*., 2009). Nicotine can reduce oxidative stress by inhibiting MAO in the brain, and caffeine serves as an adenosine A_{2A} receptor antagonist (Lees *et al*., 2009). Both these pharmacological activities contribute to antiparkinsonian activity (Lees *et al*., 2009).

2.1.4 Pathogenesis

Although the exact causes of Parkinson's disease are not fully known (Lees *et al*., 2009), several mechanisms that may play a role have been identified as contributors to the disease. These include oxidative stress, neuroinflammation, excitotoxicity, apoptosis and the loss of certain neurotrophic factors.

2.1.4.1 Oxidative stress

An unusual build-up of iron in the substantia nigra, variation in the concentration of iron-binding proteins, enhanced oxidative stress and a deficit in mitochondrial complex I can contribute to the biochemical abnormalities identified in Parkinson's disease (Silva & Schapira, 2001).

Various neurodegenerative diseases are characterised by alterations in iron metabolism (Ward *et al.,* 1995). In Parkinson's disease, excessive iron deposits are found in the substantia nigra of the brain which may contribute to oxidative stress

(Ward *et al.,* 1995). By catalysing oxidative reactions, iron generates hydrogen peroxide and the hydroxyl ion, which lead to oxidative stress and damage to dopaminergic neurons (Silva & Schapira, 2001).

There are additional factors contributing to oxidative stress and damage in Parkinson's disease. Lowered antioxidant defence is found due to a decrease in glutathione concentration in the substantia nigra (Silva & Schapira, 2001). Due to the presence of the enzyme superoxide dismutase, superoxide generation adds to the oxidative stress observed in Parkinson's disease (Silva & Schapira, 2001). Oxidative damage is also implied when products such as polyunsaturated fatty acids, malondialdehyde, and hydroperoxides are increased by free-radical damage to lipid membranes (Silva & Schapira, 2001).

Prolonged exposure to MPP^+ (1-methyl-4-phenylpyridinium), the active metabolite of MPTP, inhibits the multimeric protein, complex I (Silva & Schapira, 2001). Complex I form part of the respiratory chain and oxidative phosphorylation system in mitochondria (Silva & Schapira, 2001). Free radicals are generated with inhibition of complex I and can damage the respiratory chain and cause oxidative stress (Silva & Schapira, 2001).

Mitochondrial DNA (deoxyribonucleic acid) is particularly susceptible to free radical damaging due to the absence of a histone coat and restricted range of repair enzymes (Silva & Schapira, 2001). Somatic or inherited mitochondrial DNA mutations may lead to mitochondrial dysfunctions, which are thought to contribute to the pathogenesis in Parkinson' s disease (Silva & Schapira, 2001).

2.1.4.2 Neuroinflammation

Ramsey and Tansey (2014) reviewed the role of neuroinflammation in neurotoxin-induced animal models of Parkinson's disease. Various stimuli can activate brain microglia which subsequently leads to the release of cytokines, chemokines, reactive oxygen species (ROS) and reactive nitrogen species (RNS) (Ramsey & Tansey, 2014). MPTP, 6-hydroxydopamine, paraquat and lipopolysaccharide can cause microglial activation (Ramsey & Tansey, 2014). In the study by Ramsey and Tansey (2014), it

was concluded that the neuroinflammation that resulted from these neurotoxins, directly induced nigral dopamine cell death. According to Yacoubian and Standaert (2009), the aggregated and nitrated forms of α-synuclein can directly activate microglial response.

2.1.4.3 Excitotoxicity

High levels of glutamate receptors occur on dopaminergic neurons in the substantia nigra (Yacoubian & Standaert, 2009). Glutamate is a primary driver of the excitotoxic process by activating NMDA (N-methyl-D-aspartate) channels (Yacoubian & Standaert, 2009). Excessive NMDA channel activation can lead to increased intracellular calcium influx and promote cell death pathways (Yacoubian & Standaert, 2009). Elevated intracellular calcium can ultimately lead to peroxynitrite production by activating nitric oxide synthase (Yacoubian & Standaert, 2009).

2.1.4.4 Apoptosis

Another factor that may play a role in dopaminergic neuron loss in Parkinson's disease is apoptosis (Zhang *et al.,* 2013). Apoptotic pathways may be activated through oxidative stress, protein aggregation, inflammation or excitotoxicity (Yacoubian & Standaert, 2009). MPTP induced apoptosis is often used in studies to investigate dopaminergic neuron degeneration both *in vivo* and *in vitro* (Zhang *et al.,* 2013). According to Zhang *et al*. (2013), an increase in acetylcholinesterase expression is present during apoptosis. Inhibition of acetylcholinesterase has shown to protect cells from MPP^+ induced apoptosis and therefore has been suggested as possible treatment in Parkinson's disease (Zhang *et al.,* 2013).

2.1.4.5 Loss of neurotrophic factors

According to Yacoubian and Standaert (2009), it has been demonstrated that Parkinson's disease patients have reduced levels of glial cell line-derived neurotrophic factor (or neurturine), brain-derived neurotrophic factor and nerve growth factor. Loss of these neurotrophic factors may contribute to the cell death observed in Parkinson's disease (Yacoubian & Standaert, 2009). Treatment with neurotrophic factors are

currently under investigation as potential neuroprotective therapy in Parkinson's disease (Garbayo *et al*., 2013).

2.1.5 Treatment

2.1.5.1 Levodopa

Available pharmacotherapy in Parkinson's disease aims to improve a patient's quality of life (Tugwell, 2008). This only includes the treatment of symptoms and not the prevention of disease progression (Tugwell, 2008). The metabolic precursor of dopamine, levodopa (Figure 2.1), still remains the most effective therapy for restoring the dopamine deficit that accompanies Parkinson's disease (Standaert & Roberson, 2011). Levodopa should be considered when monotherapy with a MAO-B (selective type B monamine oxidase) inhibitor or dopamine agonist are insufficient (Wells, 2009).

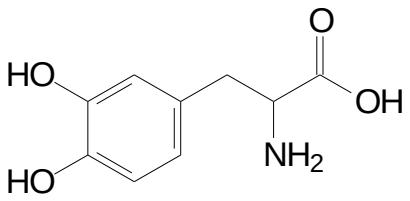

Levodopa

Figure 2.1: The chemical structure of levodopa (Standaert & Roberson, 2011).

2.1.5.2 Dopa decarboxylase (DDC) inhibitors

Due to extensive peripheral decarboxylation and O-methylation, less than 1% of a levodopa dose reaches the brain (Kaakkola, 2000). Thus, initial therapy usually consists of a combination of levodopa and a DDC inhibitor, for example beserazide or carbidopa (Figure 2.2) (Lees *et al*., 2009). By inhibiting the peripheral metabolism of levodopa, delivery to the brain is improved (Kaakkola, 2000). Chronic use of levodopa may initially exhibit stable and sustained benefits, but may later result in motor complications (Bonifati & Meco, 1999). Maintaining effective pharmacotherapy may become more challenging as the disease progresses and levodopa-induced

dyskinesia and wearing-off effects start to occur (Tugwell, 2008).

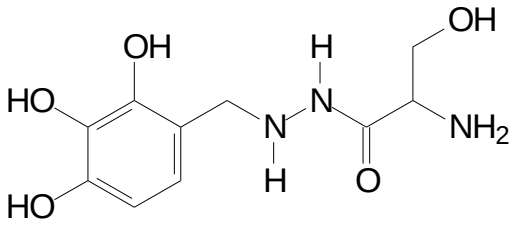

Benserazide

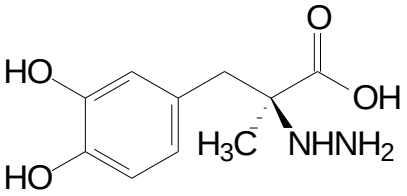

Carbidopa

Figure 2.2: Dopa decarboxylase inhibitors (Adams, 1996).

2.1.5.3 Catechol-*O*-methyltransferase (COMT) inhibitors

COMT inhibitors are added to levodopa treatment when motor fluctuations start to occur (Wells, 2009). A detailed discussion on COMT inhibitors are given in Section 3 of this chapter. Clinical relevant nitrocatechol-type COMT inhibitors include entacapone and tolcapone (Figure 2.1) (Kaakkola, 2000). Wearing-off symptoms can be reduced with entacapone (Maranis *et al*., 2011). The therapeutic effects of levodopa are enhanced by a COMT inhibitor's ability to reduce the central elimination of levodopa (Kaakkola, 2000).

2.1.5.4 Dopamine agonists

Dopamine-receptor agonists can serve as an alternative to levodopa treatment (Standaert & Roberson, 2011). Monotherapy with non-ergoline dopamine agonists, for example ropinirole and pramipexole (Figure 2.3), are mainly used as first-line treatment in younger patients and do not provoke the dyskinesia associated with levodopa (Lees *et al*., 2009). According to Standaert and Roberson (2011), dopamine-receptor agonists have the ability to reduce the endogenous release of dopamine and lower the need for exogenous levodopa. This contributes to a decrease in the formation of free radicals, which can possibly change the course of Parkinson's disease (Standaert & Roberson, 2011). However, within 3 years of diagnosis, levodopa is usually required (Lees *et al*., 2009). Dopamine agonists also display early gastrointestinal and psychiatric adverse effects that may result in drug withdrawal in

certain patients (Lees *et al*., 2009). According to Lees (2005), there is evidence that dopamine agonists delay the onset of motor fluctuations. The dopamine agonist, apomorphine (Figure 2.3), is used as acute "rescue therapy" when "off" symptoms occur in patients who display a fluctuating dopaminergic response towards treatment (Standaert & Roberson, 2011).

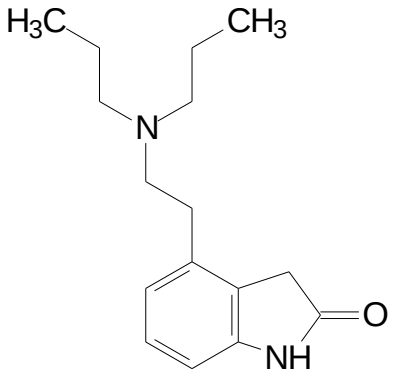

Ropinirole

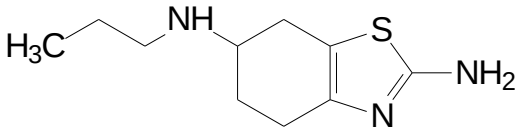

Pramipexole

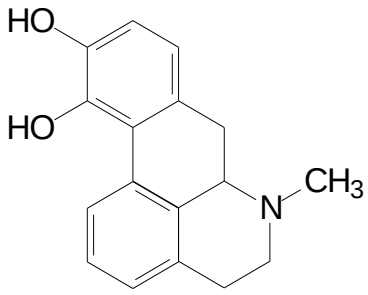

Apomorphine

Figure 2.3: Examples of dopamine-receptor agonists: ropinirole, pramipexole and apomorphine (Varga *et al*., 2009; Koch *et al*., 1968).

2.1.5.5 Monoamine oxidase B inhibitors

Another approach to treatment is the use of selective type B MAO inhibitors (Lees *et al*., 2009). These include selegiline and rasagiline (Figure 2.4), which are suitable for initial treatment of Parkinson's disease where mild symptoms are experienced

(Tugwell, 2008). They are well-tolerated drugs and seem to slow the disease progression (Lees *et al*., 2009). When MAO is inhibited, the formation of free radicals that may be potentially toxic are reduced (Standaert & Roberson, 2011). This may contribute to the neuroprotective effects of MAO inhibitors (Standaert & Roberson, 2011). Selegiline, but not rasagiline, give rise to amphetamine metabolites that may display undesirable adverse effects (Standaert & Roberson, 2011). As an adjunctive to levodopa therapy, monotherapy with rasagiline may reduce the "wearing off" symptoms associated with advanced Parkinson's disease (Standaert & Roberson, 2011).

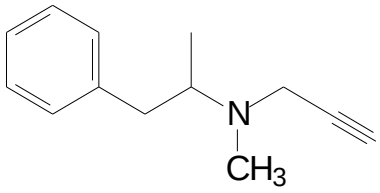

Selegeline

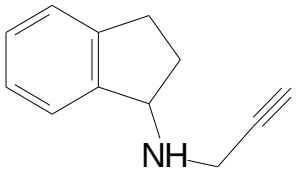

Rasagiline

Figure 2.4: Selective type B MAO inhibitors (Bertoni & Torres-Russotto, 2013).

2.1.5.6 Amantadine and anticholinergic agents

Amantadine and anticholinergic drugs are much less frequently used as treatments in Parkinson's disease and are not regarded as first-line therapy (Tugwell, 2008). When tremor is the main complaint, anticholinergic agents and beta-blockers may be adequate treatment (Tugwell, 2008). Present anticholinergic drugs that are used in Parkinson's disease include benztropine, trihexyphenidyl and diphenhydramine (Standaert & Roberson, 2011). Mild anti-parkinsonian effects are displayed by amantadine (Lees *et al*., 2009). Dyskinesia as a result of levodopa therapy can be treated with amantadine (Wells, 2009).

2.1.6 Current developments

Pulsatile stimulation by short-acting dopaminergic agents (such as levodopa) on receptors is responsible for the development of motor complications (Maranis *et al*.,

2011). New developments focus on continuous stimulation of receptors that leads to reduced side-effects and improved tolerability (Garbayo *et al*., 2013). This is achieved by extending the length of treatment or continuous drug release (Garbayo *et al*., 2013). Recent studies have aimed to address disease progression by promoting disease-modifying agents (Garbayo *et al*., 2013). New drug development strategies include disruption of the blood-brain barrier and using alternative drug delivery systems such as micro- and nanosystems (Garbayo *et al*., 2013).

Current drug development for Parkinson's disease concentrate on reformulating drugs that already exists, reconsidering compounds that originally are indicated for other clinical uses and developing unique small molecules along with gene and cell-based therapies (Garbayo *et al*., 2013). These approaches mainly focus on motor symptom control and less attention is given to disease modification and relief of non-motor symptoms (Garbayo *et al*., 2013).

LeWitt and Taylor (2008) published a review article on neuroprotective drug treatments that have been investigated. Although some treatments are very promising, none have been proven to impair disease progression (LeWitt & Taylor, 2008). Some treatment strategies have been proven to be disease modifying, but limited benefits questioned their practical application (LeWitt & Taylor, 2008). Examples of disease modifying agents include mitochondrial energy enhancers (coenzyme Q_{10} and creatine), MAO type B inhibitors, dopaminergic drugs (ropinirole, pramipexole), minocycline (antiapoptotic agent), α-tocopherol (antioxidant), GPI-1485 and riluzole (antiglutamatergic compounds) (LeWitt & Taylor, 2008).

Neurotrophic factors such as glial cell line-derived neurotrophic factor or neurturine are under investigation for neuroprotective treatment in Parkinson's disease (Garbayo *et al*., 2013). Disease modifying therapy has been encouraged by the identification of genes that are relevant to Parkinson's disease (Garbayo *et al*., 2013). Promising results have been obtained by agents that target α-synuclein, parkin and leucin-rich repeat serine/threonine protein kinase 2. These agents are, however, still under investigation (Garbayo *et al*., 2013).

Several micro- and nanosystems address brain drug delivery issues and improve

pharmacotherapeutic outcomes (Garbayo *et al*., 2013). Effective drug delivery systems include hydrogels and polymeric or lipid microparticles, and nanoparticles (Garbayo *et al*., 2013). These systems facilitate the delivery of antiparkinsonian drugs to the brain (Garbayo *et al*., 2013).

Since more than one factor may contribute to the pathogenesis of Parkinson's disease, multiple treatments may be required to treat Parkinson's disease (LeWitt & Taylor, 2008). In the future, a sustained dopaminergic system together with antioxidant molecules and different neurotrophic factors could be incorporated in a smart drug delivery system that is conjugated with specific ligands to optimise Parkinson's disease therapy (Garbayo *et al*., 2013).

2.2 COMT

2.2.1 General background and tissue distribution

O-Methylation of catecholamines was first defined in 1958 by Julius Axelrod where the characteristics of COMT were analysed (Männistö & Kaakkola, 1999; Bonifati & Meco, 1999). COMT is localised intracellular and is widely distributed in the body (Männistö & Kaakkola, 1999).

In the brain, low intracellular activity of COMT is present in post synaptic dopaminergic neurons, but considerable activity is found in glial cells, the space around synapses, capillary walls and in postsynaptic dendritic spines (Männistö & Kaakkola, 1999). The liver contains the highest COMT activity, with the kidneys, stomach and intestine also possessing high COMT activity (Männistö & Kaakkola, 1999). The spleen, submaxillary glands, pancreas β and δ cells, erythrocytes, heart, lungs, skin and eyes also possess COMT activity (Männistö & Kaakkola, 1999). COMT that occurs in erythrocytes is used as a convenient method of monitoring COMT inhibitory therapy (Männistö & Kaakkola, 1999).

The first COMT inhibitors were introduced by Guldberg and Marsden in 1975 (Männistö & Kaakkola, 1999). More interest in COMT arose when the selective second-generation COMT inhibitors were discovered in the 1980's (Männistö &

Kaakkola, 1999).

2.2.2 Biological function of COMT

2.2.2.1 Substrate specificities

Regardless of substituents on the aromatic nucleus, most COMT substrates have a catechol configuration (Figure 1.2) in its chemical structure (Guldberg & Marsden, 1975). Catecholamines [epinephrine, NE, dopamine (Figure 2.5)], levodopa (Figure 2.1), hydroxylated metabolites of catecholamines, catecholestrogens, dihydroxyindolic intermediates of melanin and ascorbic acid (Figure 2.8) are all substrates of COMT (Männistö & Kaakkola, 1999). An electron-withdrawing group on the catechol ring at position 5 can increase the affinity of the substrate for binding to the enzyme (Reenilä, 1999). Certain high affinity side chains of catechol substrates are apolar and co-planar with the catechol ring. These substrates have good binding affinities (Reenilä, 1999). Other catechols, including arterenone, adrenalone, 3,4-dihydroxycinnamic acid, triphenols and substituted catechols, also serve as COMT substrates (Guldberg & Marsden, 1975). Several medicinal substances, for example, apomorphine, benserazide, carbidopa, dobutamine, isoprenaline, methyldopa and rimiterol also contain a catechol structure that is susceptible to O-methylation (Kaakkola, 2000).

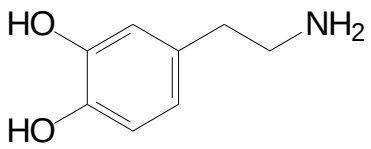

Dopamine

Figure 2.5: Dopamine, a COMT substrate (Guldberg & Marsden, 1975).

2.2.2.2 Genes and COMT

Two major isoforms exists for the enzyme: MB-COMT and S-COMT (Robinson *et al*., 2012). S-COMT and MB-COMT are encoded by the same gene (Männistö & Kaakkola, 1999). This gene is located on chromosome 22, band q11.2 and contains six exons (Männistö & Kaakkola, 1999). The two isoforms of COMT are encoded from

two AUG start codons that are situated in exon 3 (Tunbridge, 2010). 50 Hydrophobic amino acids are encoded for MB-COMT's membrane-spanning region and are not included in the 221 amino acids of S-COMT (Tunbridge, 2010). The two distinct promoters from exon 3 that control COMT gene expression in humans, are the P1 promoter that is responsible for the transcription of 1.3-kb mRNA (messenger ribonucleic acid) and the distal 5' promoter (P2) that regulates the transcription of the longer 1.5-kb mRNA (Männistö & Kaakkola, 1999). P2 can code for both S-COMT and MB-COMT (Männistö & Kaakkola, 1999). P1 can only code transcripts for S-COMT due to the absence of the MB-COMT AUG translation initiation codon (Männistö & Kaakkola, 1999).

S-COMT is mainly found in peripheral tissue, while MB-COMT is dominant in the brain (Tunbridge, 2010). Both transcripts occur in most human tissues, but only the longer transcript is found in the brain (Männistö & Kaakkola, 1999). According to Tunbridge (2010), the reason for this lies in the putative transcription binding sites where COMT promoters show different expression profiles (Tunbridge, 2010). This also explains the variation in the proportion of S-COMT and MB-COMT in different peripheral tissues (Tunbridge, 2010). Differences in COMT expression may be due to environmental factors, nutritional factors, differences between males and females, changes in growth as well as certain drug treatments (Tunbridge, 2010). A study done by Zhao *et al.* (2001) concluded that levodopa therapy may lead to increased COMT activity.

2.2.2.3 Polymorphisms of COMT

According to Robinson *et al*. (2012) numerous functional single nucleotide polymorphisms (SNPs) exists for the COMT gene. At codon 108, the replacement of valine (Val) with methionine (Met) is the most common polymorphism of S-COMT. This polymorphism corresponds to the same replacement at codon 158 of MB-COMT (Robinson *et al*., 2012). Männistö and Kaakkola (1999) explain that genetic polymorphisms can lead to different levels of COMT enzyme activity. Different populations may also display variation between low and high COMT activity alleles, which may lead to differences in levodopa response (Männistö & Kaakkola, 1999).

2.2.3 Role of COMT in Parkinson's disease

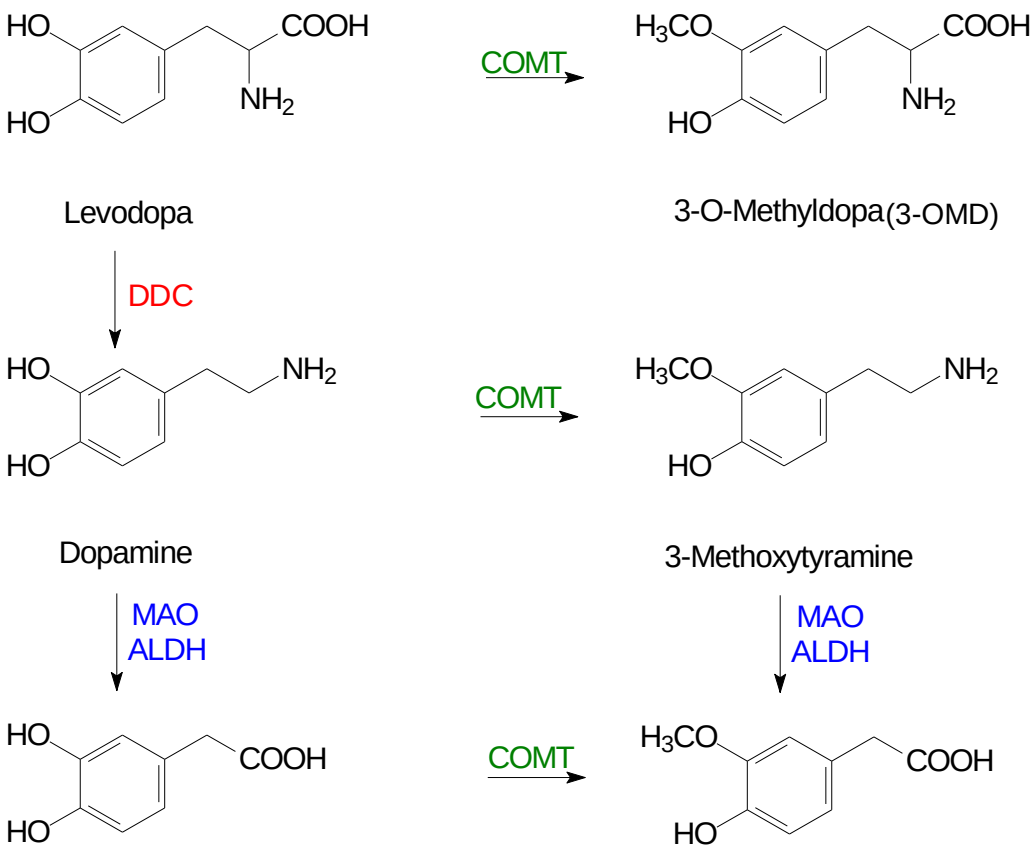

Figure 2.6: The metabolism of levodopa. COMT, catechol-*O*-methyltransferase; DDC, dopa decarboxylase; MAO, monoamine oxidase; ALDH, aldehyde dehydrogenase (Standaert & Roberson, 2011).

2.2.3.1 The metabolism of levodopa and dopamine

Levodopa is primarily metabolised to dopamine by aromatic L-amino acid decarboxylase (AADC), also called DDC. This reaction occurs mainly in the gut and liver (Figure 2.6) (Nissinen, 2010). The metabolism of levodopa by DDC occurs both in the periphery and the central nervous system (Figure 2.7) (Tugwell, 2008). COMT, MAO and ALDH are responsible for dopamine metabolism (Standaert & Roberson, 2011). Homovanillic acid (3-methoxy-4-hydroxyphenylacetic acid or HVA) and 3,4-dihydroxyphenylacetic acid (DOPAC) are the major metabolites that results from

dopamine metabolism (Halkias *et al*., 2007). Less than 1% of a levodopa dose reaches the brain due to its extensive peripheral metabolism (Kaakkola, 2000). Adding a peripheral DDC inhibitor to levodopa therapy, for example carbidopa or benserazide, result in a reduction of the levodopa dose to approximately one tenth of the original dose (Nissinen, 2010). This leads to an improved side-effect profile, such as reduced nausea after levodopa treatment (Tugwell, 2008), as well as higher levodopa concentrations the brain after a specific dose of levodopa (Nissinen, 2010).

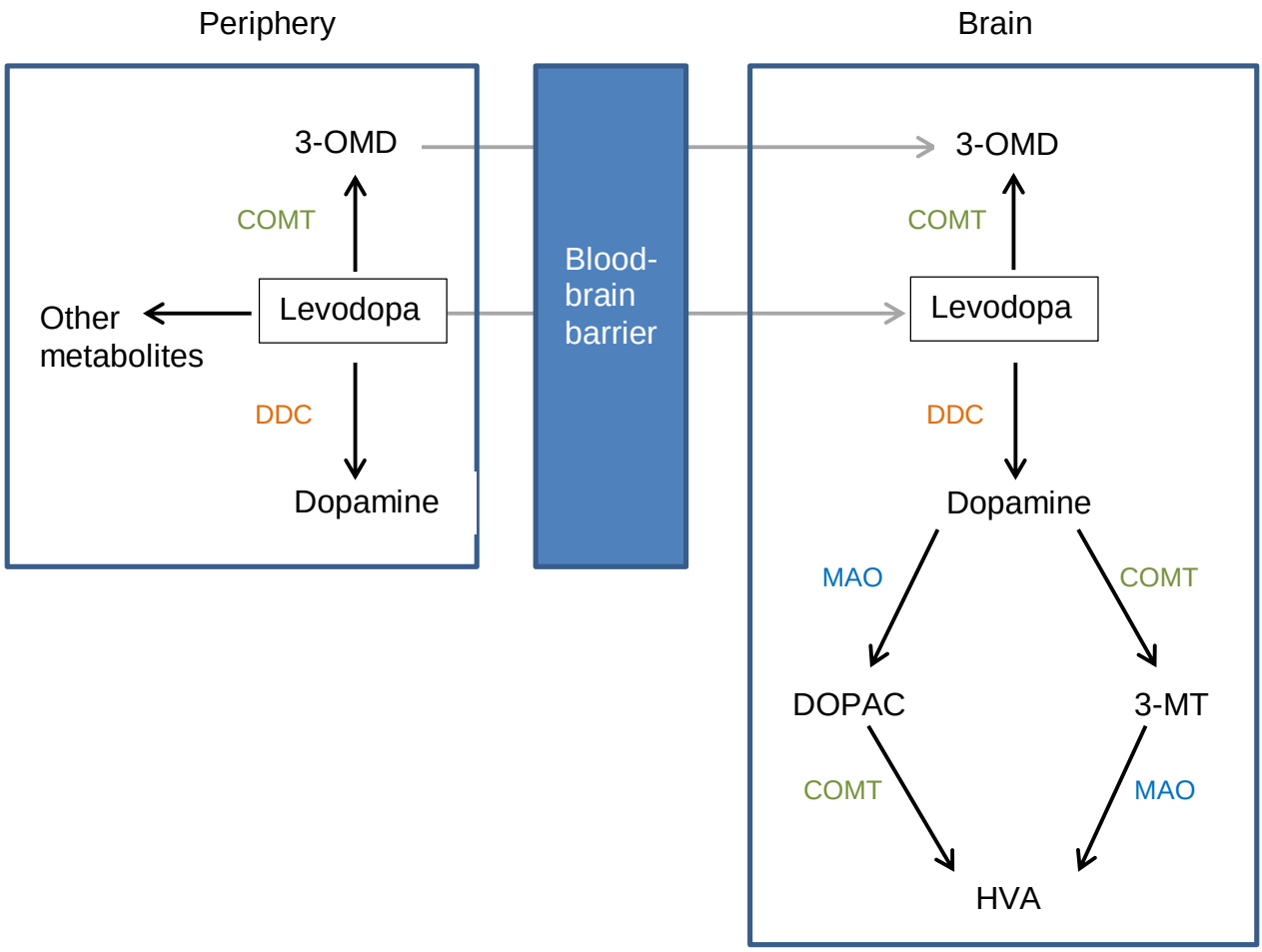

Figure 2.7: The metabolic pathways of levodopa and dopamine in the periphery and central nervous system. 3-OMD, 3-O-methyldopa; 3-MT, 3-methoxytyramine, COMT, catechol-*O*-methyltransferase; DDC, dopa decarboxylase; MAO, monoamine oxidase; DOPAC, 3,4-dihydroxyphenylacetic acid; HVA, homovanillic acid (Kaakkola, 2000).

When decarboxylation by DDC is inhibited, *O*-methylation becomes the main metabolic pathway for the metabolism of levodopa. Levodopa is O-methylated by COMT to yield 3-*O*-methyldopa (3-OMD) (Kaakkola, 2000). In the gut and blood-brain barrier, the 3-OMD metabolite can compete with levodopa for uptake by neutral amino acid transporters (Nissinen, 2010). By administering peripheral COMT inhibitors, the conversion of levodopa to 3-OMD is blocked (Standaert & Roberson, 2011). This leads to decreased peripheral breakdown and prolonged plasma half-life of levodopa, and thus a higher fraction of the levodopa dosage reaches the brain (Maranis *et al*., 2011).

As mentioned above, levodopa is metabolised by COMT to yield 3-OMD. Dopamine is also metabolised by COMT to yield 3-MT (3-methoxytyramine). Both these metabolites are pharmacologically inactive (Standaert & Roberson, 2011). Levodopa is absorbed by the saturable large neutral amino acid (LNAA) transporter system in the gastrointestinal tract and blood-brain barrier (Bonifati & Meco, 1999). 3-OMD has a higher affinity for the LNAA transporters than levodopa (Bonifati & Meco, 1999). This could lead to fluctuations in levodopa therapy when 3-OMD and levodopa have to compete for transport across the blood-brain barrier and intestinal mucosa (Kaakkola, 2000). 3-OMD has a long elimination half-life of 15 h (Männistö & Kaakkola, 1999). During chronic levodopa therapy where COMT is not inhibited, 3-OMD and levodopa accumulate in skeletal muscle (Bonifati & Meco, 1999). The accumulated 3-OMD may thus affect the maintenance of levodopa plasma levels as well as the entry of levodopa into the brain (Bonifati & Meco, 1999). Levodopa-induced dyskinesia or a decrease in the response to therapy can occur with high 3-OMD plasma levels (Bonifati & Meco, 1999).

In spite of the above mentioned, Bonifati and Meco (1999) explained that high 3-OMD levels do not necessarily lead to a significant inhibition of levodopa uptake into the brain, because 3-OMD represents only approximately 10% of circulating LNAAs. Rapid equilibrium between the plasma and the brain is also achieved owing to 3-OMD's high affinity to LNNAs (Bonifati & Meco, 1999). The wearing-off phenomenon, however, has been associated with high 3-OMD levels (Bonifati & Meco, 1999).

2.2.3.2 COMT levels in the brain and aging

Various studies have been carried out to determine if correlations exist between high and low COMT activities and several diseases (Hirano *et al*., 2005). However, differentiation between S-COMT and MB-COMT were not made in these studies (Hirano *et al*., 2005). Diseases that are associated with low COMT activity include Parkinson's disease, obsessive-compulsive disorder, aggressive schizophrenia and bipolar affective disorder (Hirano *et al*., 2005). Anorexia nervosa, the abuse of polysubstances and suicide are all associated with high COMT activity (Hirano *et al*., 2005). According to Guldberg & Marsden (1975), COMT activity increases approximately tenfold from birth to adulthood. However, after the age of 60, there is a decrease in COMT activity (Guldberg & Marsden, 1975). Bonifati and Meco (1999) also report that aging in rats is associated with reduced affinity for COMT substrates as well as lowered sensitivity to enzyme inhibition.

2.2.4 COMT inhibitors

2.2.4.1 First generation inhibitors of COMT

Early COMT inhibitors are discussed in detail in a study done by Guldberg and Marsden (1975). These include pyrogallol and its derivatives, catechol derivatives, tropolones, 8-hydroxyquinolines, iodophenol derivatives, 3-mercaptotyramine, S-adenosylhomocysteine (SAH), pyridoxal-5'-phosphate, l-ascorbic acid as well as pyrones and pyridones (Figure 2.8) (Guldberg & Marsden, 1975). These compounds showed adequate *in vitro* enzyme inhibition, but poor results *in vivo* and high toxicity levels were frequently observed (Guldberg & Marsden, 1975). According to Männistö and Kaakkola (1999), early COMT inhibitors lack selectivity and are short-acting. These early COMT inhibitors have poor oral bioavailability profiles and are thus excluded from routine clinical use (Bonifati & Meco, 1999). A trial with butylgallate and U-0521 (3,4-dihydroxy-2-methylpropiophenone) were performed in combination with levodopa therapy in Parkinson's disease, but promising results were not obtained, and these compounds are thus not clinically useful (Kaakkola, 2000).

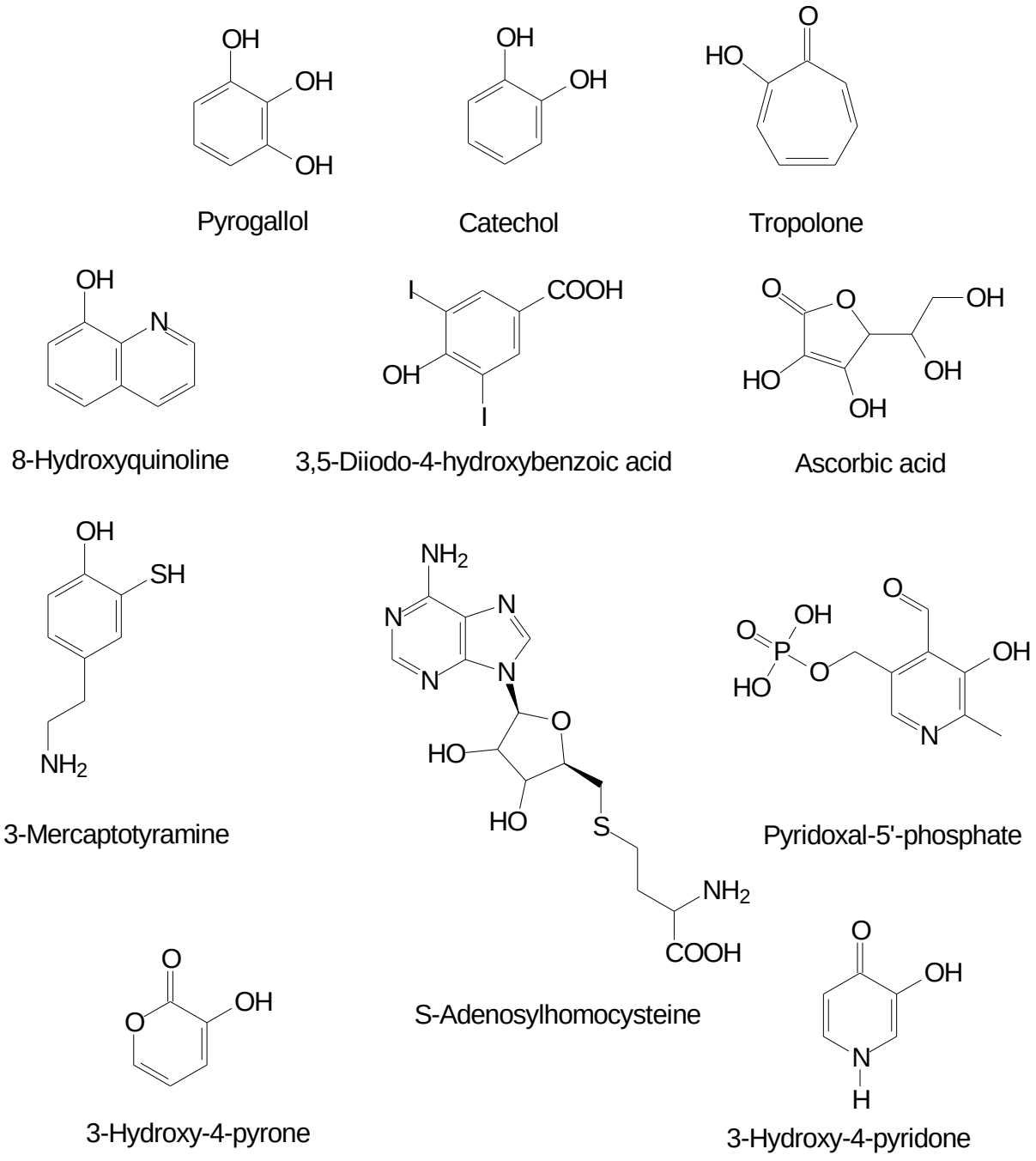

Figure 2.8: Miscellaneous first generation COMT inhibitors (Guldberg & Marsden, 1975).

2.2.4.2 Second generation inhibitors of COMT

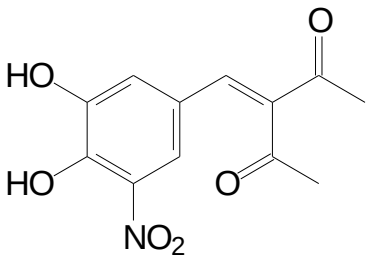

Nitecapone

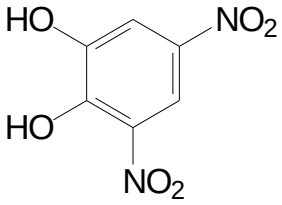

Dinitrocatechol

Figure 2.9: Examples of nitrocatechol COMT inhibitors (Männistö and Kaakkola, 1999).

According to Männistö and Kaakkola (1999), new generation COMT inhibitors mostly contain a nitrocatechol group as a key structural feature. Second generation COMT inhibitors include nitecapone and dinitrocatechol (OR-486) (Figure 2.9), entacapone and tolcapone (Figure 1.1), 2-(3,4-dihydroxy-2-nitrophenyl)vinylketone, dihydroxy-nitrobenzaldehyde and 6-nitronorepinephrine (Männistö & Kaakkola, 1999). CGP 28014 (Figure 2.10) is also a second generation COMT inhibitor but does not contain a nitrocatechol moiety (Männistö & Kaakkola, 1999).

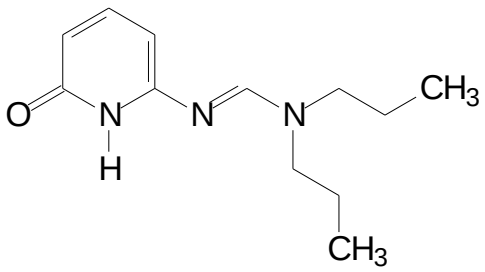

CGP 28014

Figure 2.10: A second generation non-nitrocatechol COMT inhibitor (Männistö & Kaakkola, 1999).

Tolcapone and entacapone have successfully been used in the treatment of Parkinson's disease (Robinson *et al*., 2012). When treated with levodopa and

carbidopa, both COMT inhibitors reduce the so called “wearing off” symptoms (Standaert & Roberson, 2011). The clinical use of these nitrocatechol COMT inhibitors is sometimes limited due to tolcapone’s association with hepatotoxicity and entacapone’s association with severe diarrhoea (Robinson *et al*., 2012). The hepatotoxicity of tolcapone may be due to the inhibition of peripheral S-COMT (Robinson *et al*., 2012). Present therapy that makes use of tolcapone thus requires appropriate monitoring of hepatic function (Standaert & Roberson, 2011). Other possible adverse effects of tolcapone and entacapone that are dopamine related include nausea, vivid dreams, confusion, hallucinations and orthostatic hypotension (Standaert & Roberson, 2011).

Robinson *et al.* (2012) reported that non-nitrocatechol COMT inhibitors, such as 3-hydroxypyridin-4-ones that are MB-COMT specific, possess improved safety profiles. It must however be kept in mind that interference with dopamine synthesis can occur with 3-hydroxypyridine-4-ones due to the chelation of iron and subsequent inhibition of Tyr and tryptophan (Trp) hydroxylases (Männistö & Kaakkola, 1999).

2.2.5 Mechanism of action of COMT

COMT serves as a catalyst of SAMe methyl transmission (Standaert & Roberson, 2011). In the presence of magnesium, the methyl group of SAMe is transferred to one of the catechol substrate’s hydroxyl groups (Figure 2.11) (Männistö & Kaakkola, 1999). O-Methylation occurs through a direct nucleophilic attack of the catechol substrate’s hydroxyl group on the methyl carbon of SAMe in a S_N2-like transition state (Männistö & Kaakkola, 1999).

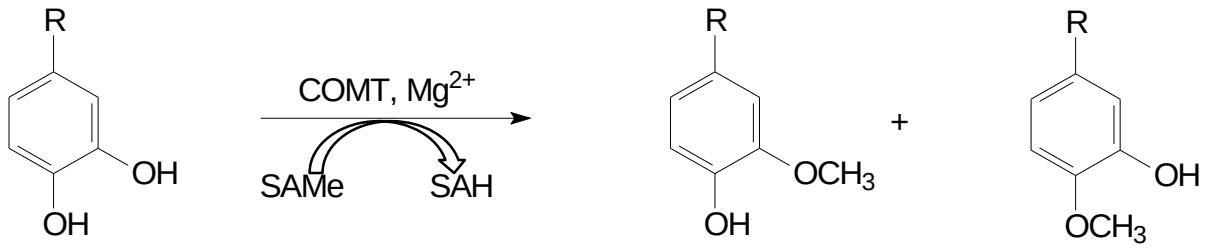

Figure 2.11: Mechanism of action of COMT. SAMe, S-adenosyl-L-methionine; SAH, S-adenosylhomocysteine (Männistö & Kaakkola, 1999).

The order in which this *O*-methylation reaction takes place starts with the binding of SAMe to the enzyme, followed by magnesium, and lastly the catechol substrate (Bonifati & Meco, 1999). The order, in which the molecules are released, follows the reversed order (Reenilä, 1999). This reaction may also be facilitated by other divalent cations such as Ca^{2+} and Hg^{2+}, but is noncompetitively inhibited by Ca^{2+} ions (Bonifati & Meco, 1999). According to Reenilä (1999), both isoforms of COMT should follow the same reaction mechanism. 3- and 4-*O*-methylation depends on the chemical nature of the substrate as well as the reaction pH (Guldberg & Marsden, 1975). 4'-Hydroxy methylation is much less common than 3'-hydroxy methylation (Männistö & Kaakkola, 1999) and is only rarely found *in vivo* (Reenilä, 1999).

2.2.6 The 3D-structure of COMT

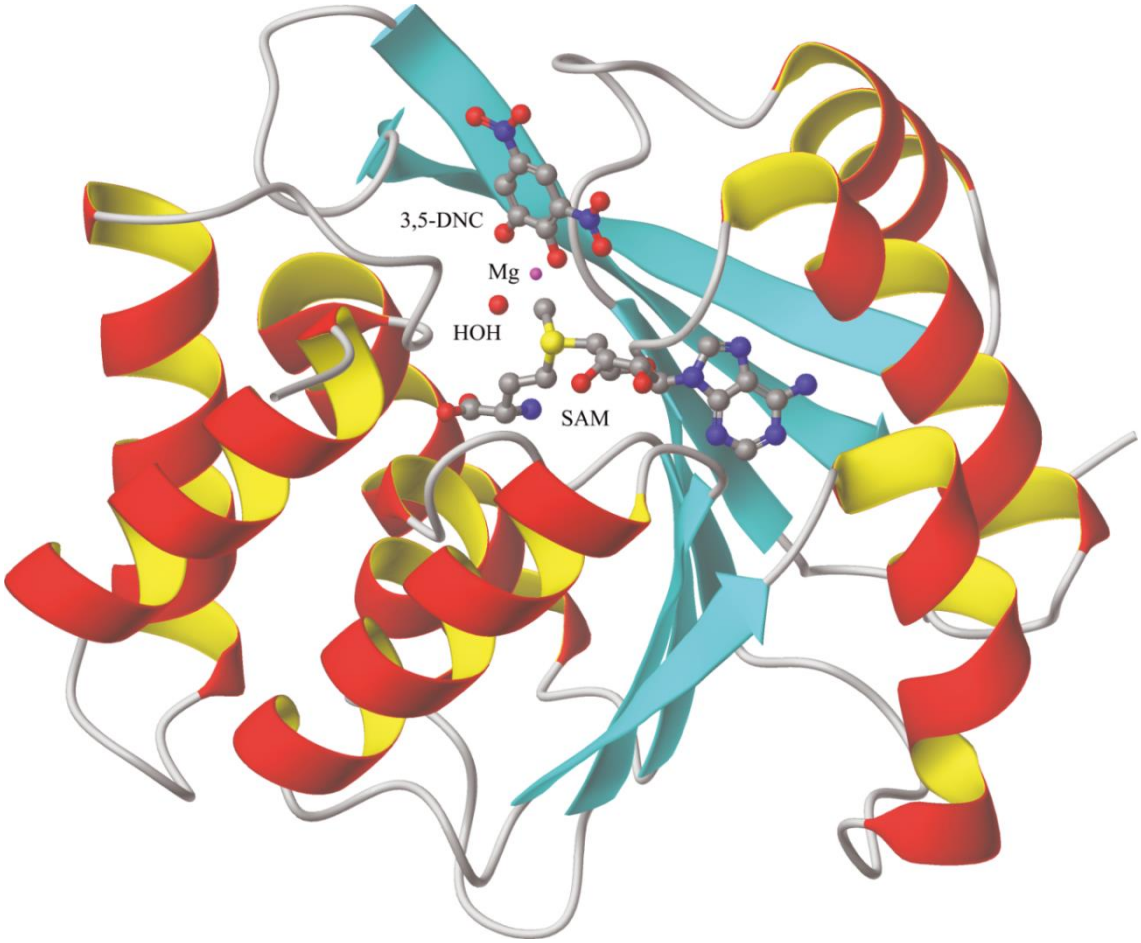

Figure 2.12: The three-dimensional structure of rat S-COMT. 3,5-DNC, 3,5-dinitrocatechol; SAM, S-adenosyl-L-methionine (Bonifácio *et al*., 2007).

In this representation of the 3D-structure of rat S-COMT (Figure 2.12), SAMe, magnesium, the COMT inhibitor 3,5-DNC and a coordinated water molecule are illustrated. The central seven-stranded β-sheet core is surrounded by eight α-helices (Rutherford *et al*., 2008). The active site of COMT is made up by two distinct parts: SAMe is situated in a deep cleft inside the COMT protein, while the magnesium ion and the substrate/inhibitor are located in a shallower groove (Learmonth *et al*., 2010).

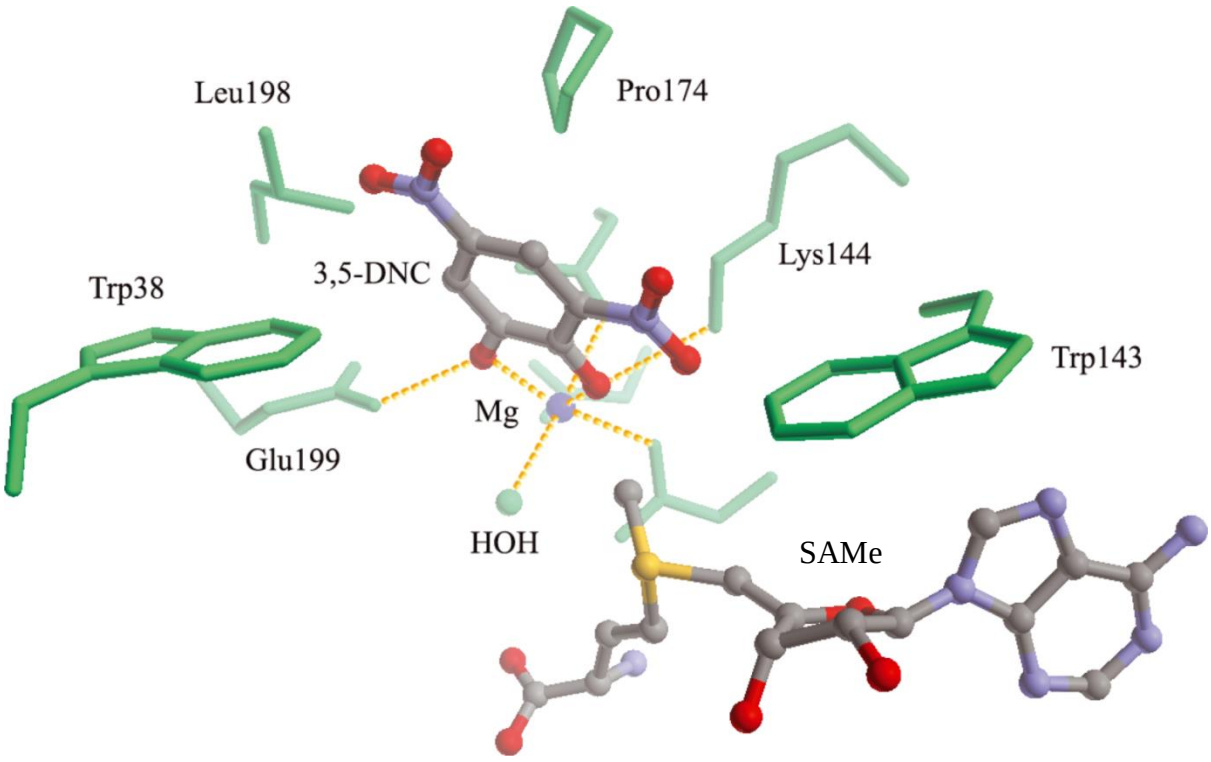

Figure 2.13: The catalytic site of COMT (Bonifácio *et al*., 2007).

The catalytic domain of S-COMT (Figure 2.13) is identical to that of MB-COMT (Orłowski *et al*., 2011). Although their catalytic domains are identical, their enzymatic kinetics differ significantly (Orłowski *et al*., 2011). The difference between the two isoforms of COMT is that S-COMT consists of 221 residues (Jee-Young & Yangmee, 2005) while MB-COMT contains an extra 50 residues at the N-terminus of the protein (Orłowski et al., 2011).

The octahedral coordination of magnesium is essential for COMT catalytic activity (Learmonth *et al*., 2010). It is coordinated towards one asparagine (Asn) residue (Asn170), two aspartic acid (Asp) residues (Asp141 and Asp169), and one water

molecule (Bonifácio *et al*., 2007). It also chelates the two hydroxyl groups of the catechol substrate which serves as final preparation before O-methylation occurs (Learmonth *et al*., 2010). Another function of magnesium is that it brings one of the hydroxyl groups closer to the donor's methyl group to be transferred (Learmonth *et al*., 2010). Magnesium also lowers the pKa of the catechol and facilitates the first step in the catalytic cycle, which is the capturing of the more acidic proton from one of the hydroxyls by lysine (Lys) 144 (Lys144), which is deprotonated at physiological pH (Learmonth *et al*., 2010; Männisto & Kaakkola, 1999). In the second step in the catalytic cycle, the resulting nucleophilic phenolate anion attacks the trimethylsulfonium ion of SAMe, which results in methyl transmission to the oxygen (Learmonth *et al*., 2010).

Hydrogen bonding between the hydroxyl groups of the catechol substrate and the side chains of glucine (Glu) 199 (Glu199) and Lys144 leads to further anchoring of the substrate in a favourable position (Learmonth *et al*., 2010). So-called "gatekeeper" residues, namely Trp38, Trp143, Pro174 (proline) and Leu198 (leucine) offer additional support in keeping the substrate in the correct orientation (Learmonth *et al*., 2010). These "gatekeeper" residues form a hydrophobic wall and make favourable contacts with the planar catechol ring (Learmonth *et al*., 2010). Due to the interaction with side chain substituents, it is very likely that these residues are responsible for the selectivity of COMT for different substrates (Learmonth *et al*., 2010).

2.2.7 Enzyme kinetics

Potential therapeutic agents can be analysed mathematically by their ability to enhance or inhibit the rates of certain enzyme-catalysed reactions (Rodwell & Kennelly, 2003). Before kinetic data can be interpreted, it is important to understand where enzyme kinetics originates. The Michaelis-Menten equation (Equation 2.1) describes the relationship that exists between the initial reaction velocity (v_i) and the concentration of a substrate, [S] (Rodwell & Kennelly, 2003). As indicated in Figure 2.14, an increase in [S] will lead to an increase in the reaction velocity (V) until a maximum V_{max} is reached (Rodwell & Kennelly, 2003). Saturation of an enzyme with a substrate is achieved when no further increase in reaction velocity is seen with an increase in [S] (Rodwell & Kennelly, 2003). At saturated levels, the reaction velocity

relies exclusively on the dissociation of the free enzyme from the enzyme-substrate complex to combine with more substrate to form the product (Rodwell & Kennelly, 2003).

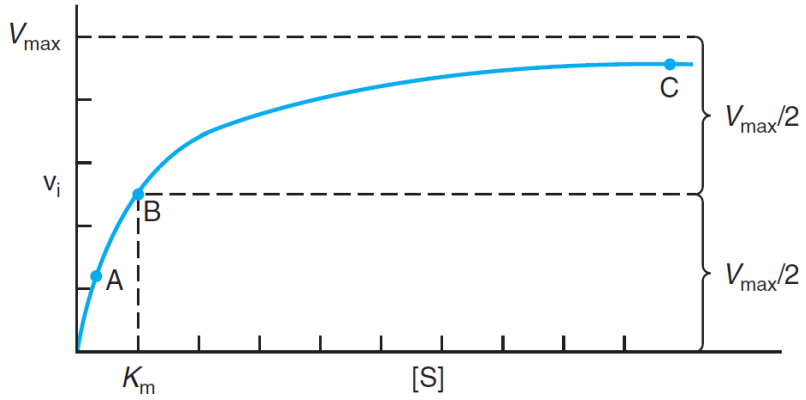

Figure 2.14: An example of a Michaelis-Menten plot (Rodwell & Kennelly, 2003). [S], substrate concentration; v_i, initial velocity; V_{max}, maximum velocity; K_m, substrate concentration when v_i is one-half of V_{max}.

(2.1): $$v_i = \frac{V_{max}[S]}{K_m + [S]}$$

K_m is the Michaelis constant that indicates the substrate concentration, [S], where the initial reaction velocity (v_i) is half of the maximum velocity ($V_{max}/2$) (Rodwell & Kennelly, 2003). Impractical high concentrations of the substrate are sometimes needed to directly calculate the numeric value of V_{max} and K_m (Rodwell & Kennelly, 2003). This can be overcome by the inversion of the Michaelis-Menten equation, which leads to the formation of the Lineweaver-Burk plot (Figure 2.15) (Rodwell & Kennelly, 2003).

Inversion and fractionation of Equation 2.1 firstly yield Equation 2.2 and then Equations 2.3 and 2.4:

(2.2): $$\frac{1}{v_i} = \frac{K_m + [S]}{V_{max}[S]}$$

(2.3): $$\frac{1}{v_i} = \frac{K_m}{V_{max}[S]} + \frac{[S]}{V_{max}[S]}$$

(2.4): $\frac{1}{v_i} = \left(\frac{K_m}{V_{max}}\right)\frac{1}{[S]} + \frac{1}{V_{max}}$

Inversion and fractionation of the Michaelis-Menten equation gives the equation of a straight line (Equation 2.4), y = mx + c (Dixon, 1953). A plot of $1/v_i$ on the y-axis versus 1/[S] on the x-axis gives a slope of K_m/V_{max} and an intercept of $1/V_{max}$ (Rodwell & Kennelly, 2003). This plot is termed the double reciprocal plot or Linweaver-Burk plot. V_{max} can thus be calculated by using the y-intercept of the Linweaver-Burk plot (Dixon, 1953). K_m values can be determined in two different ways (Dixon, 1953): (1) by using the slope of the Lineweaver-Burk plot to calculate K_m and (2) by extrapolation of the straight line to its intercept on the x-axis (where y = 0) giving $x = -1/K_m$.

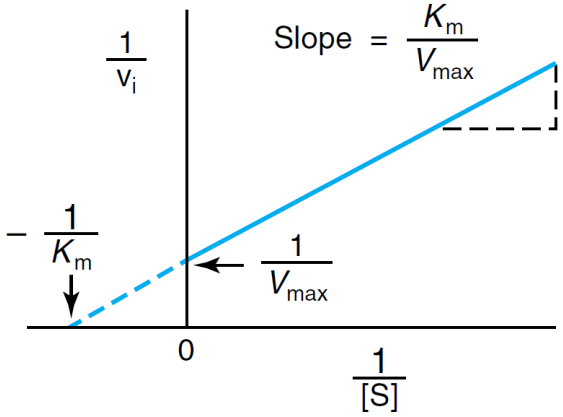

Figure 2.15: An example of a Linweaver-Burk plot (Rodwell & Kennelly, 2003).

The enzyme-inhibitor dissociation constant (K_i) indicates the equilibrium that exists for the reversible combination of an enzyme with a competitive inhibitor (Dixon, 1953). The amount of free enzyme available to bind to substrate is decreased when a competitive inhibitor is added (Rodwell & Kennelly, 2003). To distinguish between competitive and noncompetitive inhibitors, Linweaver-Burk plots may be used. Linweaver-Burk plots also simplify the determination of K_i (Figure 2.16) (Rodwell & Kennelly, 2003).

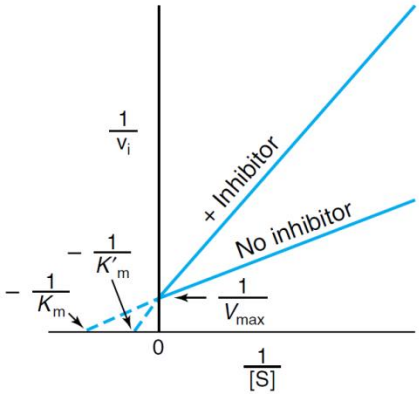

Figure 2.16: The Lineweaver-Burk plot of competitive inhibition (Rodwell & Kennelly, 2003).

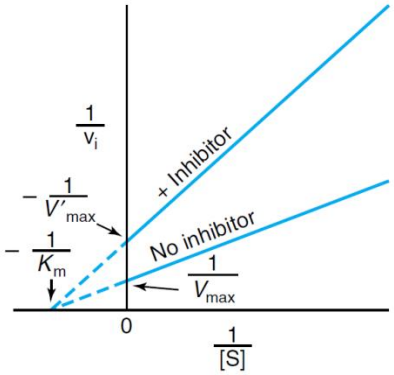

Figure 2.17: The Lineweaver-Burk plot of non-competitive inhibition (Rodwell & Kennelly, 2003).

Considering the Lineweaver-Burk plot of competitive inhibition (Figure 2.16), it is clear that when 1/[S] is equal to 0, the reaction velocity (v_i) is independent of the inhibitor's presence (Rodwell & Kennelly, 2003). A competitive inhibitor thus has no effect on V_{max} but increases the K_m value of the substrate (Rodwell & Kennelly, 2003). When K_m is known, K_i may be determined by using Equation 2.5, with x signifying the intercept on the x axis (in the presence of inhibitor) and [I] indicating the inhibitor's concentration (Rodwell & Kennelly, 2003). Higher K_i values are an indication of a reduction in the effectiveness of the inhibitor (Rodwell & Kennelly, 2003).

(2.5): $x = \frac{-1}{K_m}\left(1 + \frac{[I]}{K_i}\right)$

Noncompetitive inhibitors do not affect the substrate's ability to bind to the enzyme (Rodwell & Kennelly, 2003). Thus, enzyme-inhibitor complexes can be formed as well as enzyme-inhibitor-substrate complexes, but the ability of transforming these substrates to products are reduced as reflected by reduction in the V_{max} value demonstrated in Figure 2.17 (Rodwell & Kennelly, 2003). The free enzymes and enzyme-inhibitor complexes exhibit identical affinities for the substrate when noncompetitive inhibition occurs (Rodwell & Kennelly, 2003). When noncompetitive inhibition occurs, K_m remains unchanged.

2.2.7.1 COMT specific enzyme kinetics to consider

S-COMT has a higher *O*-methylation catalytic activity, but lower affinity for catecholamine substrates than MB-COMT (Reenilä, 1999). This is confirmed by substrate K_m values being much higher for S-COMT than MB-COMT (Reenilä, 1999). V_{max} values of natural catecholamines can differ by as much as tenfold between S-COMT and MB-COMT (Reenilä, 1999).

2.2.8 *In vitro* measures of COMT

In vitro methods used to determine COMT activity are based on the principle that COMT catalyses the donation of a methyl group from SAMe to a catechol substrate in the presence of magnesium ions or any divalent cation (Guldberg & Marsden, 1975). Any substrate that contains a catechol grouping can be used, for example NE (Guldberg & Marsden, 1975). Formation of the *O*-methylated end product is then determined and quantified (Guldberg & Marsden, 1975, Creveling & Daly, 1971).

- The rare use of colourimetric measures is reported for early COMT assays (Guldberg & Marsden, 1975). Catecholamines react with hydroxylamine to form a coloured complex in the presence of ferric chloride (Pihlavisto & Reenilä, 2002). This was used to determine COMT catalysed *O*-methylation of catecholamines and is based on monitoring the disappearance of the catechol substrate colourometrically (Pihlavisto & Reenilä, 2002). Repeatability of these assays was reasonable, but desired sensitivity and stability were not always achieved (Pihlavisto & Reenilä, 2002). The accidental monitoring of other O-

methylation reactions that took place and recording the disappearance of the substrate, rather than the production of the product also made results unreliable (Pihlavisto & Reenilä, 2002).

- Spectrophotometry is an analytical method used to identify and quantify samples based on the measurement of their ultraviolet (UV) or visible light absorption spectra (Karpinska, 2012). A spectrophotometric assay for COMT is described by Borchardt (1974), where 3,4-dihydroxyacetophenone is used as a substrate. Spectrophotometric detection of the end-products, 3-hydroxy-4-methoxyacetophenone and 4-hydroxy-3-methoxyacetophenone (Figure 2.18) (Borchardt, 1974), is possible since the products absorb at longer absorption wavelengths than the parent compound (Pihlavisto & Reenilä, 2002). This method made quantitation of the *O*-methylated products possible without separating them from the parent compound, but required knowledge of the relative amounts of the regioisomeric products formed (Pihlavisto & Reenilä, 2002).

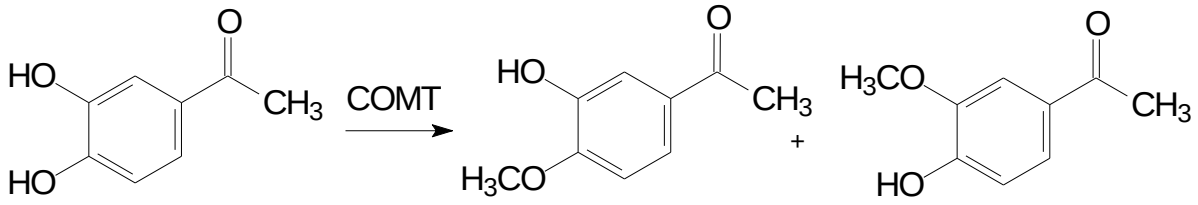

Figure 2.18: *O*-Methylation of 3,4-dihyroxyacetophenone, yielding 3-hydroxy-4-methoxyacetophenone and 4-hydroxy-3-methoxy-acetophenone as reaction products (Borchardt, 1974).

Products formed during a COMT-catalysed reaction, include not only methoxy derivatives, but also SAH which is the demethylated end product of SAMe (Pihlavisto & Reenilä, 2002). Coward and Wu (1973) made use of a spectrophotometric COMT assay which was based on the difference in UV absorption spectra of SAH and S-inosylhomocysteine. S-Inosylhomocysteine is formed from SAH when adenosine deaminase is added to the reaction mixture (Pihlavisto & Reenilä, 2002). This method, however, delivered high

background noise at the analytical wavelength of 265 nm (Pihlavisto & Reenilä, 2002).

- *O*-Methylated products from COMT incubation mixtures can be identified by comparing their *Rf* values to those of authentic reference compounds by using paper or thin layer chromatography (TLC) (Pihlavisto & Reenilä, 2002). Colour reagents or UV light are used to visualise spots that represent different compounds (Pihlavisto & Reenilä, 2002). Spots representing certain compounds can be eluted from the plate and can also be quantitated fluorometrically or with liquid scintillation counting (Pihlavisto & Reenilä, 2002). For example, after separation and derivatisation with isothiocyanate, 4-*O*-methyldopamine can be quantitated fluorometrically directly from the silica gel plate (Pihlavisto & Reenilä, 2002). However, distinguishing between 3-OMD and 4-*O*-methyldopa (Figure 2.19) is difficult to achieve with the use of paper or TLC, but can be accomplished after extraction of the co-eluted compounds and applying it to a resin column (Pihlavisto & Reenilä, 2002).

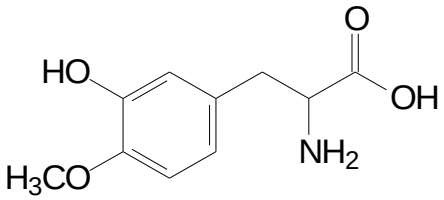

4-O-methyldopa

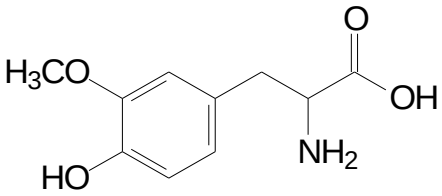

3-O-methyldopa

Figure 2.19: Illustration of 4-*O*-methyldopa and 3-OMD (Pihlavisto & Reenilä, 2002).

- Liquid-liquid extraction with organic solvents was another of the early methods used for the separation of an *O*-methylated metabolite from the parent compound (Pihlavisto & Reenilä, 2002). After evaporation of the organic phase, a product present in the residue may be quantitated with different detection methods (Pihlavisto & Reenilä, 2002). Liquid-liquid extraction is mainly used as a sample preparation method, making analytes easier to separate and detect

before injecting into the chromatographic system of choice (Gonçalves *et al*., 2012). It thus eliminates substances that could possibly interfere with the analyte peaks of interest (Gonçalves *et al*., 2012).

An example where liquid-liquid extraction was used as sample preparation step is the fluorometric detection of the COMT-catalysed products of epinephrine and NE. Epinephrine or NE was thus used as substrate, and after reaction the incubations were extracted from borate buffer (pH 10) with organic solvents. This was followed by re-extraction with 0.1 N HCl to an acidic aqueous phase (Pihlavisto & Reenilä, 2002). Measurement of the end-product, metanephrine or NMN, respectively, was accomplished fluorometrically (Figure 2.20) (Creveling & Daly, 1971).

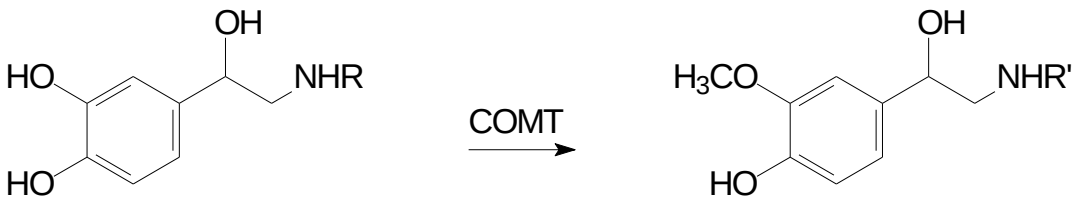

R = CH_3, Epinephrine
R = H, Norepinephrine

R' = CH_3, Metanephrine
R' = H, Normetanephrine

Figure 2.20: Metabolism of epinephrine and NE by COMT (Creveling & Daly, 1971).

- Gas chromatography is a technique used to separate components in a mixture and to gain information regarding their molecular compositions and amounts (Blumberg, 2012). Components of a vaporised sample are carried through a column and partition between a stationary phase, which consists of a large surface area, and a gas mobile phase, which permeates through the stationary bed (McNair & Miller, 2009). Components separate based on the relative vapour pressures of the sample components and their affinities for the stationary bed (McNair & Miller, 2009). Maurer *et al*. (2000) presented a procedure for the determination of the COMT activity using 3,4-dihydroxyphenethylamine (dopamine) as substrate. Gas chromatographic-

mass spectrometry (MS) was used to quantify 3-methoxy-4-hydroxyphenethylamine as product (Figure 2.21) (Maurer *et al*., 2000).

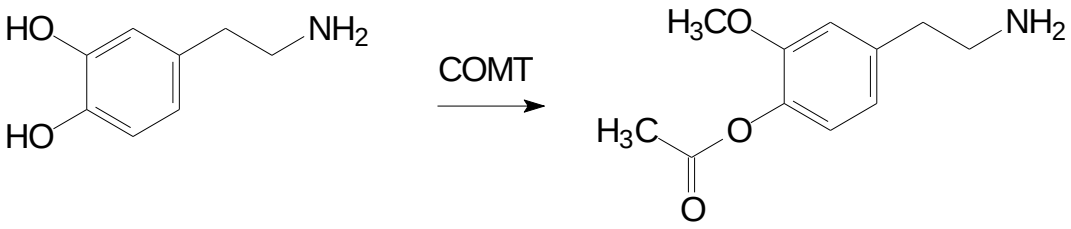

3,4-dihydroxyphenethylamine 3-methoxy-4-hydroxyphenethylamine

Figure 2.21: *O*-Methylation of 3,4-dihydroxyphenethylamine (Maurer *et al*., 2000).

- HPLC (high-performance liquid chromatography) methods are used to separate reaction products by making use of different columns that include ion exchange, normal-phase or reversed-phase columns (Reenilä, 1999). Different detection systems, for example UV, electrochemical, fluorometric (Reenilä, 1999) and radiochemical detectors are employed in HPLC methods to determine COMT activity (Lautala *et al*., 1999). According to Hirano *et al.* (2005), HPLC coupled with fluorescence detection exhibit better sensitivity compared to HPLC-electrochemical and radiochemical detection assays.

HPLC detection systems

- UV detection: The O-methylated products of 3,4-dihydroxybenzoic acid (Figure 2.22) have been detected in a HPLC system with UV detection by Pennings and Van Kempen (1979). UV detection is however less common than other detection systems, due to poor selectivity and sensitivity associated with it (Pihlavisto & Reenilä, 2002).

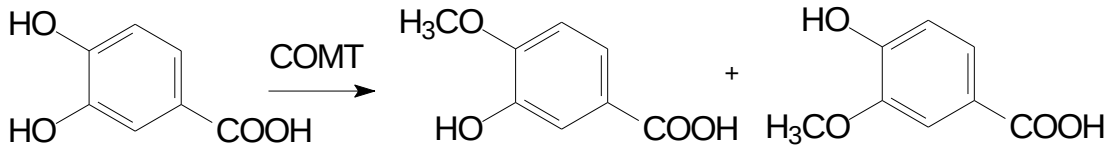

Figure 2.22: Reaction pathway of 3,4-dihydroxybenzoic acid subjected to COMT metabolism, yielding 3-hydroxy-4-methoxy-benzoic acid (isovanillic acid) and 4-hydroxy-3-methoxybenzoic acid (vanillic acid) (Pennings & van Kempen, 1979).

- Radiochemical detection: Quantitation of the O-methylated products with radiochemical detection is based on the measurement of the radioactivity of the product after separating it from the substrates or co-substrates (Pihlavisto & Reenilä, 2002). Lautala *et al*. (1999) carried out a COMT assay using S-adenosyl-L-[methyl-^{14}C]methionine as methyl donor. After transferring the labeled methyl to 3,4-dihydroxybenzoic acid, the product is separated by HPLC and quantitated by radiochemical detection (Lautala *et al*., 1999). Regioisomeric products can also be separated from each other and determined with radiochemical detection (Pihlavisto & Reenilä, 2002). Often the use of radiochemical assays for COMT is uncommon due to concerns and restrictions associated with radioactive material (Pihlavisto & Reenilä, 2002).

- Electrochemical detection: COMT HPLC assays may also make use of electrochemical detection since the catechols of the substrates and phenolic hydroxyls of the *O*-methylated products are susceptible to oxidation (Pihlavisto & Reenilä, 2002). Reenilä *et al*. (1995) quantitated vanillic acid and isovanillic acid, products of the methylation of dihydroxybenzoic acid, using reversed-phase HPLC with coulometric detection. A dual-cell coulometric system was used, which contained an oxidative conditioning cell and an analytical cell. Both oxidative and reductive electrodes were used to detect the reaction products (Reenilä *et al*., 1995).

- Fluorescence detection: *O*-Methylated compounds exhibiting native fluorescence themselves can directly be analysed with fluorescence detection

(Pihlavisto & Reenilä, 2002). Aoyama *et al.* (2005) reported an improved HPLC assay with fluorescence detection, using NE as a natural substrate. With this method the inhibition potencies of COMT inhibitors may be measured. This assay can analyse one sample in 5 min (Aoyama *et al.*, 2005). This is made possible by avoiding time consuming pretreatments, and injecting the enzymatic reaction solution directly into the HPLC system (Aoyama *et al.*, 2005). NE was incubated with COMT and the test inhibitor and the formation of NMN quantified with HPLC fluorescence detection (Aoyama *et al.*, 2005). Decreased formation of normetanepinephrine indicates successful inhibition of COMT activity.

2.2.9 *In vivo* measures of COMT

Extracellular levels of various neurotransmitters and their metabolites can be measured by making use of microdialysis techniques and are used extensively (Männistö & Kaakkola, 1999). Fujii *et al*. (2004) implanted dialyses probes into the skeletal muscle of anesthetised rabbits to monitor catecholamines and their metabolites in the dialysate. For this study, they determined the catecholamine concentrations by HPLC analysis. They administered entacapone and found a decrease in the formation of 3-methoxy-4-hydroxyphenylglycol levels in the diasylate. This correlates with reduced skeletal muscle COMT activity (Fujii *et al*., 2004). Positron emission tomography (PET) studies are another approach and make use of 6-[^{18}F]-fluorodopa (6-FD), which is an analogue of levodopa (Kaakkola, 2000). 3-Methyl-6-[^{18}F]-fluorodopa (3-OMFD) formation is reduced when COMT is selectively inhibited. This reduction is accompanied by an increase in 6-FD levels in brain (Kaakkola, 2000). PET studies have been carried out in both animals and humans (Männistö & Kaakkola, 1999).

2.2.10 Conclusion

Parkinson's disease is a neurodegenerative disorder, resulting from the death of dopaminergic neurons in the basal ganglia of the brain. The metabolic precursor of dopamine, levodopa, still remains the most effective treatment for restoring central dopamine levels. By inhibiting the peripheral metabolism of levodopa, delivery to the

brain is improved. This can be achieved through the use of COMT inhibitors. Non-nitrocatechol COMT inhibitors have shown to possess better bioavailability and side-effect profiles than nitrocatechol COMT inhibitors like entacapone and tolcapone. In the following chapter, the 3-hydroxypyridin-4-one scaffold was selected for the design of novel COMT inhibitors, since the COMT inhibitory potential of this class has been illustrated. Such compounds may represent useful agents for the treatment of Parkinson's disease with improved safety profiles compared to nitrocatechol COMT inhibitors.

CHAPTER 3

SYNTHESIS AND CHARACTERISATION

3.1 INTRODUCTION

In order to discover non-nitrocatechol COMT inhibitors, a series consisting of ten 3-hydroxypyridin-4-one derivatives (Table 3.1) was synthesised. These structures were docked into the reported crystal structure of the COMT enzyme in a preliminary attempt to predict inhibition activity. SARs regarding both the size and rigidity of the nitrogen substituent were thus explored. Different structural aspects that were explored were simple aromatic and aliphatic substitution (JDB1, JDB10, and JDB11), chain elongation and increasing flexibility (JDB3, JDB4, JDB5, and JDB9), as well as halogen and methyl substitution of the side chain phenyl ring (JDB12, JDB13, and JDB14).

3.2 MOLECULAR DOCKING STUDIES

3.2.1 Cleaning and preparing the COMT protein for modelling

Discovery Studio 3.1 (Accelrys®) was used to carry out molecular docking studies to investigate the binding of the synthesised compounds to the S-COMT protein. The protein model was obtained from the Protein Data Bank (PDB code: 3BWM). After generating a protein report, the default 'prepare protein' option was used to prepare and clean the protein. Invalid residues were corrected and all crystal water molecules were deleted, except for HOH411, HOH441 and HOH458 present in the active site. These waters undergo hydrogen bonding with the crystallised co-factor SAMe. The protein was typed with the CHARMm forcefield and hydrogen atoms were subsequently added to the structure. The ionisation states of the ionisable residues were calculated at a physiological pH of 7.4. The structure was minimised using a fixed backbone constraint with a Generalised Born approximation with Molecular Volume (GBMV) as solvent model (50 000 steps). The protocol followed is illustrated in Figure 3.1.

Table 3.1: Synthesised 3-hydroxypyridin-4-one derivatives.

JDB1	*JDB3*	*JDB4*	*JDB5*
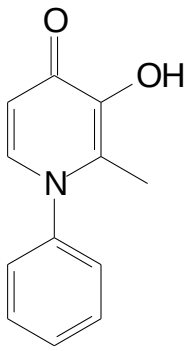	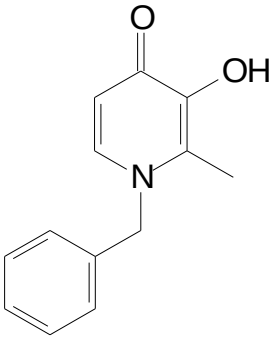	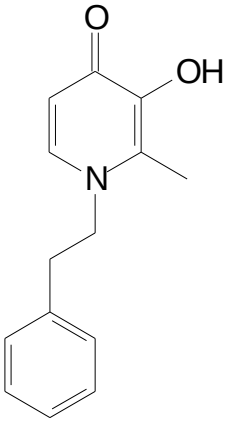	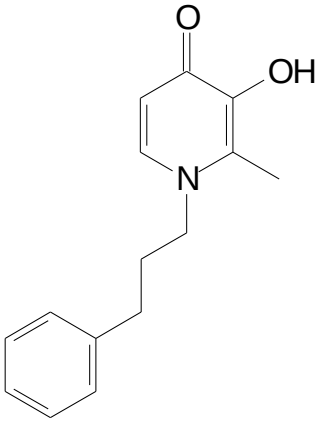
JDB9	*JDB10*	*JDB11*	*JDB12*
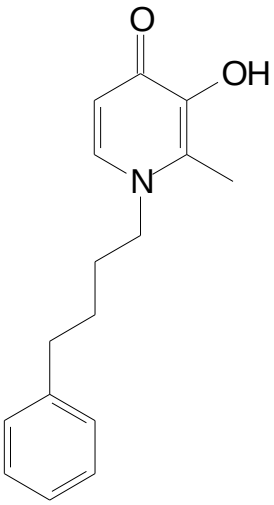	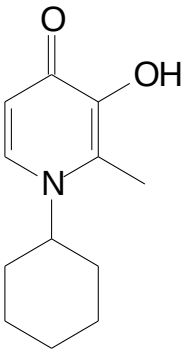	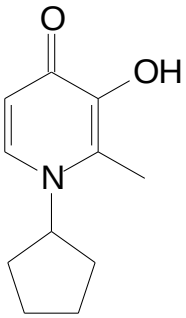	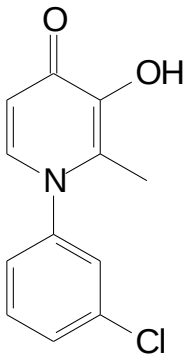
JDB13	*JDB14*		
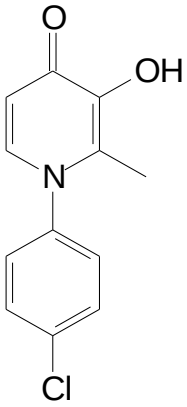	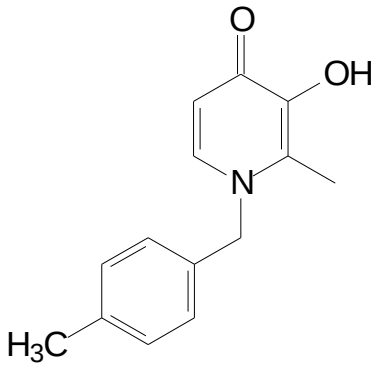		

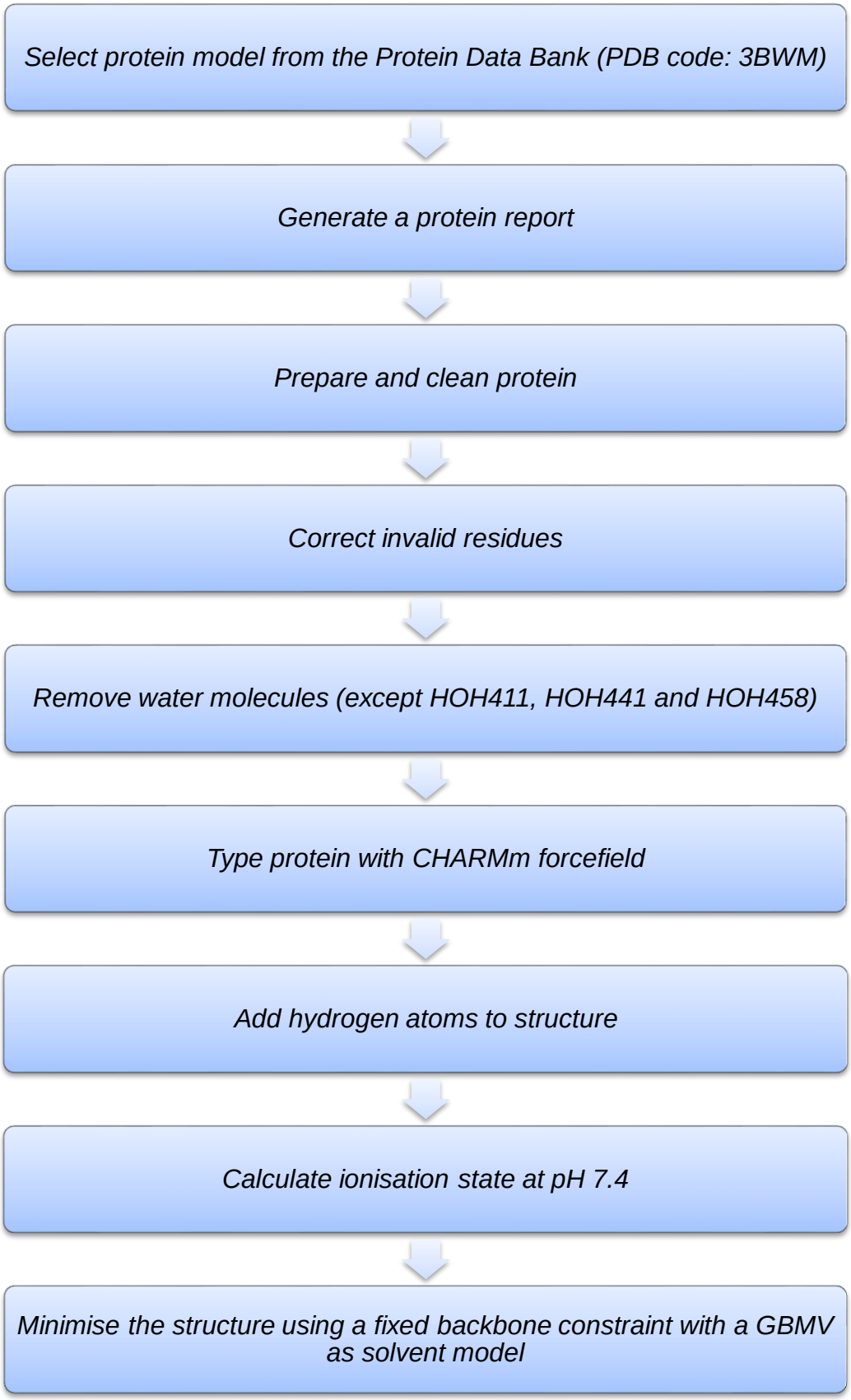

Figure 3.1: Protocol followed for cleaning and preparing the COMT protein for modelling.

3.2.2 Molecular docking

Structures of the 3-hydroxypyridin-4-one ligands (Table 3.1) were drawn in ChemWindow 6.0, transferred to the Discovery Studio 3.1 environment and prepared using the 'prepare ligands' function. The prepared ligands were then docked using the CDOCKER algorithm. Ten random ligand conformations were generated with the heating target temperature set to 700 K in full potential mode. The pose of each compound with the most favourable CDOCKER interaction was selected on which *in situ* minimisation was performed. Finally, binding energies were calculated for the minimised poses.

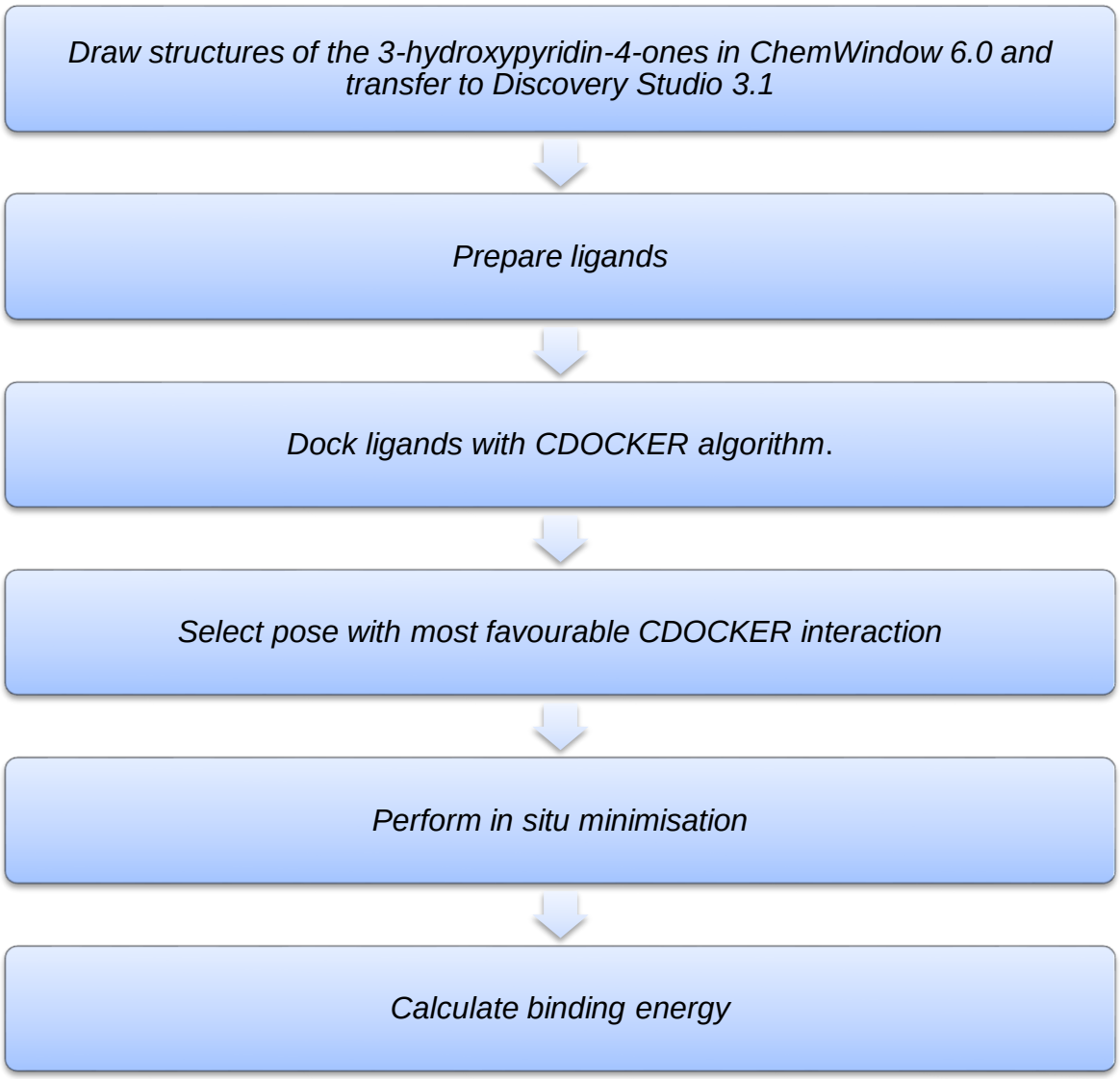

Figure 3.2: Protocol followed for molecular docking.

3.2.2.1 Results

To validate the docking protocol, 3,5-DNC, the co-crystallised ligand located in the binding site, was redocked into the binding site using the CDOCKER protocol (Figure 3.2). The root-mean-square deviation (RMSD) between the orientations of the docked and crystallised ligands was calculated. A RMSD value (for all atoms) of 0.42 Å was obtained, which may be regarded as an acceptable value.

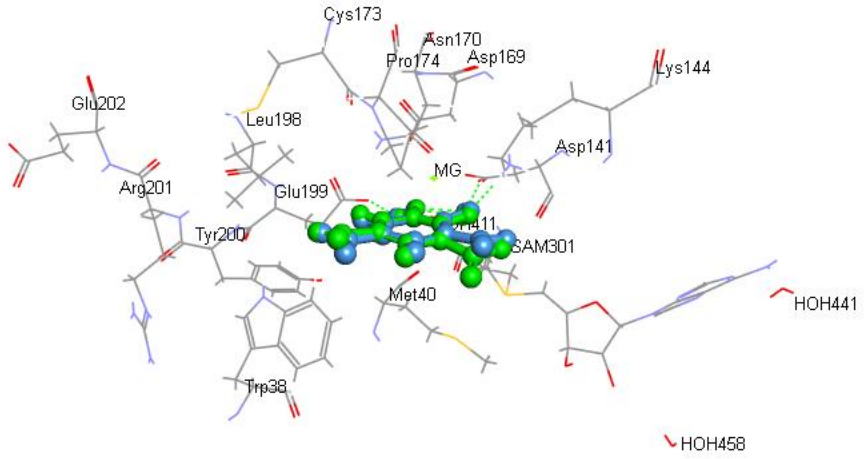

Figure 3.3: 3,5-DNC (in green) crystallised in the catechol-binding site, superimposed on 3,5-DNC docked into the binding site (in light blue). The green lines represent hydrogen bond interactions.

Docking was also successful with the proposed 3-hydroxypyridin-4-one derivatives (Table 3.1), indicating that these compounds would fit into the catechol binding site of COMT. The catechol binding site of COMT presents as a shallow cleft on the protein surface (Rutherford *et al*., 2008). It is defined by Met40, Leu198, Tyr200 as well as the "gatekeeper" residues Trp38 and Pro174, which ensures the correct orientation of the substrate for methylation (Rutherford *et al*., 2008). Mg^{2+}, which is a co-factor for the methylation reaction, is octahedral coordinated to the side chains of Asp141 and Asp169, Asn170, the two hydroxyl groups of the catechol substrate, and a water molecule trans to Asn170 (Rutherford *et al*., 2008). 3,5-DNC undergoes hydrogen bonding with Glu199, Asp141 and Lys144 in the shallow catechol binding site (Figure 3.3). As expected all ligands (Table 3.1) docked with the 3-hydroxypyridin-4-one moiety of the molecule orientated towards the magnesium ion located in this site. In most cases, hydrogen bonding occurs between the 3-hydroxyl group and Glu199 (Figure 3.4 – 3.6), except for JDB5, where the 3-hydroxyl group forms hydrogen bonds

with both Lys144 and Asp141 (Figure 3.6). The side chains of the different compounds are mostly solvent-exposed and have minimum interaction with the binding site. Interestingly for some of the phenyl derivatives, such as JDB3, JDB4 and JDB14, π-interactions were observed between the phenyl ring and either Trp143 or Lys144 (Figure 3.5 – 3.6).

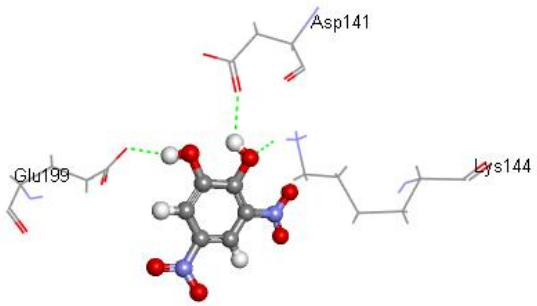

Figure 3.4: Hydrogen bonding interactions (green lines) with 3,5-DNC in the catechol-binding site.

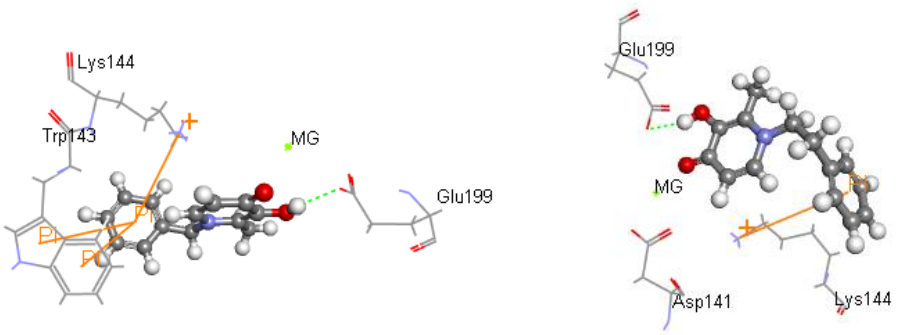

Figure 3.5: Compounds JDB3 (left) and JDB4 (right) docked within the catechol-binding site, undergoing hydrogen bonding (green lines) with Glu199 and π-stacking (orange lines) with Lys144 and/or Trp143.

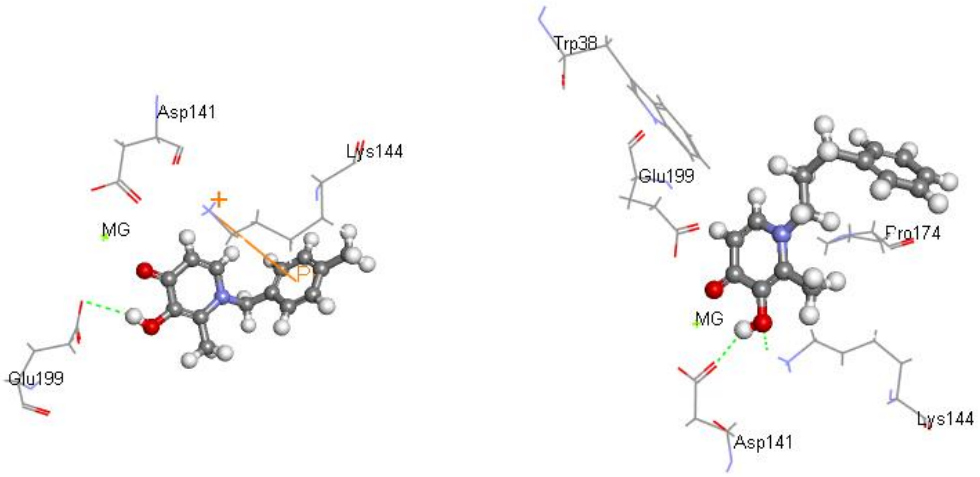

Figure 3.6: Compounds JDB14 (left) and JDB5 (right) docked within the catechol-binding site, undergoing hydrogen bonding (green lines) with Glu199 (JDB14), and with Asp141 and Lys144 (JDB5). JDB 14 undergoes π-stacking (orange line) with Lys144.

3.2.2.2 IC_{50} values versus CDOCKER interaction energies

The CDOCKER interaction energies of the docked ligands are given in Table 3.2. Also provided are the corresponding IC_{50} values (Chapter 5). The correlation between the interaction energies and IC_{50} values are provided in Figure 3.7. JDB4 had the most favourable CDOCKER interaction energy of -32.15 kcal/mol which compared well with 3,5-DNC (-33.05 kcal/mol). As previously stated, the phenyl ring of this compound undergoes a π-interaction with Lys144. This may have contributed to the more favourable CDOCKER interaction energy, improving the stability of the compound in the binding site. π-Interactions have also been observed for JDB3 and JDB14 (Figure 3.5 and 3.6). According to the IC_{50} values obtained for these compounds, the CDOCKER interaction energy for JDB4 (IC_{50} 15.0 μM) does not correlate well with the measured IC_{50} value as this compound proved to be among the weaker COMT inhibitors of the series. In contrast, the favourable CDOCKER energies of JDB3 (IC_{50} 4.55 μM) and JDB14 (IC_{50} 5.76 μM) correlates better with the finding that these compounds are among the more potent COMT inhibitors of the series. The results of the inhibition studies further show that JDB9 is a moderately potent inhibitor with an IC_{50} value of 9.05 μM. Since JDB9 possesses the least favourable CDOCKER interaction energy of the series (-22.32 kcal/mol), the modelling results and findings of

the inhibition studies also do not correlate well for this compound. This discrepancy is well illustrated by the fact that JDB9 is an outlier on the scatter plot (Figure 3.7). Considering that CDOCKER interaction energies of the remaining 3-hydroxypyridin-4-one derivatives were in a close range, it would have been difficult to predict that JDB5 and JDB11 would display the least favourable inhibition potencies. Thus a definite recognisable trend between CDOCKER interaction energies and IC_{50} values could not be established, but did give a slight indication that JDB3 and JDB14 would display better inhibition activity.

Table 3.2: The CDOCKER interaction energies and measured IC_{50} values of the proposed 3-hydroxypyridin-4-one derivatives.

Compound	*CDOCKER Interaction Energies (kcal/mol)*	*COMT inhibition IC_{50} (µM)*
3,5-DNC	-33.0450	*
JDB4	-32.1538	14.98
JDB3	-31.4834	4.55
JDB14	-31.2112	5.76
JDB10	-30.6102	12.19
JDB12	-30.2285	11.17
JDB5	-29.6636	18.37
JDB11	-29.4026	19.79
JDB13	-28.7331	9.31
JDB1	-28.3698	10.93
JDB9	-22.3199	9.05

**IC_{50} value not determined with the method of Aoyama et al. (2005).*

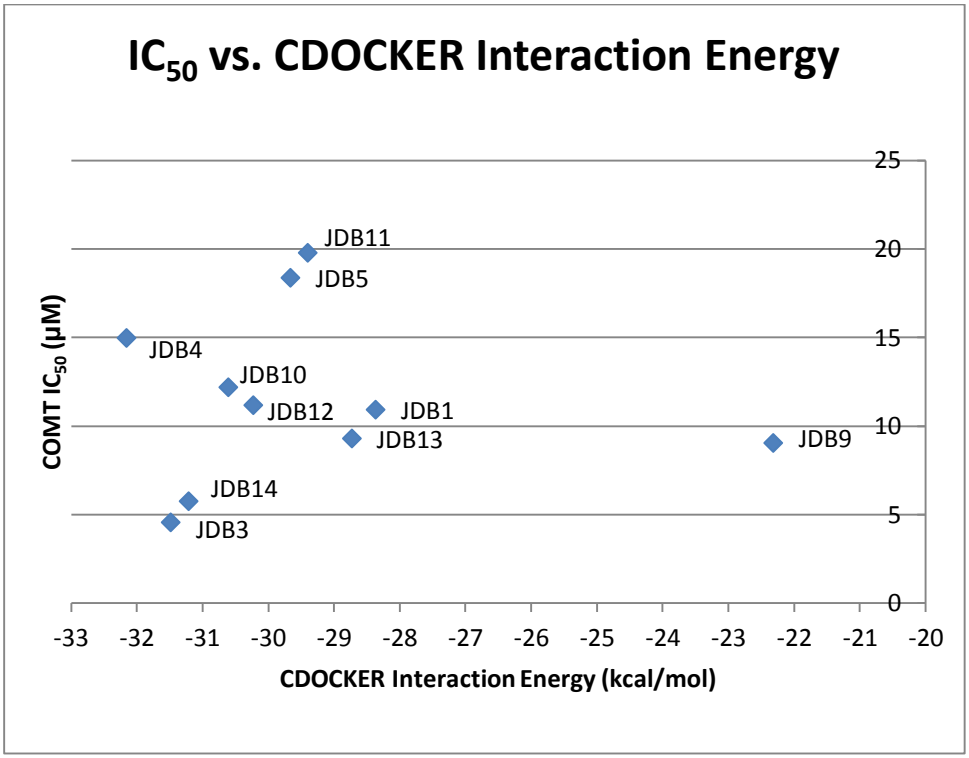

Figure 3.7: IC_{50} values versus CDOCKER interaction energies of the synthesised 3-hydroxypyridin-4-one derivatives.

3.2.2.3 IC_{50} values versus binding energies

The calculated binding energies of the docked ligands are given in Table 3.3 and are correlated with the corresponding IC_{50} values in Figure 3.8. The relatively weak binding energy of JDB5 (30.31 kcal/mol) correlates with the finding that it exhibits lower inhibition activity considering that it has an IC_{50} value of 18.37 µM. In contrast, JDB11 possesses a more favourable binding energy (-24.61 kcal/mol) but exhibits the highest IC_{50} (19.79 µM) value of the series. Although JDB3 and JDB14 displays better inhibition potencies, it could not have been predicted with their calculated binding energies of -20.82 kcal/mol and -17.87 kcal/mol, respectively. Considering that binding energies of the remaining 3-hydroxypyridin-4-one derivatives were in a close range, and JDB5 as an outlier, no definite correlations could be established between IC_{50} values and the respective binding energies.

Table 3.3: The binding energies and measured IC_{50} values of the proposed 3-hydroxypyridin-4-one derivatives.

Compound	*Binding Energies (kcal/mol)*	*COMT inhibition IC_{50} (µM)*
3,5-DNC	-28.5226	*
JDB11	-24.6114	19.79
JDB10	-22.8473	12.19
JDB4	-22.7214	14.98
JDB13	-22.1555	9.31
JDB1	-21.5958	10.93
JDB3	-20.8178	4.55
JDB12	-18.1209	11.17
JDB14	-17.8689	5.76
JDB9	-7.36277	9.05
JDB5	30.3111	18.37

IC_{50} value not determined with the method of Aoyama et al. (2005).

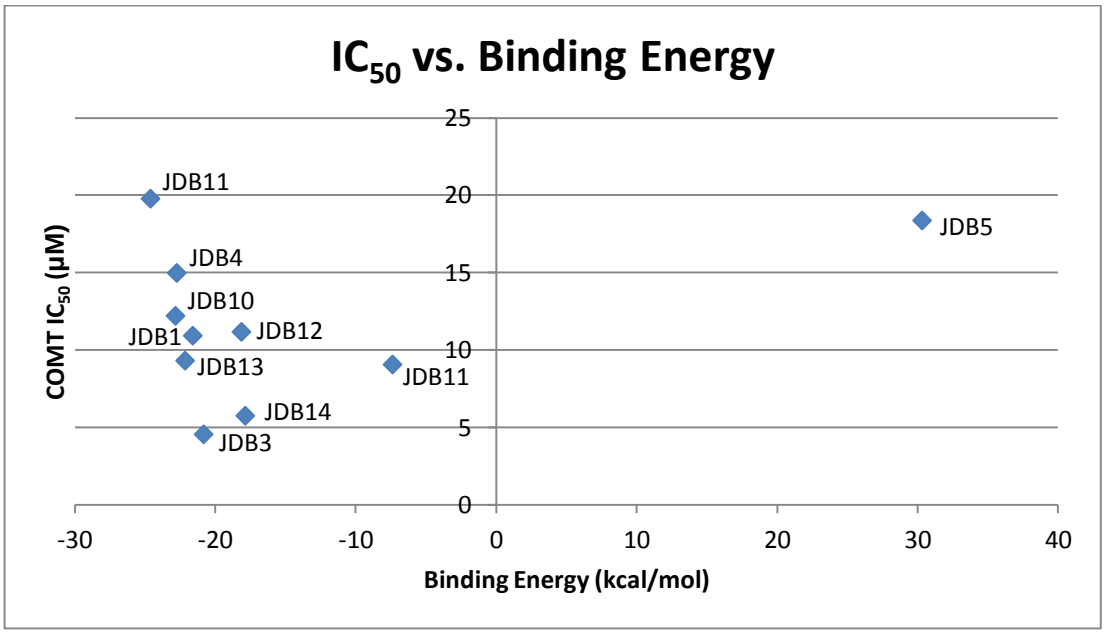

Figure 3.8: IC_{50} values vs. binding energies of the synthesised 3-hydroxypyridin-4-one derivatives.

3.3 SYNTHESIS

3.3.1 General approach for the synthesis of the 3-hydroxypyridin-4-one derivatives

The compounds of interest (Table 3.1) were synthesised by using a modification of the literature procedure described by Fassihi *et al*. (2009). In this protocol maltol is heated under reflux with a suitable primary amine in an acidic environment with ethanol serving as solvent (Figure 3.9) (Fassihi *et al*., 2009). After completion of the reaction [as judged by TLC], the crude product is collected by filtration and purified by recrystallisation from hot methanol. Target compounds are characterised by ^{1}H-NMR (proton nuclear magnetic resonance) spectroscopy, ^{13}C-NMR (carbon nuclear magnetic resonance) spectroscopy, infrared (IR) spectroscopy and MS, and purities are estimated by HPLC analysis.

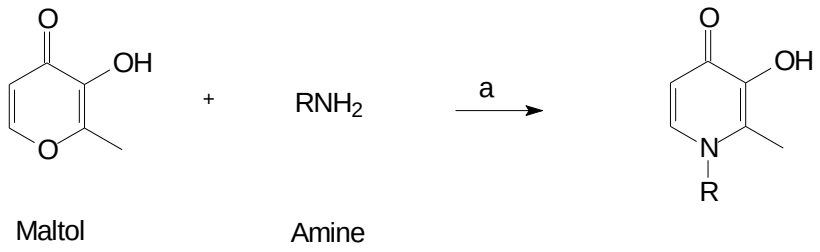

Figure 3.9: General synthetic route for the preparation 3-hydroxypyridin-4-one derivatives *via* a single step synthetic pathway. (a) HCl, H_2O, ethanol, 72 h, 110 °C (Fassihi *et al*., 2009).

3.3.2 Materials and instrumentation

3.3.2.1 Materials

The required reagents and solvents were obtained from Sigma-Aldrich and Rochelle, respectively, and were used without any further purification. Deuterated solvents for NMR spectroscopy were purchased from Merck.

3.3.2.2 Thin layer chromatography (TLC)

TLC is the method that was used to monitor the progress of the reactions and to determine whether the reactions were complete. The reagents and products were dissolved in methanol, applied to silica gel 60 aluminium coated TLC sheets (Merck) and developed in an appropriate mobile phase. The mobile phase that was used to monitor compounds JDB1, JDB3, JDB12 and JDB13 was ethyl acetate. A mixture of methanol and ethyl acetate (9:1) was used as mobile phase to monitor the synthesis of compounds JDB4, JDB5, JDB9, JDB10, JDB11 and JDB14. The developed TLC sheets were visualised under an UV-lamp at a wavelength of 254 nm.

3.3.2.3 Melting point (mp)

To determine the mps (melting points) of the synthesised compounds, a Büchi B-545 mp apparatus was used and the mps are uncorrected.

3.3.2.4 IR spectroscopy

IR spectra were obtained for each synthesised compound using an Alpha Bruker Fourier Transform Infrared (FT-IR) spectrometer. Opus 7.0.129 software was used to process and record IR data, reporting absorption bands in cm^{-1}.

3.3.2.5 Mass spectrometry (MS)

A Bruker micrOTOF-Q II mass spectrometer functioning in atmospheric-pressure chemical ionisation (APCI) mode was used to record high resolution mass spectra (HRMS).

3.3.2.6 Nuclear magnetic resonance (NMR) spectroscopy

A Bruker Avance III 600 spectrometer was used to record proton (^{1}H) and carbon (^{13}C) NMR spectra at 600 MHz and 150 MHz, respectively. Deuterated dimethylsulfoxide (DMSO-*d6* or DMSO) was used to dissolve the synthesised compounds. To process and analyse the NMR data obtained, MestReNova2 was used. Data reported included

integration (e.g. 1H), multiplicity and coupling constants (*J*) given in hertz (Hz). Chemical shifts (δ), in parts per million (ppm), were referenced to the residual solvent (DMSO-*d6*) signal at 2.5 ppm for ^{1}H NMR and 39.5 ppm for ^{13}C NMR. Spin multiplicities were presented as s (singlet), br s (broad singlet), d (doublet), br d (broad doublet), ddd (doublet of doublet of doublets), t (triplet), br t (broad triplet), p (pentet) or m (multiplet).

3.3.2.7 High-performance liquid chromatography (HPLC)

HPLC analyses were performed to estimate the purities of the synthesised compounds. These were conducted with an Agilent 1100 HPLC system equipped with a quaternary pump and an Agilent 1100 series diode array detector. HPLC grade acetonitrile (Merck) and Milli-Q water (Millipore) were used for the preparation of the mobile phase. A Venusil XBP C18 column (4.60 x 150 mm, 5 µm) was used as analytical column. Initially, the mobile phase consisted of 30% acetonitrile and 70% Milli-Q water and the flow rate was set to 1 ml/min. A solvent gradient program was initiated at the beginning of each HPLC run. This was done by linearly increasing the composition of the acetonitrile in the mobile phase to 85% acetonitrile over a 5 min period. HPLC runs lasted 15 min and a 5 min period was allowed for equilibration of the system. The test compounds were dissolved in acetonitrile to a concentration of 1 mM and 20 µl of these solutions were injected into the HPLC system. The eluent was monitored at a wavelength of 254 nm.

3.3.3 Synthesis of 3-hydroxypyridin-4-one derivatives

3.3.3.1 General procedure for the synthesis of 3-hydroxypyridin-4-one derivatives JDB1, JDB3, JDB4, JDB5, JDB9, JDB12, JDB13, JDB14:

The synthesis of the 3-hydroxypyridin-4-one derivatives was achieved in a single step synthetic pathway and is based on a modification of the procedure reported by Fassihi *et al*. (2009). Commercially available maltol (20 mmol, 2.52 g, 1 equiv.) was heated under reflux at 110 °C with a suitable primary amine (30 mmol, 1.5 equiv.) in the presence of HCl (32%, 0.8 ml), water (36 ml) and ethanol (4 ml) for 72 h. By monitoring the progress of the reaction with TLC, it was determined if it was necessary to add

another 10 mmol (0.5 equiv.) of the primary amine to complete the reaction. After reflux was completed, dark oily residues were allowed to separate to the bottom of the round-bottom flask (Figure 3.10). While still hot, the light yellow clear solution was decanted from the oily residue. The clear solution was covered and incubated overnight at room temperature. A white solid precipitated from the solution. The precipitate was collected by filtration the following morning and allowed to air dry overnight. Recrystallisation from hot methanol gave a white crystalline solid (Figure 3.11).

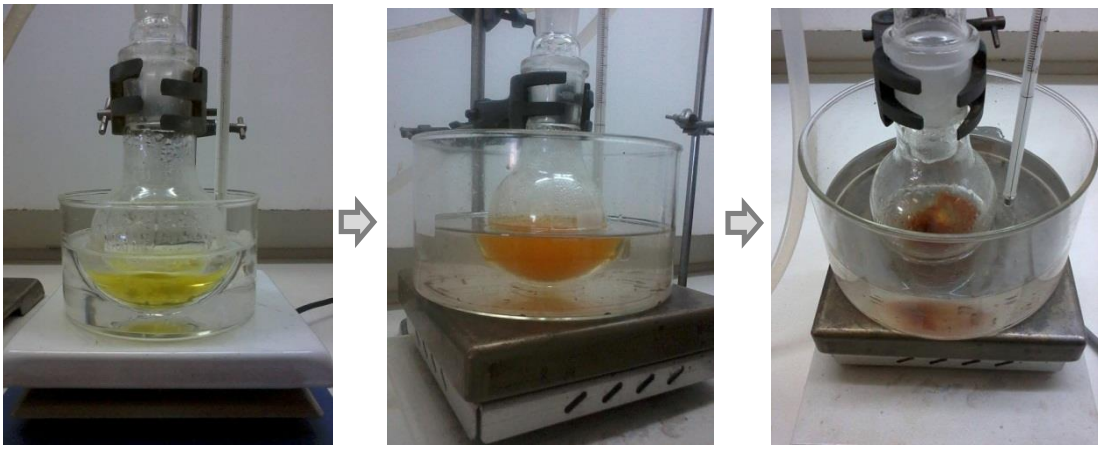

Figure 3.10: Colour change and formation of oily impurities during synthesis of 3-hydroxypyridin-4-ones: JDB1, JDB3, JDB4, JDB5, JDB9, JDB12, JDB13, and JDB14.

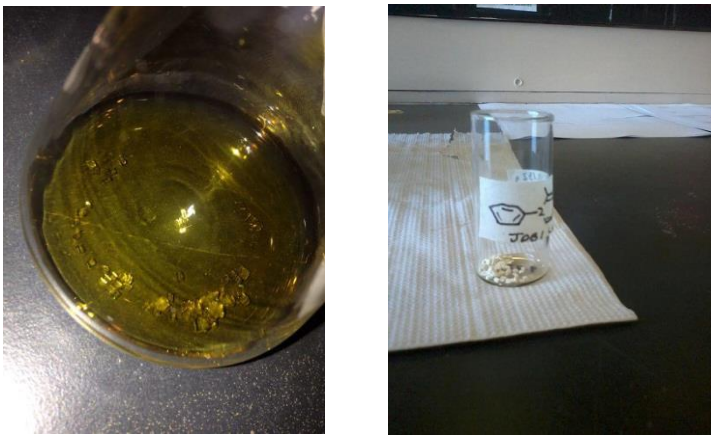

Figure 3.11: Recrystallisation of JDB1 from hot methanol and collected crystals after filtration.

3.3.3.2 Synthesis of compounds JDB10 and JDB11

The synthesis of JDB10 and JDB11 follows the same general procedure as described for the 3-hydroxypyridin-4-one derivatives above, but differs in the work-up procedure. After reflux was completed, the reactions did not yield dark oily residues, and no precipitate was obtained after cooling of the reactions. Instead, the resulting reaction mixture remained a clear red-orange solution (Figure 3.12). After cold distilled water (1 x 20 ml for JDB10; 2 x 10 ml for JDB11) was added to the reaction, it was extracted to ethyl acetate (1 x 20 ml for JDB10; 2 x 30 ml for JDB11). The combined organic layers were dried over anhydrous magnesium sulphate, filtered and the solvent was removed by rotary evaporation. The crude product was then allowed to air dry to yield a red powder that was purified with silica gel column chromatography (methanol:ethyl acetate, 9:1).

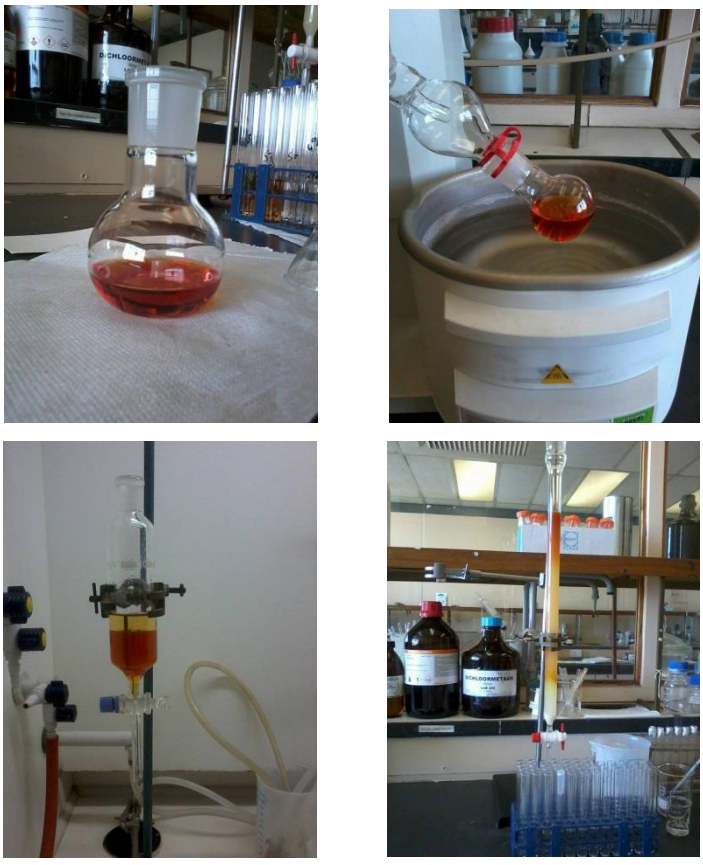

Figure 3.12: Clear red-orange solution obtained during the synthesis of JDB10 and JDB11 which were subjected to rotary evaporation, extraction and silica gel column chromatography.

3.3.4 Results and discussion

3.3.4.1 Mass spectrometry (MS)

Characterisation of the synthesised compounds was done by determining their experimental masses via MS (found) and comparing them to their corresponding calculated masses (Table 3.3) (Appendix A.3). The relative small differences between the experimental and calculated masses indicated that the structures of the synthesised 3-hydroxypyridin-4-ones correspond to the proposed structures in Table 3.4.

(3.1) Formula to determine parts per million (ppm):

$$ppm = \left[\frac{(found - calculated.)}{calculated}\right] \times 1\,000\,000$$

Table 3.4: The calculated and experimentally determined masses of the synthesised 3-hydroxypyridin-4-one derivatives.

Compound	*Calculated**	*Found**	*Formula*	*ppm*
JDB1	202.0863	202.0854	$C_{12}H_{12}NO_2$	-4.5
JDB3	216.1019	216.1003	$C_{13}H_{14}NO_2$	-7.4
JDB4	230.1176	230.1186	$C_{14}H_{16}NO_2$	4.3
JDB5	244.1332	244.1331	$C_{15}H_{18}NO_2$	-0.4
JDB9	258.1489	258.1481	$C_{16}H_{20}NO_2$	-3.1
JDB10	208.1332	208.1344	$C_{12}H_{18}NO_2$	5.8
JDB11	194.1176	194.1174	$C_{11}H_{16}NO_2$	-1.0
JDB12	236.0473	236.0446	$C_{12}H_{11}ClNO_2$	-11.4
JDB13	236.0473	236.0465	$C_{12}H_{11}ClNO_2$	-3.4
JDB14	230.1176	230.1166	$C_{14}H_{16}NO_2$	-4.3

**All masses are given as M+H*

3.3.4.2 IR spectroscopy

The IR spectra (Appendix A.2) recorded for all of the synthesised compounds were interpreted based on comparison with previous literature IR spectra obtained reported by Fox and Taylor (1999) and Fassihi *et al.* (2009). Only selected functional groups of the 3-hydroxypyridin-4-one moiety will be discussed: The broad OH absorption band was mainly detected at 3047 – 3204 cm^{-1} for all compounds. The carbonyl absorption band of the 3-hydroxypyridin-4-one moiety was observed at 1619 – 1627 cm^{-1}. C=C bands were present at 1558 – 1582 cm^{-1} and the C-N band at 1212 – 1245 cm^{-1}. These stretching vibrations are consistent with the structures of the synthesised compounds and confirm the presence of the 3-hydroxypyridin-4-one moiety in each compound.

3.3.4.3 NMR spectroscopy

Structures were confirmed using ^{1}H-NMR, ^{13}C-NMR, DEPT90 and DEPT135 (DEPT: distortionless enhancement by polarization transfer) spectra obtained for each synthesised compound. Two-dimensional (2-D) spectroscopic data were obtained and include ^{1}H-^{1}H correlation spectroscopy (COSY), heteronuclear single-quantum correlation spectroscopy (HSQC) and heteronuclear multi-bond correlation spectroscopy (HMBC) data. Assignments of NMR signals were based on analysis of 1-D spectra in conjunction with the 2-D spectra (COSY, HSQC and HMBC) of these compounds (Appendix A.1).

For all of the synthesised compounds, structure characteristics of the 3-hydroxypyridin-4-one moiety were evident in both the ^{1}H NMR and ^{13}C NMR spectra. Proton signals of the ^{1}H NMR spectra were assigned based on the chemical shifts, integration, coupling constant values, multiplicities of signals and comparison with COSY data. Assignment of carbon signals were achieved by analysing chemical shifts and interpreting selected HSQC and HMBC spectroscopic data. Assigning quaternary carbons was supported by comparing ^{13}C NMR signals with their corresponding DEPT spectra.

The assignments of compound JDB3 will be discussed as an example:

^{1}H NMR

- The doublet at 7.75 ppm which integrates for 1 proton was assigned as H-6. The assignment was based on a coupling constant of 7.3 Hz, correlating with the coupling constant of H-5 (7.2 Hz); a COSY correlation with H-5; and HMBC correlations with C-1′′, C-2, C-3, C-4, C-5 and the methyl carbon, C-2.
- The aromatic protons, H-3′ and H-5′ correspond to the broad triplet at 7.37 ppm, integrating for 2 protons. HMBC correlations were observed with C-1′, C-2′/6′ and C-4′.
- The multiplet at 7.27–7.33 ppm, which integrates for 1 proton, corresponds to the aromatic H-4′ signal. A HMBC correlation was observed with C-2′/6′.
- The broad doublet at 7.06 ppm, integrating for 2 protons, was assigned as the aromatic protons, H-2′ and H-6′. This was confirmed with HMBC correlations with C-4′ and C-1′′ (which was used to distinguish between H-2′/H-6′ and H-3′/H-5′).
- The doublet at 6.21 ppm integrating for 1 proton was assigned as H-5. This was confirmed by the coupling constant of 7.2 Hz, correlating with the coupling constant of H-6 (7.3 Hz); a COSY correlation with H-6; as well as HMBC correlations with C-4, C-3 and C-6.
- The aliphatic CH_2 (H-1′′) is represented by the singlet at 5.25 ppm integrating for 2 protons. This was confirmed with a HSQC correlation observed with the carbon at 56.0 ppm, which was identified as a CH_2 on the DEPT135 spectrum.
- The methyl substituent at C-2 corresponds to the singlet at 2.12 ppm, integrating for 3 protons. This was confirmed with a HSQC correlation observed with the carbon at 11.6 ppm, which was identified as a CH_3 using the DEPT135 spectrum in conjunction with the DEPT90 spectrum.

^{13}C NMR

- The most downfield signal at 169.3 ppm was identified as the carbonyl carbon, C-4. This assignment was based on the shift, and the fact that this signal was not present in the DEPT90 and DEPT135 spectra. HMBC correlations were observed with H-6.

- Remaining quaternary carbons: These signals were not present in the DEPT90 and DEPT135 spectra. The more downfield signal at 145.8 ppm was assigned as C-3, since this carbon is adjacent to the more electron withdrawing hydroxy group. HMBC correlations observed with the methyl group at C-2, as well as H-5 further supported this assignment. The signal at 129.1 ppm was thus assigned as C-2 as HMBC correlations were observed with H-6 and H-1′′. Since the signal at 137.1 ppm showed HMBC correlations with H2′/6′ and H-1′′ it was assigned as C-1′.
- Assignment of CH carbons: The signal at 138.6 ppm was assigned as C-6 since a HSQC correlation was observed with H-6 (δ_H 7.75 ppm). HMBC correlations were further observed with H-5 and H-1′′. Similarly the signal at 110.9 ppm was assigned as C-5, as it has a HSQC correlation to H-5 (δ_H 6.21 ppm). A HMBC correlation was also observed with H-6. The signals at 126.1, 127.7 and 129.0 were assigned as C-2′/6′, C-4′ and C-3′/5′ respectively, based *inter alia* on the HSQC correlations to their respective protons.
- The aliphatic CH_2, C-1′′, is represented by the signal at 56.0 ppm and was easily identifiable on the DEPT135 spectrum. The methyl substituent at C-2 corresponds to the signal at 11.6 ppm, showing an HSQC correlation to the methyl singlet at δ_H 2.12 ppm.

Since the structures of all compounds are related, a detailed discussion will not be provided, but the HMBC assignments of substituents are tabulated in Table 3.5.

Table 3.5: HMBC assignments of the synthesised 3-hydroxypyridin-4-ones.

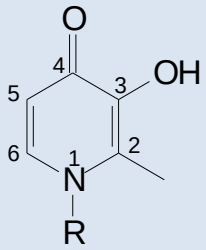

R	Atom no.	δ_H (multiplicity, *J* in Hz)	δ_C (Type)	HMBC (δ_H to δ_C)
JDB1 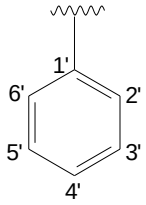	2′/6′	7.43 – 7.48 (m)	127.0 (CH)	1′, 3′/5′
	3′/5′, 4′	7.50 – 7.60 (m)	129.7 (CH), 129.1 (CH)	1′, 4′, 2′/6′, 3′/5′
	1′		141.6 (C)	2′/6′, 3′/5, 4′, 6
JDB3 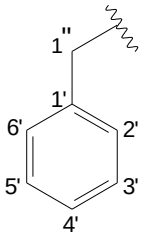	1′′	5.25 (s)	56.0 (CH_2)	6
	2′/6′	7.06 (br d, 7.0 Hz)	126.1 (CH)	1′′, 4′
	4′	7.33 – 7.27 (m)	127.7 (CH)	2′/6′
	3′/5′	7.37 (br t, 7.6 Hz)	129.0 (CH)	2′/6′, 4′, 1′
	1′		137.1 (C)	2′/6′, 1′′
JDB4 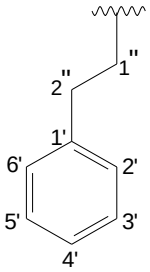	1′′	4.14 (t, 7.5 Hz)	53.9 (CH_2)	2′′, 2′/6′, 6 or 1′
	2′′	2.95 (t, 7.5 Hz)	36.3 (CH_2)	1′′, 2′/6′, 6 or 1′
	2′/6′, 4′	7.26 – 7.17 (m)	126.7 (CH) / 128.5 (CH), 126.7 (CH-4′)	2′′, 3′/5′, 4′
	3′/5′	7.29 (br t, 7.3 Hz)	128.5 (CH)	2′/6′, 1′
	1′		137.46 (C)	1′′, 2′′

JDB5 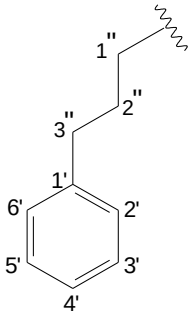	1′′	3.94 (t, 7.4 Hz)	52.4 (CH_2)	6, 2′′, 3′′
	2′′, 3′′	1.94 (p, 7.8 Hz), 2.60 (t, 7.8 Hz)	31.8 (CH_2)	1′′, 2′′, 3′′, 2′/6′
	2′/6′, 4′	7.25 – 7.16 (m)	128.4 (CH) / 128.2 (CH), 126.0 (CH-4′)	4′, 2′/6′, 3′/5′, 2′′, 3′′
	3′/5′	7.31 – 7.25 (m)	128.4 (CH) / 128.2 (CH)	2′/6′, 1′
	1′		140.8 (C)	2′′, 3′′
JDB9 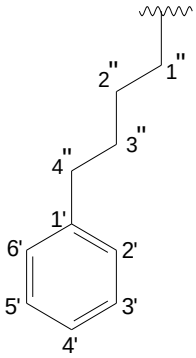	1′′	3.94 (t, 7.3 Hz)	52.7 (CH_2)	2′′, 3′′, 2, 6
	2′′	1.68 – 1.50 (m)	29.8 (CH_2)	1′′, 3′′
	3′′	1.68 – 1.50 (m)	27.7 (CH_2)	2′′, 4′′
	4′′	2.59 (t, 7.6 Hz)	34.6 (CH_2)	1′, 2′/6′, 3′′
	2′/6′,	7.21 – 7.14 (m)	128.32(CH) / 128.28 (CH)	3′/5′, 4′, 4′′
	4′	7.21 – 7.14 (m)	125.8 (CH)	2′/6′
	3′/5′	7.30 – 7.24 (m)	128.32(CH) / 128.28 (CH)	1′, 2′/6′
	1′		141.8 (C)	4′′, 3′/5′
JDB10 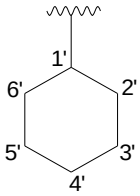	2′/6′	2.09 – 0.74 (m)	32.5 (CH_2)	*
	4′	2.09 – 0.74 (m)	24.6 (CH_2)	*
	3′/5′	2.09 – 0.74 (m)	25.3 (CH_2)	*
	1′	4.02 (br s)	59.0 (CH)	*
JDB11	1′	4.61 (br s)	60.9 (CH)	*
	2′/5′	2.46 – 1.28 (m)	32.5 (CH_2)	*

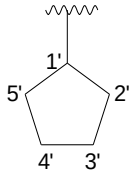	3′/4′	2.46 – 1.28 (m)	23.7 (CH_2)	*
JDB12 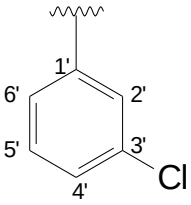	2′	7.68 (br t, 2.0 Hz)	127.3	1′, 3′
	5′ and 6′	7.64 – 7.55 (m)	129.4 (CH-5′), 131.2 (CH-6′)	5′, 3′, 1′
	4′	7.46 (ddd, 7.7, 2.1, 1.2 Hz)	126.2 (CH)	1′, 5′
	3′		133.8 (C)	5′ and 6′
	1′		142.7 (C)	6, 5′ and 6′, 2′, 4′
JDB13 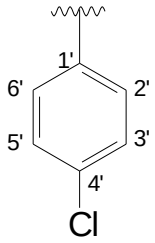	2′/6′	δ 7.63 (d, 8.7 Hz) / 7.51 (d, 8.7 Hz)	129.7 / 129.1 (CH)	1′, 4′, 3′/5′
	4′		133.7 (C)	3′/5′, 2′/6′
	3′/5′	δ 7.63 (d, 8.7 Hz) / 7.51 (d, 8.7 Hz)	129.7 (CH) / 129.1 (CH)	4′, 1′, 2′/6′
	1′		140.4 (C)	2′/6′, 3′/5′, 6
JDB14 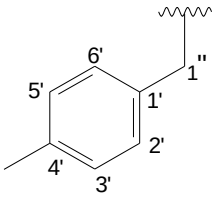	1′′	5.19 (s)	55.8 (CH_2)	6, 1′, 2′/6′
	2′/6′	6.96 (d, 7.9 Hz)	126.1 (CH)	1′′, 4′
	4′		134.0 (C)	CH_3 (benzyl), 2′/6′,
	3′/5′	7.18 (d, 7.8)	129.5 (CH)	CH_3 (benzyl), 2′/6′, 1′
	1′		137.0 (C)	1′′, 2′/6′
	CH_3	2.27 (s)	20.7 (CH_3)	4′, 3′/5′

**HMBC signals unclear. Refer to Appendix A.1.*

3.3.4.4 Structures of the synthesised 3-hydroxypyridin-4-ones

3.3.4.4.1 JDB1: 3-Hydroxy-2-methyl-1-phenylpyridin-4-one

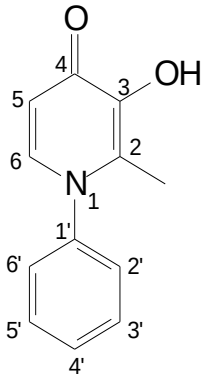

JDB1 was prepared from maltol and aniline in a yield of 6.56% (132 mg): mp 223.3 – 223.9 °C (methanol) (lit. Fassihi *et al*., 2009, 221 – 222 °C), white crystals. ^{1}H NMR (600 MHz, DMSO-*d6*) δ 7.60 – 7.50 (m, 4H, H-6, H-3′/5′, H-4′), 7.48 – 7.43 (m, 2H, H-2′/6′), 6.22 (d, *J* = 7.3 Hz, 1H, H-5), 1.96 (s, 3H, C<u>H</u>$_3$). ^{13}C NMR (151 MHz, DMSO-*d6*) δ 169.7 (C-4), 145.1 (C-3), 141.6 (C-1′), 137.9 (C-6), 129.7 (C-3′/5′), 129.1 (C-4′), 128.8 (C-2), 127.0 (C-2′/6′), 111.0 (C-5), 13.4 (<u>C</u>H$_3$). APCI-HRMS *m/z*: calcd for $C_{12}H_{11}NO_2$ (MH^+), 201.0790, found 202.0854; Purity (HPLC): 99% (254 nm). FT-IR *v*/cm^{-1}: 3197 (broad OH), 1626 (C=O), 1578 (C=C), 1235 (C-N).

3.3.4.4.2 JDB3: 1-Benzyl-3-hydroxy-2-methylpyridin-4-one

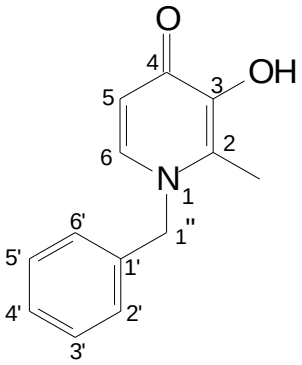

JDB3 was prepared from maltol and benzylamine in a yield of 4.88% (105 mg): mp 205.6 – 207.1 °C (methanol), white crystals. ^{1}H NMR (600 MHz, DMSO-*d6*) δ 7.75 (d, J = 7.3 Hz, 1H, H-6), 7.37 (br t, J = 7.6 Hz, 2H, H-3′/5′), 7.33 – 7.27 (m, 1H, H-4′), 7.06 (br d, J = 7.0 Hz, 2H, H-2′/6′), 6.21 (d, J = 7.2 Hz, 1H, H-5), 5.25 (s, 2H, H-1′′), 2.12 (s, 3H, C<u>H</u>$_3$). ^{13}C NMR (151 MHz, DMSO-*d6*) δ 169.3 (C-4), 145.8 (C-3), 138.6 (C-6), 137.1 (C-1′), 129.1 (C-2), 129.0 (C-3′/5′), 127.7 (C-4′), 126.1 (C-2′/6′), 110.9 (C-5),

56.0 (C-1′′), 11.6 (<u>C</u>H_3). APCI-HRMS *m/z*: calcd for $C_{13}H_{13}NO_2$ (MH^+), 215.0946, found 216.1003; Purity (HPLC): 99% (254 nm). FT-IR *v*/cm^{-1}: 3175 (broad OH), 1626 (C=O), 1574 (C=C), 1234 (C-N).

3.3.4.4.3 JDB4: 3-Hydroxy-2-methyl-1-(2-phenylethyl)pyridin-4-one

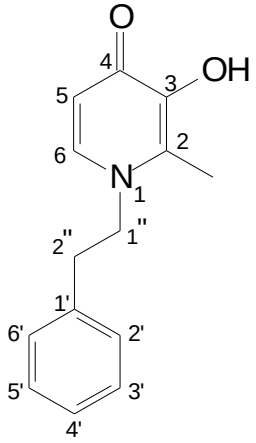

JDB4 was prepared from maltol and 2-phenyl-1-ethylamine in a yield of 6.42% (147 mg): mp 159.4 – 160.8 °C (methanol), white crystals. ^{1}H NMR (600 MHz, DMSO-*d6*) δ 7.45 (d, J = 7.3 Hz, 1H, H-6), 7.29 (br t, J = 7.3 Hz, 2H, H3′/5′), 7.26 – 7.17 (m, 3H, H-2′/6′, H-4′), 6.06 (d, J = 7.2 Hz, 1H, H-5), 4.14 (t, J = 7.5 Hz, 2H, H-1′′), 2.95 (t, J = 7.5 Hz, 2H, H-2′′), 2.25 (s, 3H, C<u>H</u>$_3$). ^{13}C NMR (151 MHz, DMSO-*d6*) δ 168.9 (C-4), 145.4 (C-3), 137.52 (C-6), 137.46 (C-1′), 129.0 (C-2′/6′ or C-3′/5′), 128.7 (C-2), 128.5 (C-2′/6′ or C-3′/5′), 126.7 (C-4′), 110.6 (C-5), 53.9 (C-1′′), 36.3 (C-2′′), 11.3 (<u>C</u>H_3). APCI-HRMS *m/z*: calcd for $C_{14}H_{15}NO_2$ (MH^+), 229.1102, found 230.1186; Purity (HPLC): 99% (254 nm). FT-IR *v*/cm^{-1}: 3188 (broad OH), 1625 (C=O), 1558 (C=C), 1231 (C-N).

3.3.4.4.4 JDB5: 3-Hydroxy-2-methyl-1-(3-phenylpropyl)pyridin-4-one

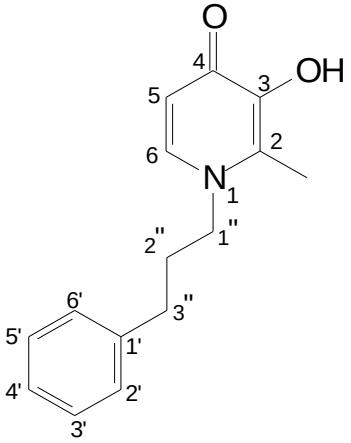

JDB5 was prepared from maltol and 3-phenyl-1-propylamine in a yield of 12.92% (294 mg): mp 157.2 – 159.3 °C (methanol), white crystals. ^{1}H NMR (600 MHz, DMSO-*d6*) δ 7.57 (d, *J* = 7.3 Hz, 1H, H-6), 7.31 – 7.25 (m, 2H, H-3′/5′), 7.25 – 7.16 (m, 3H, H-2′/6′, H-4′), 6.13 (d, *J* = 7.2 Hz, 1H, H-5), 3.94 (t, *J* = 7.4 Hz, 2H, H-1′′), 2.60 (t, *J* = 7.8 Hz, 2H, H-3′′), 2.23 (s, 3H, C<u>H</u>$_3$), 1.94 (p, *J* = 7.8 Hz, 2H, H-2′′). ^{13}C NMR (151 MHz, DMSO-*d6*) δ 168.9 (C-4), 145.5 (C-3), 140.8 (C-1′), 137.5 (C-6), 128.6 (C-2), 128.4 (C-2′/6′ or C-3′/5′), 128.2 (C-2′/6′ or C-3′/5′), 126.0 (C-4′), 110.7 (C-5), 52.4 (C-1′′), 31.8 (C-2′′, C-3′′), 11.3 (<u>C</u>H$_3$). APCI-HRMS *m/z*: calcd for $C_{15}H_{17}NO_2$ (MH^+), 243.1259, found 244.1331; Purity (HPLC): 99% (254 nm). FT-IR *v*/cm^{-1}: 3118 (broad OH), 1624 (C=O), 1572 (C=C), 1219 (C-N).

3.3.4.4.5 JDB9: 3-Hydroxy-2-methyl-1-(4-phenylbutyl)pyridin-4-one

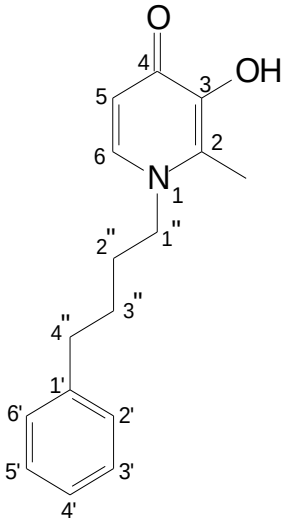

JDB9 was prepared from maltol and 4-phenyl-1-butylamine in a yield of 4.90% (126 mg): mp 171.6 – 173.7 °C (methanol), white crystals. ^{1}H NMR (600 MHz, DMSO-*d6*) δ 7.55 (d, *J* = 7.3 Hz, 1H, H-6), 7.30 – 7.24 (m, 2H, H-3′/5′), 7.21 – 7.14 (m, 3H, H-2′/H-6′, H-4′), 6.09 (d, *J* = 7.2 Hz, 1H, H-5), 3.94 (t, *J* = 7.3 Hz, 2H, H-1′′), 2.59 (t, *J* = 7.6 Hz, 2H, H-4′′), 2.25 (s, 3H, C<u>H</u>$_3$), 1.68 – 1.50 (m, 4H, H-2′′, H-3′′). ^{13}C NMR (151 MHz, DMSO-*d6*) δ 168.8 (C-4), 145.5 (C-3), 141.8 (C-1′), 137.6 (C-6), 128.5 (C-2), 128.32 (C-2′/6′ or C-3′/5′), 128.28 (C-2′/6′ or C-3′/5′), 125.8 (C-4′), 110.5 (C-5), 52.7 (C-1′′), 34.6 (C-4′′), 29.8 (C-2′′ or C-3′′), 27.7 (C-2′′ or C-3′′), 11.3 (<u>C</u>H$_3$). APCI-HRMS *m/z*: calcd for $C_{16}H_{19}NO_2$ (MH^+), 257.1416, found 258.1481; Purity (HPLC): 98% (254 nm). FT-IR *v*/cm^{-1}: 3079 (broad OH), 1626 (C=O), 1567 (C=C), 1223 (C-N).

3.3.4.4.6 JDB10: 1-Cyclohexyl-3-hydroxy-2-methylpyridin-4-one

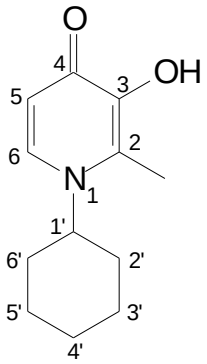

JDB10 was prepared from maltol and cyclohexylamine in a yield of 6.86% (142 mg): mp 191.6 – 202.8 °C (methanol), red solid. ^{1}H NMR (600 MHz, DMSO-*d6*) δ 7.67 (br s, 1H, H-6), 6.15 (br s, 1H, H-5), 4.02 (br s, 1H, H-1′), 2.32 (s, 3H, C$\underline{H}_3$), 2.09 – 0.74 (m, 10H, H-2′/6′, H-3′/5′, H-4′). ^{13}C NMR (151 MHz, DMSO-*d6*) δ 168.6 (C-4), 145.3 (C-3), 133.3 (C-6), 128.8 (C-2), 110.8 (C-5), 59.0 (C-1′), 32.5 (C-2′/6′), 25.3 (C-3′/5′), 24.6 (C-4′), 11.3 (C$\underline{H}_3$). APCI-HRMS *m/z*: calcd for $C_{12}H_{17}NO_2$ (MH^+), 207.1259, found 208.1344; Purity (HPLC): 92% (254 nm). FT-IR *v*/cm^{-1}: 3081 (broad OH), 1619 (C=O), 1566 (C=C), 1216 (C-N).

3.3.4.4.7 JDB11: 1-Cyclopentyl-3-hydroxy-2-methylpyridin-4-one

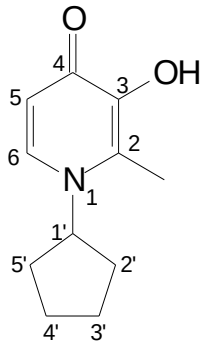

JDB11 was prepared from maltol and cyclopentylamine in a yield of 8.39% (162 mg): mp 51.4 – 51.5 °C (methanol), red solid. ^{1}H NMR (600 MHz, DMSO-*d6*) δ 7.62 (br s, 1H, H-6), 6.17 (br s, 1H, H-5), 4.61 (br s, 1H, H-1′), 2.46 – 1.28 (m, 11H, H-2′/5′, H-3′/4′, C$\underline{H}_3$). ^{13}C NMR (151 MHz, DMSO-*d6*) δ 168.7 (C-4), 145.4 (C-3), 133.1 (C-6), 129.3 (C-2), 111.1 (C-5), 60.9 (C-1′), 32.5 (C-2′/5′), 23.7 (C-3′/4′), 11.7 (C$\underline{H}_3$). APCI-HRMS *m/z*: calcd for $C_{11}H_{15}NO_2$ (MH^+), 193.1103, found 194.1174; Purity (HPLC): 91% (254 nm). FT-IR *v*/cm^{-1}: 3078 (broad OH), 1621 (C=O), 1562 (C=C), 1212 (C-N).

3.3.4.4.8 JDB12: 1-(3-Chlorophenyl)-3-hydroxy-2-methylpyridin-4-one

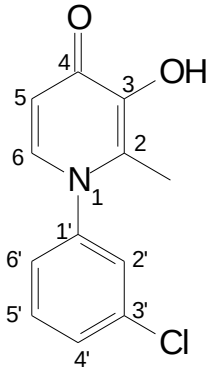

JDB12 was prepared from maltol and 3-chloroaniline in a yield of 5.06% (119 mg): mp 185.6 – 186.2 °C (methanol), white solid. ^{1}H NMR (600 MHz, DMSO-*d6*) δ 7.68 (br t, *J* = 2.0 Hz, 1H, H-2′), 7.64 – 7.55 (m, 3H, H-6′, H-5′, H-6), 7.46 (ddd, *J* = 7.7, 2.1, 1.2 Hz, 1H, H-4′), 6.23 (d, *J* = 7.3 Hz, 1H, H-5), 1.97 (s, 3H, C$\underline{H}_3$). ^{13}C NMR (151 MHz, DMSO-*d6*) δ 169.8 (C-4), 145.1 (C-3), 142.7 (C-1′), 137.9 (C-6), 133.8 (C-3′), 131.2 (C-6′), 129.4 (C-5′), 128.9 (C-2), 127.3 (C-2′), 126.2 (C-4′), 111.2 (C-5), 13.4 ($\underline{C}H_3$). APCI-HRMS *m/z*: calcd for $C_{12}H_{10}ClNO_2$ (MH^+), 235.0400, found 236.0446; Purity (HPLC): 94% (254 nm). FT-IR *v*/cm^{-1}: 3057 (broad OH), 1627 (C=O), 1561 (C=C), 1245 (C-N).

3.3.4.4.9 JDB13: 1-(4-Chlorophenyl)-3-hydroxy-2-methylpyridin-4-one

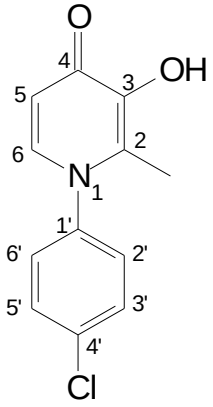

JDB13 was prepared from maltol and 4-chloroaniline in a yield of 5.09% (120 mg): mp 298.1 – 298.4 °C (methanol), white solid. ^{1}H NMR (600 MHz, DMSO-*d6*) δ 7.63 (d, *J* = 8.7 Hz, 2H, H-2′/6′ or H-3′/5′), 7.55 (d, *J* = 7.3 Hz, 1H, H-6), 7.51 (d, *J* = 8.7 Hz, 2H, H-2′/6′ or H-3′/5′), 6.22 (d, *J* = 7.3 Hz, 1H, H-5), 1.96 (s, 3H, C$\underline{H}_3$). ^{13}C NMR (151 MHz, DMSO-*d6*) δ 169.8 (C-4), 145.1 (C-3), 140.4 (C-1′), 137.9 (C-6), 133.7 (C-4′), 129.7 (C-2′/6′ or C-3′/5′), 129.1 (C-2′/6′ or C-3′/5′), 128.7 (C-2), 111.1 (C-5), 13.4 ($\underline{C}H_3$). APCI-HRMS *m/z*: calcd for $C_{12}H_{10}ClNO_2$ (MH^+), 235.0400, found

236.0465; Purity (HPLC): 90% (254 nm). FT-IR *v*/cm^{-1}: 3047 (broad OH), 1622 (C=O), 1582 (C=C), 1233 (C-N).

3.3.4.4.10 JDB14: 3-Hydroxy-2-methyl-1-(4-methylbenzyl)pyridin-4-one

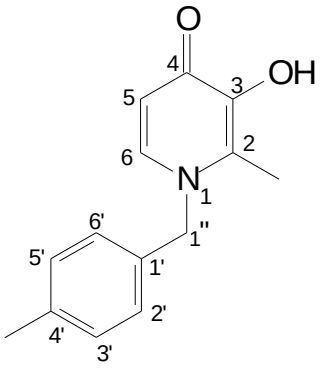

JDB14 was prepared from maltol and 4-methylbenzylamine in a yield of 7.68% (176 mg): mp 213.7 – 226.0 °C (methanol), white solid. ^{1}H NMR (600 MHz, DMSO-*d6*) δ 7.73 (d, *J* = 7.3 Hz, 1H, H-6), 7.18 (d, *J* = 7.8 Hz, 2H, H-3′/5′), 6.96 (d, *J* = 7.9 Hz, 2H, H-2′/6′), 6.19 (d, *J* = 7.2 Hz, 1H, H-5), 5.19 (s, 2H, H-1′′), 2.27 (s, 3H, C$\underline{H}_3$ benzyl), 2.12 (s, 3H, C$\underline{H}_3$ pyridone). ^{13}C NMR (151 MHz, DMSO-*d6*) δ 169.2 (C-4), 145.8 (C-3), 138.5 (C-6), 137.0 (C-1′), 134.0 (C-4′), 129.5 (C-3′/5′), 129.0 (C-2), 126.1 (C-2′/6′), 110.8 (C-5), 55.8 (C-1′′), 20.7 (C$\underline{H}_3$ benzyl), 11.6 (C$\underline{H}_3$ pyridone). APCI-HRMS *m/z*: calcd for $C_{14}H_{15}NO_2$ (MH^+), 229.1103, found 230.1166; Purity (HPLC): 93% (254 nm). FT-IR *v*/cm^{-1}: 3203 (broad OH), 1627 (C=O), 1576 (C=C), 1239 (C-N).

3.3.4.5 HPLC analyses and purity estimation

HPLC analyses were used to estimate the purities of the 3-hydroxypyridin-4-one derivatives (Appendix A.4). For these analyses a reversed phase column was used and the derivatives were eluted with 30% acetonitrile that linearly increased to 85%. The eluent was monitored at a wavelength of 254 nm. This wavelength is commonly used to detect the UV light absorption of organic analytes and impurities. Purity estimations were based on the integrated surface areas of each peak present on the chromatogram. Single peaks indicated a high level of purity and where additional peaks occurred, the percentage purity was calculated. Table 3.6 lists the purities of the synthesised compounds, which ranged between 90–99%. These values may be

regarded as acceptable purities. The chromatograms of each of the synthesised 3-hydroxypyridin-4-one derivatives are given in Appendix A.

Table 3.6: HPLC purities of the synthesised 3-hydroxypyridin-4-ones.

Compound	*HPLC Purity (%)*
JDB1	99
JDB3	99
JDB4	99
JDB5	99
JDB9	98
JDB10	92
JDB11	91
JDB12	94
JDB13	90
JDB14	93

3.3.5 Conclusion

In this chapter, the synthesis and characterisation of ten 3-hydroxypyridin-4-one derivatives were described. The proposed derivatives were firstly docked into the COMT enzyme's binding site by making use of molecular modelling software. All the derivatives fitted within the catechol binding site of COMT and formed productive interactions with the residues of the enzyme. The proposed 3-hydroxypyridin-4-one derivatives were successfully synthesised by reacting maltol and a suitable primary amine. Characterisation of the synthesised compounds was carried out by NMR spectroscopy, IR spectroscopy and MS. The NMR, IR and MS data corresponded well with the proposed structures. The purities of the synthesised compounds were determined by HPLC analyses and determining their melting points. The results showed that the estimated purities are at least 90%. The purities of the 3-hydroxypyridin-4-one derivatives are thus acceptable for these compounds to be subjected to biological evaluation experiments. In the next chapter, the 3-hydroxypyridin-4-one derivatives will be evaluated as potential COMT inhibitors.

CHAPTER 4

VALIDATION OF THE CHROMATOGRAPHIC ASSAY OF COMT ACTIVITY

4.1 INTRODUCTION

In this chapter a literature method for determining COMT activity will be validated. This is of importance since this protocol will be used to determine IC_{50} values for the inhibition of COMT by the synthesised 3-hydroxypyridin-4-ones (Chapter 3). The determination of IC_{50} values will thus be carried out *in vitro* and COMT activity will be measured by the method of Aoyama *et al*. (2005). This method measures the formation of NMN, the metabolite that forms when NE is *O*-methylated by COMT. The reaction for this biotransformation is illustrated in Figure 4.1. NMN will be quantified by reversed-phase HPLC separation with fluorescence detection. The principle of the IC_{50} determination is based on the fact that test inhibitors would decrease the formation of NMN. A typical enzyme reaction contains the substrate, NE, the cofactor SAMe, and the test inhibitors. The solvent for these reactions will be sodium phosphate buffer (pH 7.8) containing dithiothreitol and $MgCl_2$. After incubation for 60 min, the reactions will be terminated with the addition of perchloric acid. Following centrifugation, the supernatant fractions will be analysed by HPLC for NMN content. In this chapter the HPLC protocol for the measurement of NMN will be validated. A detailed description of the enzymatic reactions and IC_{50} determinations will be provided in the next chapter.

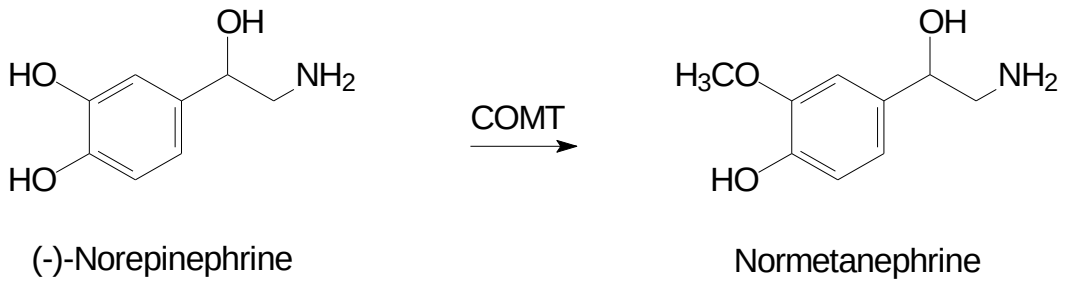

(-)-Norepinephrine Normetanephrine

Figure 4.1: *O*-Methylation of NE by COMT.

4.2 CHEMICALS AND INSTRUMENTATION

Table 4.1: Reagents and materials used for enzyme reactions and HPLC analyses.

Reagent	*Abbreviation / Formula*	*Molecular Weight (g/mol)*	*Supplier*
(-)-Norepinephrine	NE	319.26	Sigma-Aldrich
COMT purified from porcine liver (≥ 150 units/mg)	COMT		Sigma-Aldrich
Normetanephrine.HCl	NMN	145.16	Sigma-Aldrich
S-Adenosyl-L-methionine	SAMe	507.82	Sigma-Aldrich
Magnesium chloride	$MgCl_2$	95.21	Sigma-Aldrich
HPLC grade acetonitrile		41.05	Merck
Boric acid		61.83	Sigma-Aldrich
Sodium 1-hexanesulfonate monohydrate		206.24	Sigma-Aldrich
Dithiothreitol	DTT	154.25	Sigma-Aldrich
70% Perchloric acid	$HClO_4$	100.46	Sigma-Aldrich
Sodium dihydrogen orthophosphate dihydrate	$NaH_2PO_4.2H_2O$	156.01	Merck
Sodium phosphate dibasic	$Na_2HPO_4.2H_2O$	177.99	Sigma-Aldrich

4.2.1 Instrumentation and HPLC requirements

- An Agilent HP1100 HPLC system, equipped with a Shimadzu RF-551 fluorescence detector was used to perform HPLC analyses. An USP L1 Luna C18 column (250 x 4.6 mm, 5 µm) was used for chromatographic separation (Phenomenex, Torrance, CA).
- A mixture of an aqueous phase and an organic phase was used to prepare the mobile phase. The aqueous phase consisted of 10 mM sodium phosphate buffer (pH 7.0), 80 mM boric acid and 4 mM sodium 1-hexanesulfonate. The

organic phase consisted of acetonitrile and the aqueous and organic phases were mixed in a ratio of 85:15.

- The HPLC system was set to a flow rate of 1 ml/min with a sample injection volume of 20 µl. A retention time of ± 4.7 min was recorded for NMN and the stop time of each run was thus set to 7.0 min. Milli-Q water was used in all instances.
- Fluorescence detection was recorded at an excitation wavelength of 283 nm and an emission wavelength of 315 nm (response time 0.5; range x 1; low sensitivity).

4.3 METHOD VALIDATION

4.3.1 Linearity

By analysing a set of calibration standards containing known amounts of NMN, linear calibration curves were constructed. The calibration standards were analysed with every inhibition assay and served as reference to monitor any changes that the HPLC instrument may undergo from day to day. The calibration standards were made up to a final volume of 137.5 µl and contained known amounts of NMN (0, 1, 2, 5, 10 and 30 µM) dissolved in a 25 mM sodium phosphate buffer (pH 7.8). Perchloric acid (1 M; 12.5 µl) was added to each calibration standard. To prepare the calibration standards, the order of addition was first the buffer, then NMN and then perchloric acid. Calibration curves were constructed by graphing the peak area versus the known concentrations of NMN. A blank sample was also included in each series of calibration standards and consisted of 35 µl substrate (NE), 50 µl sodium phosphate buffer, 10 µl $MgCl_2$, 5 µl DMSO, 25 µl SAMe and 12.5 µl perchloric acid.

4.3.2 Precision and accuracy

Selected calibration standards were analysed to establish inter- and intra-day precision and accuracy. Inter-day precision and accuracy were determined by analysing solutions containing 5, 10 and 30 µM NMN once for three consecutive days. Intra-day precision and accuracy were determined by analysing solutions containing 10 and 50 µM NMN on a single day. For intra-day precision and accuracy each standard was analysed three times on the same day. Precision was assessed from the relative standard deviation (SD) from the mean of each selected calibration standard. Accuracy is reported as the percentages of the actual known concentrations of the selected calibration standards. The criteria for acceptability of the accuracy of the method are ±15% deviation from the actual concentration. The criteria for acceptability for the precision of the method should not exceed a coefficient of variation (CV) of 15%.

4.3.3 Stability

The stability of the calibration standard which contained 10 µM NMN was determined. The first sample injected served as reference point and was followed by reinjection of the same selected calibration standard every hour for a period of 12 h. The samples were incubated at room temperature during the 12 h time period by placing them in the auto-sampler tray. The mean ± SD of the analysed samples was reported with the first sample serving as reference point for determining the stability.

4.3.4 Repeatability

Two selected calibration standards (5 µM and 10 µM NMN) were injected into the HPLC system for six consecutive times to determine the repeatability of the method. The repeatability of each sample is reported as the mean ± SD of each calibration standard. A CV of 5% is regarded as an acceptable value for the repeatability of a method.

4.4 RESULTS

4.4.1 Linearity

Calibration curves were constructed for NMN and were evaluated by their correlation coefficients, R^2. For this purpose, two calibration curves were constructed, one for a lower concentration range (1–10 µM) and another for a higher concentration range (5–30 µM). Linearity was excellent over the respective calibration ranges, with correlation coefficients >0.99. The R^2 values of these curves are given in Table 4.2. An example of a chromatogram showing the peak of NMN (10 µM) is given in Figure 4.2. These data show that the linearity of detection of NMN is excellent and the protocol is thus acceptable when quantifying NMN for the determination of IC_{50} values.

Table 4.2: Linearity of detection of NMN.

	Range	*Equation*	*R^2*
Lower concentrations	1–10 µM	y = 245x + 51.8	0.9992
Higher concentrations	5–30 µM	y = 238x + 119.2	0.9999

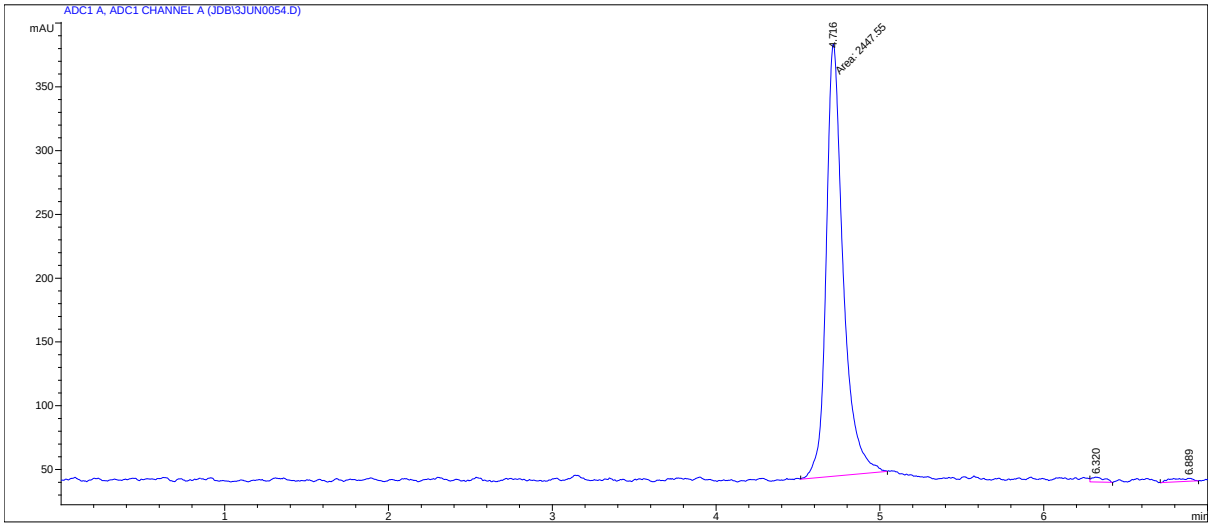

Figure 4.2: An example of the HPLC chromatogram for the analysis of a sample containing 10 µM NMN.

4.4.2 Precision and accuracy

The inter- and intra-day precision and accuracy of the selected calibration standards containing NMN are given in Tables 4.3 and 4.4. Inter-day precision was determined for three calibration standards (5, 10 and 30 µM) by injecting each standard once for three consecutive days, and intra-day precision was determined for two calibration standards (10 and 50 µM) by injecting each standard three times on the same day. The intra-day precision (%CV) for the measurement of NMN at both concentrations (10 µM and 50 µM) were below 9%, which is deemed to be acceptable. The intra-day accuracy at both concentrations was also within the acceptable range. The inter-day precision (%CV) for all three measured concentrations (5, 10 and 30 µM) was found to be ≤6.7% and the accuracies between 101.9% and 110.1%. These inter-day precision and accuracy values were within the acceptable range of 15% variation. These data show that samples containing NMN can be quantified with good precision and accuracy.

Table 4.3: Intra-day precision and accuracy of quantification of NMN.

NMN concentration (µM)	*Measured concentration (µM) ± SD*	*Precision (%CV)*	*Accuacy (% ± SD)*
10	10.3 ± 0.91	8.9	103.1 ± 9.1
50	48.6 ± 1.97	4.0	97.2 ± 3.9

Table 4.4: Inter-day precision and accuracy of quantification of NMN.

NMN concentration (µM)	*Measured concentration (µM) ± SD*	*Precision (%CV)*	*Accuacy (%) ± SD*
5	5.1 ± 0.34	6.7	101.9 ± 6.8
10	10.2 ± 0.68	6.7	101.9 ± 6.8
30	33.0 ± 1.67	5.1	110.1 ± 5.1

4.4.3 Stability and repeatability

The stability of the calibration standard which contained 10 µM NMN was determined (Table 4.5). This sample proved to be stable at room temperature over a period of 12 h. The mean of the measured concentrations over the 12 h period were within 97.9 ± 2.64% of the concentration measured at t = 0, with a CV of 2.70%. Repeatability was measured for the 5 µM and 10 µM NMN standards by analysing each standard six consecutive times on the same day (Table 4.6). The repeatability (%CV) was 2.92% and 2.07% for the 5 µM and 10 µM standards, respectively. These values are acceptable for the repeatability of a HPLC detection method (<5%).

Table 4.5: The percentage stability of 10 µM NMN stock solutions at room temperature.

Time (hrs)	*% Stability*
0	100.00
1	90.00
2	99.12
3	97.78
4	99.12
5	99.51
6	98.69
7	98.66
8	97.65
9	97.04
10	99.47
11	98.25
Mean	97.94
Deviation	2.64
%CV	2.70

Table 4.6: The repeatability of 5 µM and 10 µM NMN standards.

Injection	*Measured concentrations*	
	5 µM	*10 µM*
1	5.19	10.44
2	4.81	10.56
3	5.17	10.81
4	5.03	10.37
5	5.13	10.18
6	4.95	10.60
Mean	5.05	10.49
Deviation	0.15	0.22
%CV	2.92	2.07

4.5 THE DETECTION OF NMN IN THE PRESENCE OF NE

An important consideration is that NMN should be measurable in the presence of NE since, for the determination of IC_{50} values, NE will serve as substrate and will thus be present in the samples to be analysed. As mentioned, in the enzyme reactions, NE is *O*-methylated by COMT to yield NMN. The enzyme reactions will be terminated at 60 min after the addition of COMT, a time point at which relatively little NE has been converted to NMN. In Figure 4.3, the chromatogram shows that NMN (10 µM) is readily detectable in the presence of an excessive amount of NE (250 µM). As discussed later, NE at a concentration of 250 µM will be used for the enzyme reactions. Also shown is a typical chromatogram containing only NMN (Figure 4.4).

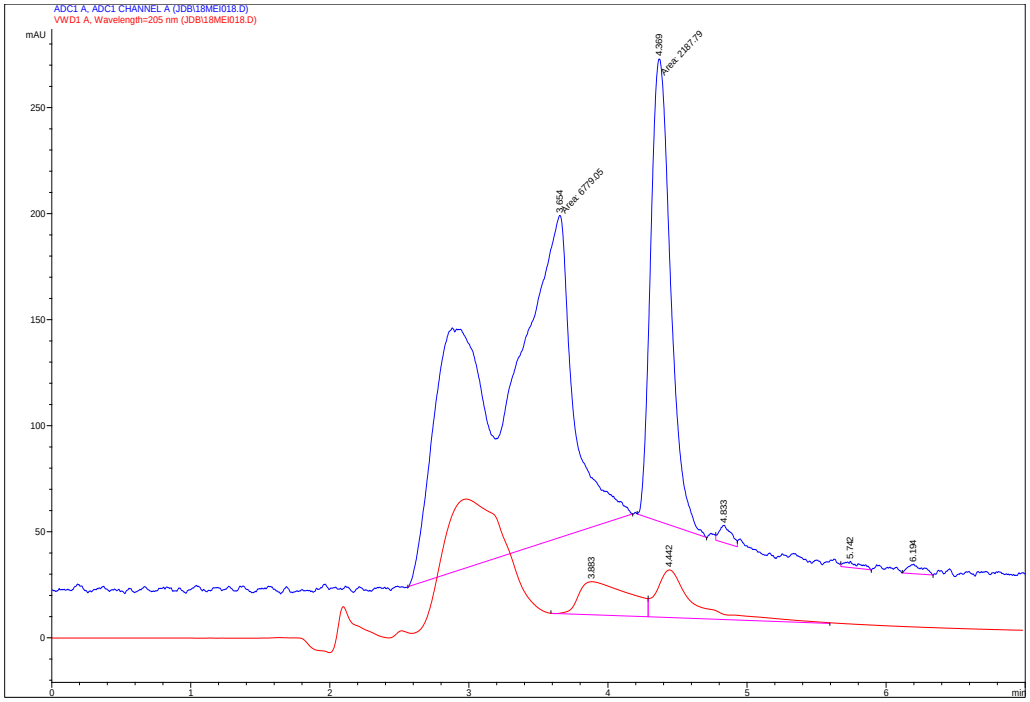

Figure 4.3: A chromatogram of the analysis of NMN (10 µM) in the presence of NE (250 µM) by HPLC with fluorescence detection (blue trace).

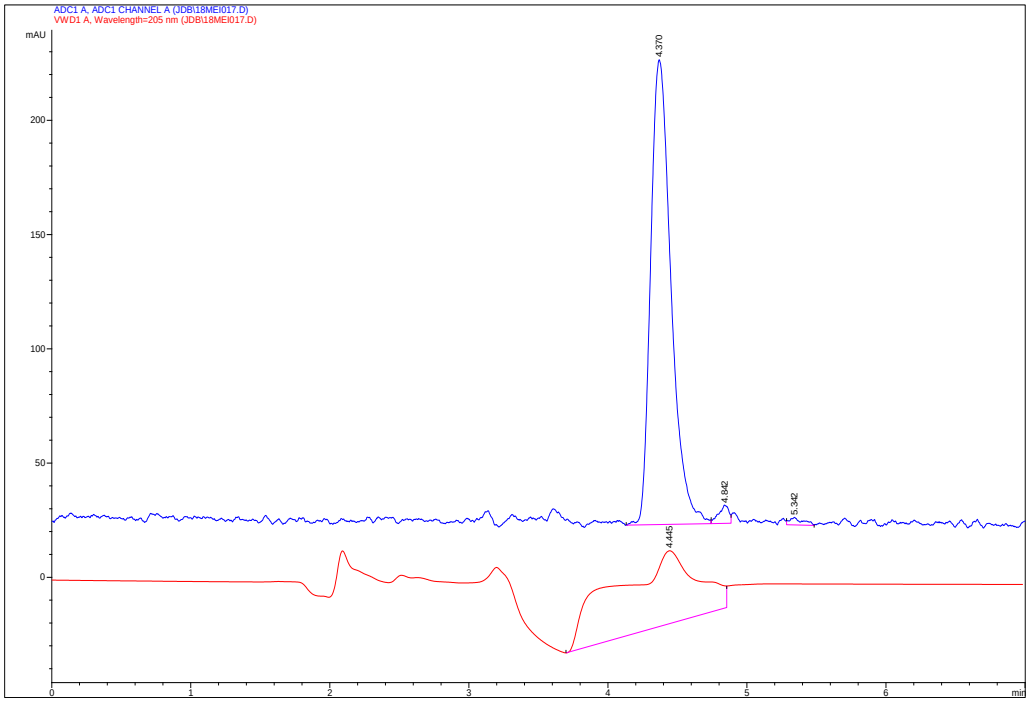

Figure 4.4: A chromatogram of the analysis of NMN (10 µM) by HPLC with fluorescence detection (blue trace).

4.6 THE DETERMINATION OF THE MICHAELIS CONSTANT, K_M

When determining IC_{50} values for the inhibition of a specific enzyme (such as COMT) the Michaelis constant (K_m) of the substrate to be used, should be known. K_m has the dimension of molar concentration and represents the substrate concentration [S] when the enzyme is functioning at exactly half the rate of maximal velocity (V_{max}). When [S] is approximately equal to K_m, the initial velocity of enzyme catalysis (V_i) is very responsive to changes in [S] and to the presence of an inhibitor. In contrast, when the enzyme is functioning at V_{max}, changes in V_i will not be readily observed when an inhibitor is present. Therefore, when determining IC_{50} values, [S] should be approximately equal to K_m. In the following section K_m for the metabolism of NE by COMT will be determined.

4.6.1 Method

The enzyme stock solution was prepared by dissolving the purified COMT (750 units/5 ml) in 20 ml of sodium phosphate buffer (pH 7.8) containing 0.5 mM dithiothreitol. Different concentrations of NE (Table 4.7) were used to determine the K_m value. Each enzyme reaction was prepared to a final volume of 137.5 µl and contained NE (at the various concentrations given in Table 4.7), 2 mM $MgCl_2$ (10 µl) and 200 µM SAMe (25 µl). Sodium phosphate buffer (25 mM) served as reaction solvent and the reactions were initiated with the addition of the COMT stock solution (50 µl). The order of addition was as follows: First the buffer was added followed by $MgCl_2$, NE and then SAMe. After the mixtures were pre-incubated at 37 °C in a water bath for at least 10 min, a 50 µl aliquot of the enzyme stock solution was added. The reactions were incubated for 60 min and subsequently terminated by adding 12.5 µl perchloric acid. The samples were centrifuged at 16 000 x g for 10 min and the supernatants were analysed by the validated HPLC method described earlier.

The peak areas of NMN formed in these enzyme reactions were recorded (Figure 4.5) and the corresponding concentrations of NMN formed were calculated using a calibration curve. The calibration curve was constructed by analysing known concentrations of NMN (1–5 µM). For this purpose, the calibration standards were prepared as described in the method validation section. Using the Prism 5 (GraphPad)

software package, the data were fitted to the Michaelis-Menten equation to obtain a plot of V_i versus [S]. From this fit, the K_m value was estimated.

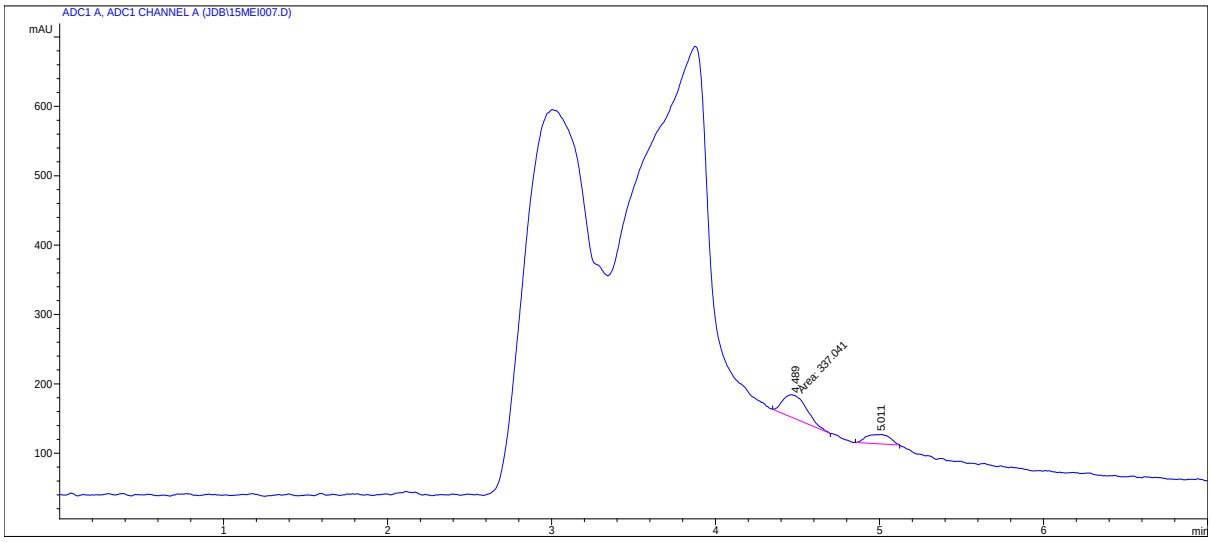

Figure 4.5: Example of a HPLC chromatogram showing the presence of normethanephrine in an enzyme reaction with 500 µM NE as substrate.

4.6.2 Results

Table 4.7: HPLC determined concentrations, retention times and areas for the K_m determination.

NE concentration (µM)	*Retention time (min)*	*Peak area*	*Concentration of NMN (µM)*
25	4.674	35.6	0.070
50	4.580	53.8	0.140
100	4.457	139.3	0.469
175	4.428	291.8	1.054
500	4.593	715.5	2.681
1 000	4.333	595.8	2.221

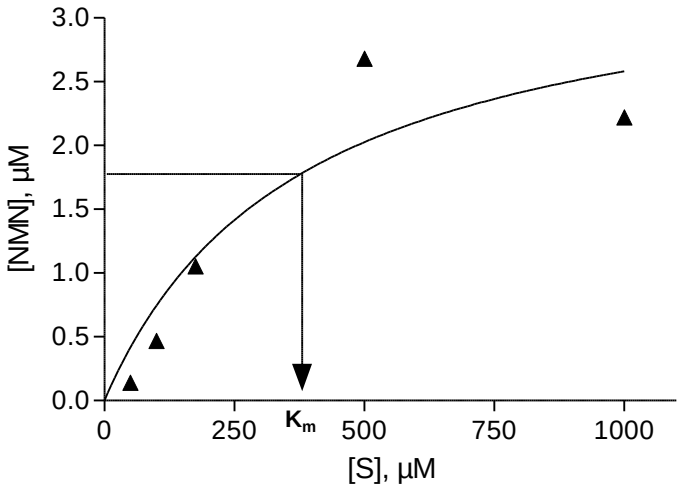

Figure 4.6: The Michaelis-Menten graph of the concentration of NMN formed versus substrate (NE) concentration.

In this study, different concentrations of the COMT substrate, NE, were incubated with the COMT enzyme and the concentrations of NMN that formed were measured (Table 4.7). These data were fitted to the Michaelis-Menten equation to obtain a graph of concentration of NMN versus [S] (Figure 4.6). From the fit, a K_m value of 379 µM were estimated for the methylation of NE by COMT. This value is similar to that reported in literature of 488 ± 51 µM (Aoyama *et al*., 2005). As mentioned, for the determination of IC_{50} values, the enzyme reactions should be carried out with the [S] approximately equal to K_m. It was thus decided to set [S] equal to 250 µM for the enzyme reactions described in the next chapter.

4.7 CONCLUSION

In this chapter, the procedure for the determination of COMT activity described by Aoyama *et al*. (2005) was validated. This protocol involves the measurement of NMN by HPLC analysis with fluorescence detection. NMN is the product that forms when the enzyme substrate, NE, is metabolised by COMT. The linearity, repeatability, stability and inter-day and intra-day precision and accuracy were determined. All parameters were acceptable and this method may thus be used to measure NMN concentrations. It is recommended that samples containing NMN should be analysed on the same day as preparation. In this chapter, the K_m value for the metabolism of

NE by COMT was measured. This value is required since the enzymatic reactions for the determination of IC_{50} values should be conducted at a [S] approximately equal to K_m.

CHAPTER 5

ENZYMOLOGY

5.1 INTRODUCTION

To determine if the synthesised 3-hydroxypyridin-4-ones (Chapter 3) are *in vitro* inhibitors of COMT, commercially available lyophilised COMT powder from porcine liver (≥150 units/mg) was used as enzyme source. A modified procedure of Aoyama *et al.* (2005) was employed to measure COMT activity. NE, a natural substrate of COMT (Dauvilliers *et al.*, 2015), was incubated with COMT in the presence of various concentrations of the test inhibitors. The formation of the enzyme-catalysed product (Figure 5.1), NMN, was quantified by reversed-phase HPLC with fluorescence detection. The principle of the assay is based on the fact that the test inhibitors would decrease the formation of NMN. In this chapter, the experimental methods, equipment, materials and results of the COMT inhibition studies are presented. Some preliminary SARs are also discussed.

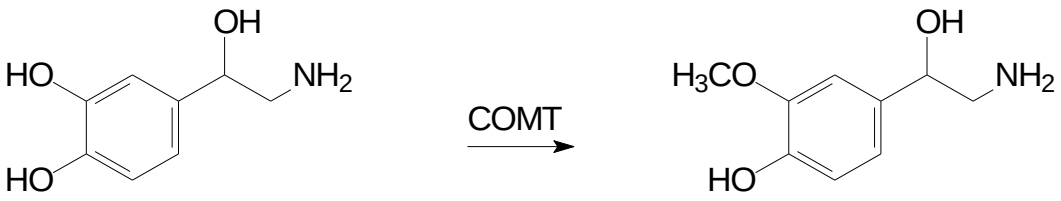

(-)-Norepinephrine Normetanephrine

Figure 5.1: *O*-Methylation of NE (Dauvilliers *et al*., 2015).

5.2 CHEMICALS AND INSTRUMENTATION

All the reagents and materials used for the inhibition studies are listed in Table 4.1.

5.2.1 Instrumentation and HPLC requirements

The HPLC system used for the measurement of NMN was described in the previous chapter (Chapter 4, subsection 4.2.1).

5.3 METHODS

5.3.1 Calibration curve

As described in the previous chapter, the calibration standards were made up to a final volume of 137.5 µl and contained known amounts of NMN (0, 1, 2, 5, 10 and 30 µM) dissolved in a 25 mM sodium phosphate buffer (pH 7.8). Perchloric acid (1 M; 12.5 µl) was added to each calibration standard. A linear calibration curve was constructed by graphing the peak areas of NMN (as measured by the HPLC system) versus NMN concentration. This calibration curve was used to quantify normethanephrine produced in the enzyme reactions by COMT from NE.

5.3.2 IC_{50} Determination

The IC_{50} value is the concentration of an inhibitor that reduces the rate of an enzymatic reaction by 50% (Burlingham & Widlanski, 2003). For the purpose of this study, IC_{50} values were determined in triplicate as a measure of the average COMT inhibitory potencies of the synthesised compounds.

The enzyme stock solution used for the enzyme reactions was prepared by dissolving the purified COMT (750 units/5 ml) in 20 ml of 25 mM sodium phosphate buffer (pH 7.8) containing 0.5 mM dithiothreitol (DTT) (Figure 5.2). Different concentrations of the test inhibitor were prepared in DMSO and added to the enzyme reactions to yield the following concentration range: 0.0, 0.1, 0.3, 1.0, 3.0, 10.0, 30.0 and 100.0 µM (Table 5.1). As reference inhibitors the known COMT inhibitors, tolcapone and entacapone, were also evaluated. Tolcapone and entacapone were also prepared in DMSO and added to the enzyme reactions to yield the following concentration range: 0, 0.0003, 0.001, 0.003, 0.01, 0.1 and 1 µM. This lower concentrations range was used since tolcapone and entacapone were found to be several orders of magnitude more potent than the synthesised 3-hydroxypyridin-4-ones as COMT inhibitors.

Table 5.1: Composition of each enzyme reaction (137.5 µl).

Reagents and final concentrations in the incubations	*Volume (per 137.5 µl)*	*Storage conditions*
2 mM $MgCl_2$	10 µl	Room temperature
250 µM Substrate (NE)	35 µl	–20 °C
200 µM SAMe	25 µl	–20 °C
Test inhibitor (dissolved in DMSO)	5 µl	Room temperature
COMT solution	50 µl	–86 °C
1 M $HClO_4$	12.5 µl	2–8 °C

To prepare the enzyme reactions 10 µl $MgCl_2$ was firstly added followed by 35 µl of the substrate (NE), 25 µl SAMe and lastly 5 µl of the test inhibitor. This yielded concentrations of the constituents of: $MgCl_2$ 2 mM; NE 250 µM; SAMe 200 µM. After the mixtures were pre-incubated at 37 °C in a water bath for at least 10 min, a 50 µl aliquot of the enzyme stock solution was added. The reactions were incubated for 60 min and subsequently terminated by adding 12.5 µl perchloric acid (1 M). The samples were centrifuged at 16 000 x g for 10 min and the supernatants were analysed by the validated HPLC method. The peak areas of NMN (Figure 5.3) were recorded and the corresponding concentrations of NMN formed were calculated using the calibration curve. Using the Prism 5 (GraphPad) software package, the data were fitted to the equation for one-site competition to yield a sigmoidal curve of concentration of NMN formed versus inhibitor concentration. From this fit, the IC_{50} value was estimated. For each test inhibitor the IC_{50} values were determined in triplicate and expressed as mean ± SD.

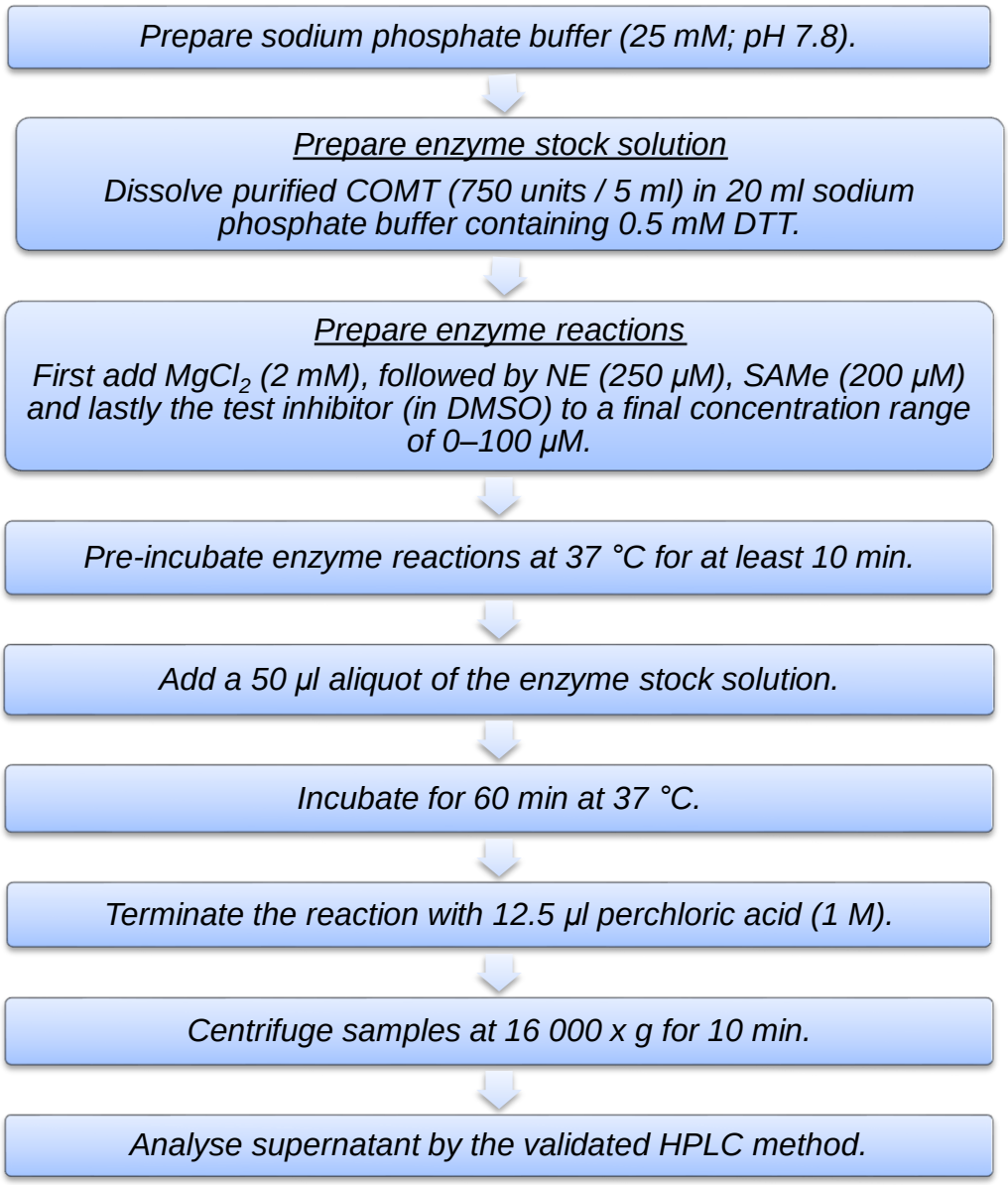

Figure 5.2: Diagrammatic representation of the method followed to determine IC_{50} values for the inhibition of COMT.

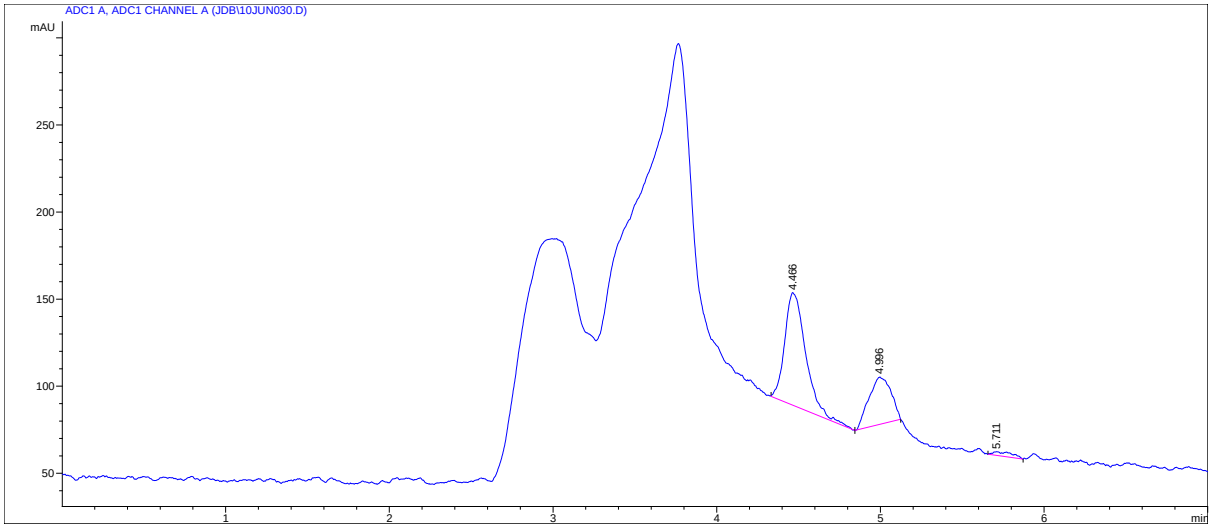

Figure 5.3: Example of a chromatogram showing the presence of NMN, produced by the metabolism of NE by COMT. This enzyme reaction also contained JDB14 at a concentration of 0.1 µM.

5.4 RESULTS: IC_{50} VALUES

The IC_{50} values of the test inhibitors are given in Table 5.2. The IC_{50} values of the reference inhibitors, entacapone and tolcapone, are also provided. The sigmoidal curves constructed for the inhibition of COMT by the 3-hydroxypyridin-4-ones are shown in Figures 5.4 and 5.5.

Table 5.2: The IC_{50} values for the inhibition of COMT by the synthesised 3-hydroxypyridin-4-ones and the reference inhibitors, entacapone and tolcapone.

Compound	*COMT IC_{50} (µM) Mean ± SD**
JDB1	10.9 ± 1.060
JDB3	4.55 ± 0.545
JDB4	15.0 ± 2.100
JDB5	18.4 ± 0.974
JDB9	9.05 ± 1.250
JDB10	12.2 ± 3.060
JDB11	19.8 ± 5.860
JDB12	11.2 ± 1.010
JDB13	9.31 ± 2.940
JDB14	5.76 ± 0.664
Entacapone	0.00047 ± 0.00007
Tolcapone	0.0068 ± 0.0027

**All values are expressed as the mean ± SD of triplicate determinations.*

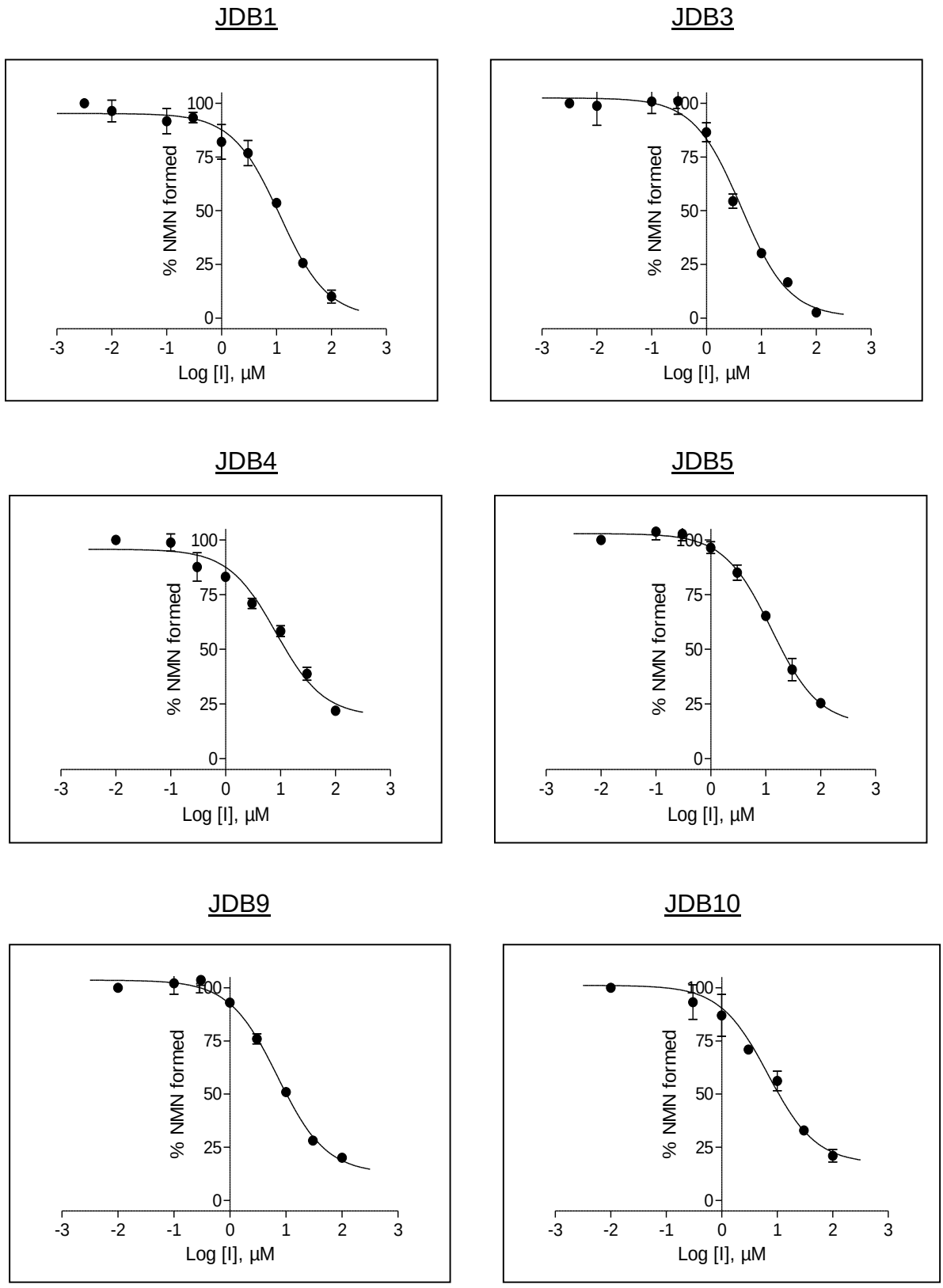

Figure 5.4: The sigmoidal dose-response curves for the inhibition of COMT by JDB1, JDB3, JDB4, JDB5, JDB9 and JDB10. These curves were used to determine IC_{50} values for COMT inhibition.

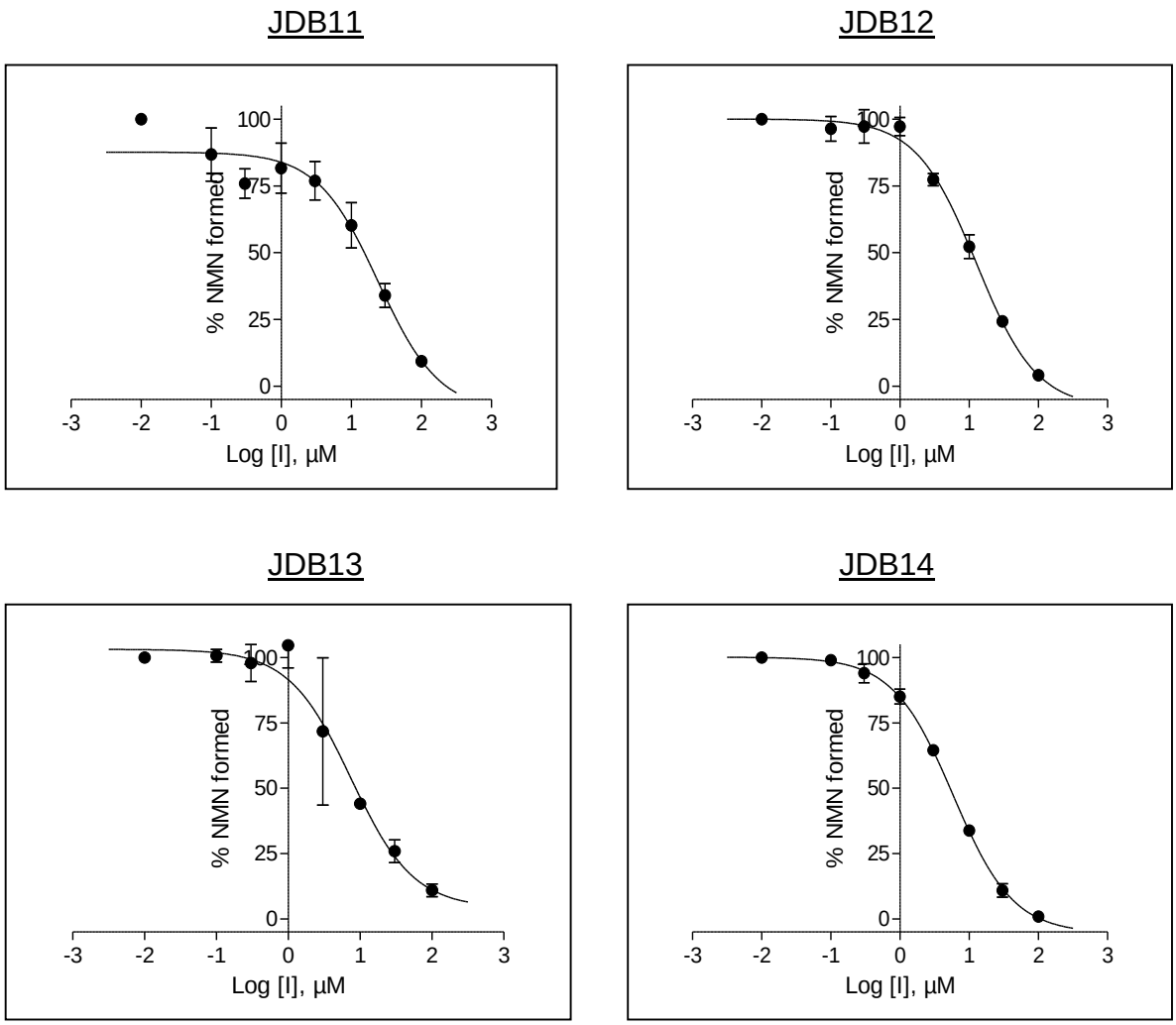

Figure 5.5: The sigmoidal dose-response curves for the inhibition of COMT by JDB11, JDB12, JDB13 and JDB14. These curves were used to determine IC_{50} values for COMT inhibition.

5.4.1 Discussion

From the IC_{50} values obtained for each of the synthesised 3-hydroxypyridin-4-one derivatives (Table 5.2), the following can be concluded:

- The 3-hydroxypyridin-4-one derivatives exhibit COMT inhibitory activity.
- Some preliminary SARs may be derived for the inhibition of COMT by the 3-hydroxypyridin-4-ones.

- Phenyl substitution of the 3-hydroxypyridin-4-one moiety (JDB1, IC_{50} = 10.9 μM) results in a higher IC_{50} value (and thus lower inhibition potency) compared to benzyl substitution (JDB3, IC_{50} = 4.55 μM).
- Benzyl substitution of the 3-hydroxypyridin-4-one moiety also results in improved COMT inhibition compared to phenylethyl (JDB4, IC_{50} = 15.0 μM), phenylpropyl (JDB5, IC_{50} = 18.4 μM) and phenylbutyl (JDB9, IC_{50} = 9.05 μM) substitution. This shows that chain elongation of the substituent reduces COMT inhibition potency and that the methylene (CH_2) linker between the 3-hydroxypyridin-4-one moiety and phenyl ring is more optimal than the other linkers considered [$(CH_2)_2$, $(CH_2)_3$ and $(CH_2)_4$].
- When comparing phenyl substitution of the 3-hydroxypyridin-4-one moiety JDB1 (IC_{50} = 10.9 μM) with cyclohexyl substitution (JDB10, IC_{50} = 12.2 μM), the aromatic substituent yields slightly more favourable inhibition than the aliphatic substituent.
- When comparing cyclohexyl substitution of the 3-hydroxypyridin-4-one moiety (JDB10, IC_{50} = 12.2 μM) with cyclopentyl substitution (JDB11, IC_{50} = 19.8 μM), a reduction in COMT inhibition potency is observed. In fact, JDB11 is the weakest COMT inhibitor of the series of 3-hydroxypyridin-4-one derivatives.
- When comparing the phenyl substituted derivative, JDB1 (IC_{50} = 10.9 μM), with the derivatives containing chlorine on the phenyl ring, JDB12 (IC_{50} = 11.2 μM) and JDB13 (IC_{50} = 9.31 μM), it is apparent that chlorine substitution on the *meta* and *para* positions of the phenyl ring does not significantly affect COMT inhibition potency.
- Similarly, when the benzyl substituted derivative, JDB3 (IC_{50} = 4.55 μM) is substituted with a methyl substituent on the *para* position of the phenyl ring (to yield JDB14, IC_{50} = 5.76 μM), COMT inhibitory activity remains relatively unchanged. Benzyl substitution of the 3-hydroxypyridin-4-one moiety (JDB3 and JDB14) thus yielded the most potent COMT inhibitory activity among the compounds evaluated.

- The effects of substitution of the 3-hydroxypyridin-4-one moiety in this study may be illustrated by the following figure:

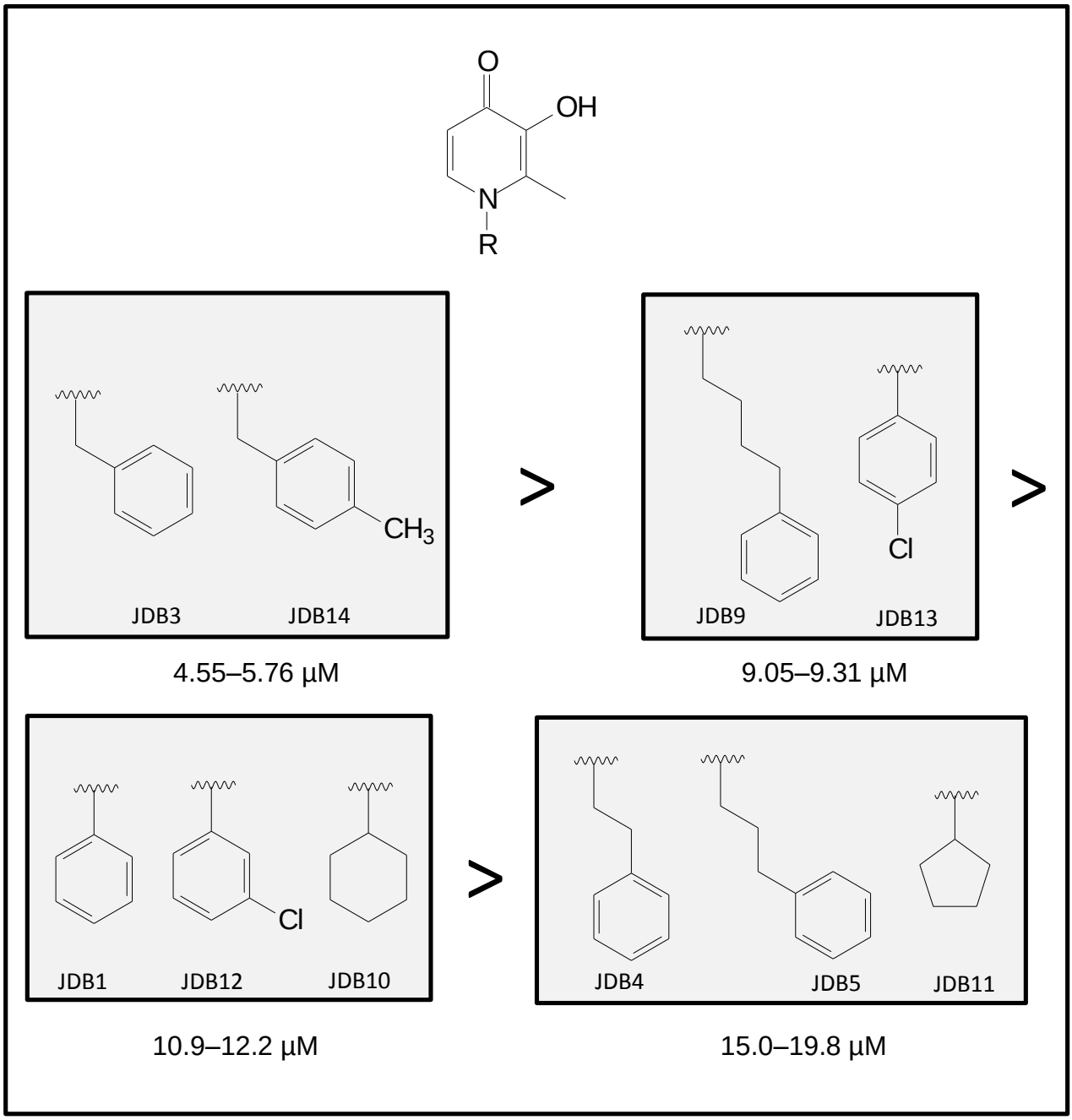

Figure 5.6: Effects of substitution of the 3-hydroxypyridin-4-one moiety on IC_{50} values, ranging from favourable to less favourable COMT inhibition.

- The reference inhibitors, entacapone (IC_{50} = 0.00047 µM) and tolcapone (IC_{50} = 0.0068 µM), proved to be highly potent COMT inhibitors. The measured IC_{50} values are similar to those reported in literature of 0.00016 µM and 0.000036 µM for entacapone and tolcapone, respectively (Bonifati & Meco, 1999).

JDB3 and JDB14 were thus the most potent COMT inhibitors of the series with IC_{50} values of 4.55 µM and 5.76 µM, respectively. The higher activity of these compounds, when compared to the other compounds of the series, has been predicted by the modelling studies since these two compounds displayed more favourable CDOCKER interaction energies (Chapter 3). Although these non-nitrocatechol COMT inhibitors are not as potent as entacapone (IC_{50} = 0.00047 µM) or tolcapone (IC_{50} = 0.0068 µM), the 3-hydroxypyridin-4-ones may act as leads for the development of non-nitrocatechol derivatives with possibly better side-effect profiles (Robinson *et al*., 2012). Further investigation in this regard is required.

5.5 CONCLUSION

In this chapter it was shown that the synthesised 3-hydroxypyridin-4-ones are *in vitro* inhibitors of COMT. Based on the IC_{50} values obtained, preliminary SARs were derived. Benzyl substitution of the 3-hydroxypyridin-4-one moiety (JDB3 and JDB14) yielded the most potent COMT inhibitory activity among the compounds evaluated. These 3-hydroxypyridin-4-one derivatives are not as potent as reference inhibitors, entacapone and tolcapone, but may serve as leads for the design of more potent non-nitrocatechol COMT inhibitors for the treatment of Parkinson's disease.

CHAPTER 6

CONCLUSION

Parkinson's disease is a neurodegenerative disorder and is characterised by the loss of dopaminergic neurons in the brain (Dauer & Przedborski, 2003). The metabolic precursor of dopamine, levodopa, still remains the most effective therapy for restoring the central dopamine deficit associated with the disease (Standaert & Roberson, 2011). Levodopa, however, is extensively metabolised in the periphery, which limits its availability for uptake into the brain. The inhibition of levodopa metabolism in the periphery is therefore a valid approach to enhance levodopa brain concentrations. Since COMT is an important enzyme in the metabolism of levodopa, this study will attempt to discover new COMT inhibitors for the treatment of Parkinson's disease (Standaert & Roberson, 2011). Tolcapone and entacapone are nitrocatechol COMT inhibitors that have been used in the treatment of Parkinson's disease (Robinson *et al*., 2012). The clinical value of nitrocatechol COMT inhibitors is sometimes limited by their poor bioavailabilities and side-effect profiles (Robinson *et al*., 2012). The non-nitrocatechol 3-hydroxypyridin-4-one scaffold (Table 6.1) has been reported to exhibit COMT inhibitory potential and was selected for the purpose of the study (Borchardt, 1973; Männistö & Kaakkola, 1999; Robinson *et al*., 2012).

Regardless of substituents on the aromatic nucleus, most COMT substrates have the catechol moiety in its chemical structure (Guldberg & Marsden, 1975). In the presence of magnesium, COMT serves as a catalyst in the methyl transmission from SAMe to one of the catechol substrate's hydroxy groups (Männistö & Kaakkola, 1999). 3-Hydroxypyridin-4-ones possess good affinities for COMT since they are isosteric to the catechol ring, but are not *O*-methylated by the enzyme themselves (Borchardt, 1973). Previous research indicated that 3-hydroxypyridin-4-ones, which possess COMT inhibitory activity, have either very small substituents on R^1 or large bicyclic aromatic substituents (Borchardt, 1973; Rai *et al*., 1999). It has also been reported by Robinson *et al*. (2012) that the 3-hydroxypyridin-4-ones are MB-COMT specific and may exhibit better side-effect profiles than nitrocatechol COMT inhibitors. Thus, the following ten 3-hydroxypyridin-4-one derivatives (Table 6.1) were designed and synthesised:

Table 6.1: The synthesised 3-hydroxypyridin-4-one derivatives and their respective IC_{50} values for the inhibition of COMT.

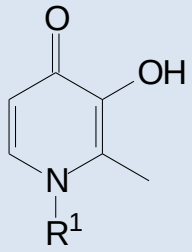

Compound	*R^1*	*COMT IC_{50} (μM)*
JDB1	$–C_6H_5$	10.9 ± 1.060
JDB3	$–CH_2C_6H_5$	4.55 ± 0.545
JDB4	$–(CH_2)_2C_6H_5$	15.0 ± 2.100
JDB5	$–(CH_2)_3C_6H_5$	18.4 ± 0.974
JDB9	$–(CH_2)_4C_6H_5$	9.05 ± 1.250
JDB10	$–C_6H_{11}$	12.2 ± 3.060
JDB11	$–C_5H_9$	19.8 ± 5.860
JDB12	$–(C_6H_4)$-3′-Cl	11.2 ± 1.010
JDB13	$–(C_6H_4)$-4′-Cl	9.31 ± 2.940
JDB14	$–CH_2(C_6H_4)$-4′-CH_3	5.76 ± 0.664

By employing molecular modelling software, the proposed 3-hydroxypyridin-4-one derivatives were docked into the COMT enzyme's binding site. All the derivatives fitted within the catechol binding site of COMT, with the 3-hydroxypyridin-4-one moiety orientated towards the magnesium ion located in this site. The side chains of the different compounds were mostly solvent-exposed and had minimum interaction with the binding site. With the exception of JDB5, hydrogen bonding occurred between the 3-hydroxyl group and Glu199. For some of the phenyl derivatives (JDB3, JDB4 and JDB14) π-interactions occurred between the phenyl ring and either Trp143 or Lys144. This may possibly explain the more favourable IC_{50} values obtained for JDB3 (4.55 μM) and JDB14 (5.76 μM).

The 3-hydroxypyridin-4-ones were synthesised by a method described by Fassihi *et al*. (2009), where maltol was refluxed with a suitable primary amine in an acidic environment with ethanol as co-solvent (Figure 6.1). After removal of an oily residue, the product precipitated from the reaction and was collected by filtration and purified by recrystallisation from hot methanol. Compounds JDB10 and JDB11 differed in the work-up procedure and were rather collected by extraction and purified by column chromatography. Characterisation of the synthesised compounds was carried out by NMR spectroscopy, IR spectroscopy and MS. The purities of the synthesised compounds were estimated by HPLC analyses. It was confirmed that the purities of the 3-hydroxypyridin-4-one derivatives were acceptable for these compounds to be subjected to biological evaluation experiments.

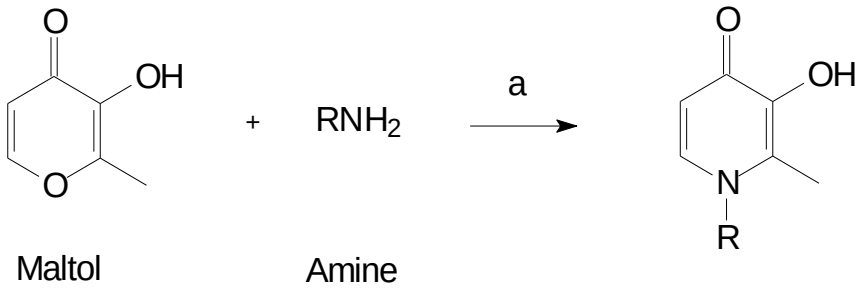

Figure 6.1: General synthetic route for the preparation 3-hydroxypyridin-4-one derivatives *via* a single step synthetic pathway. (a) HCl, H_2O, ethanol, 72 h, 110 °C (Fassihi *et al*., 2009).

The literature procedure for the determination of *in vitro* COMT activity, described by Aoyama *et al.* (2005), was validated. The measurement of NMN (the product of the *O*-methylation of NE by COMT) was carried out by HPLC analysis with fluorescence detection. Linear calibration curves were constructed and, with selected calibration standards, the repeatability, stability, and inter-day and intra-day precision and accuracy were determined. All parameters of the method proved to be acceptable and this method is therefore suitable for the measurement of NMN concentrations.

The *in vitro* COMT inhibitory potential of the synthesised 3-hydroxypyridin-4-one derivatives was determined. NE and various concentrations of the test inhibitors were incubated with COMT. The formation of NMN was quantified by HPLC with

fluorescence detection and from the inhibition data, IC_{50} values were calculated. It was concluded that the synthesised 3-hydroxypyridin-4-one derivatives exhibited COMT inhibitory activity. JDB3 and JDB4 were the most potent COMT inhibitors of the series with IC_{50} values of 4.55 µM and 5.76 µM, respectively. These 3-hydroxypyridin-4-one derivatives are not as potent as the reference inhibitors, entacapone (IC_{50} = 0.00047 µM) and tolcapone (IC_{50} = 0.00675 µM). They may, however, serve as leads for the development of non-nitrocatechol COMT inhibitors with better side-effect profiles (Robinson *et al*., 2012). Further investigation in this regard is required.

In conclusion, 3-hydroxypyridin-4-one derivatives were designed, synthesised and evaluated as inhibitors of COMT. The synthesised compounds exhibited COMT inhibitory activity, but were not as potent as nitrocatechol COMT inhibitors currently used in the clinic. It has, however, been suggested that these compounds may exhibit better side-effect profiles and thus may act as leads for the development of non-nitrocatechol COMT inhibitors.

6.1 FUTURE PERSPECTIVE

Since Robinson *et al*. (2012) proved that 3-hydroxypyridin-4-one derivatives may exhibit MB-COMT specific inhibitory activity, future exploratory work would include utilising MB-COMT as enzyme source. This may significantly affect the IC_{50} values obtained for these derivatives. Toxicity, bioavailability and physicochemical properties of the synthesised 3-hydroxypyridin-4-one derivatives still need to be explored to determine the safety profiles of this class of compounds and their suitability as potential orally active drugs. It might also be significant to test the iron chelating- and analgesic activity of the synthesised 3-hydroxypyridin-4-one derivatives. Considering the limitations of the current study, the 3-hydroxypyridin-4-one derivatives can be promising leads for the design of future non-nitrocatechol COMT inhibitors although high inhibition potencies have not been recorded.

BIBLIOGRAPHY

Adams, J.D. 1996. Agents used in neurodegenerative disorders. (*In* Wolff, M.E., *ed*. Burger's medicinal chemistry and drug discovery. New York: Wiley. p. 529-556.

Aoyama, N., Tsunoda, M. & Imai, K. 2005. Improved assay for catechol-*O*-methyltransferase activity utilizing norepinephrine as an enzymatic substrate and reversed-phase high-performance liquid chromatography with fluorescence detection. *Journal of chromatography,* 1074:47-51.

Bertoni, J. & Torres-Russotto, D.R. 2013. MAO-B inhibitors for the treatment of Parkinson's disease. (*In* Pfeiffer, R.F., *ed*. Parkinson's disease. 2nd ed. New York: CRC Press. p. 825-837).

Blumberg, L.M. 2012. Theory of gas chromatography. (*In* Poole, C.F., *ed*. Gas chromatography. Amsterdam: Elsevier. p. 20-78).

Bonifácio, M.J., Palma, P.N., Almeida, L. & Soares-da-Silva. P. 2007. Catechol-O-methyltransferase and its inhibitors in Parkinson's disease. *CNS drug reviews*, 13:352-379.

Bonifati, V. & Meco, G. 1999. New, selective catechol-O-methyltransferase inhibitors as therapeutic agents in Parkinson's disease. *Pharmacology & therapeutics,* 81:1-36.

Borchardt, R.T. 1973. Catechol-*O*-methyltransferase. 4. *In vitro* inhibition by 3-hydroxy-4-pyrones, 3-hydroxy-2-pyridones, and 3-hydroxy-4-pyridones. *Journal of medicinal chemistry*, 16:581-583.

Borchardt, R.T. 1974. A rapid spectrophotometric assay for catechol-O-methyltransferase. *Analytical biochemistry*, 58:382-389.

Burlingham, B.T. & Widlanski, T.S. 2003. An intuitive look at the relationship of K_i and IC_{50}: a more general use for the Dixon plot. *Journal of chemical education*, 80:214-218.

Chen, J.J. & Swope, D.M. 2007. Pharmacotherapy for Parkinson's disease. *Pharmacotherapy*, 27:161-173.

Coward, J.K. & Wu, F.Y. 1973. A continuous spectrophotometric assay for catechol-O-methyltransferase. *Analytical biochemistry*, 55:406-410.

Creveling, C.R. & Daly, J.W. 1971. Assay of enzymes of catecholamine biosynthesis and metabolism. (*In* Glick, D., *ed*. Analysis of biogenic amines and their related enzymes. New York: Wiley. p. 153-182).

Dauer, W. & Przedborski, S. 2003. Parkinson's disease: mechanisms and models. *Neuron,* 39:889-909.

Dauvilliers, Y., Tafti, M. & Landolt, H.P. 2015. Catechol-*O*-methyltransferase, dopamine, and sleep-wake regulation. *Sleep medicine reviews,* 22:47-53.

Dixon, M. 1953. The determination of enzyme inhibitor constants. *Biochemical journal*, 55:170-171.

Fassihi, A., Abedi, D., Saghaie, L., Sabet, R., Fazeli, H., Bostaki, G., Deilami, O. & Sadinpour, H. 2009. Synthesis, antimicrobial evaluation and QSAR study of some 3-hydroxypyridine-4-one and 3-hydroxypyran-4-one derivatives. *European journal of medicinal chemistry*, 44:2145-2157.

Fox, R.C. & Taylor, P.D. 1999. Efficient syntheses of N-alkyl-3-hydroxy-2-methyl-4(1H)-pyridinones from carbohydrate precursors. *Synthetic communications*, 29:989-1001.

Fujii, T., Yamazaki, T., Akiyama, T., Sano, S. & Mori, H. 2004. In vivo assessment of catechol *O*-methyltransferase activity in rabbit skeletal muscle. *Autonomic neuroscience: basic and clinical,* 111:140-143.

Garbayo, E., Ansorena, E. & Blanco-Prieto, M.J. 2013. Drug development in Parkinson's disease: from emerging molecules to innovative drug delivery systems. *Maturitas*, 76:272-278.

Gonçalves, D., Alves, G., Soares-da-Silva, P. & Falcão, A. 2012. Bioanalytical chromatographic methods for the determination of catechol-*O*-methyltransferase inhibitors in rodents and human samples: a review. *Analytica chimica acta*, 710:17-32.

Guldberg, H.C. & Marsden, C.A. 1975. Catechol-*O*-methyltransferase: pharmacological aspects and physiological role. *Pharmacological reviews*, 27:135-206.

Halkias, I.A.C., Haq, I., Huang, Z. & Fernandez, H.H. 2007. When should levodopa therapy be initiated in patients with Parkinson's disease? *Drugs*, 24:261-273.

Hatano, T., Kubo, S.I., Shimo, Y., Nishioka, K. & Hattori, N. 2009. Unmet needs of patients with Parkinson's disease: interview survey of patients and caregivers. *The journal of international medical research*, 37:717-726.

Hirano, Y., Tsunoda, M., Funatso, T. & Imai, K. 2005. Rapid assay for catechol-*O*-methyltransferase activity by high-performance liquid chromatography-fluorescence detection. *Journal of chromatography B*, 819:41-46.

Jee-Young, L. & Yangmee, K. 2005. Comparative homology modeling and ligand docking study of human catechol-O-methyltransferase for antiparkinson drug design. *Bulletin of the Korean Chemical Society*, 26:1695-1700.

Kaakkola, S. 2000. Clinical pharmacology, therapeutic use and potential of COMT inhibitors in Parkinson's disease. *Drugs*, 59:1233-1250.

Karpinska, J. 2012. Basic principles and analytical application of derivative spectrosphotometry. http://cdn.intechopen.com/pdfs-wm/37663.pdf Date of access: 13 Oct. 2015.

Koch, M.V., Cannon, J.G. & Burkman, A.M. 1968. Centrally acting emetics. II. Norapomorphine and derivatives. *Journal of medicinal chemistry,* 11:997-981.

Lautala, P., Ulmanen, I. & Taskinen, J. 1999. Radiochemical high-performance liquid chromatographic assay for the determination of catechol *O*-methyltransferase activity towards various substrates. *Journal of chromatography B,* 736:143-151.

Learmonth, D.A., Kiss, L.E. & Soares-da-Silva, P. 2010. The chemistry of catechol-O-methyltransferase inhibitors. (*In* Nissinen, E., *ed*. International review of neurobiology, basic aspects of catechol-O-methyltransferase and the clinical applications of its inhibitors. New York: Academic Press. p. 119-162).

Lees, A. 2005. Alternatives to levodopa in the initial treatment of early Parkinson's disease. *Drugs aging,* 22:731-740.

Lees, A.J., Hardy, J. & Revesz, T. 2009. Parkinson's disease. *Lancet*, 373:2055-2066.

LeWitt, P.A. & Taylor, D.C. 2008. Protection against Parkinson's disease progression: clinical experience. *The journal of the American society for experimental neurotherapeutics*, 5:210-225.

Liu, Z.D., Lockwood, M., Rose, S., Theobald, A.E. & Hider, R.C. 2001. Structure-activity investigation of the inhibition of 3-hydroxypyridin-4-ones on mammalian tyrosine hydroxylase. *Biochemical pharmacology*, 61:285-290.

Männistö, P.T. & Kaakkola, S. 1999. Catechol-*O*-methyltransferase (COMT): biochemistry, molecular biology, pharmacology, and clinical efficacy of the new selective COMT inhibitors. *Pharmacological reviews*, 51:594-628.

Maranis, S., Tsouli, S. & Konitsiotis, S. 2011. Treatment of motor symptoms in advanced Parkinson's disease: a practical approach. *Progress in neuro-psychopharmacology and biological psychiatry*, 35:1795-1807.

Maurer, H.H., Bickeboeller-Friedrich, J. & Kraemer, T. 2000. Gas chromatographic-mass spectrometric procedures for determination of the catechol-*O*-methyltransferase (COMT) activity and for detection of unstable catecholic metabolites in human and rat liver preparations after COMT catalyzed *in statu nascendi* derivatization using *S*-adenosylmethionine. *Journal of chromatography B*, 739:325-335.

McNair, H.M. & Miller, J.M. 2009. Basic gas chromatography. 2nd ed. Hoboken, N.J.: Wiley.

Nissinen, E. 2010. Introductory remarks: catechol-*O*-methyltransferase inhibition – an innovative approach to enhance L-dopa therapy in Parkinson's disease with dual enzyme inhibition. *International review of neurobiology*, 95:1-5.

Orłowski, A., St-Pierre, J., Magarkar, A., Bunker, A., Pasenkiewicz-Gierula, M., Vattulainen, I. & Róg, T. 2011. Properties of the membrane binding component of catechol-O-methyltransferase revealed by atomistic molecular dynamics simulations. *The journal of physical chemistry B*, 115:13541–13550.

Öztürk G., Erol, D.D., Uzbay, T. & Aytemir, M.D. 2001. Synthesis of 4(1*H*)-pyridinone derivatives and investigation of analgesic and antiinflammatory activities. *Il Farmaco,* 56:251-256.

Pennings, J.M. & van Kempen, G.M.J. 1979. Assay of catechol *O*-methyltransferase by determination of the *m*- and *p*-*O*-methylated products using high-performance liquid chromatography. *Analytical biochemistry*, 98:452-454.

Pihlavisto, P. & Reenilä, I. 2002. Separation methods for catechol *O*-methylatransferase activity assay: physiological and pathophysiological relevance. *Journal of chromatography B,* 781:359-372.

Rai, B.L., Liu, Z.D., Liu, D.Y., Lu, S.L. & Hider, R.C. 1999. Synthesis, physicochemical properties and biological evaluation of ester prodrugs of 3-hydroxypyridin-4-ones: design of orally active chelators with clinical potential. *European journal of medicinal chemistry,* 34:475-485.

Ramsey, C.P. & Tansey, M.G. 2014. A survey from 2012 of evidence for the role of neuroinflammation in neurotoxin animal models of Parkinson's disease and potential molecular targets. *Experimental neurology*, 256:126-132.

Reenilä, I., Tuomainen, P. & Männistö, P.T. 1995. Improved assay of reaction products to quantitate catechol-*O*-methyltransferase activity by high-performance liquid chromatography with electrochemical detection. *Journal of chromatography B,* 663:137-142.

Reenilä, I. 1999. Catechol-*O*-methyltrasferase activity: assay, distribution and pharmacological modification. Siltavuorenpenger: University of Helsinki. (Dissertation – PhD).

Robinson, R.G., Smith, S.M., Wolkenberg, S.E., Kandebo, M., Yao, L., Gibson, C.R., Harrison, S.T., Polsky-Fisher, S., Barrow, J.C., Manley, P.J., Mulhearn, J.J., Nanda, K.K., Schubert, J.W., Trotter, B.W., Zhao, Z., Sanders, J.M., Smith, R.F., McLoughlin, D., Sharma, S., Hall, D.L., Walker, T.L., Kershner, J.L., Bhandari, N., Hutson, P.H. & Sachs, N.A. 2012. Characterization of non-nitrocatechol pan and isoform specific catechol-*O*-methyltransferase inhibitors and substrates. *ACS chemical neuroscience*, 3:129-140.

Rodwell, V.W. & Kennelly, P.J. 2003. Enzymes: kinetics. (*In* Foltin J., *ed*. Harper's illustrated biochemistry. New York: McGraw-Hill. p.60-71).

Rutherford, K., Le Trong, I., Stenkamp, R.E. & Parson, W.W. 2008. Crystal structures of human 108V and 108M catechol-*O*-methyltransferase. *Journal of molecular biology*, 380:120-130.

Silva, M.T. & Schapira, A.H.V. 2001. Parkinson's disease. (*In* Mattson, M.P., *ed.* Pathogenesis of neurodegenerative disorders. Totowa, N.J.: Humana Press. p. 53-79).

Standaert, D.G. & Roberson, E.D. 2011. Treatment of central nervous system degenerative disorders. (*In* Brunton, L.L., *ed*. Goodman and Gilman's the pharmacological basis of therapeutics. New York: McGraw-Hill. p. 609-628).

Tugwell, C. 2008. Parkinson's disease in focus. London: Pharmaceutical Press.

Tunbridge, E.M. 2010. The catechol-*O*-methyltransferase gene: its regulation and polymorphisms. *International review of neurobiology*, 95:7-27.

Varga, L.I., Ako-Agugua, N., Colasante, J., Hertweck, L., Houser, T., Smith, J., Watty, A.A., Nagar, S. & Raffa, R.B. 2009. Critical review or ropinirole and pramipexole – putative dopamine D_3-receptor selective agonists – for the treatment or RLS. *Journal of clinical pharmacy and therapeutics*, 34:493-505.

Ward, R.J., Dexter, D., Florence, A., Aouad, F., Hider, R., Jenner, P. & Crichton, R.R. 1995. Brain iron in the ferrocene-loaded rat: its chelation and influence on dopamine metabolism. *Biochemical pharmacology*, 49:1821-1826.

Wells, B.G. 2009. Neurological disorders: Parkinson's disease. (*In* Wells, B.G., Dipiro, J.T., Schwinghammer, T.L. & Dipiro, C.V., *eds.* Pharmacotherapy handbook. 7^{Th} ed. New York: McGraw-Hill. p. 629-636).

Yacoubian T.A. & Standaert, D.G. 2009. Targets of neuroprotection in Parkinson's disease. *Biochimica et biophysica acta*, 235:1160-1163.

Zhang, X., Lu, L., Liu, S., Ye, W., Wu, J. & Zhang, X. 2013. Acetylcholinesterase deficiency decreases apoptosis in dopaminergic neurons in the neurotoxin model of Parkinson's disease. *The international journal of biochemistry and cell biology*, 45:265-272.

Zhao, W., Latinwo, L., Liu, X., Lee, E., Lamango, N. & Charlton, C.G. 2001. L-Dopa upregulates the expression and activities of methionine adenosyl transferase and catechol-*O*-methyltransferase. *Experimental neurology*, 171:127-13.

APPENDIX A

A.1 NUCLEAR MAGNETIC RESONANCE (NMR) SPECTROSCOPY

JDB1: 3-Hydroxy-2-methyl-1-phenylpyridin-4-one

- ^{1}H-NMR spectrum for JDB1:

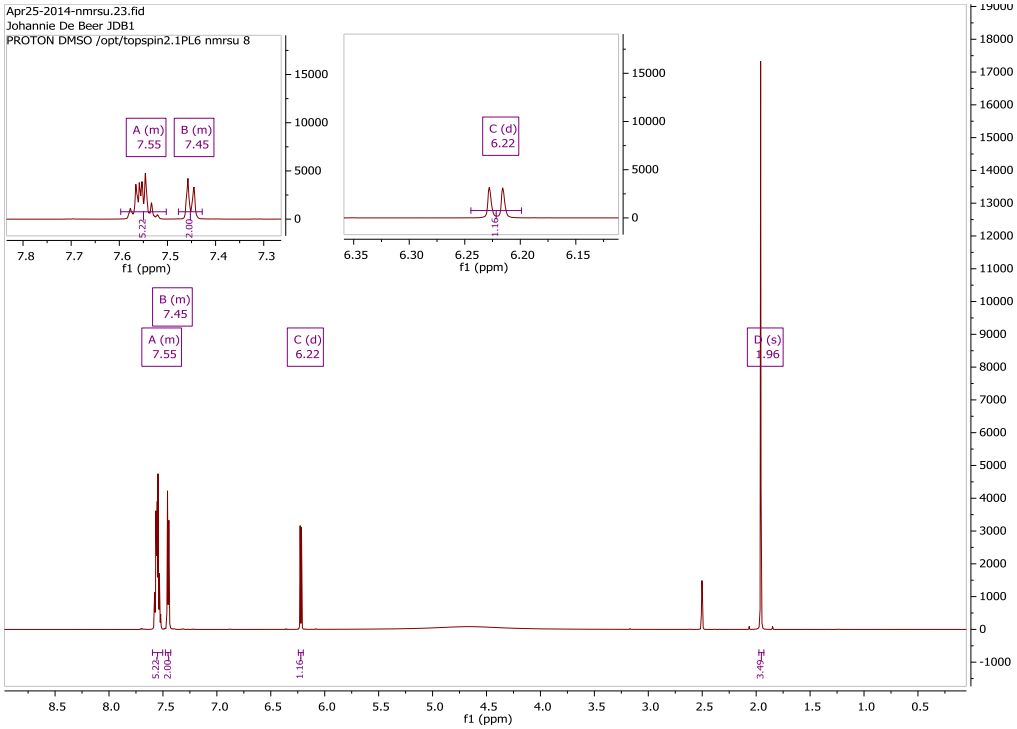

- ^{13}C-NMR spectrum for JDB1:

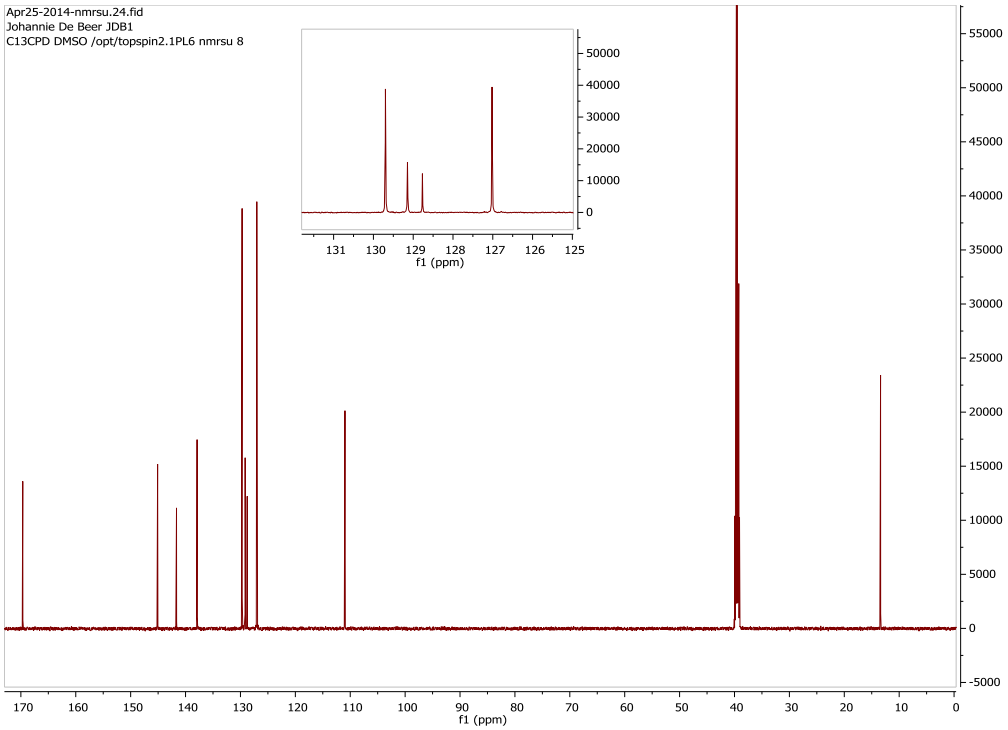

- ^{13}C-NMR, DEPT135 spectrum for JDB1:

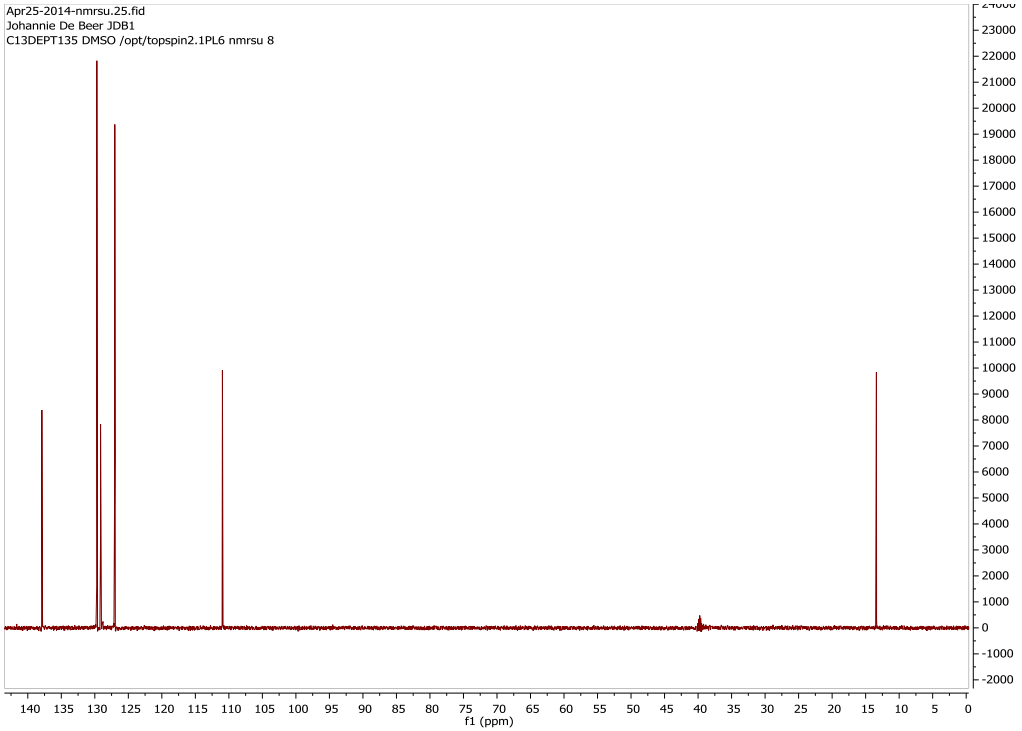

- ^{13}C-NMR, DEPT90 spectrum for JDB1:

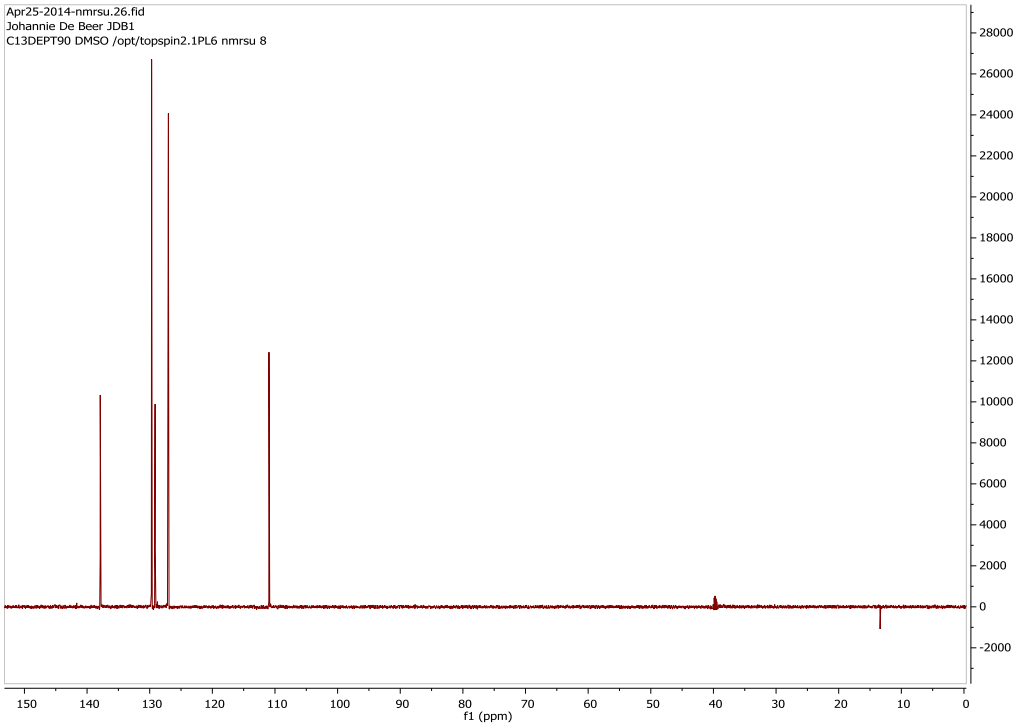

- COSY spectrum for JDB1:

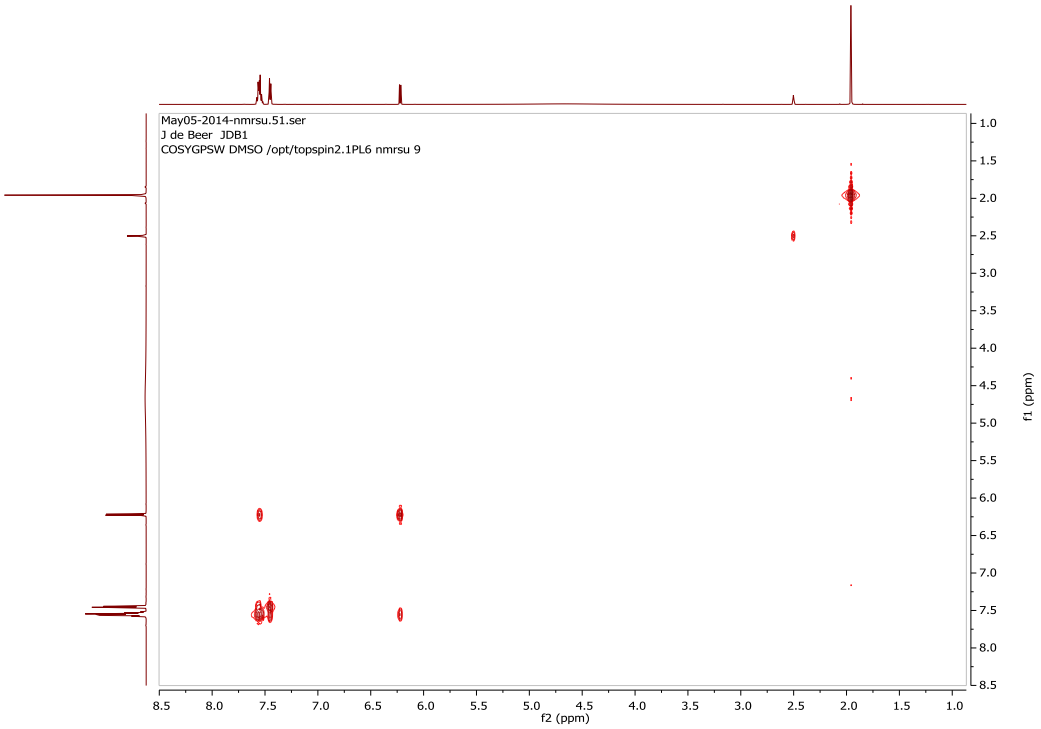

- HSQC spectrum for JDB1:

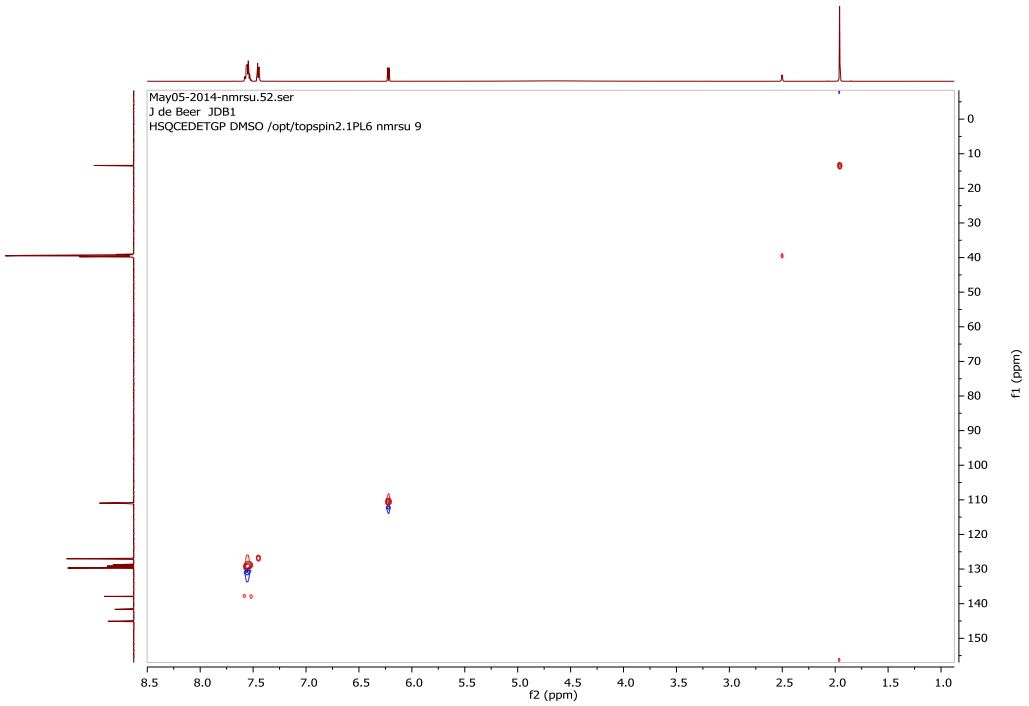

- HMBC spectrum for JDB1:

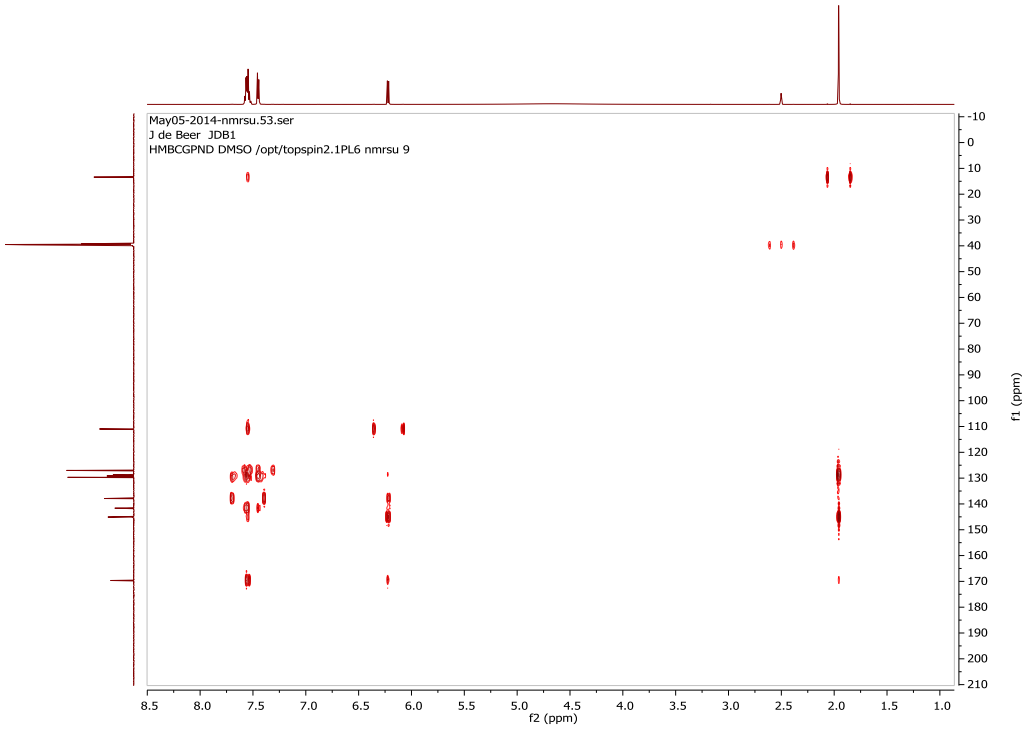

JDB3: 1-Benzyl-3-hydroxy-2-methylpyridin-4-one

- ^{1}H-NMR spectrum for JDB3:

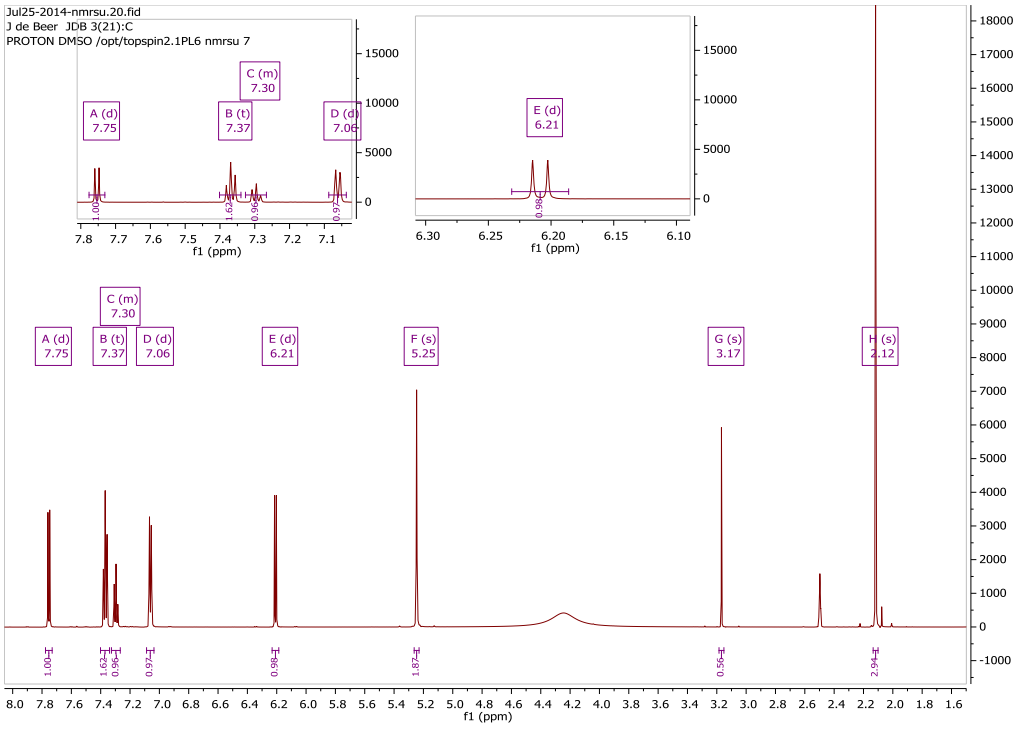

- ^{13}C-NMR spectrum for JDB3:

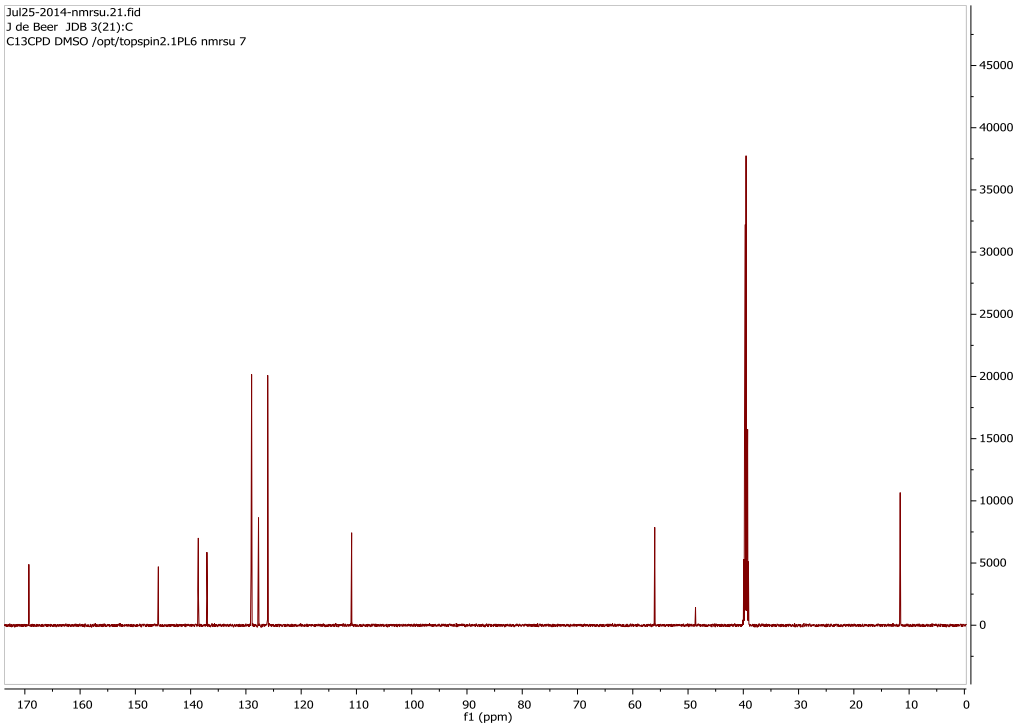

- ^{13}C-NMR, DEPT90 spectrum for JDB3:

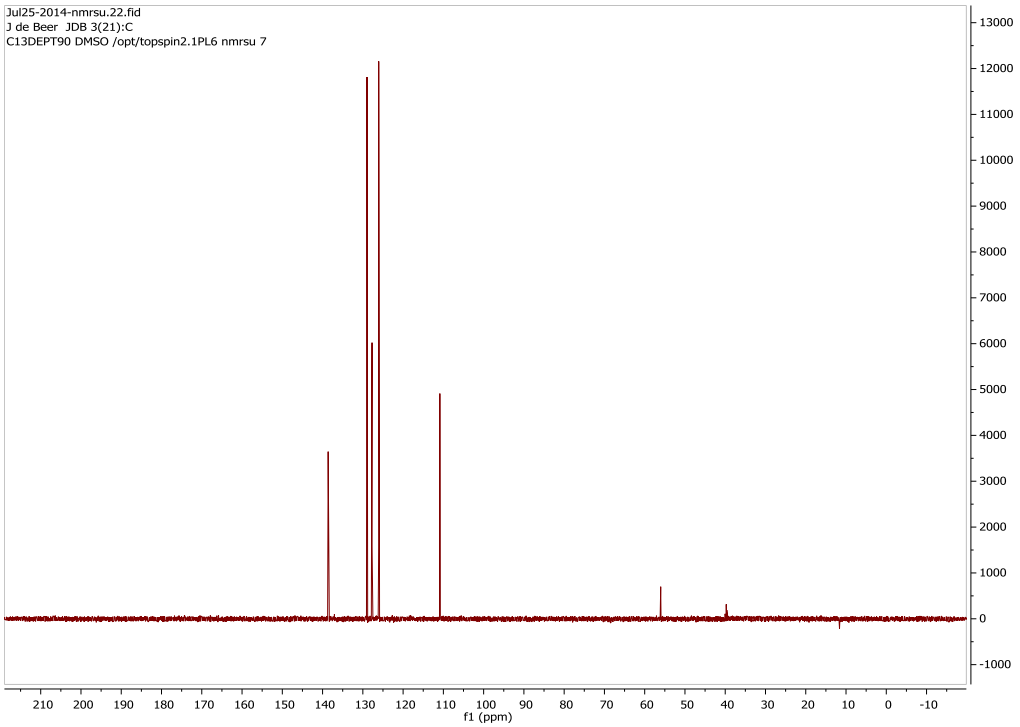

- ^{13}C-NMR, DEPT135 spectrum for JDB3:

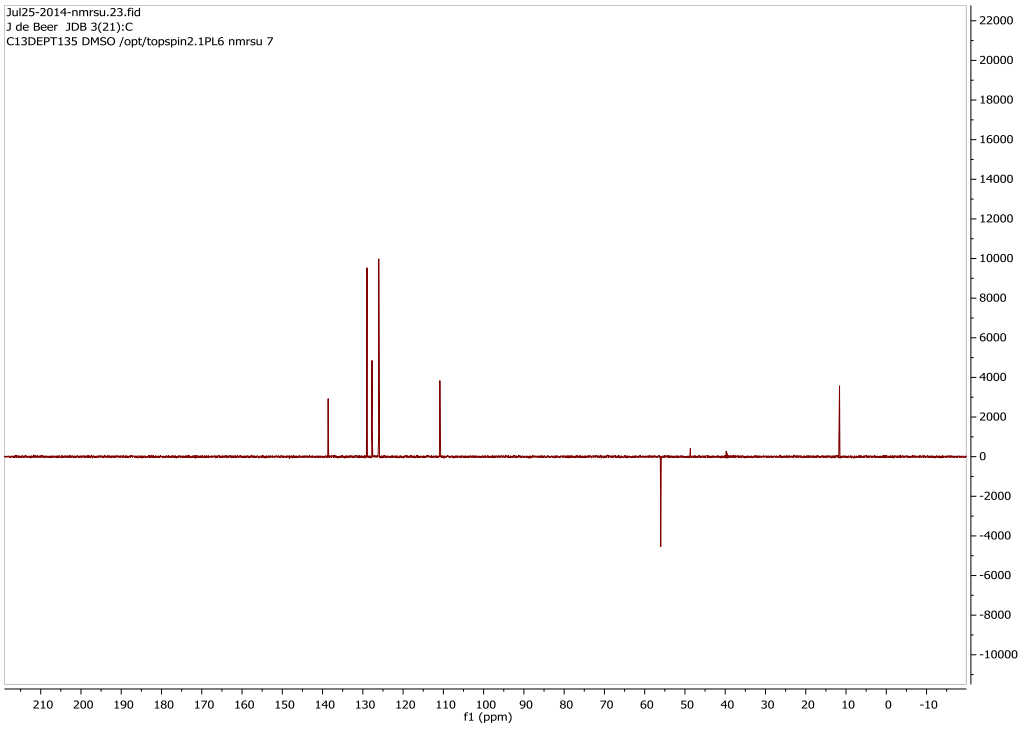

- COSY spectrum for JDB3:

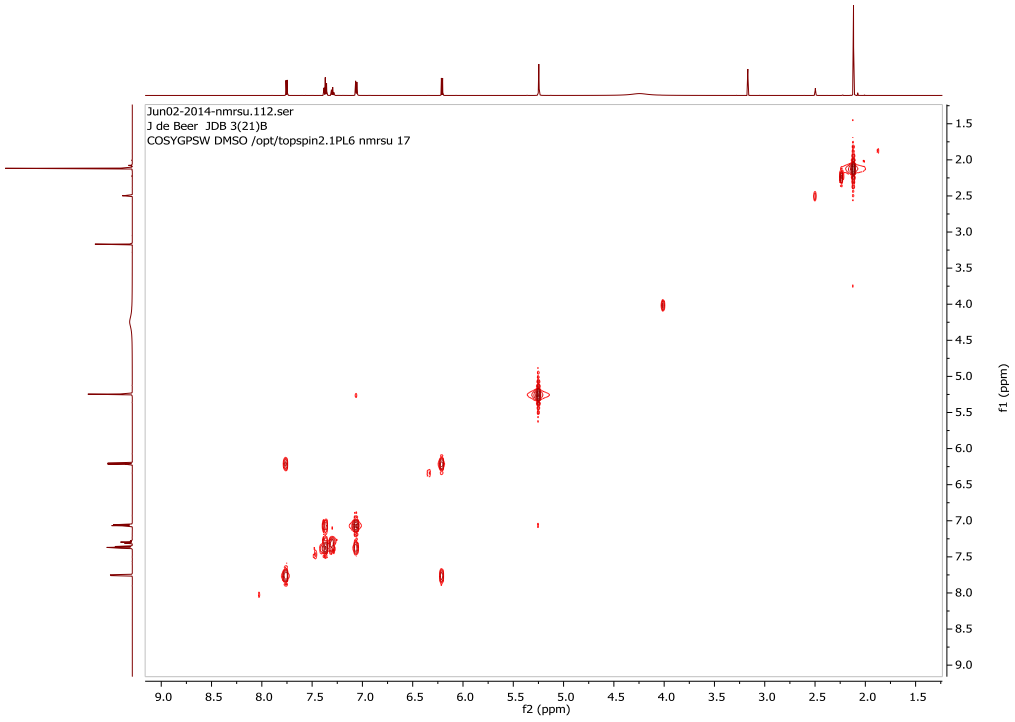

- HSQC spectrum for JDB3:

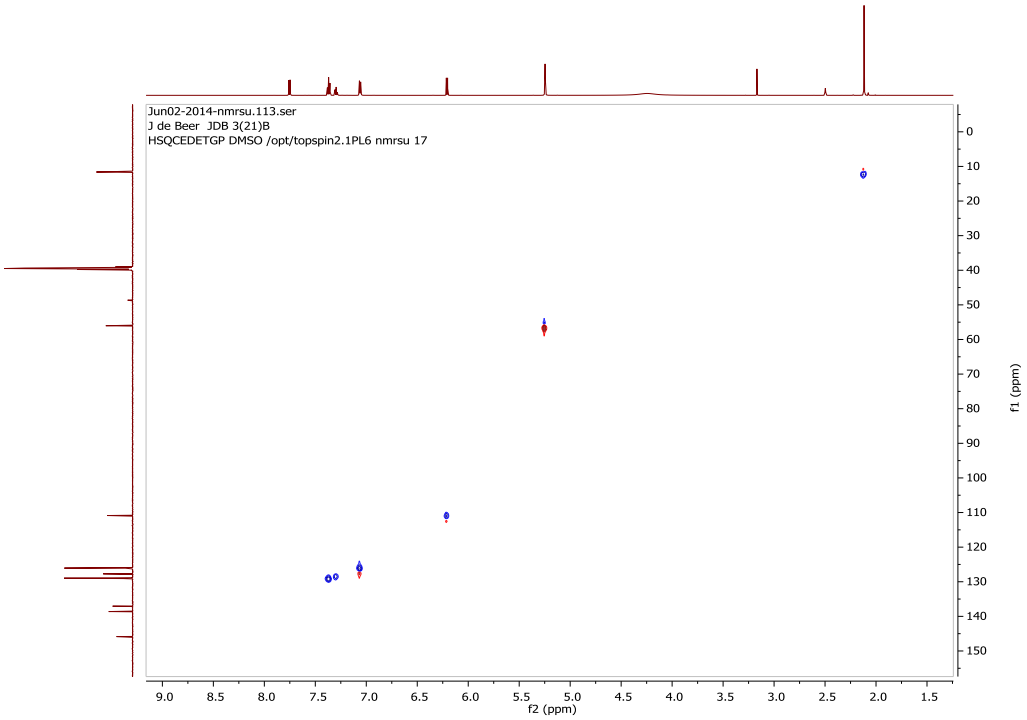

- HMBC spectrum for JDB3:

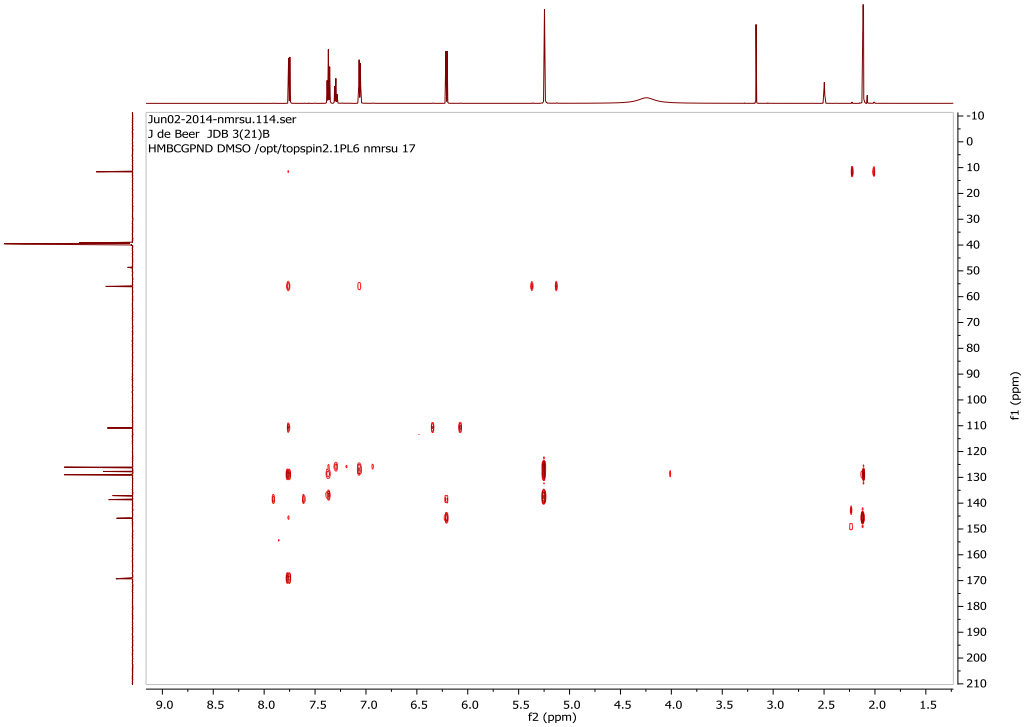

JDB4: 3-Hydroxy-2-methyl-1-(2-phenylethyl)pyridin-4-one

- ^{1}H-NMR spectrum for JDB4:

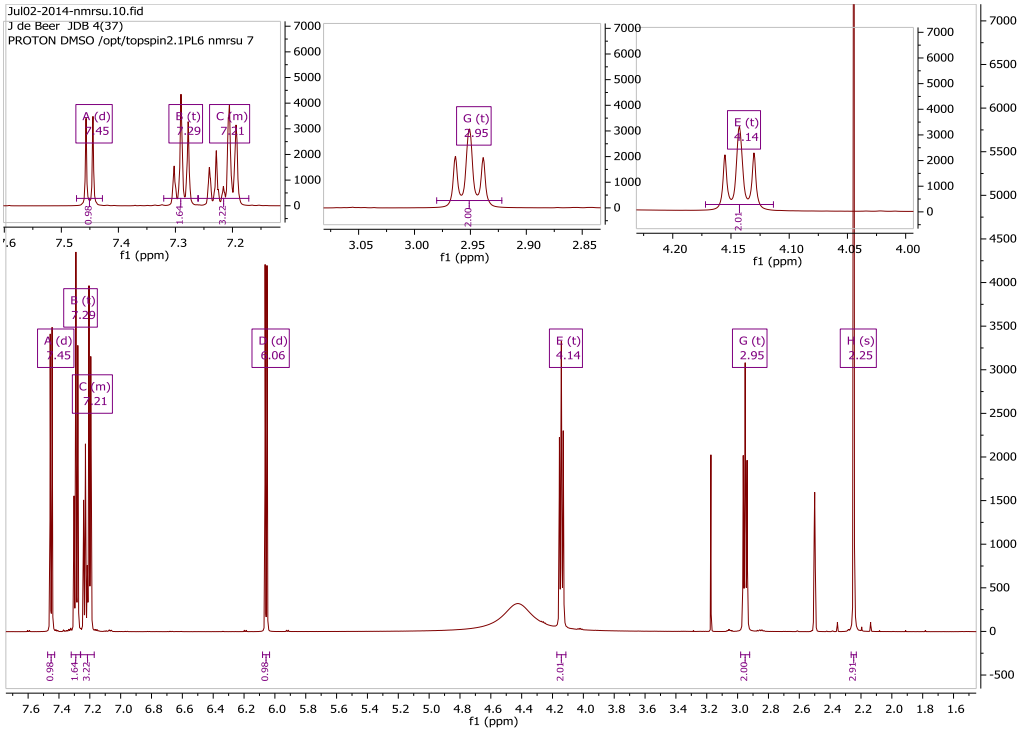

- ^{13}C-NMR spectrum for JDB4:

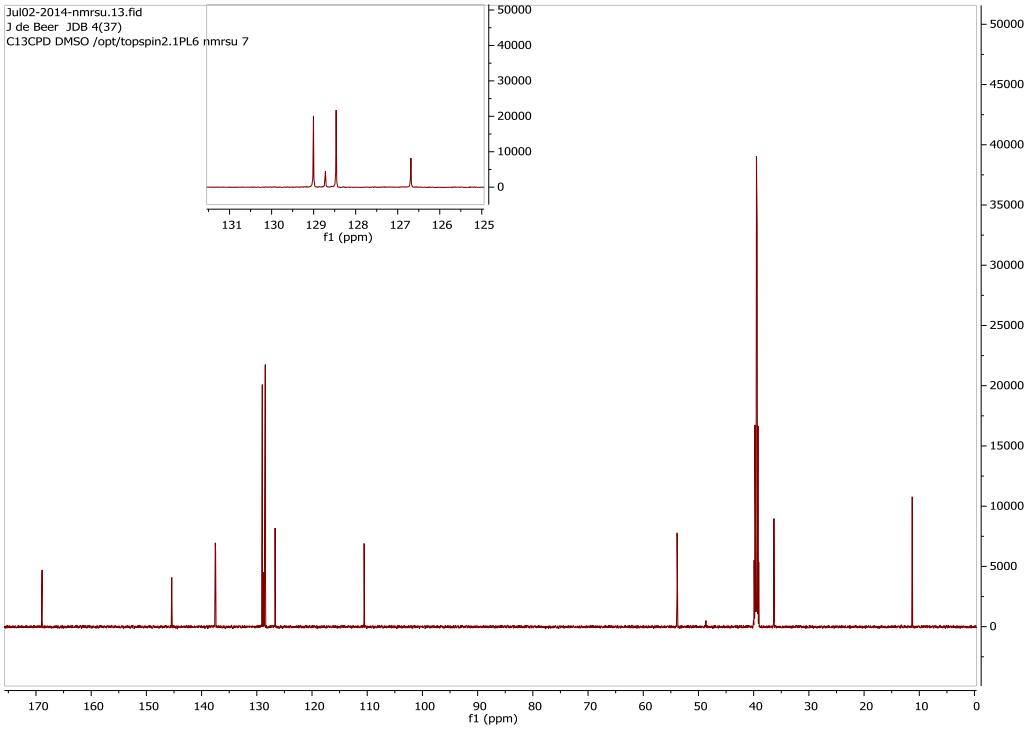

- ^{13}C-NMR, DEPT90 spectrum for JDB4:

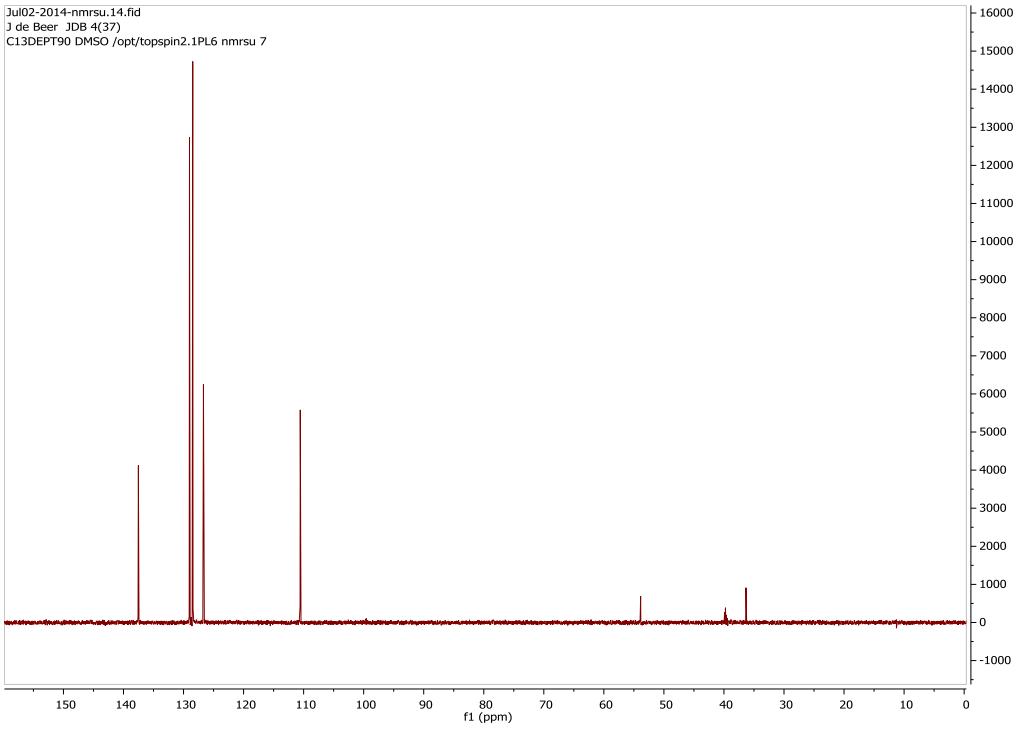

- ^{13}C-NMR, DEPT135 spectrum for JDB4:

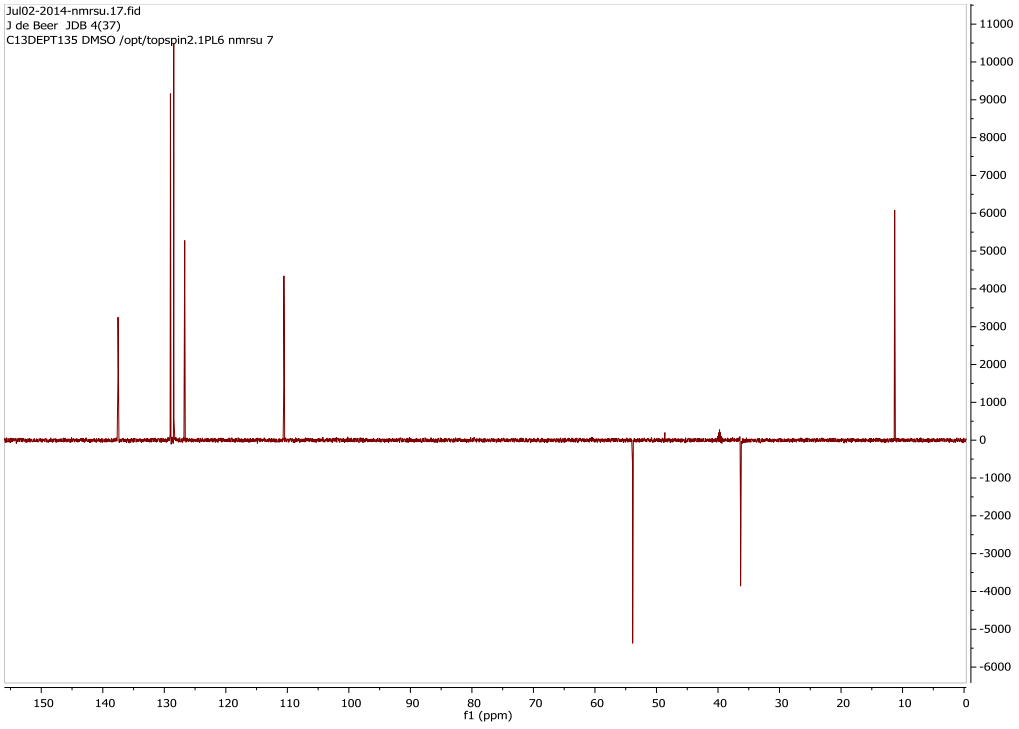

- COSY spectrum for JDB4:

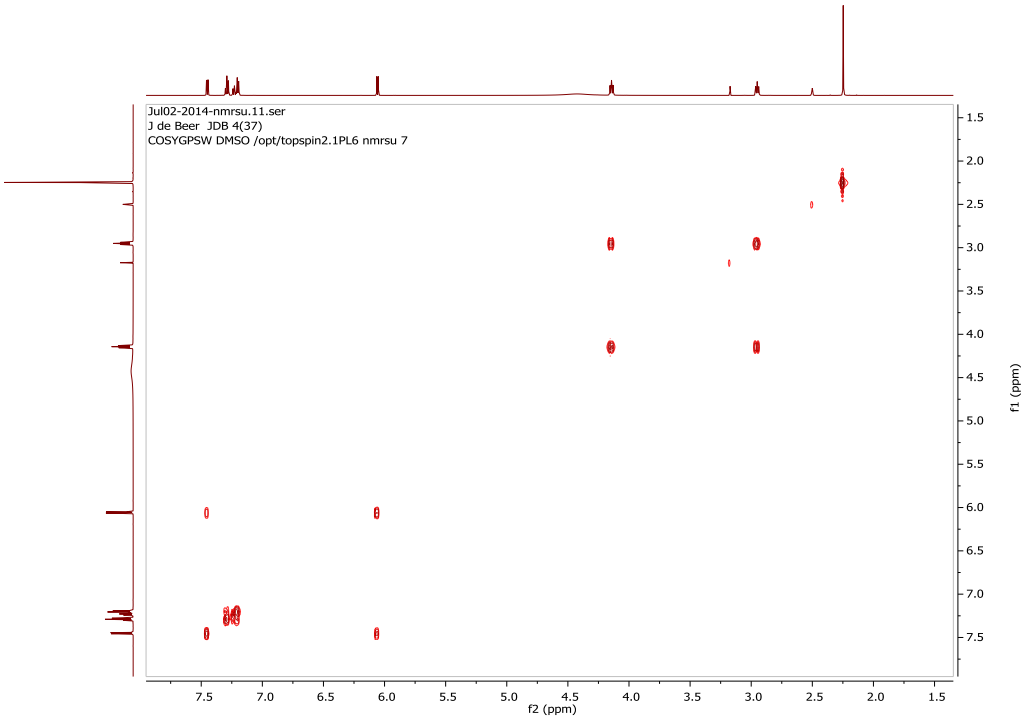

- HSQC spectrum for JDB4:

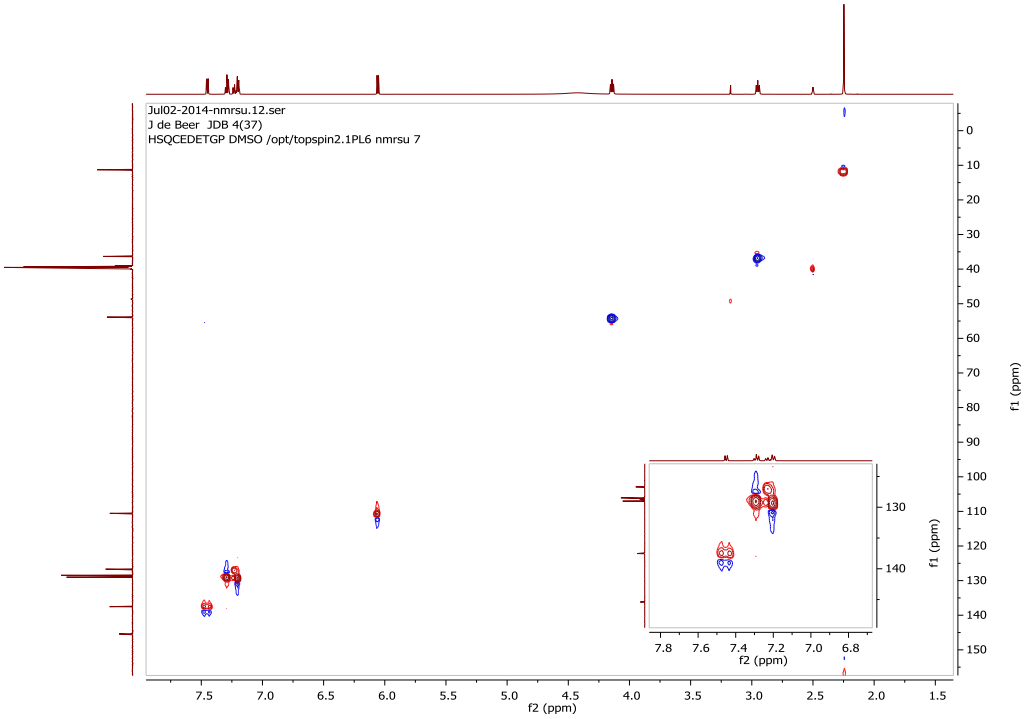

- HMBC spectrum for JDB4:

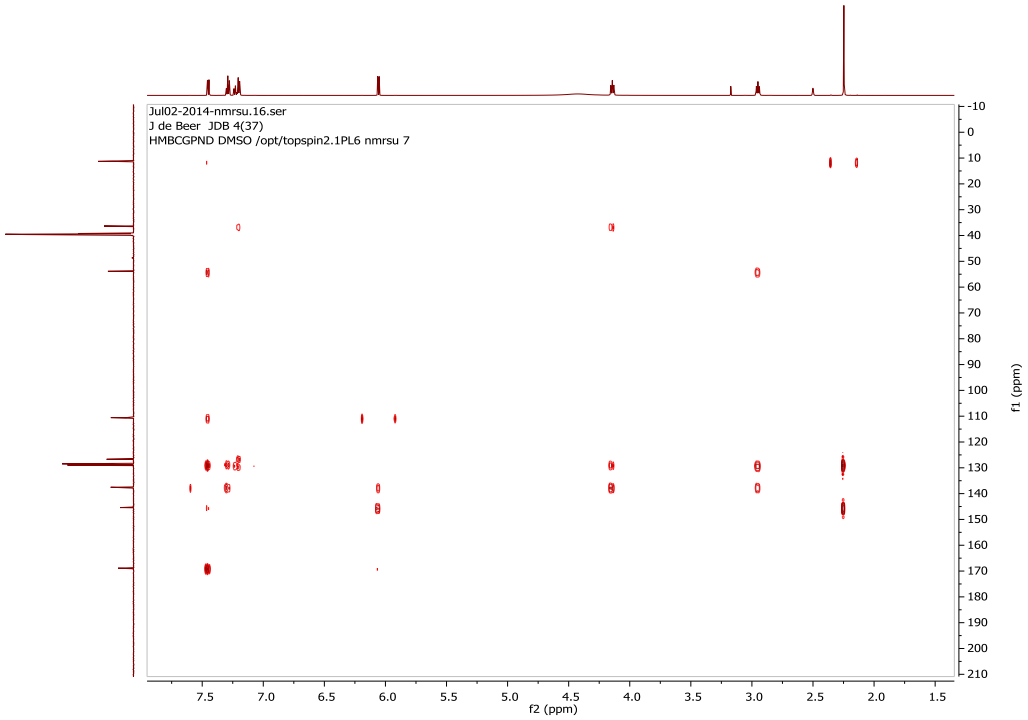

JDB5: 3-Hydroxy-2-methyl-1-(3-phenylpropyl)pyridin-4-one

- ^{1}H-NMR spectrum for JDB5:

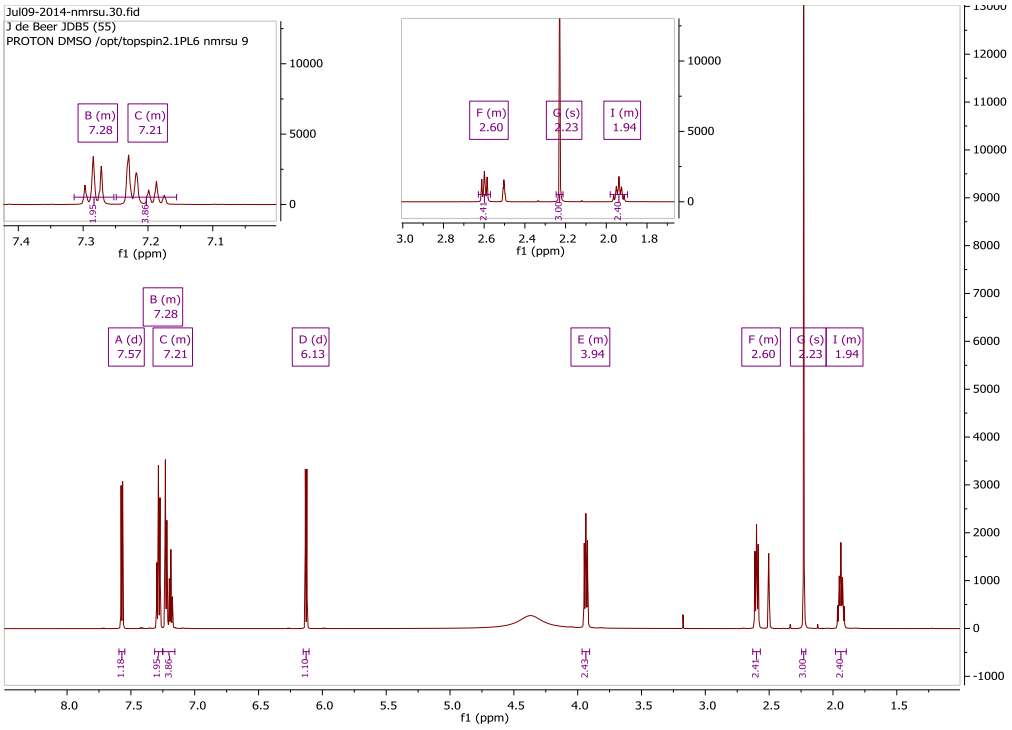

- ^{13}C-NMR spectrum for JDB5:

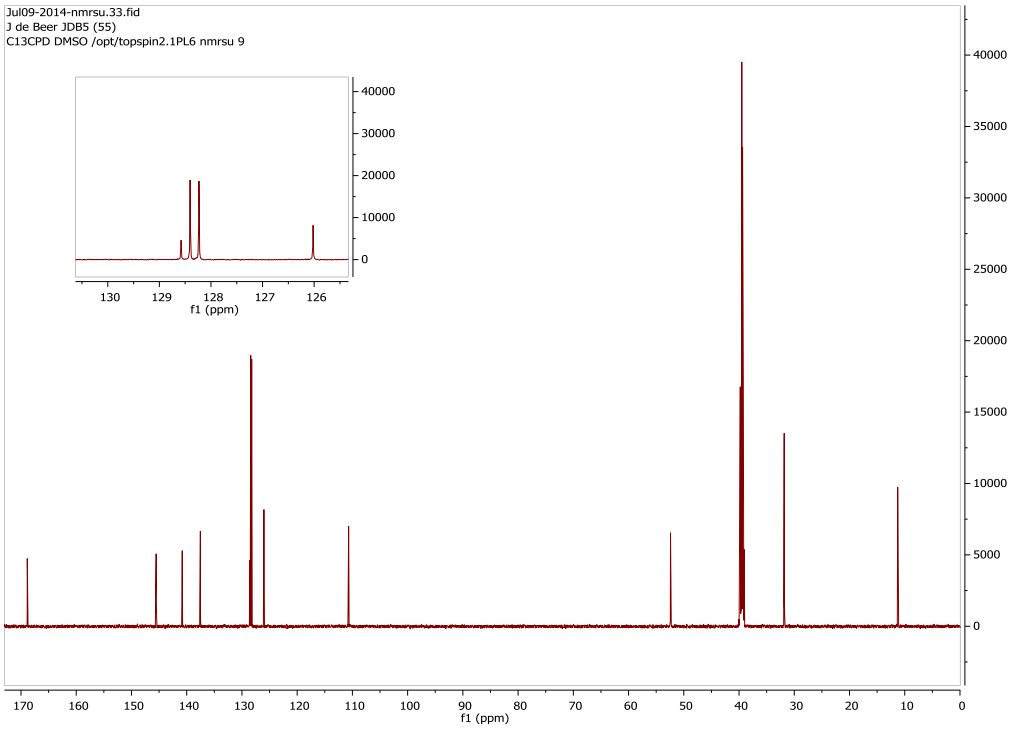

- ^{13}C-NMR, DEPT90 spectrum for JDB5:

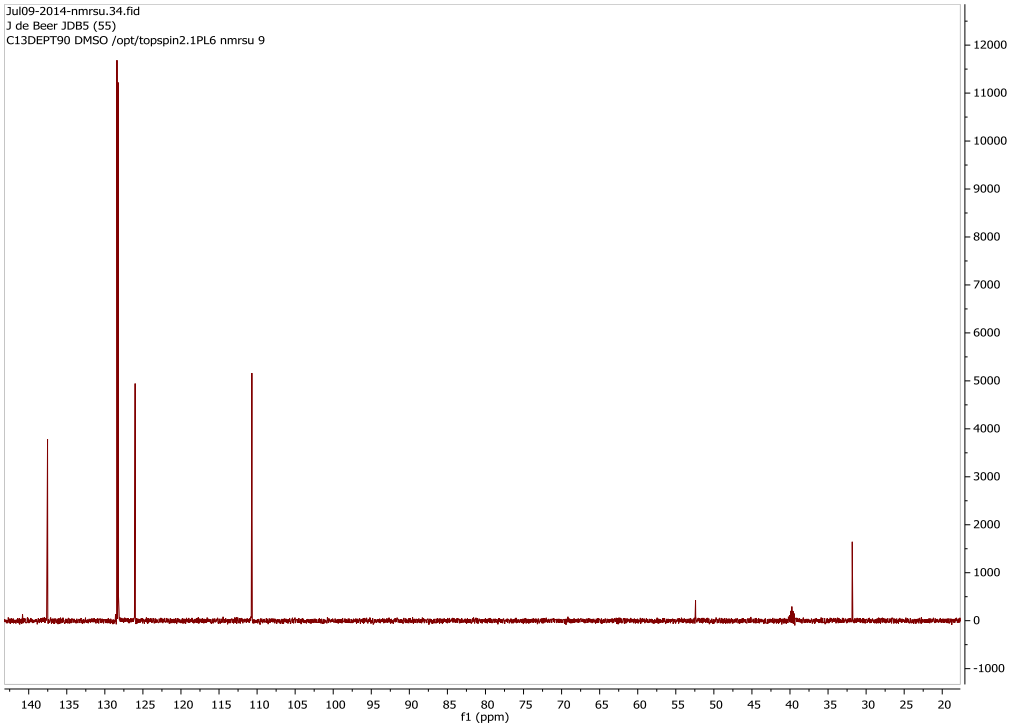

- ^{13}C-NMR, DEPT135 spectrum for JDB5:

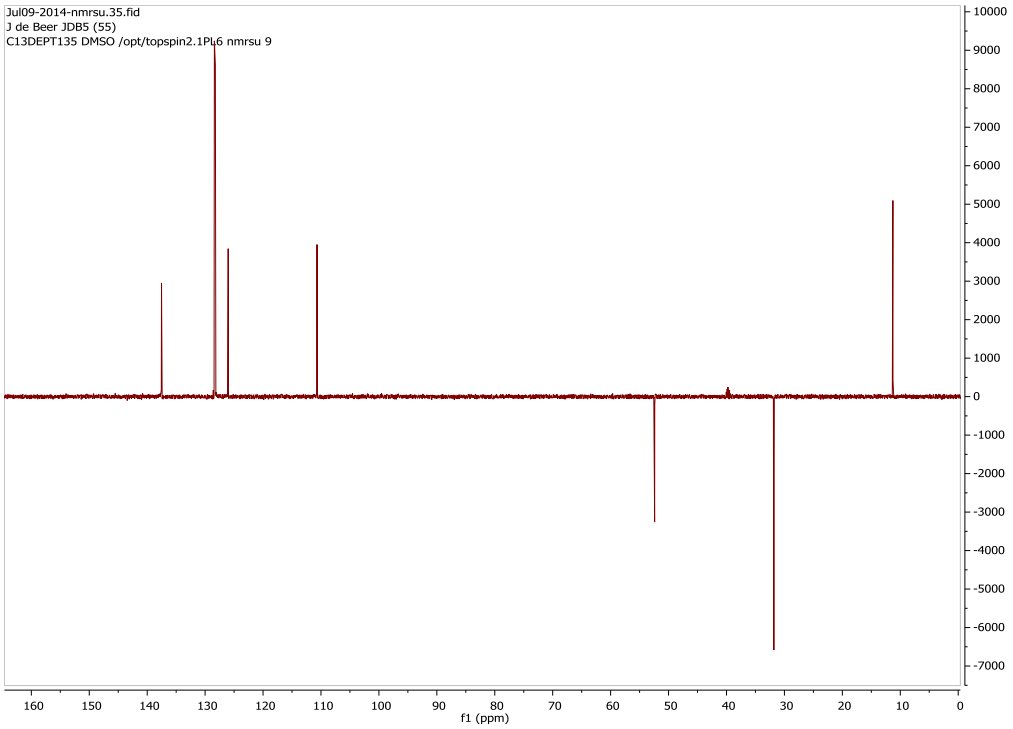

- COSY spectrum for JDB5:

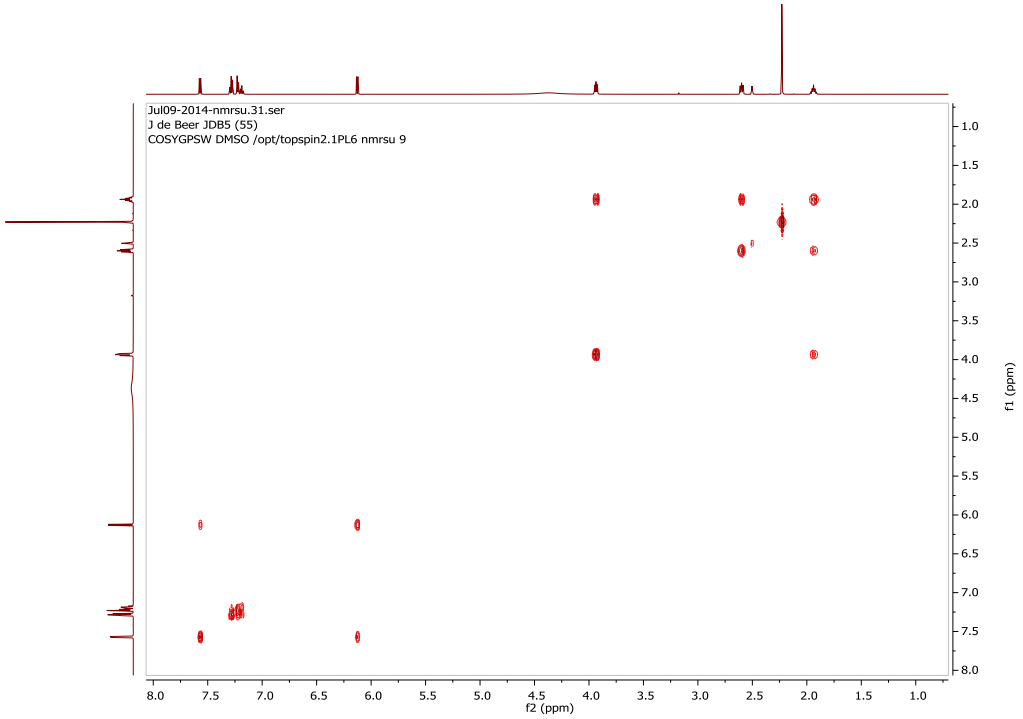

- HSCQ spectrum for JDB5:

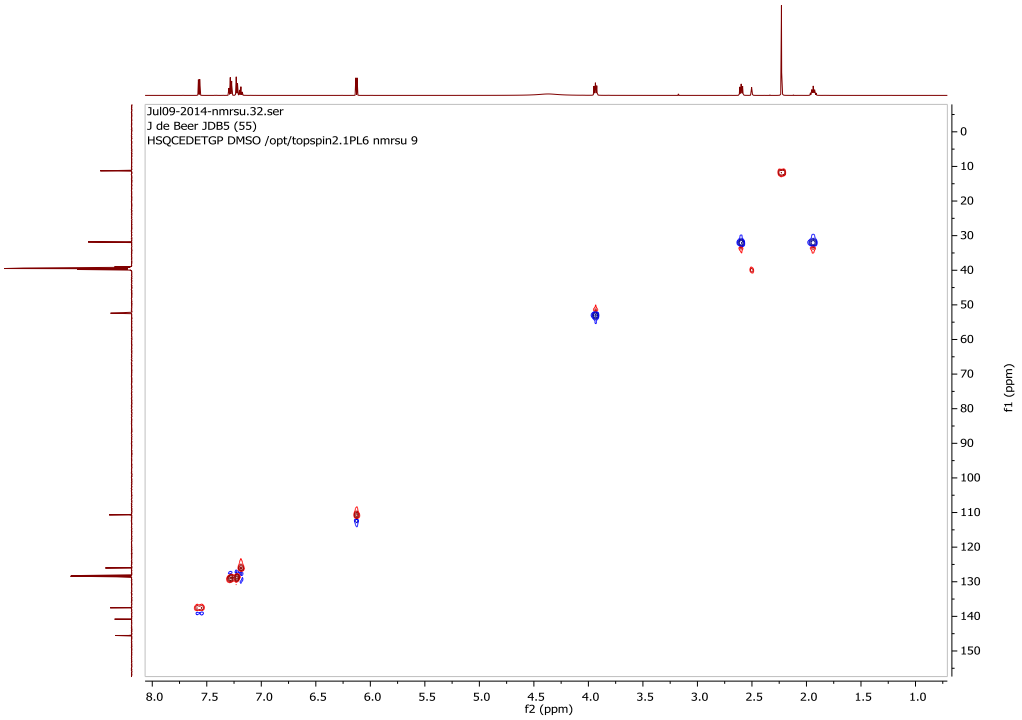

- HMBC spectrum for JDB5:

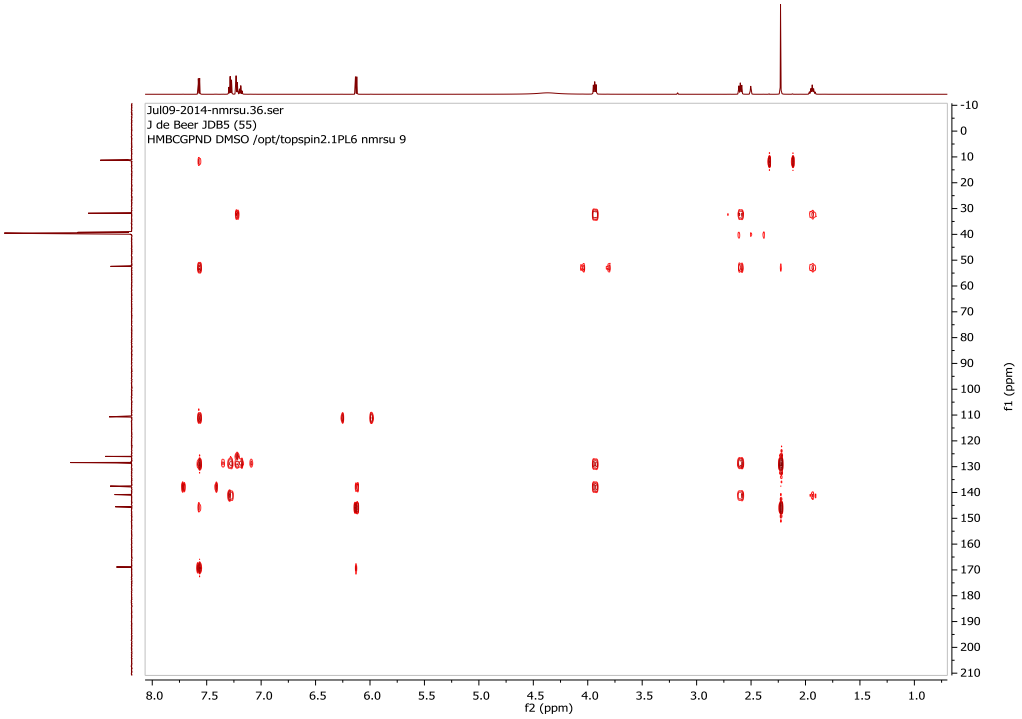

JDB9: 3-Hydroxy-2-methyl-1-(4-phenylbutyl)pyridin-4-one

- ^{1}H-NMR spectrum for JDB9:

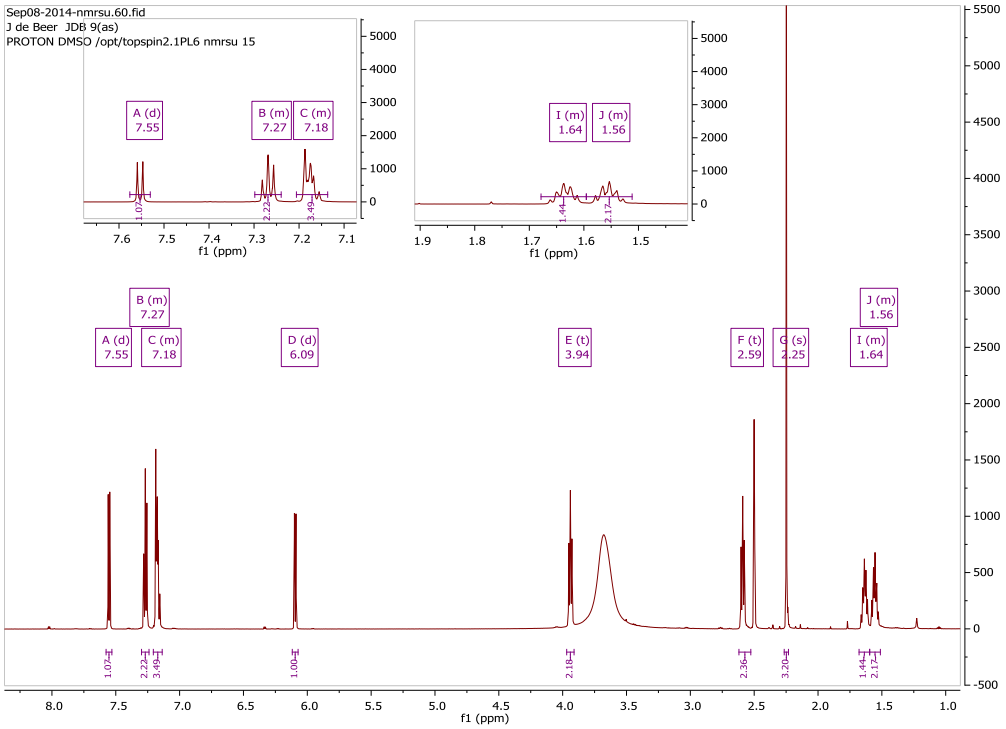

- ^{13}C-NMR spectrum for JDB9:

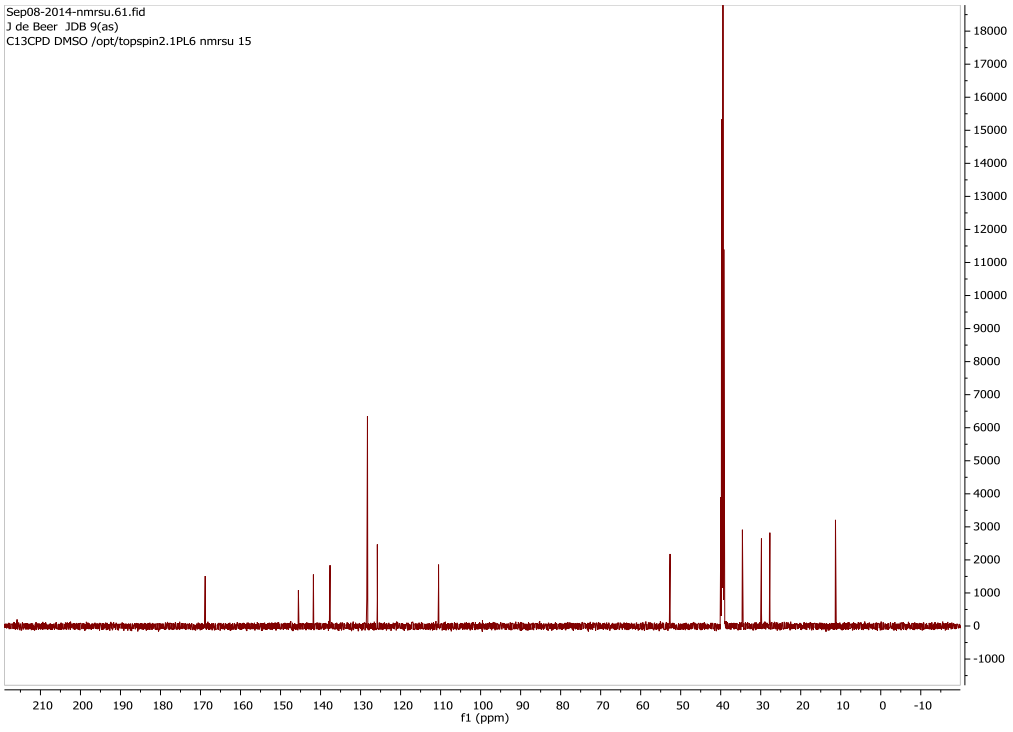

- ^{13}C-NMR, DEPT90 spectrum for JDB9:

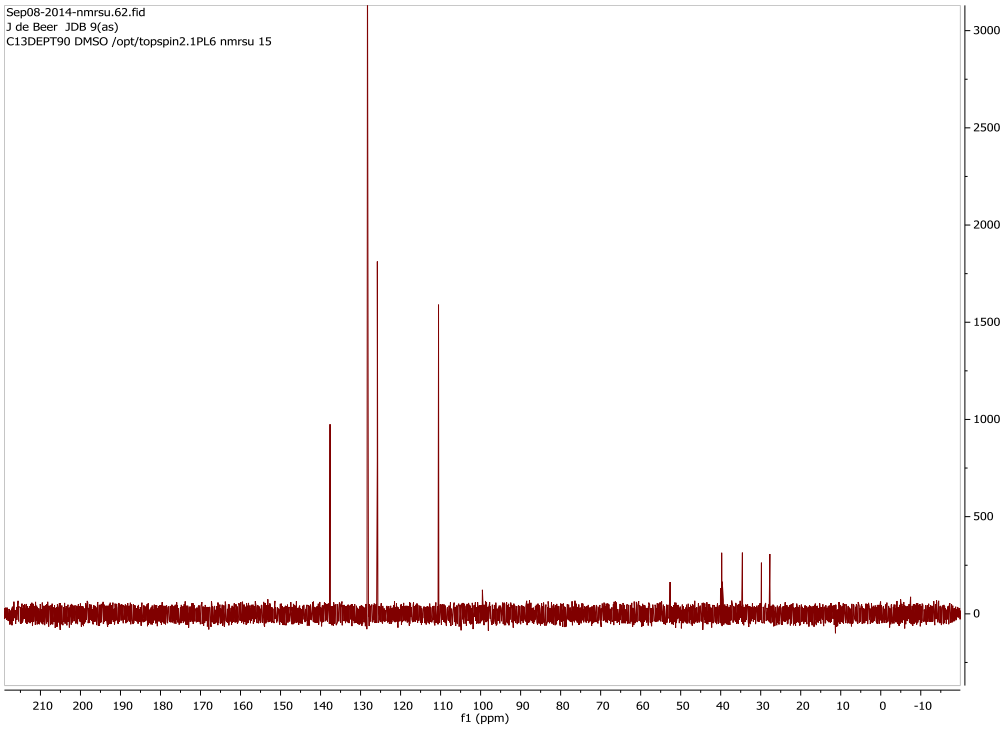

- ^{13}C-NMR, DEPT135 spectrum for JDB9:

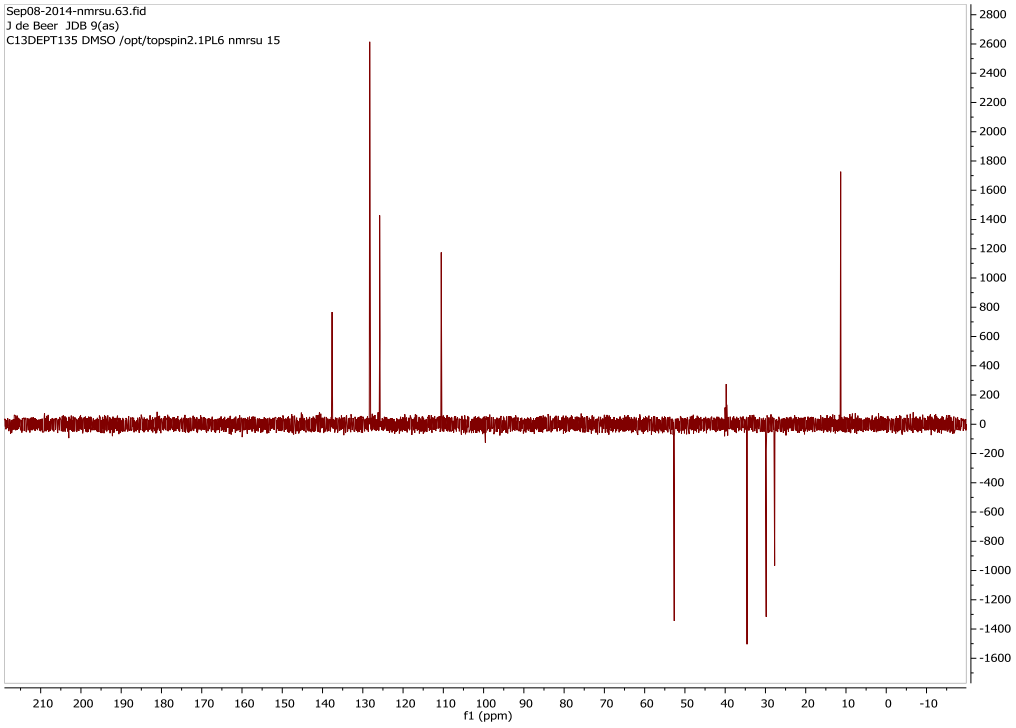

- COSY spectrum for JDB9:

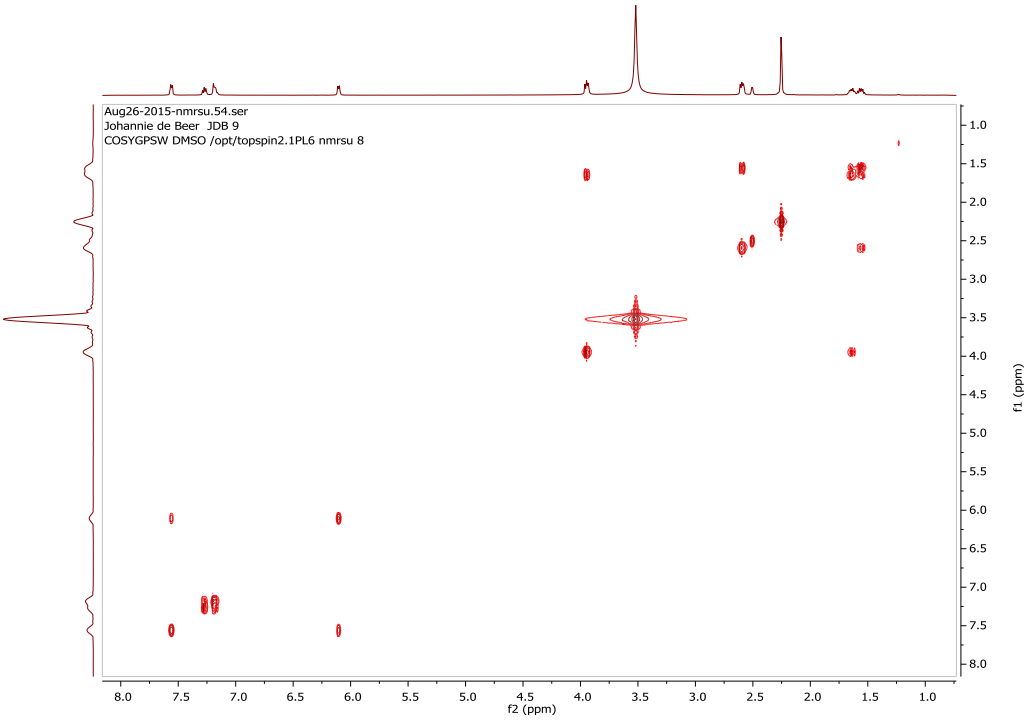

- HSQC spectrum for JDB9:

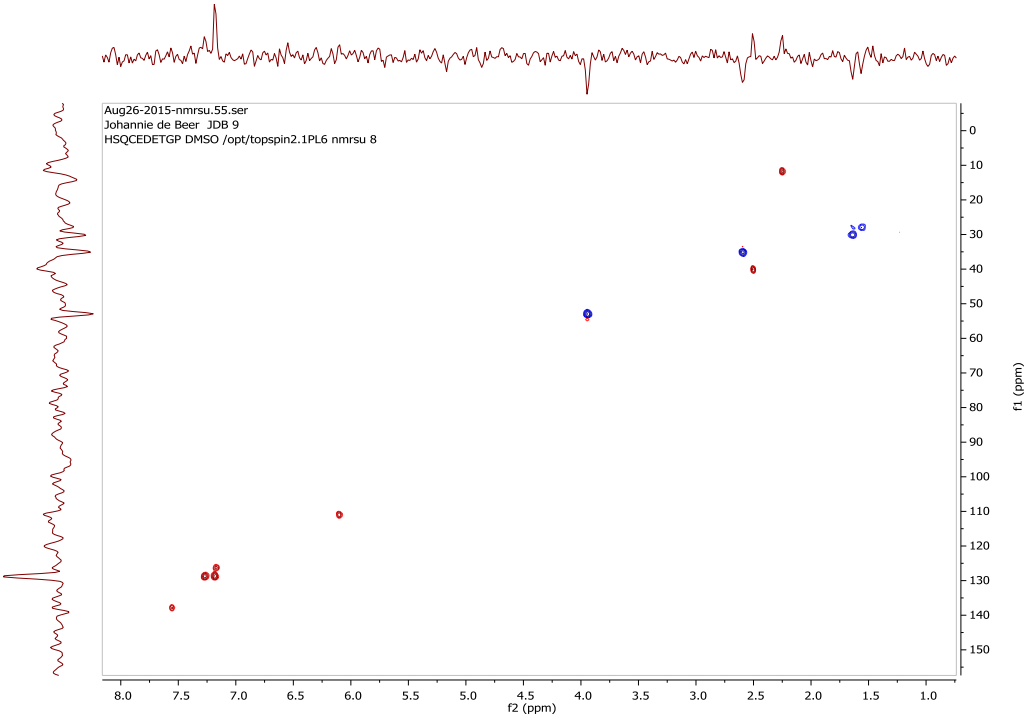

- HMBC spectrum for JDB9:

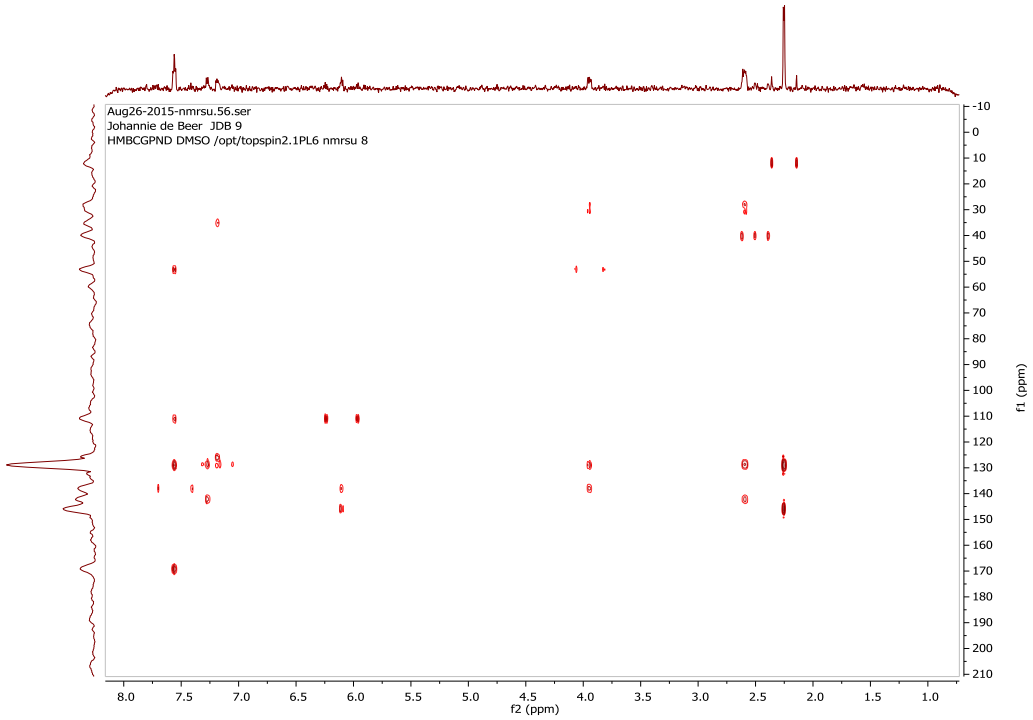

JDB10: 1-Cyclohexyl-3-hydroxy-2-methylpyridin-4-one

- ^{1}H-NMR spectrum for JDB10:

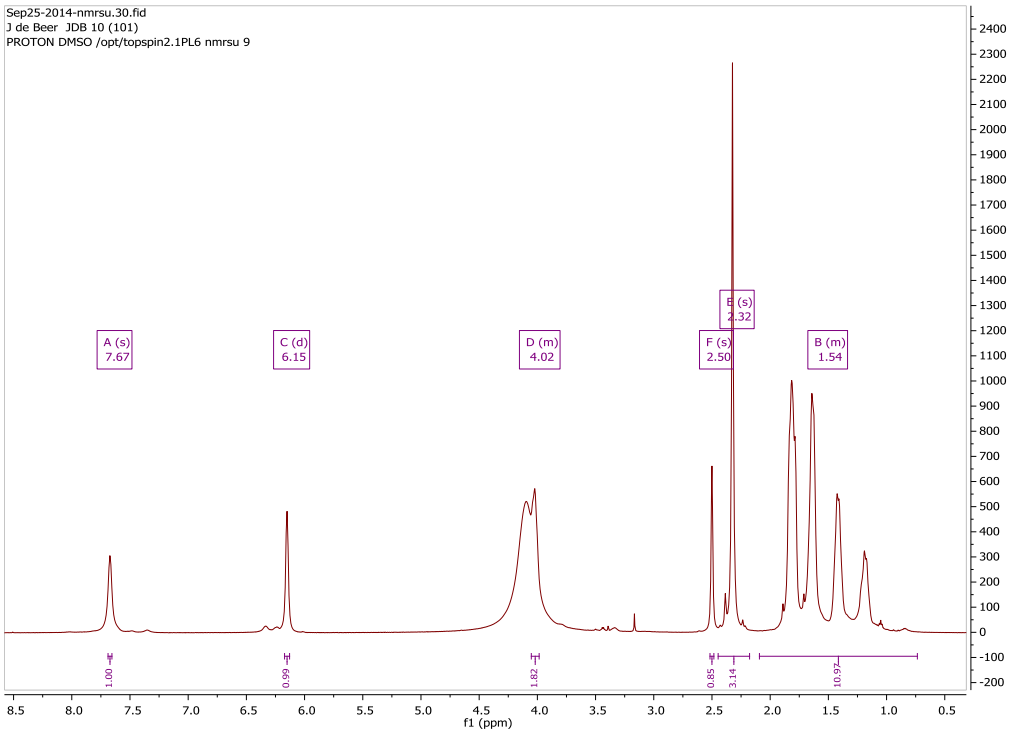

- ^{13}C-NMR spectrum for JDB10:

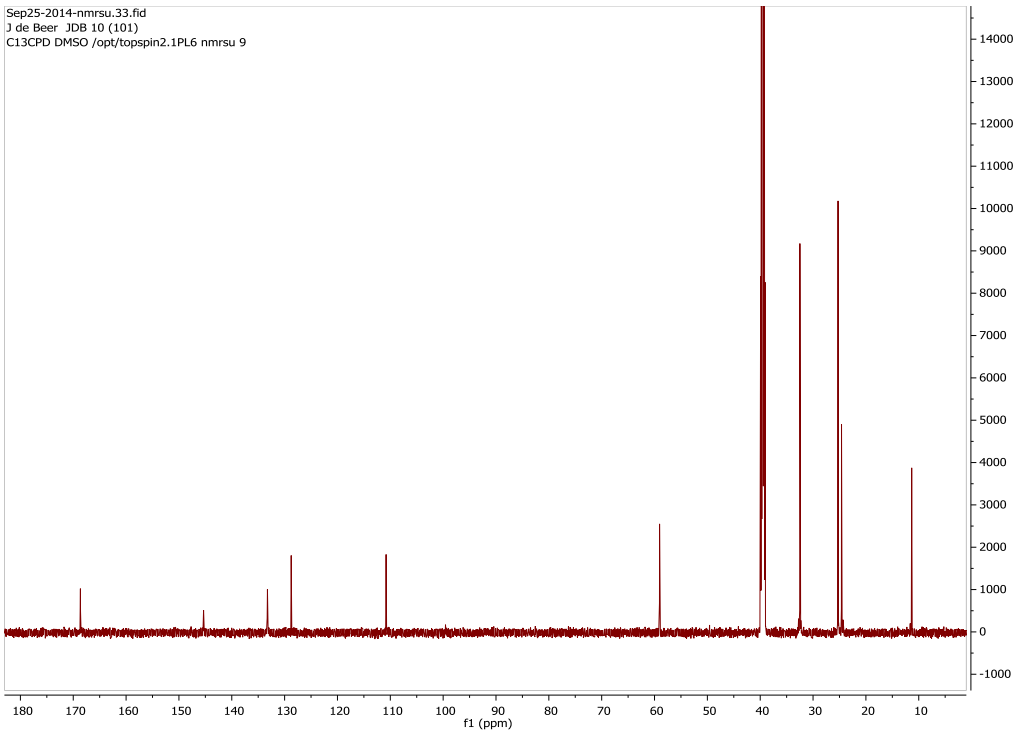

- ^{13}C-NMR, DEPT90 spectrum for JDB10:

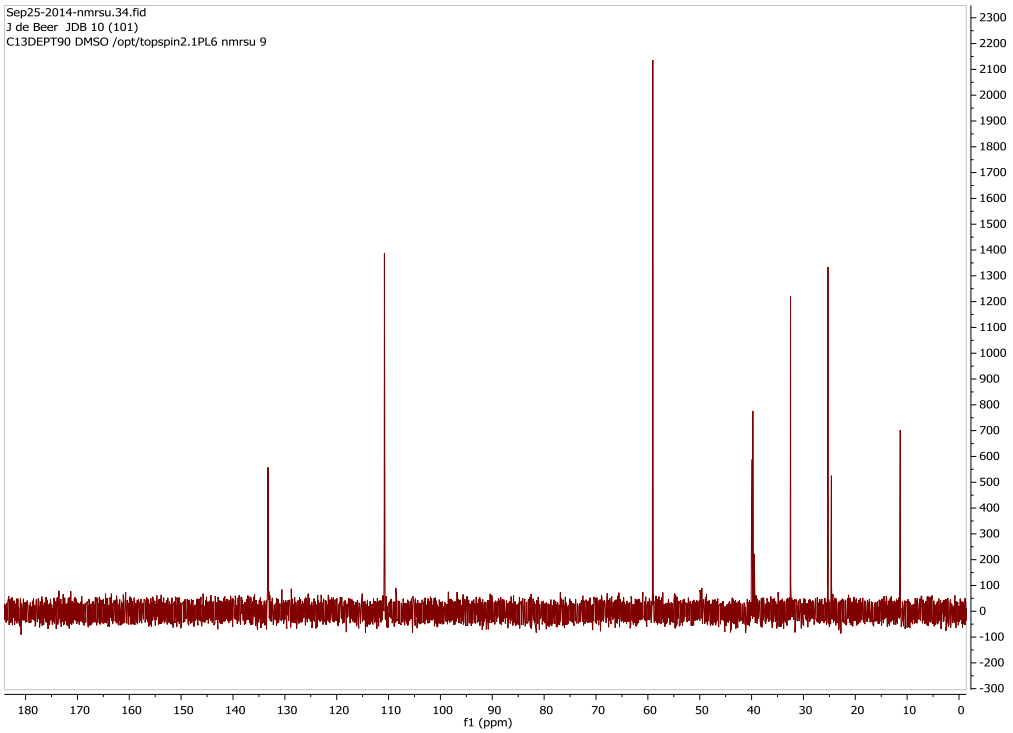

- ^{13}C-NMR, DEPT135 spectrum for JDB10:

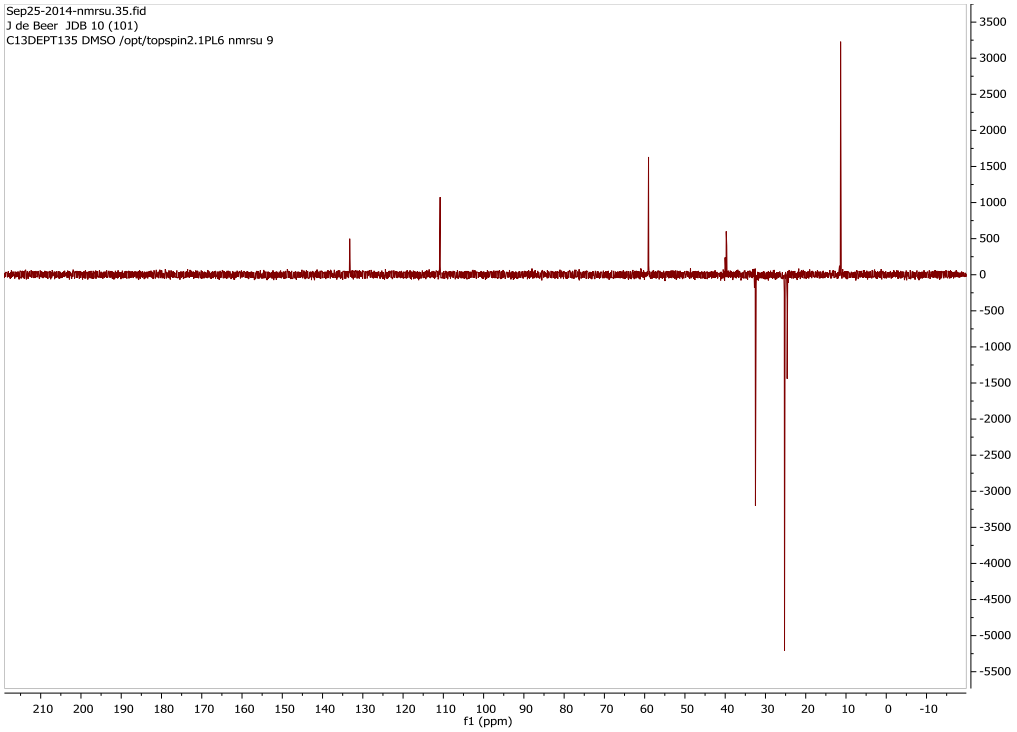

- COSY spectrum for JDB10:

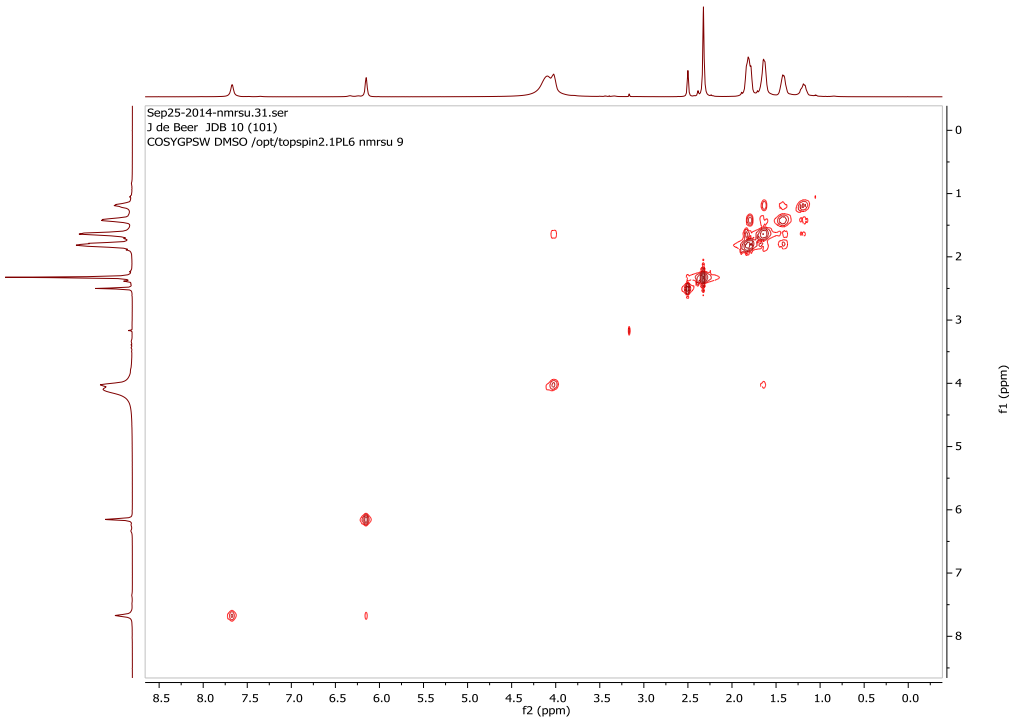

- HSQC spectrum for JDB10:

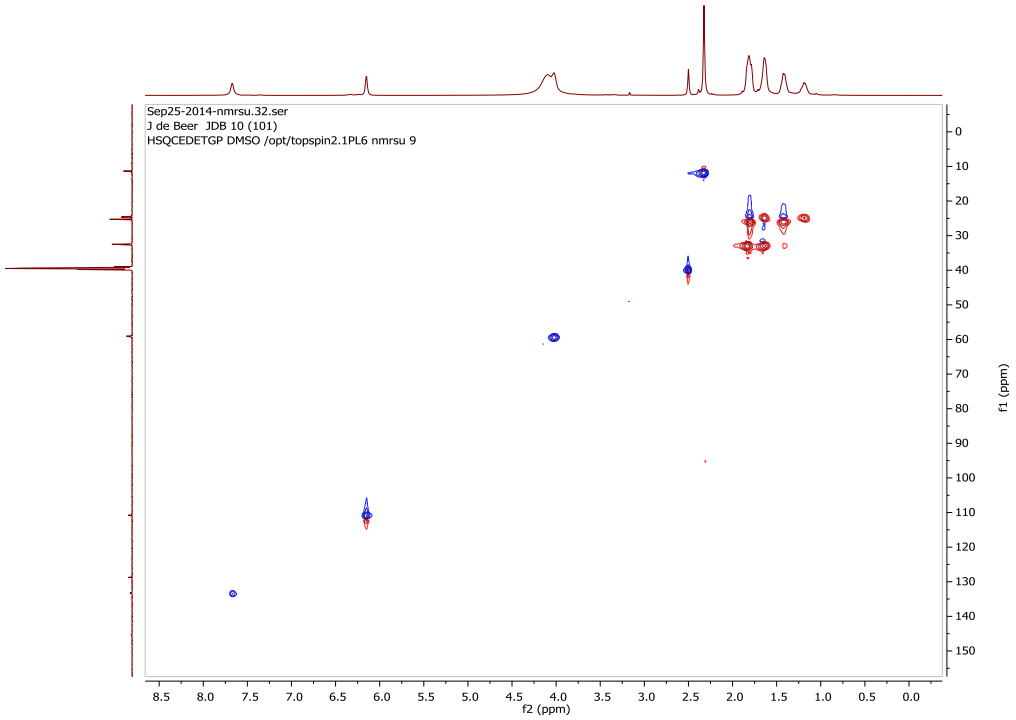

- HMBC spectrum for JDB10:

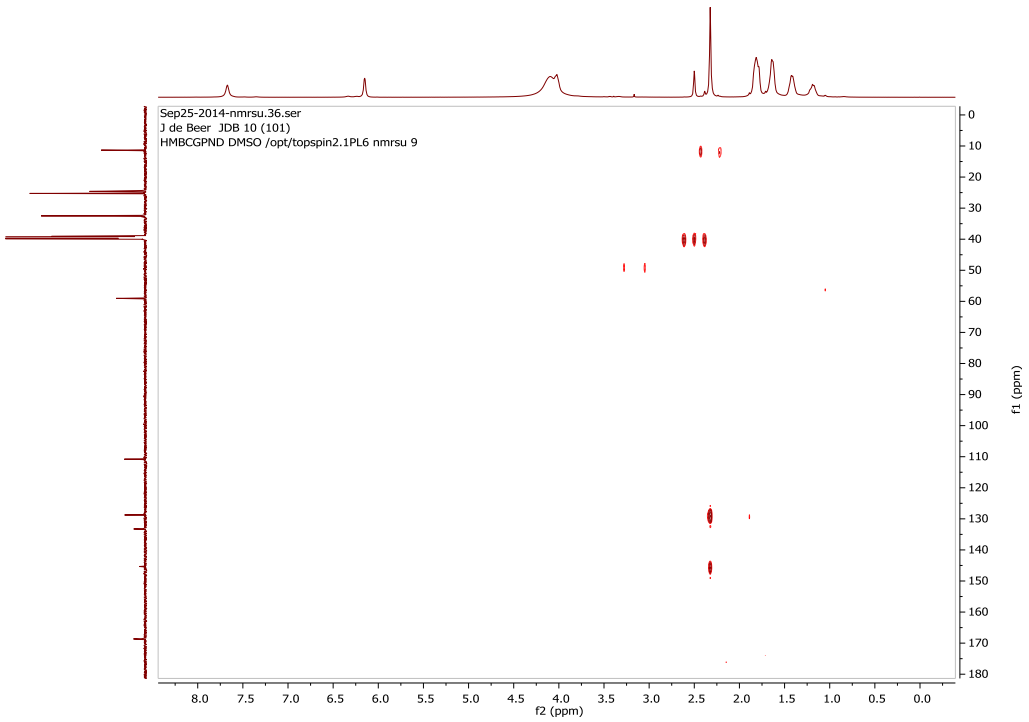

JDB11: 1-Cyclopentyl-3-hydroxy-2-methylpyridin-4-one

- ^{1}H-NMR spectrum for JDB11:

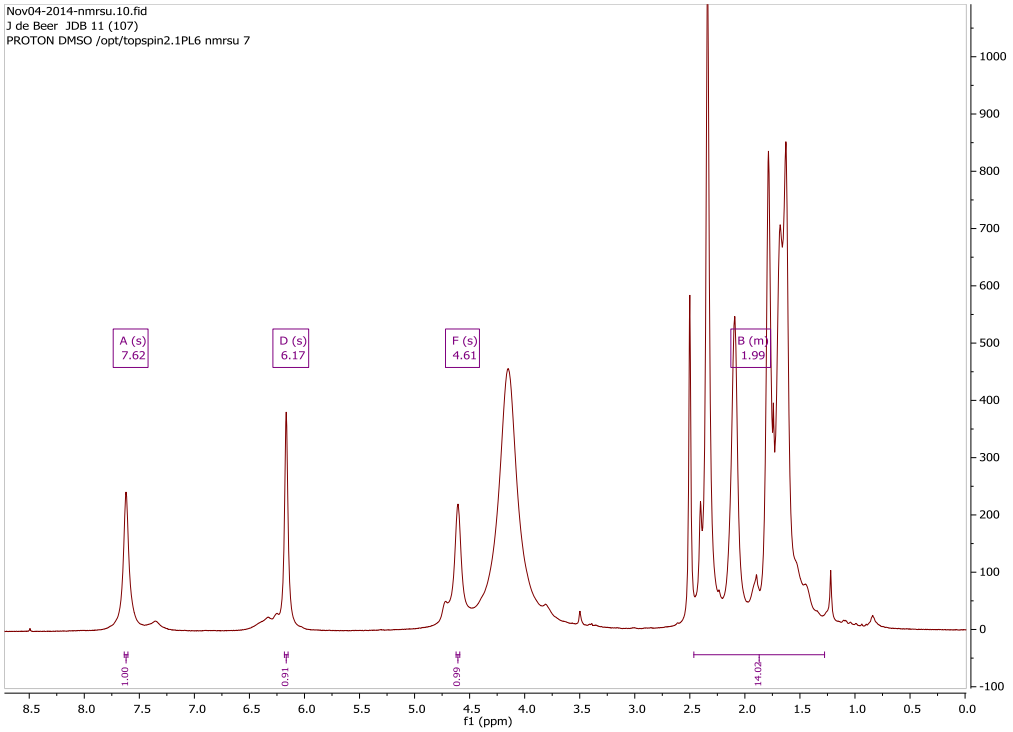

- ^{13}C-NMR spectrum for JDB11:

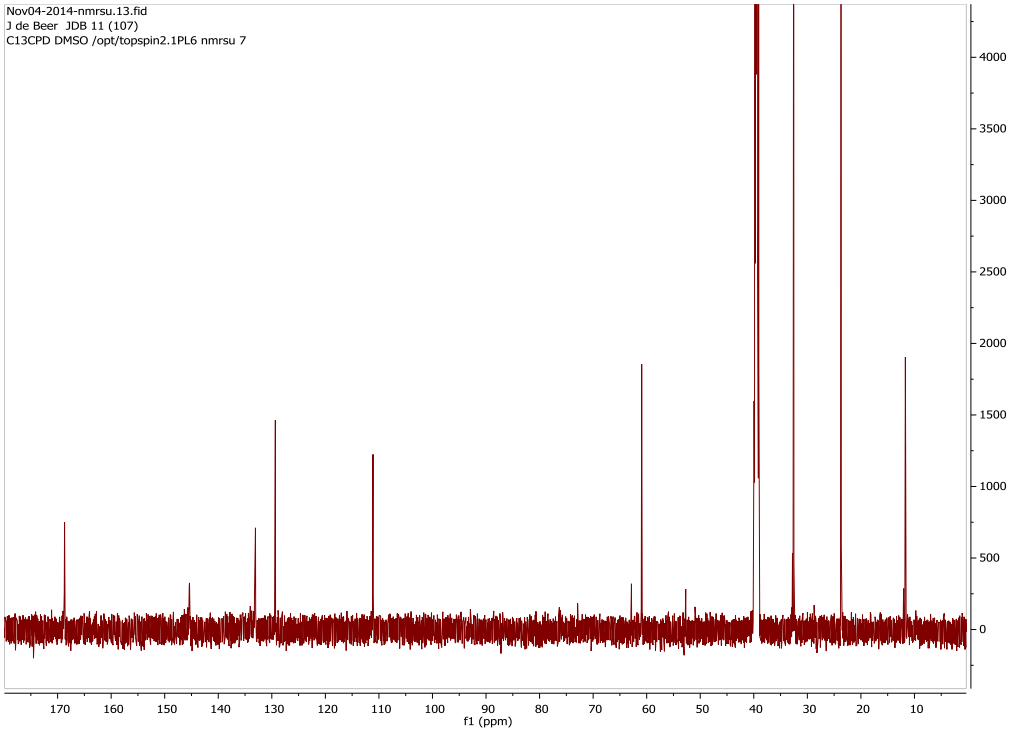

- ^{13}C-NMR, DEPT90 spectrum for JDB11:

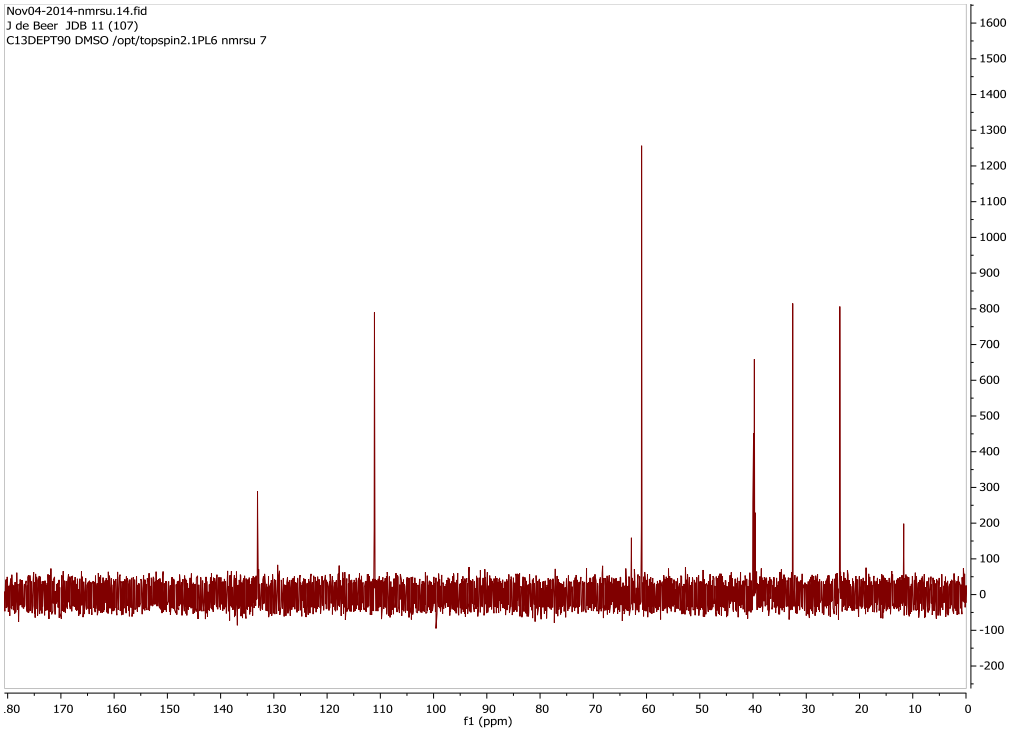

- ^{13}C-NMR, DEPT135 spectrum for JDB11:

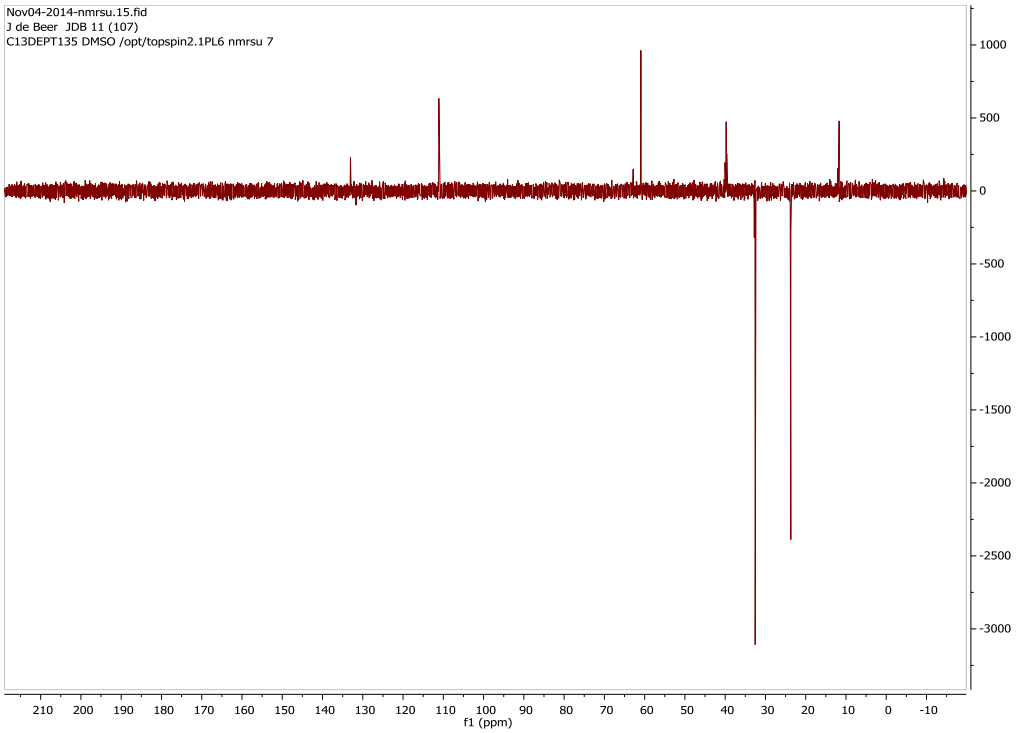

- COSY spectrum for JDB11:

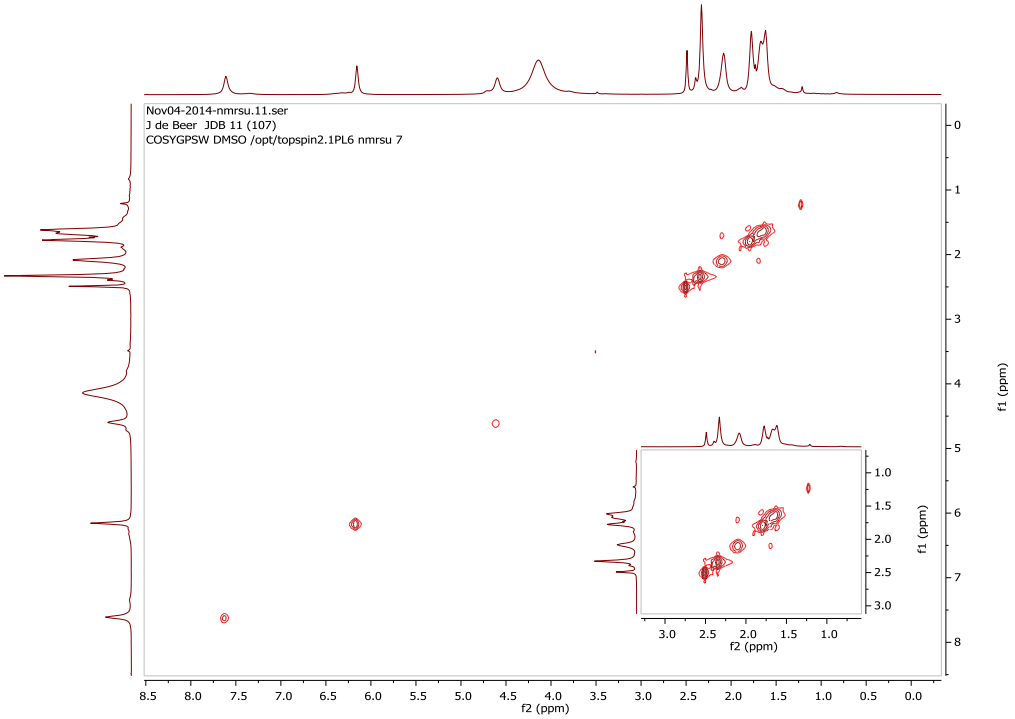

- HSQC spectrum for JDB11:

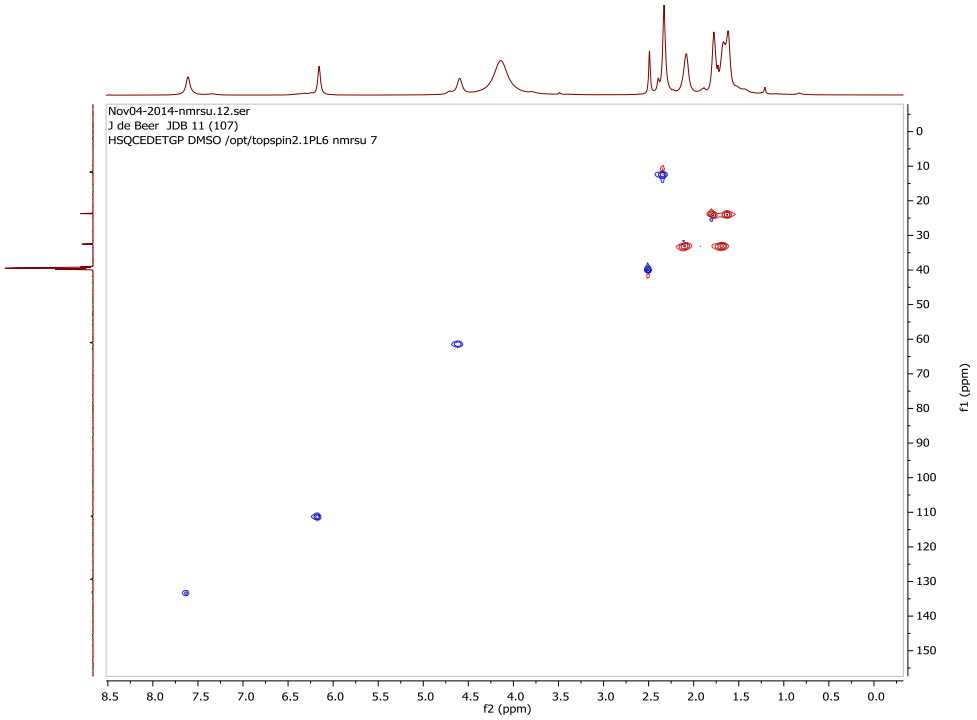

- HMBC spectrum for JDB11:

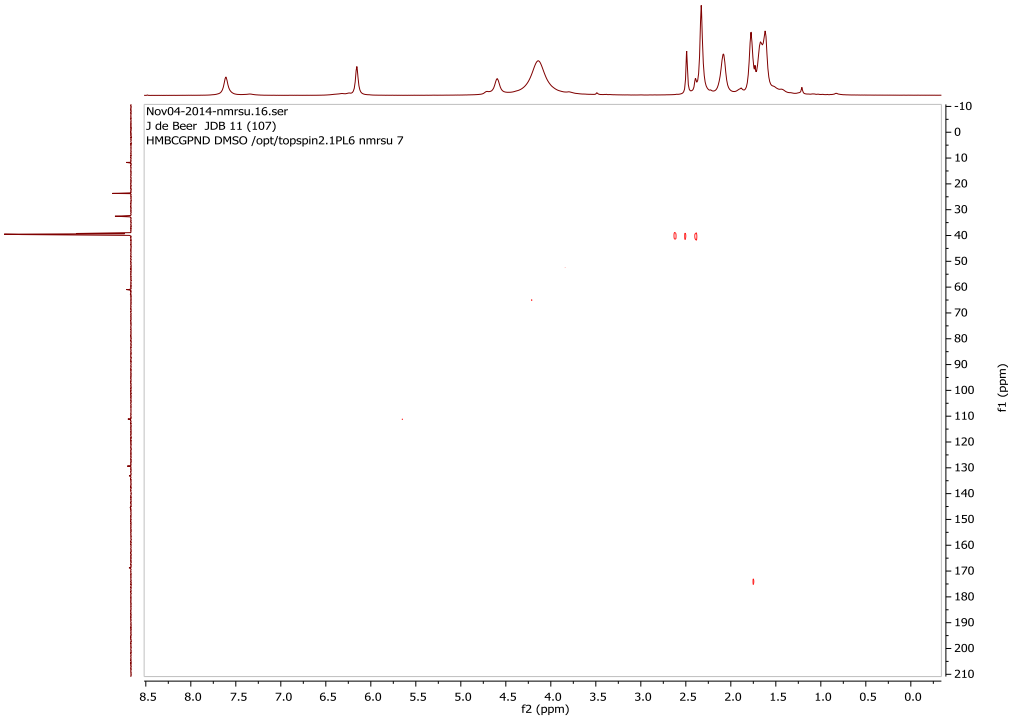

JDB12: 1-(3-Chlorophenyl)-3-hydroxy-2-methylpyridin-4-one

- ^{1}H-NMR spectrum for JDB12:

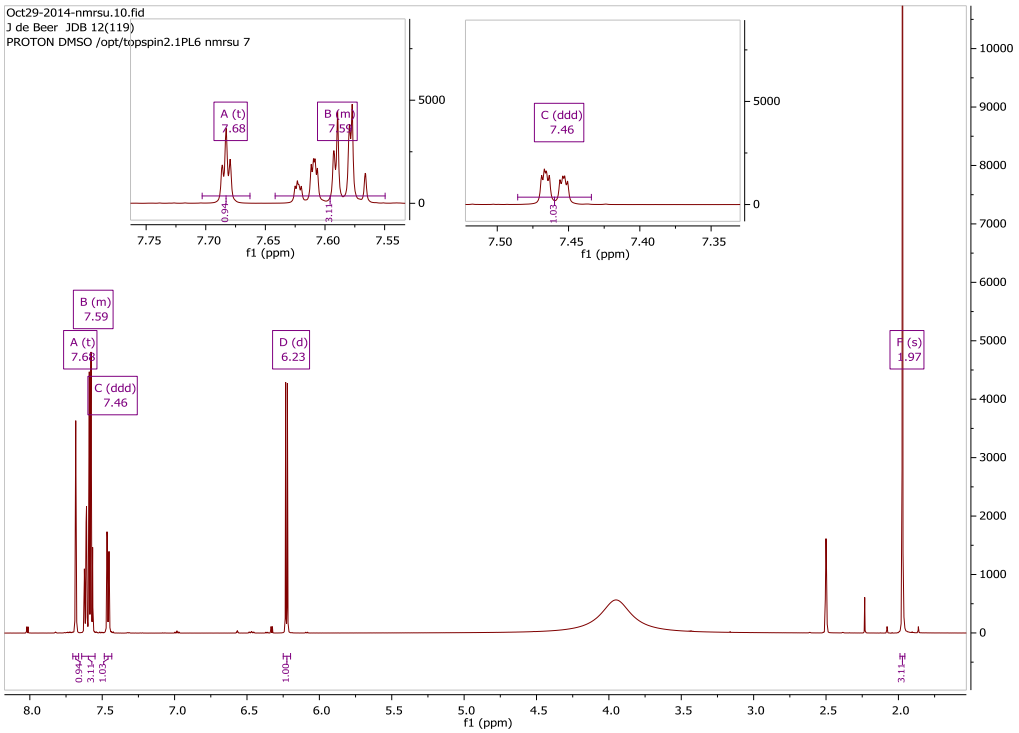

- ^{13}C-NMR spectrum for JDB12:

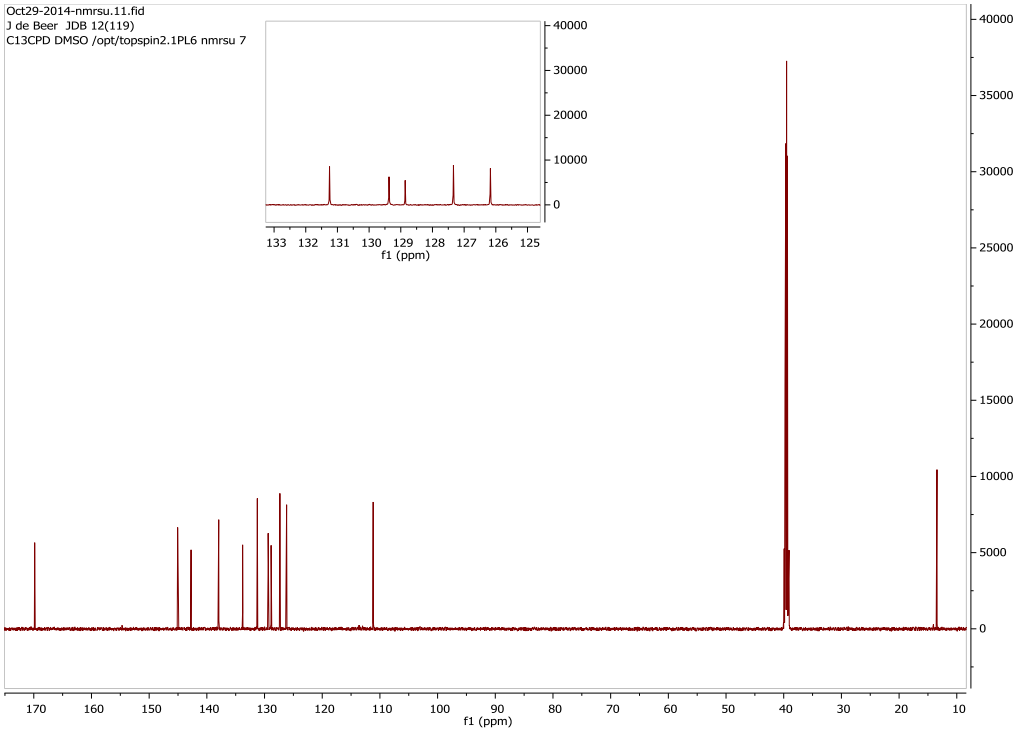

- ^{13}C-NMR, DEPT90 spectrum for JDB12:

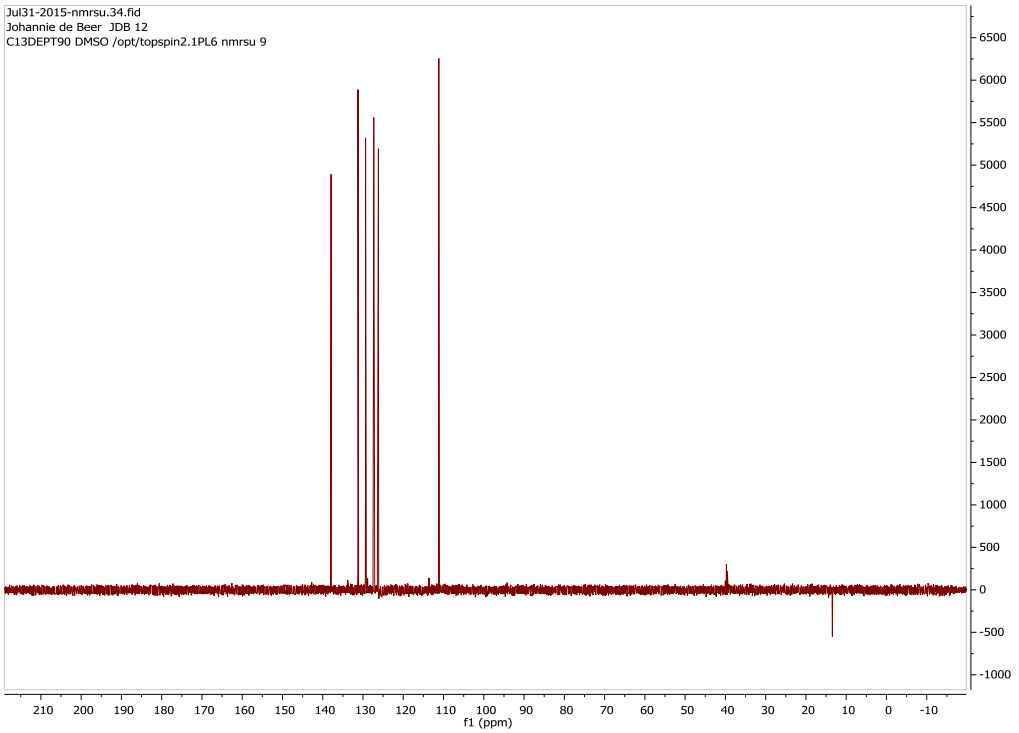

- ^{13}C-NMR, DEPT135 spectrum for JDB12:

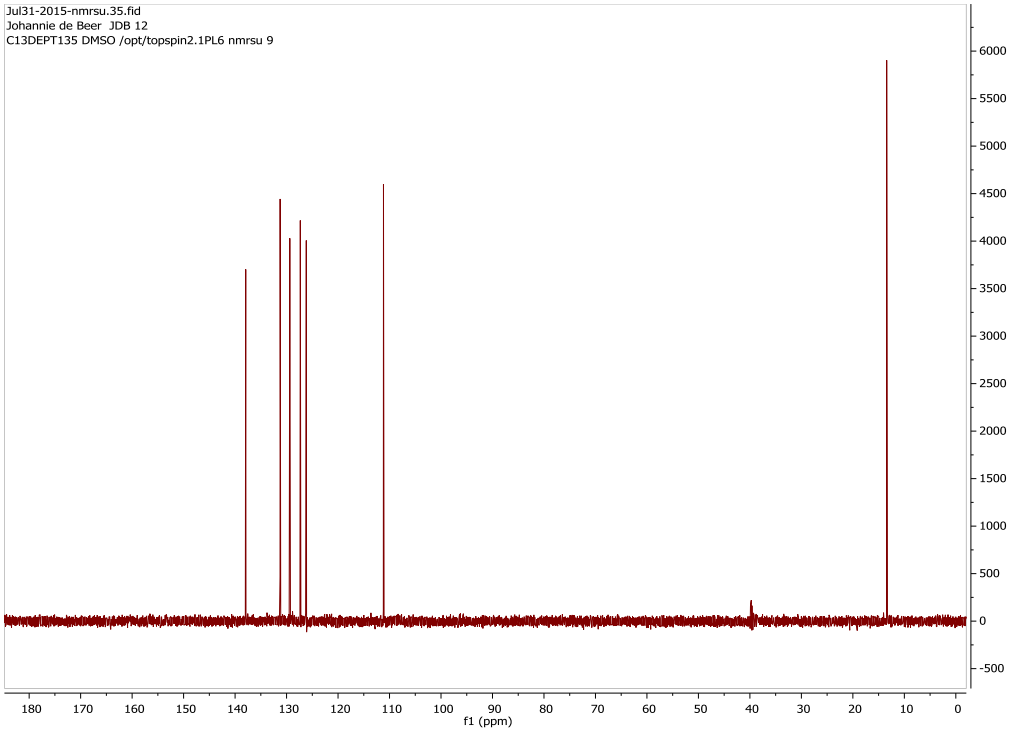

- COSY spectrum for JDB12:

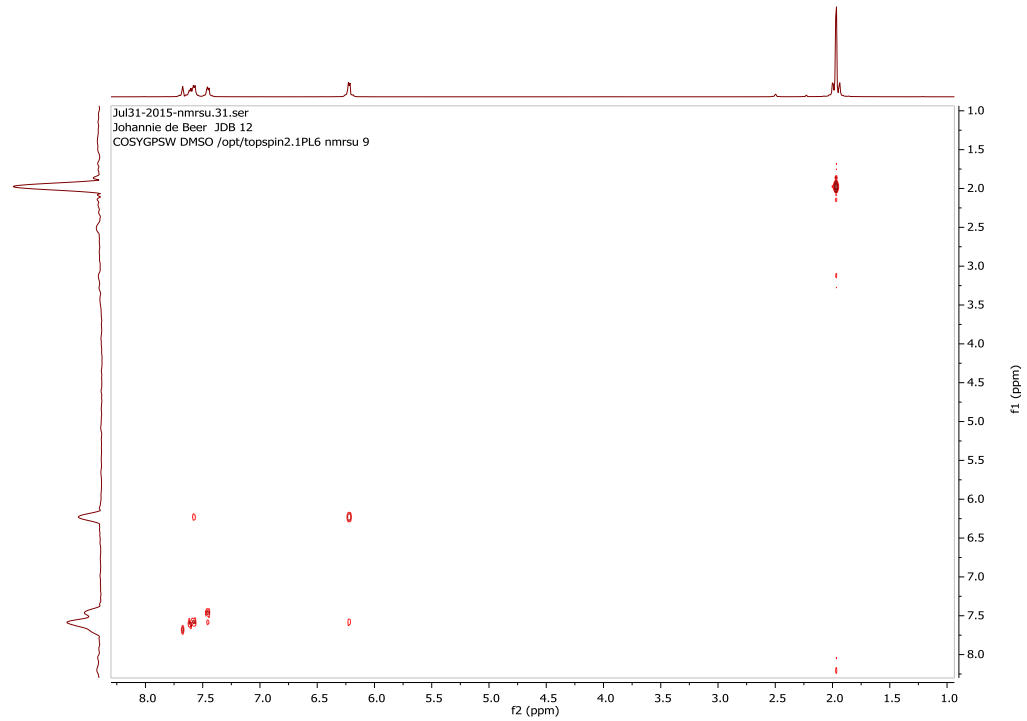

- HSQC spectrum for JDB12:

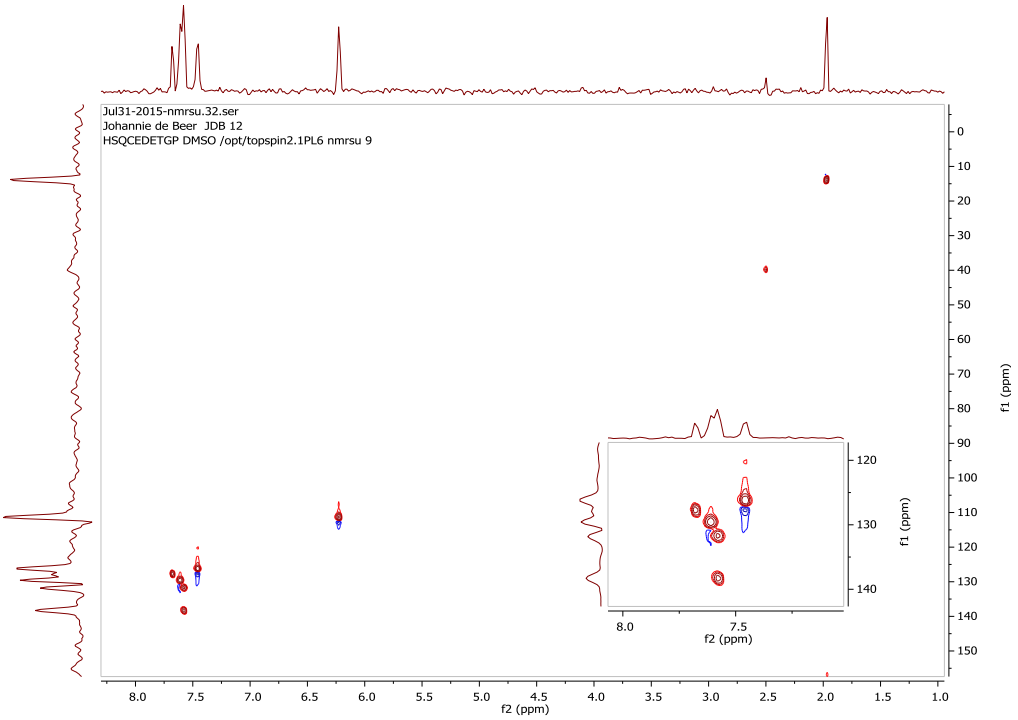

- HMBC spectrum for JDB12:

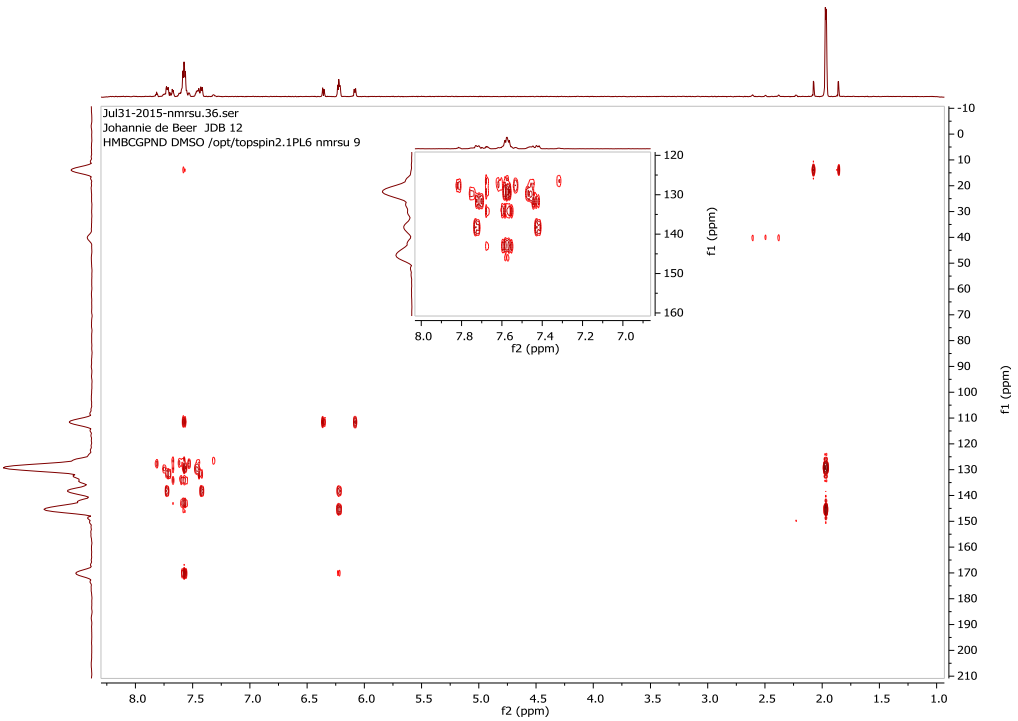

JDB13: 1-(4-Chlorophenyl)-3-hydroxy-2-methylpyridin-4-one

- ^{1}H-NMR spectrum for JDB13:

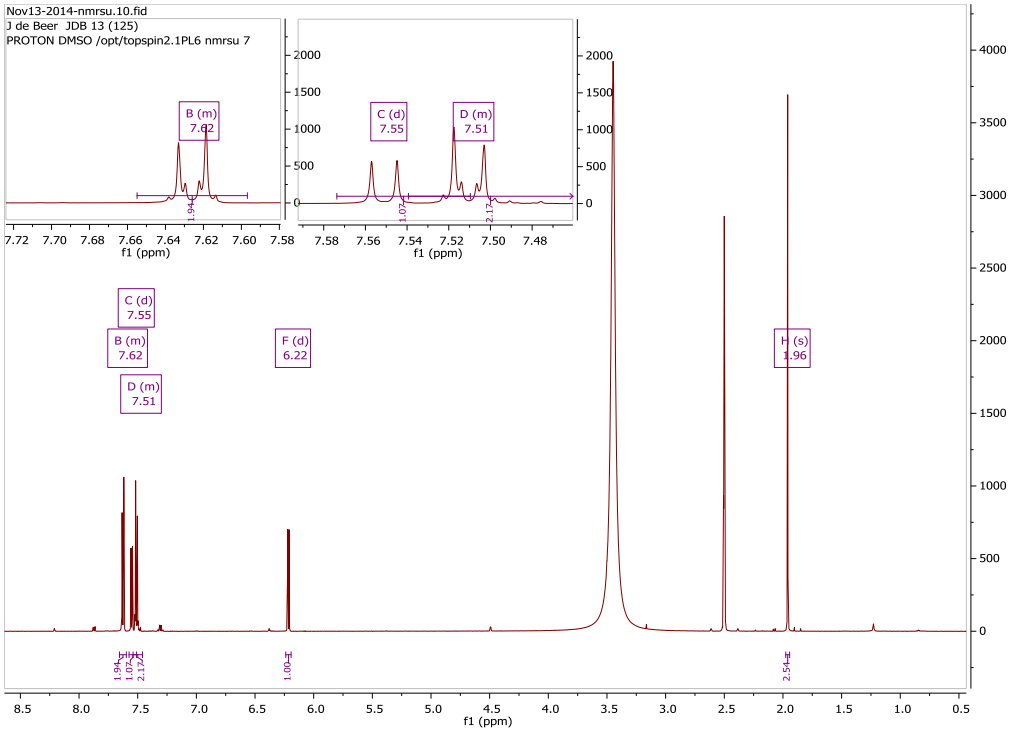

- ^{13}C-NMR spectrum for JDB13:

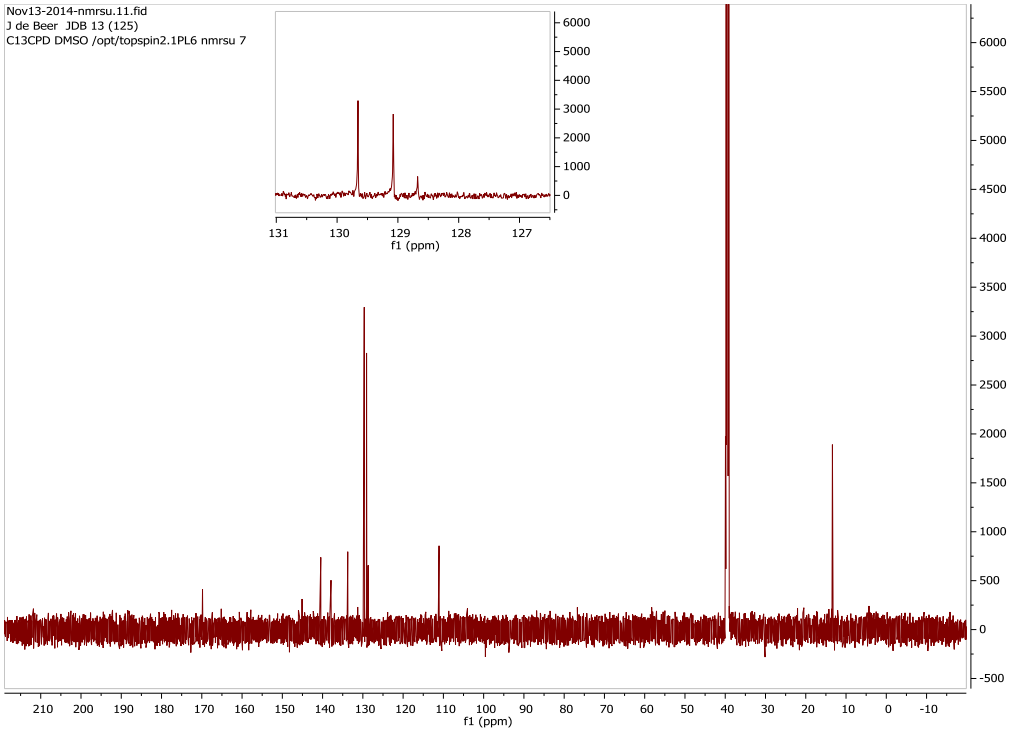

- ^{13}C-NMR, DEPT90 spectrum for JDB13:

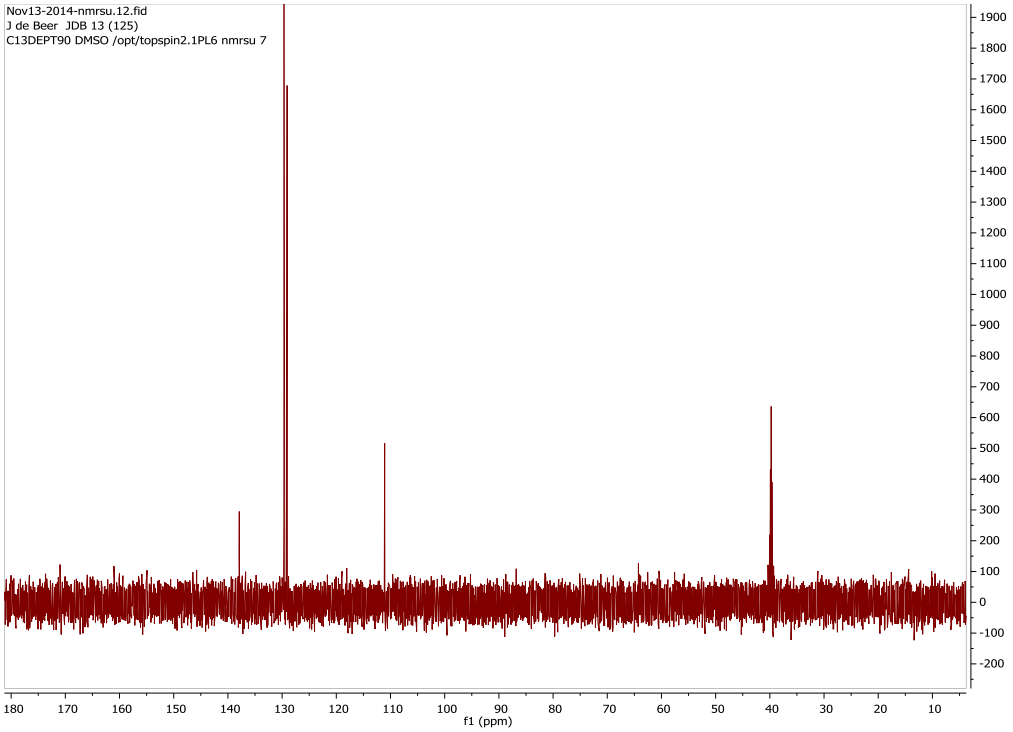

- ^{13}C-NMR, DEPT135 spectrum for JDB13:

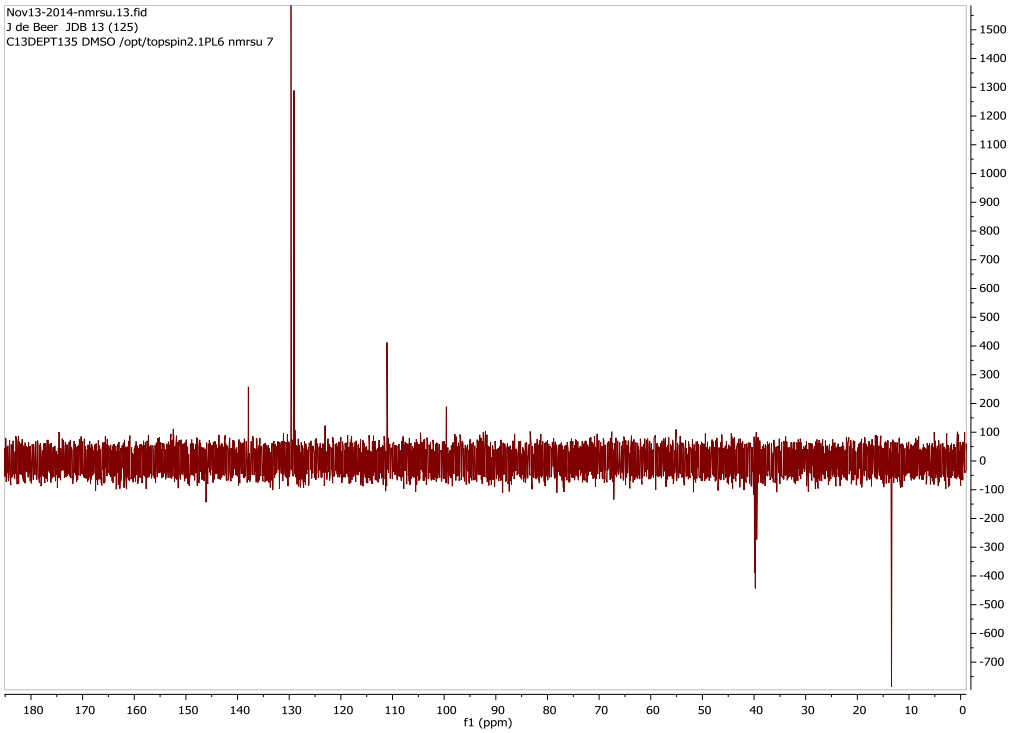

- COSY spectrum for JDB13:

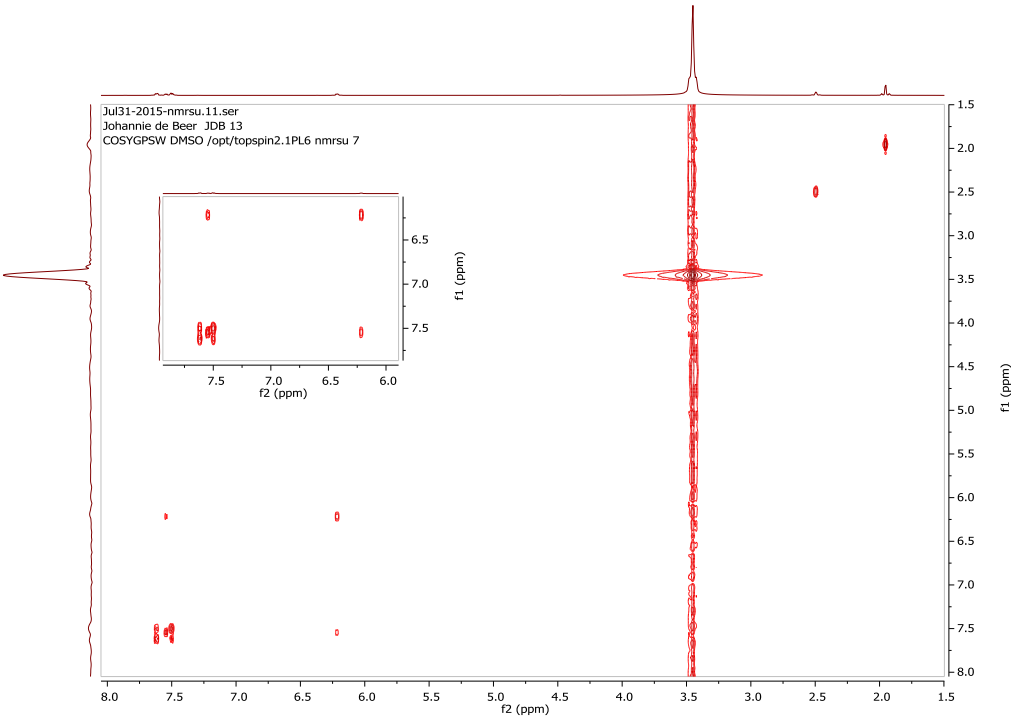

- HSQC spectrum for JDB13:

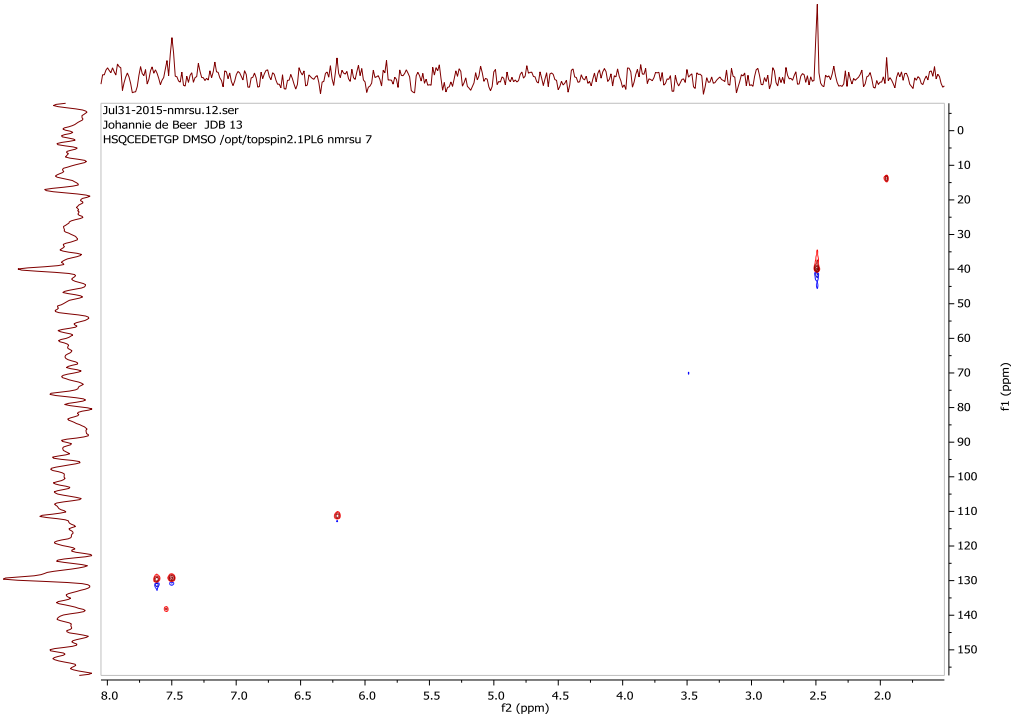

- HMBC spectrum for JDB13:

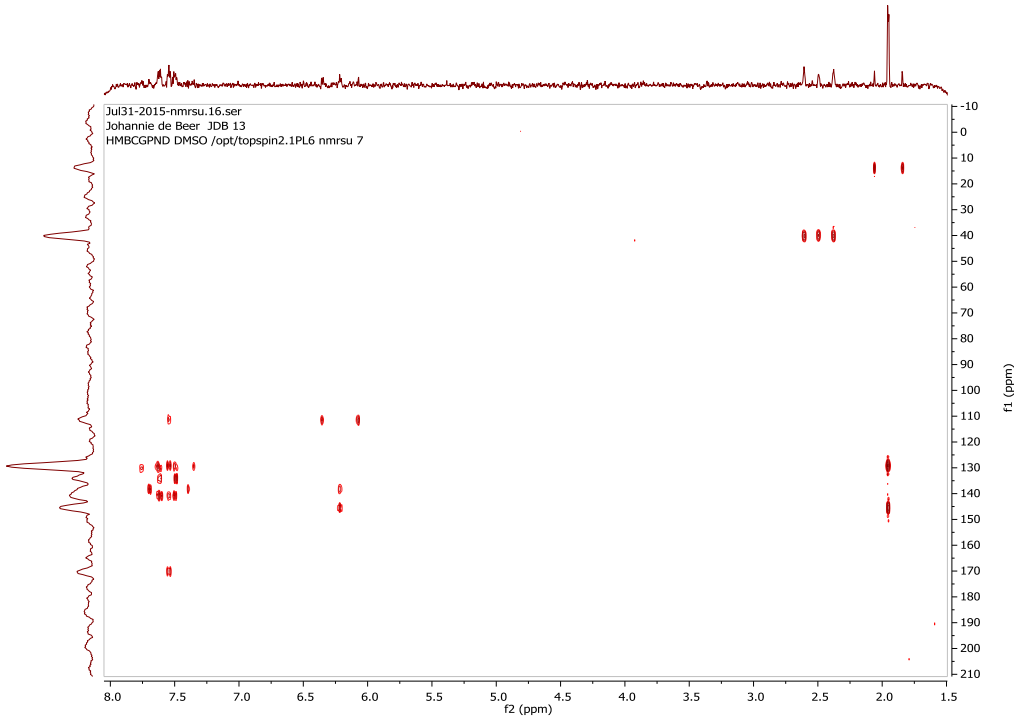

JDB14: 3-Hydroxy-2-methyl-1-(4-methylbenzyl)pyridin-4-one

- ^{1}H-NMR spectrum for JDB14:

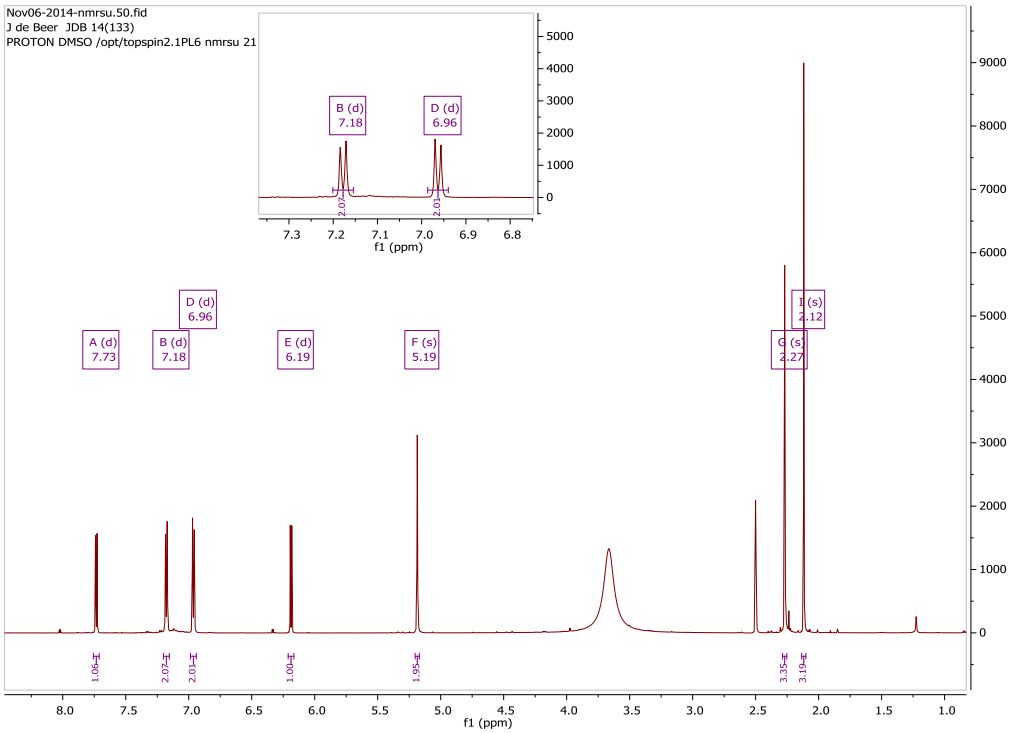

- ^{13}C-NMR spectrum for JDB14:

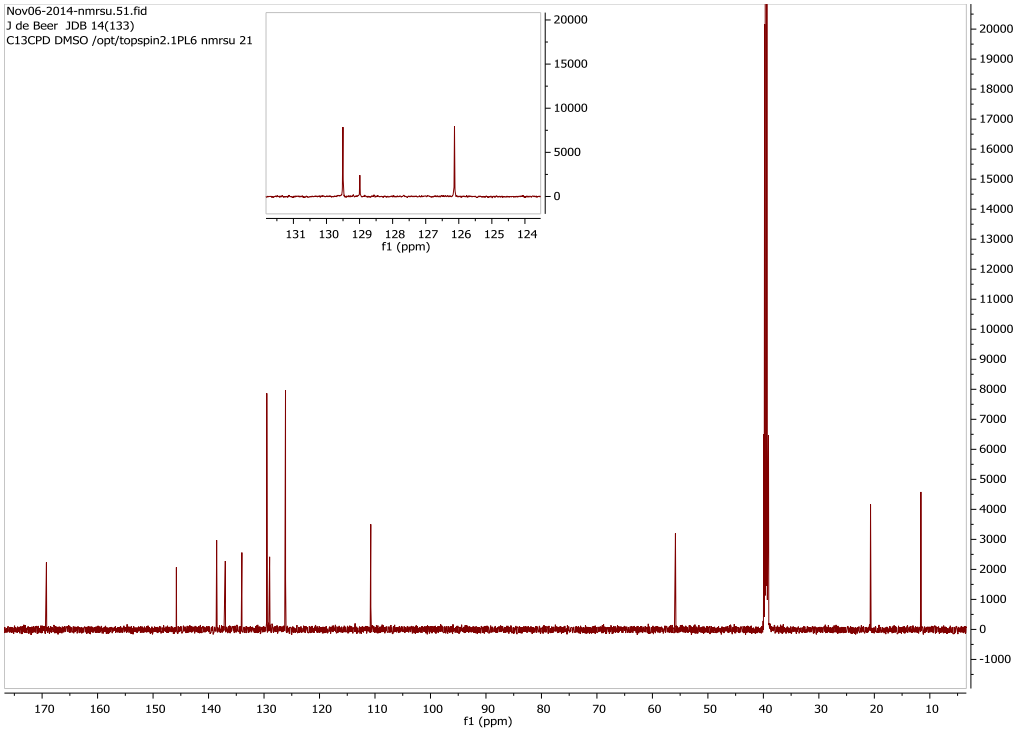

- ^{13}C-NMR, DEPT90 spectrum for JDB14:

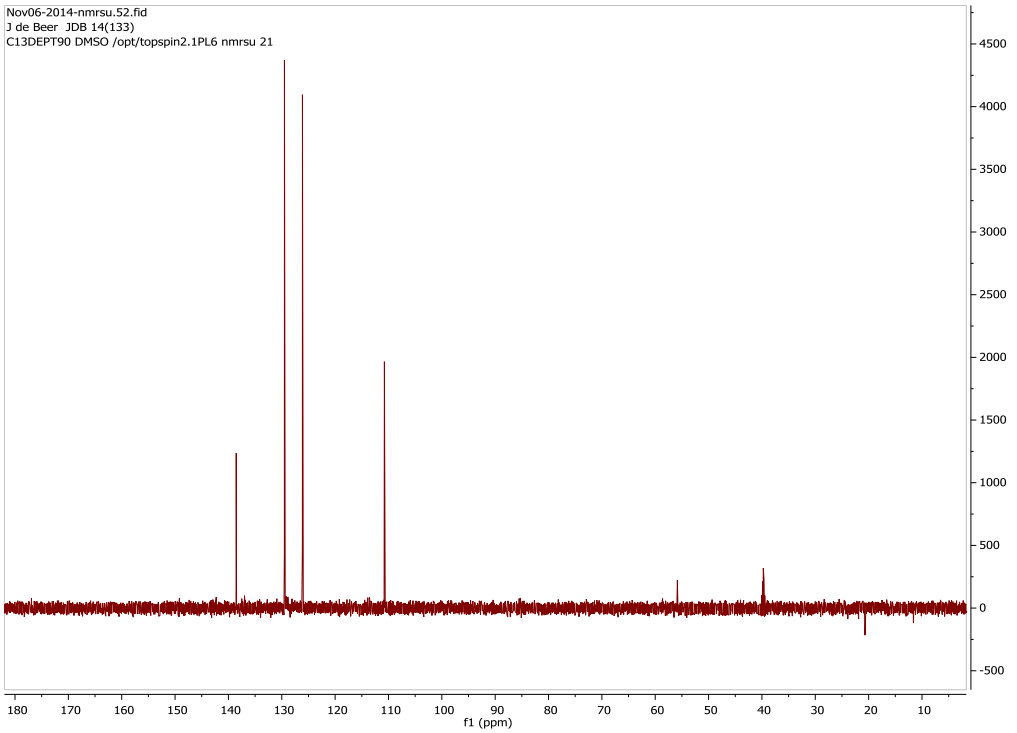

- ^{13}C-NMR, DEPT135 spectrum for JDB14:

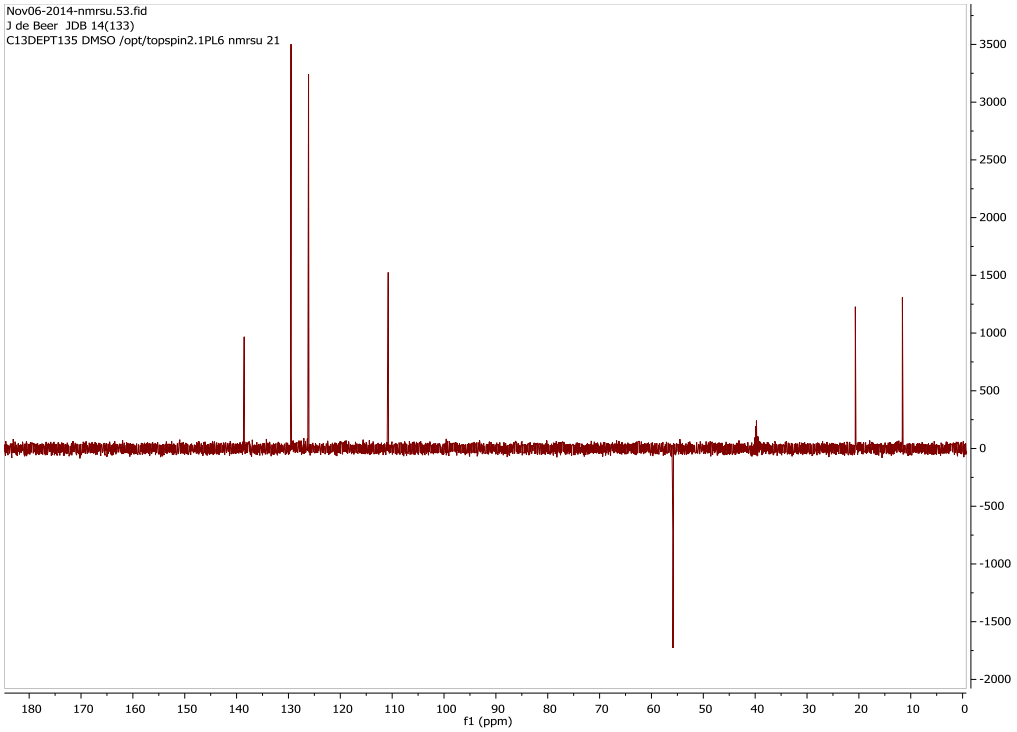

- COSY spectrum for JDB14:

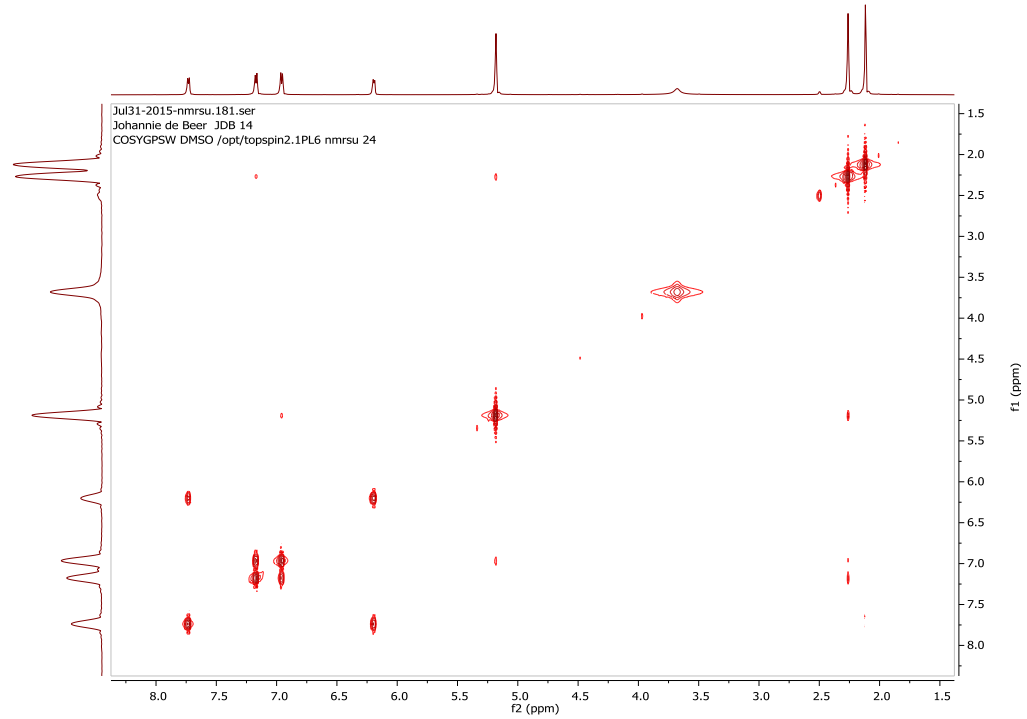

- HSQC spectrum for JDB14:

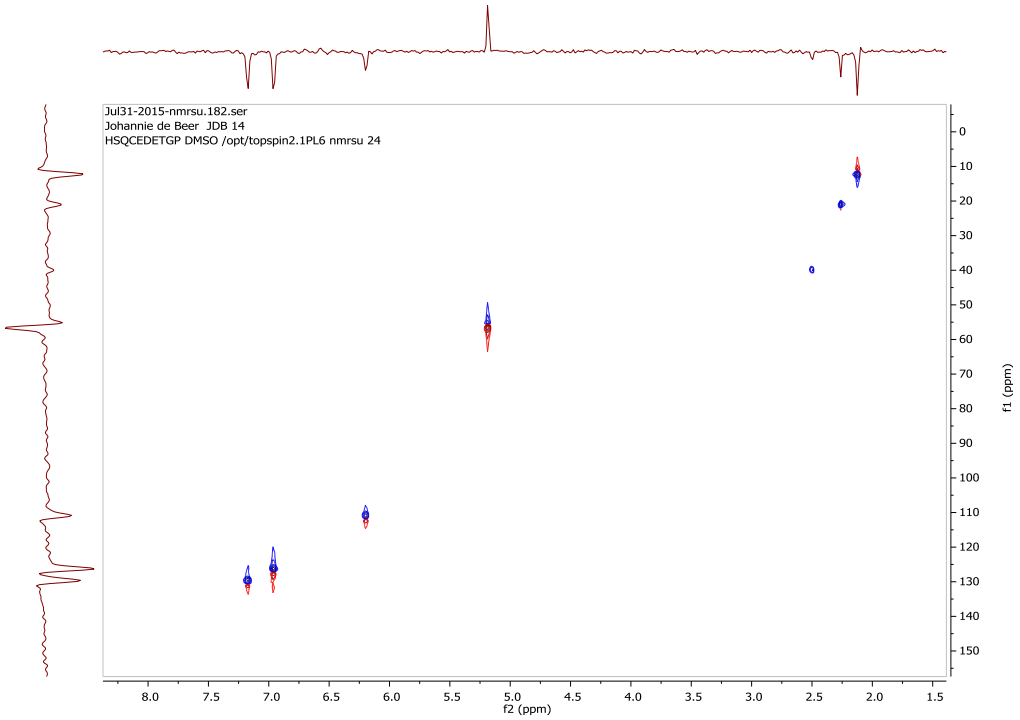

- HMBC spectrum for JDB14:

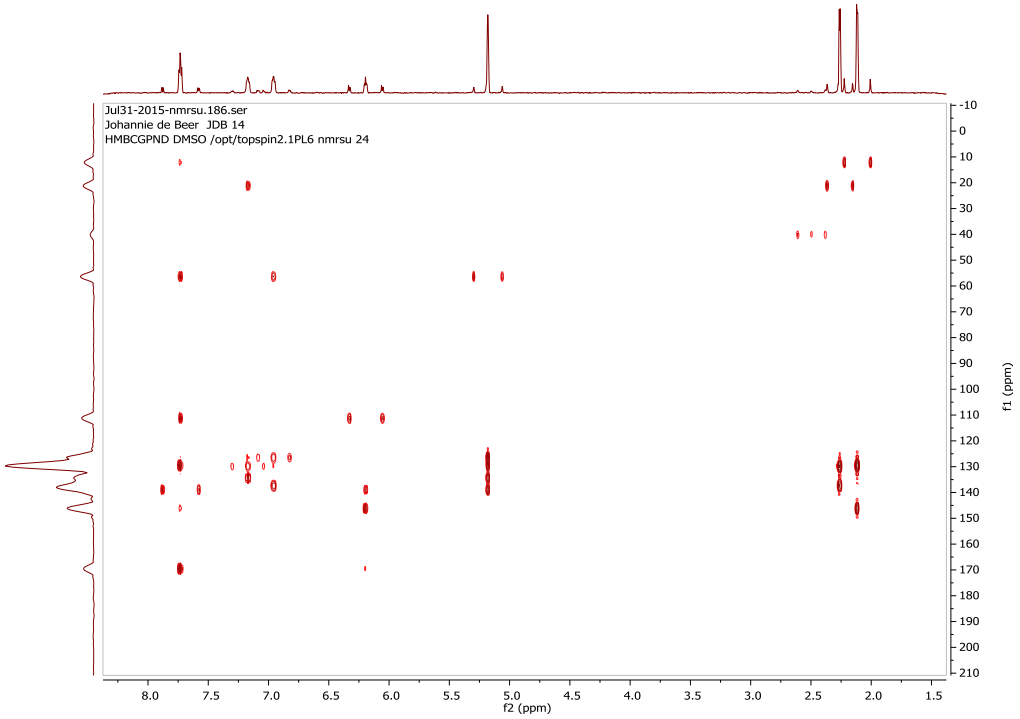

A.2 INFRARED (IR) SPECTROSCOPY

JDB1: 3-Hydroxy-2-methyl-1-phenylpyridin-4-one

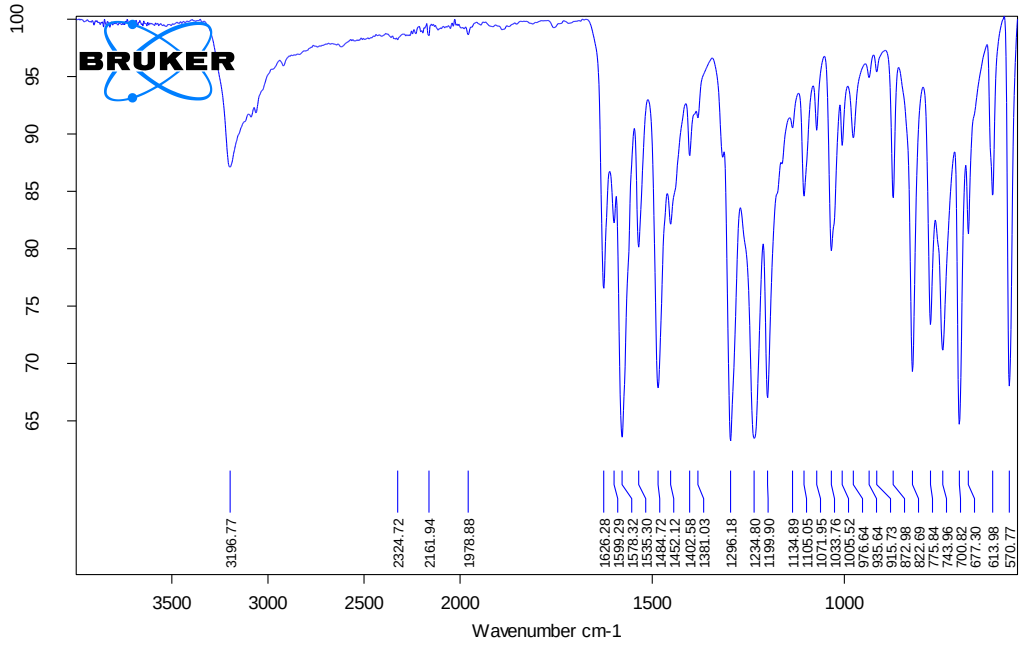

C:\NWU\Measurements\JDB1.0	JDB1	Instrument type and / or accessory	22/04/2014

Page 1/1

JDB3: 1-Benzyl-3-hydroxy-2-methylpyridin-4-one

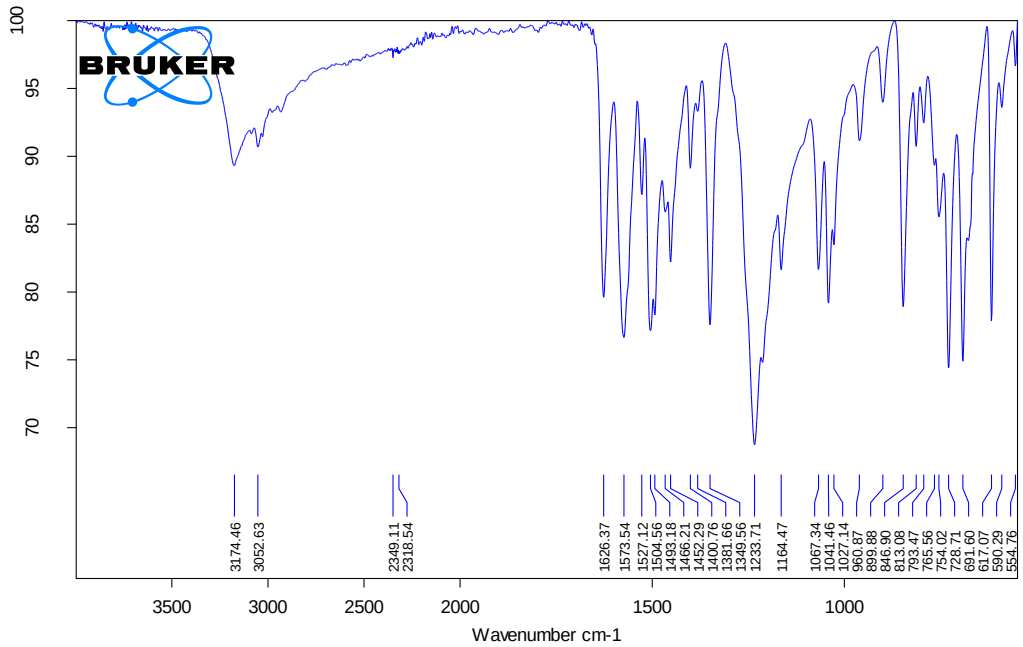

C:\Users\Administrator\Documents\Johannie\JDB3(21).0	JDB3(21)	POWDER	30/06/2014

Page 1/1

JDB4: 3-Hydroxy-2-methyl-1-(2-phenylethyl)pyridin-4-one

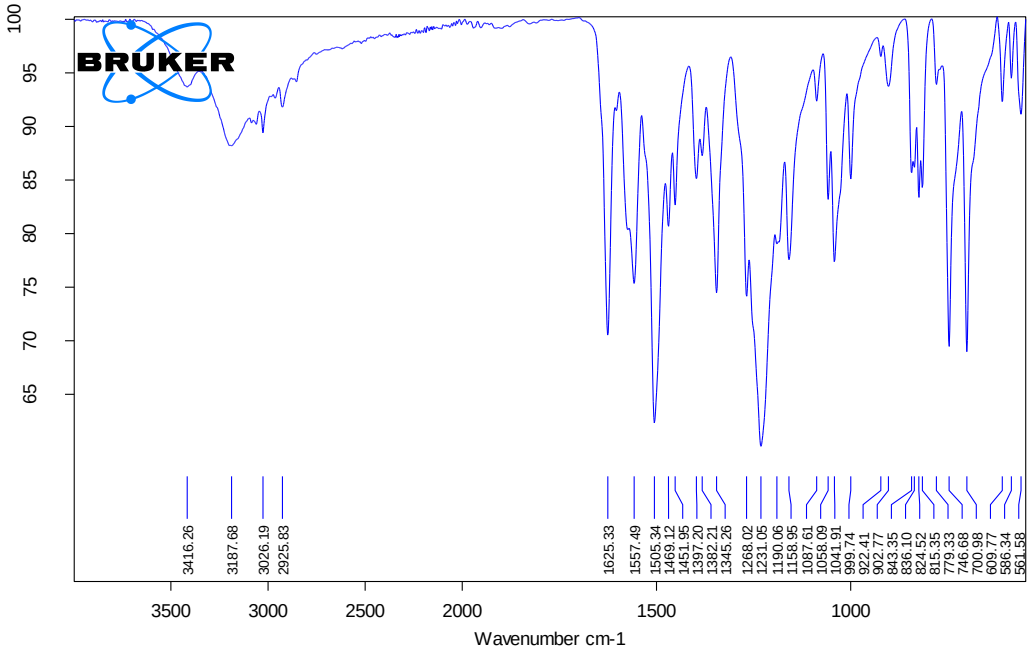

C:\Users\Administrator\Documents\Johannie\JDB4(37).0	JDB4(37)	POWDER	30/06/2014

Page 1/1

JDB5: 3-Hydroxy-2-methyl-1-(3-phenylpropyl)pyridin-4-one

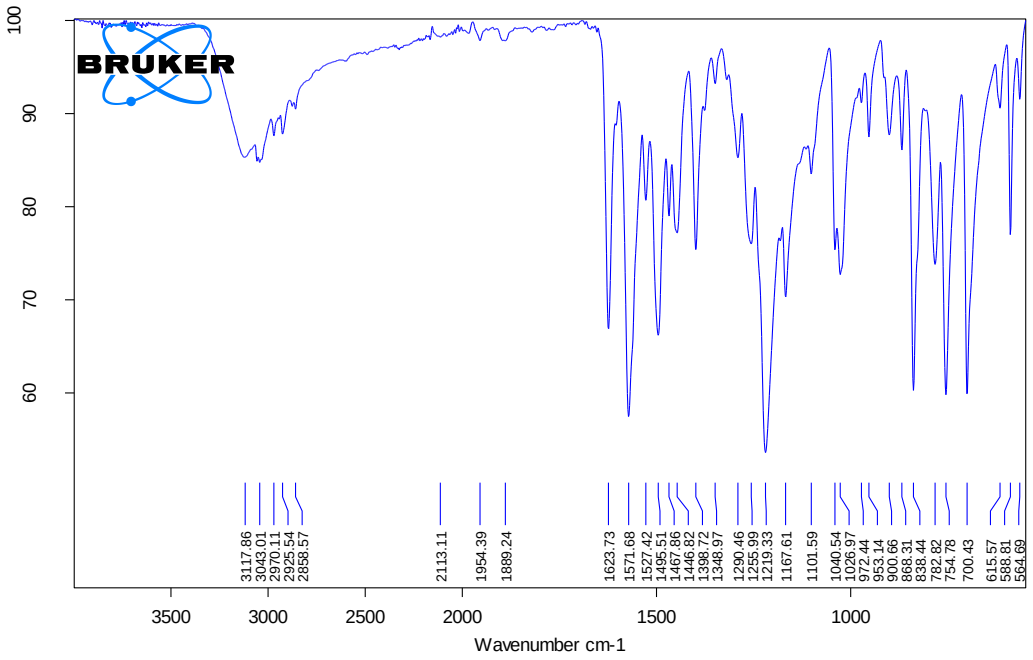

C:\Users\Administrator\Documents\Johannie\JDB5_55.0	JDB5_55	SOLID	24/11/2014

Page 1/1

JDB9: 3-Hydroxy-2-methyl-1-(4-phenylbutyl)pyridin-4-one

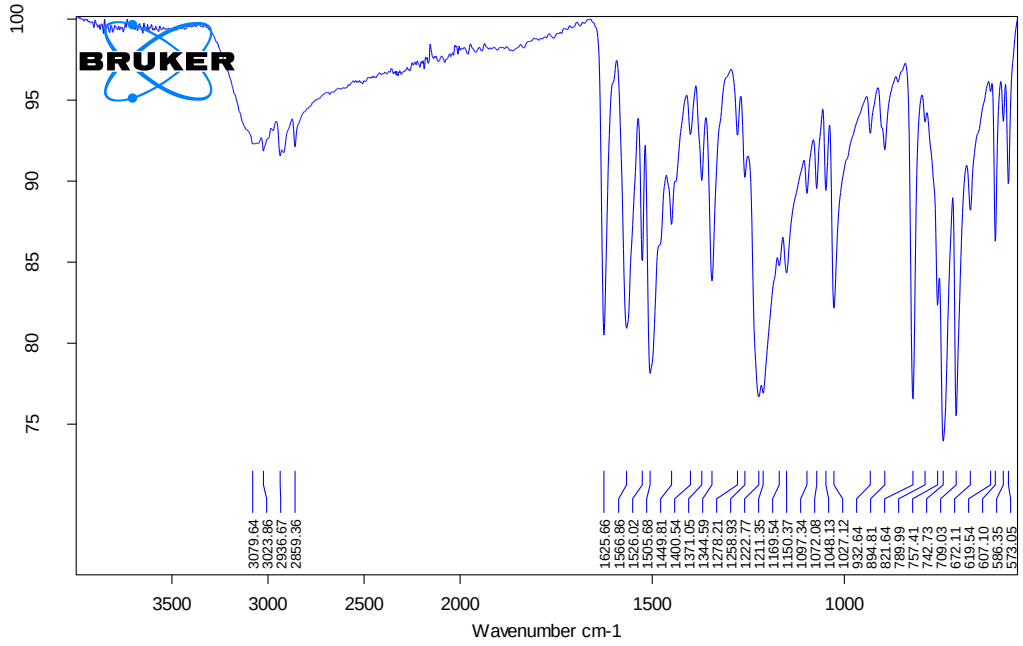

C:\Users\Administrator\Documents\Johannie\JDB9_95.0	JDB9_95	SOLID	24/11/2014

Page 1/1

JDB10: 1-Cyclohexyl-3-hydroxy-2-methylpyridin-4-one

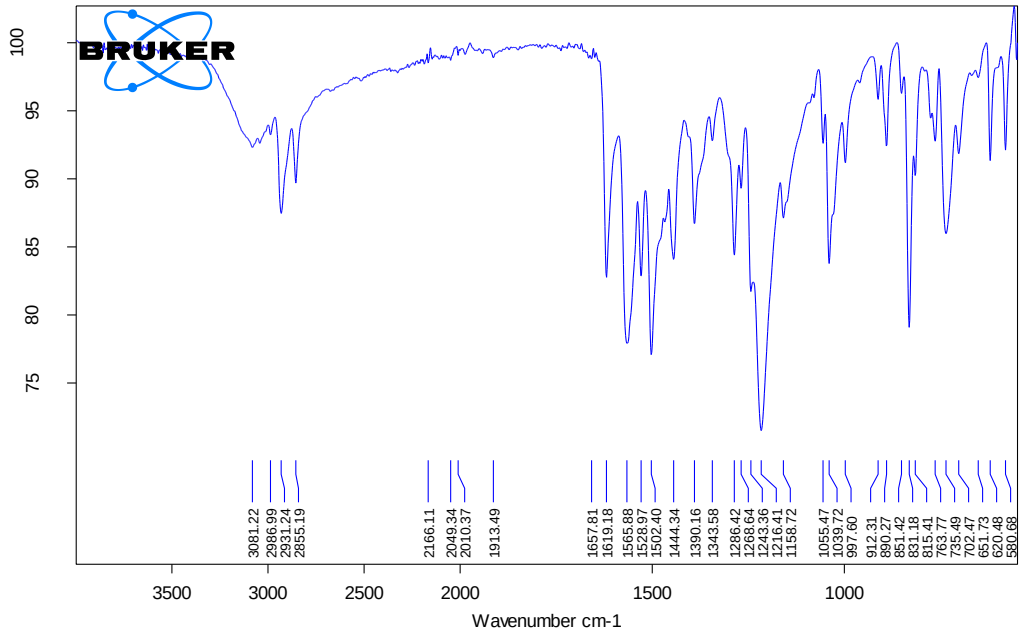

C:\Users\Administrator\Documents\Johannie\JDB10_101.0	JDB10_101	SOLID	24/11/2014

Page 1/1

JDB11: 1-Cyclopentyl-3-hydroxy-2-methylpyridin-4-one

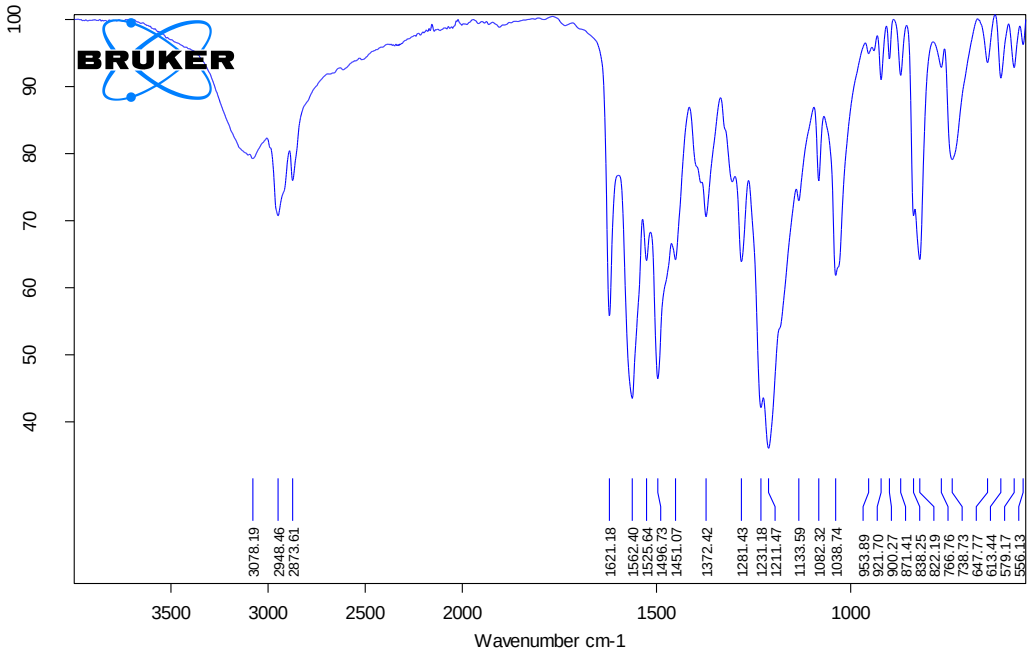

C:\Users\Administrator\Documents\Johannie\JDB11_107.0	JDB11_107	SOLID	24/11/2014

Page 1/1

JDB12: 1-(3-Chlorophenyl)-3-hydroxy-2-methylpyridin-4-one

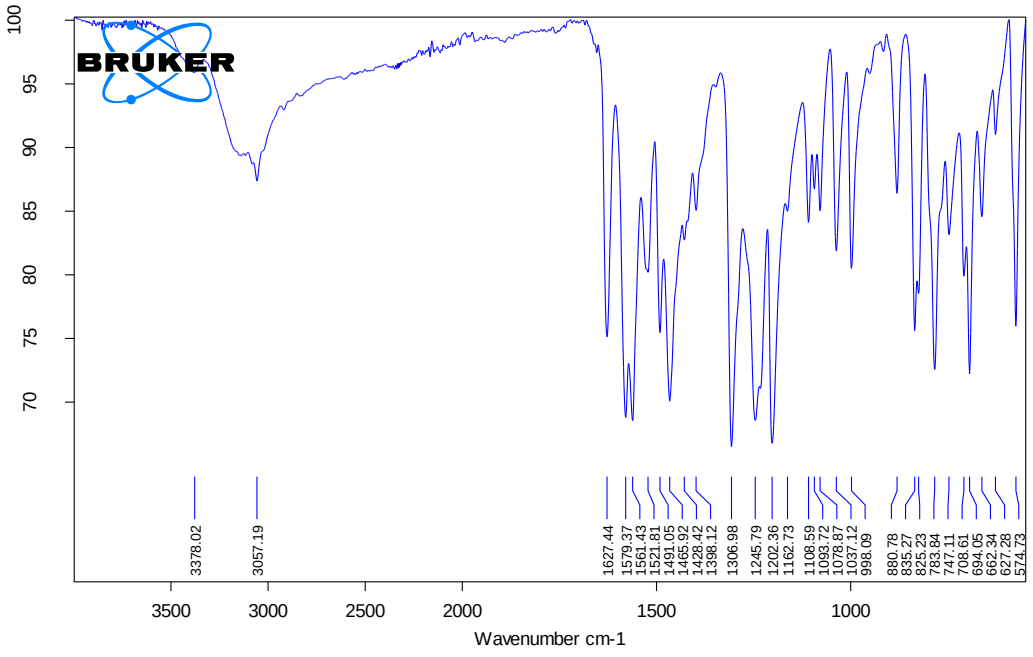

C:\Users\Administrator\Documents\Johannie\JDB12_119.0	JDB12_119	SOLID	24/11/2014

Page 1/1

JDB13: 1-(4-Chlorophenyl)-3-hydroxy-2-methylpyridin-4-one

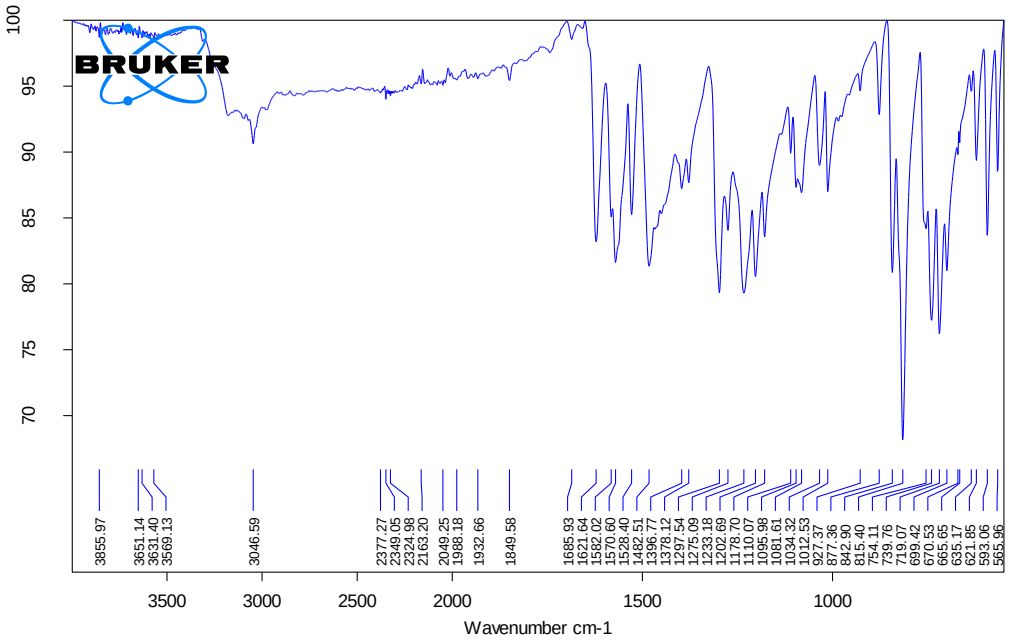

C:\Users\Administrator\Documents\Johannie\JDB13_125.0	JDB13_125	SOLID	24/11/2014

Page 1/1

JDB14: 3-Hydroxy-2-methyl-1-(4-methylbenzyl)pyridin-4-one

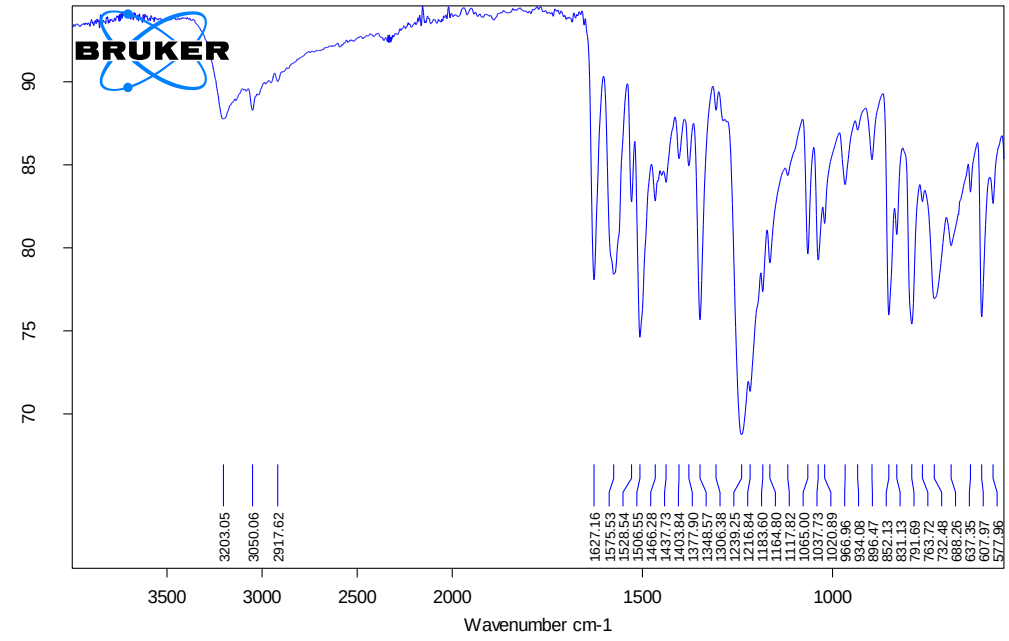

C:\Users\Administrator\Documents\Johannie\JDB14_133.0	JDB14_133	SOLID	24/11/2014

Page 1/1

A.3 MASS SPECTROMETRY

JDB1: 3-Hydroxy-2-methyl-1-phenylpyridin-4-one

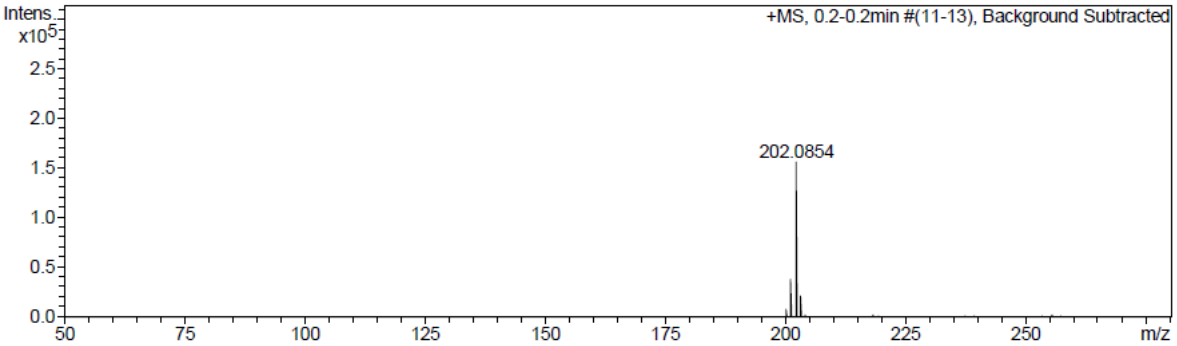

Meas. m/z	#	Formula	Score	m/z	err [mDa]	err [ppm]	mSigma	rdb	N-Rule	e⁻ Conf
202.0854	1	C 12 H 12 N O 2	100.00	202.0863	0.9	4.3	7.2	7.5	ok	even

JDB3: 1-Benzyl-3-hydroxy-2-methylpyridin-4-one

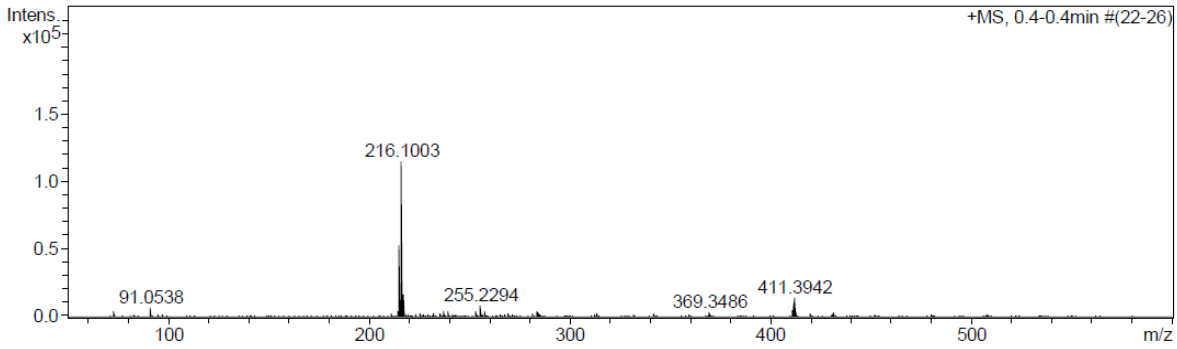

Meas. m/z	#	Formula	Score	m/z	err [mDa]	err [ppm]	mSigma	rdb	N-Rule	e⁻ Conf
216.1003	1	C 13 H 14 N O 2	100.00	216.1019	1.6	7.6	1.0	7.5	ok	even

JDB4: 3-Hydroxy-2-methyl-1-(2-phenylethyl)pyridin-4-one

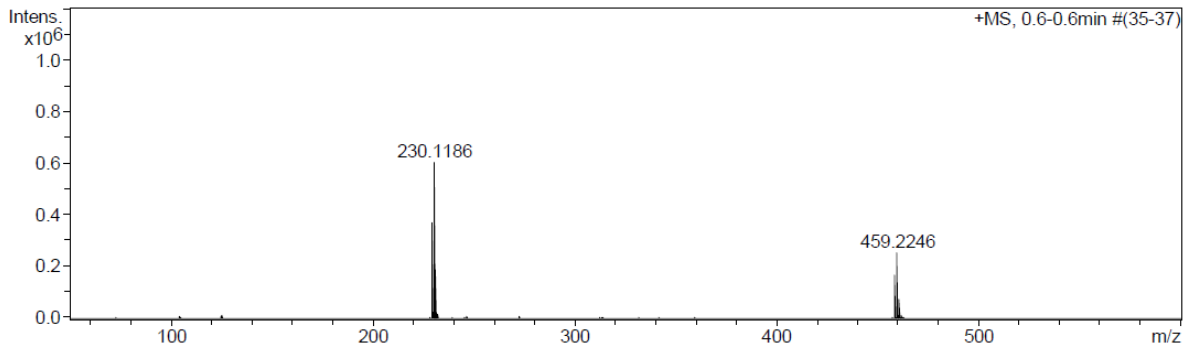

Meas. m/z	#	Formula	Score	m/z	err [mDa]	err [ppm]	mSigma	rdb	N-Rule	e¯ Conf
230.1186	1	C 14 H 16 N O 2	100.00	230.1176	-1.0	-4.5	91.6	7.5	ok	even
459.2246	1	C 28 H 31 N 2 O 4	100.00	459.2278	3.3	7.1	12.8	14.5	ok	even

JDB5: 3-Hydroxy-2-methyl-1-(3-phenylpropyl)pyridin-4-one

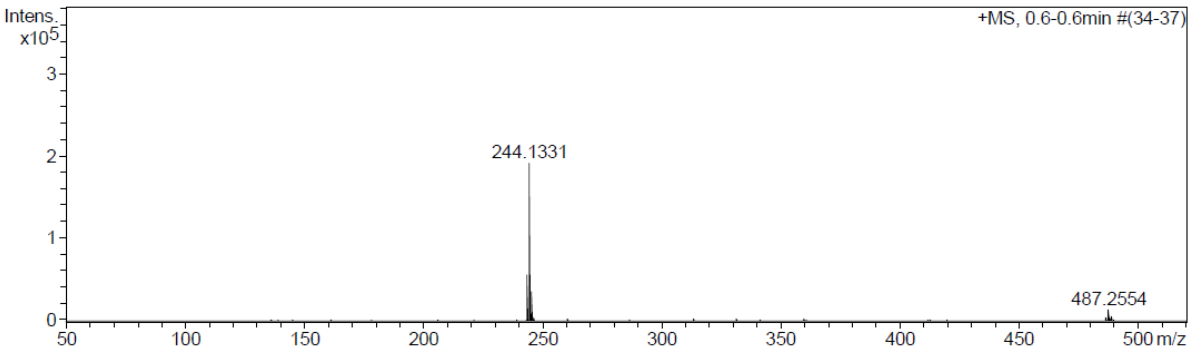

Meas. m/z	#	Formula	Score	m/z	err [mDa]	err [ppm]	mSigma	rdb	N-Rule	e¯ Conf
244.1331	1	C 15 H 18 N O 2	100.00	244.1332	0.1	0.4	9.9	7.5	ok	even
	2	C 13 H 16 N 4 O	48.70	244.1319	-1.2	-5.1	16.5	8.0	ok	odd

JDB9: 3-Hydroxy-2-methyl-1-(4-phenylbutyl)pyridin-4-one

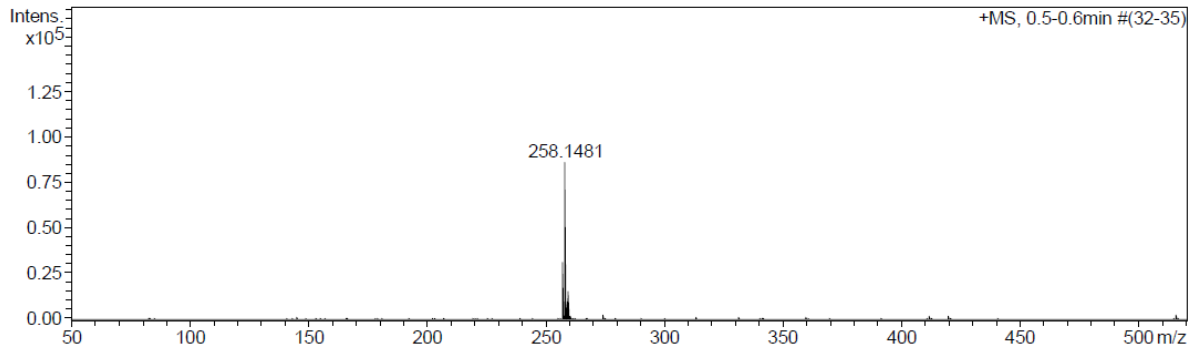

Meas. m/z	#	Formula	Score	m/z	err [mDa]	err [ppm]	mSigma	rdb	N-Rule	e¯ Conf
258.1481	1	C 16 H 20 N O 2	100.00	258.1489	0.8	3.0	0.9	7.5	ok	even
	2	C 14 H 18 N 4 O	98.17	258.1475	-0.6	-2.2	7.9	8.0	ok	odd
	3	C 12 H 16 N 7	38.29	258.1462	-1.9	-7.4	13.9	8.5	ok	even
	4	C 13 H 22 O 5	32.70	258.1462	-1.9	-7.4	21.7	3.0	ok	odd

JDB10: 1-Cyclohexyl-3-hydroxy-2-methylpyridin-4-one

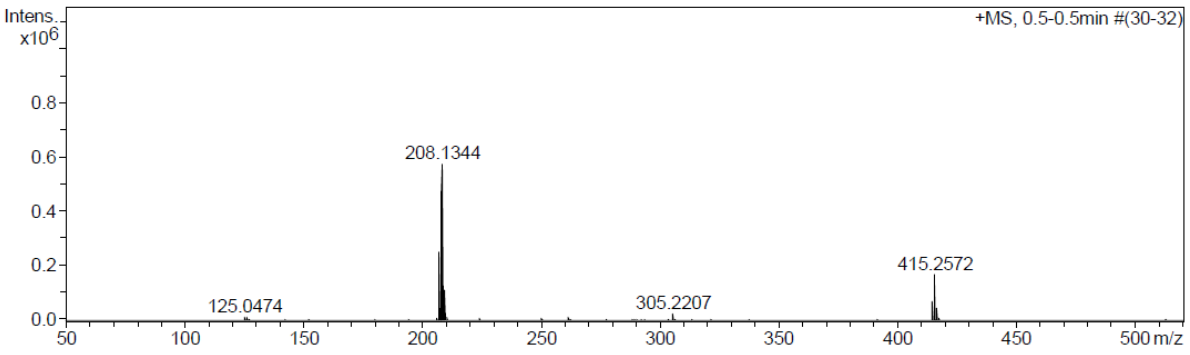

Meas. m/z	#	Formula	Score	m/z	err [mDa]	err [ppm]	mSigma	rdb	N-Rule	e⁻ Conf
208.1344	1	C 12 H 18 N O 2	100.00	208.1332	-1.2	-5.7	34.9	4.5	ok	even
415.2572	1	C 24 H 35 N 2 O 4	48.70	415.2591	2.0	4.7	3.8	8.5	ok	even
	2	C 22 H 33 N 5 O 3	100.00	415.2578	0.6	1.5	10.6	9.0	ok	odd
	3	C 20 H 31 N 8 O 2	83.00	415.2564	-0.7	-1.7	17.4	9.5	ok	even
	4	C 21 H 37 N O 7	71.32	415.2565	-0.7	-1.7	24.6	4.0	ok	odd

JDB11: 1-Cyclopentyl-3-hydroxy-2-methylpyridin-4-one

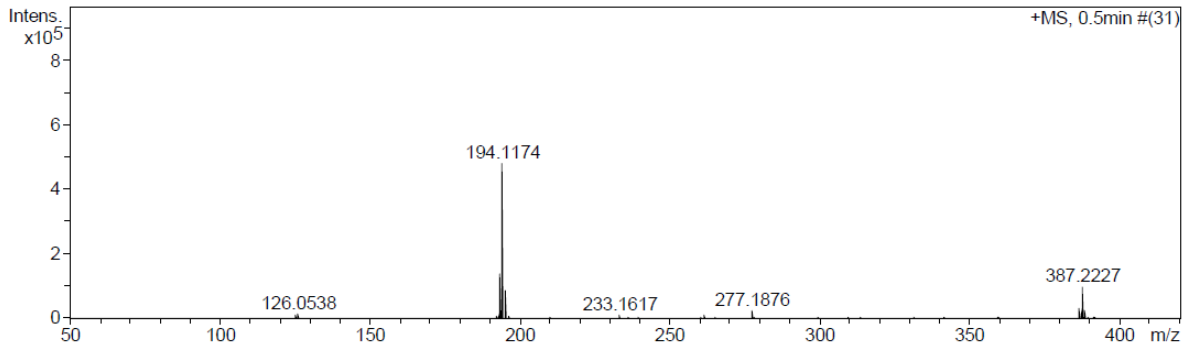

Meas. m/z	#	Formula	Score	m/z	err [mDa]	err [ppm]	mSigma	rdb	N-Rule	e⁻ Conf
194.1174	1	C 11 H 16 N O 2	100.00	194.1176	0.2	0.8	35.6	4.5	ok	even
	2	C 9 H 14 N 4 O	49.27	194.1162	-1.2	-6.1	42.1	5.0	ok	odd
387.2227	1	C 22 H 31 N 2 O 4	18.52	387.2278	5.1	13.2	5.7	8.5	ok	even
	2	C 26 H 29 N O 2	100.00	387.2193	-3.4	-8.9	26.7	13.0	ok	odd
	3	C 27 H 31 O 2	0.01	387.2319	9.1	23.6	28.8	12.5	ok	even

JDB12: 1-(3-Chlorophenyl)-3-hydroxy-2-methylpyridin-4-one

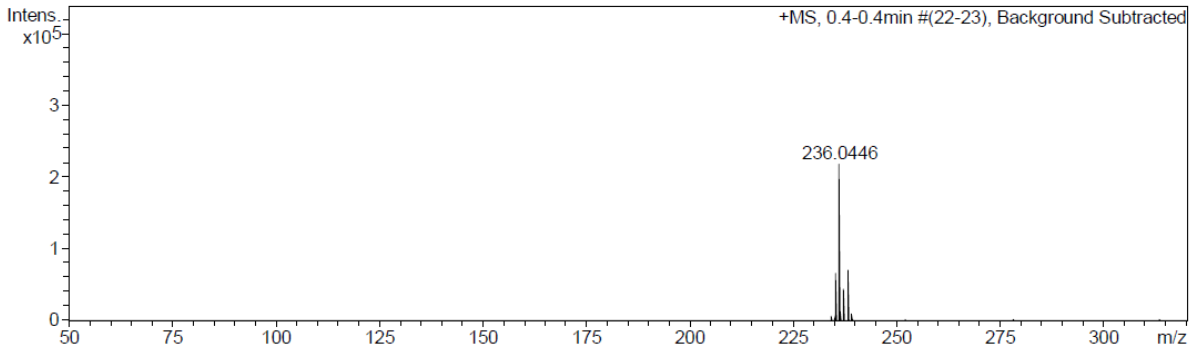

Meas. m/z	#	Formula	Score	m/z	err [mDa]	err [ppm]	mSigma	rdb	N-Rule	e⁻ Conf
235.0365	1	C 9 H 13 Cl 2 N 2 O	100.00	235.0399	3.5	14.7	507.5	3.5	ok	even
	2	C 12 H 10 Cl N O 2	0.00	235.0395	3.0	12.7	576.1	8.0	ok	odd
	3	C 15 H 7 O 3	0.00	235.0390	2.5	10.6	637.8	12.5	ok	even
236.0446	1	C 12 H 11 Cl N O 2	100.00	236.0473	2.7	11.5	36.7	7.5	ok	even
	2	C 15 H 8 O 3	0.13	236.0468	2.2	9.4	176.9	12.0	ok	odd

JDB13: 1-(4-Chlorophenyl)-3-hydroxy-2-methylpyridin-4-one

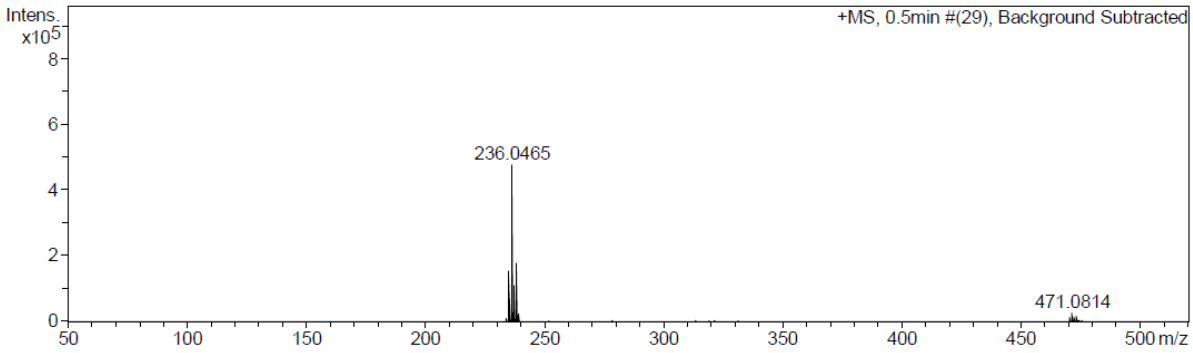

Meas. m/z	#	Formula	Score	m/z	err [mDa]	err [ppm]	mSigma	rdb	N-Rule	e⁻ Conf
236.0465	1	C 12 H 11 Cl N O 2	100.00	236.0473	0.7	3.2	51.2	7.5	ok	even
	2	C 15 H 8 O 3	0.01	236.0468	0.3	1.1	207.1	12.0	ok	odd
471.0814	1	C 24 H 21 Cl 2 N 2 O 4	100.00	471.0873	5.9	12.4	118.3	14.5	ok	even

JDB14: 3-Hydroxy-2-methyl-1-(4-methylbenzyl)pyridin-4-one

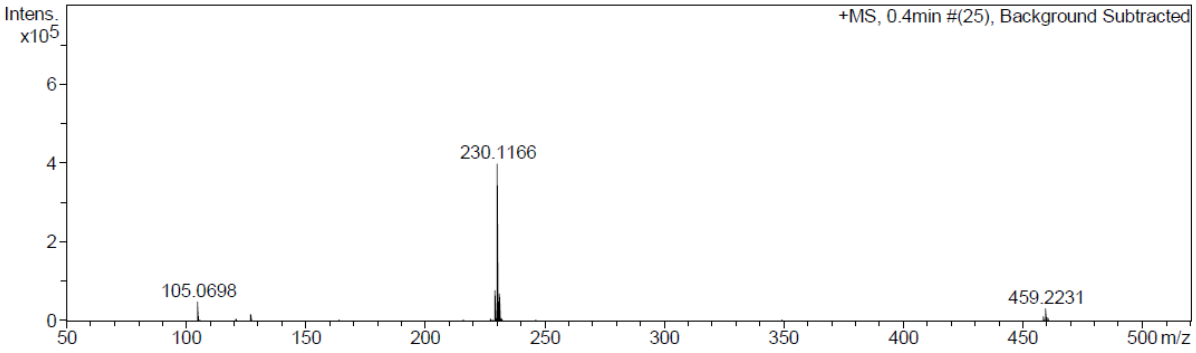

Meas. m/z	#	Formula	Score	m/z	err [mDa]	err [ppm]	mSigma	rdb	N-Rule	e¯ Conf
230.1166	1	C 14 H 16 N O 2	88.52	230.1176	0.9	4.0	11.3	7.5	ok	even
	2	C 12 H 14 N 4 O	100.00	230.1162	-0.4	-1.8	17.8	8.0	ok	odd
459.2231	1	C 28 H 31 N 2 O 4	50.93	459.2278	4.7	10.2	7.8	14.5	ok	even
	2	C 32 H 29 N O 2	100.00	459.2193	-3.9	-8.4	25.6	19.0	ok	odd
	3	C 33 H 31 O 2	0.02	459.2319	8.7	19.0	31.2	18.5	ok	even

A.4 HPLC CHROMATOGRAMS

JDB1: (3-Hydroxy-2-methyl-1-phenylpyridin-4-one)

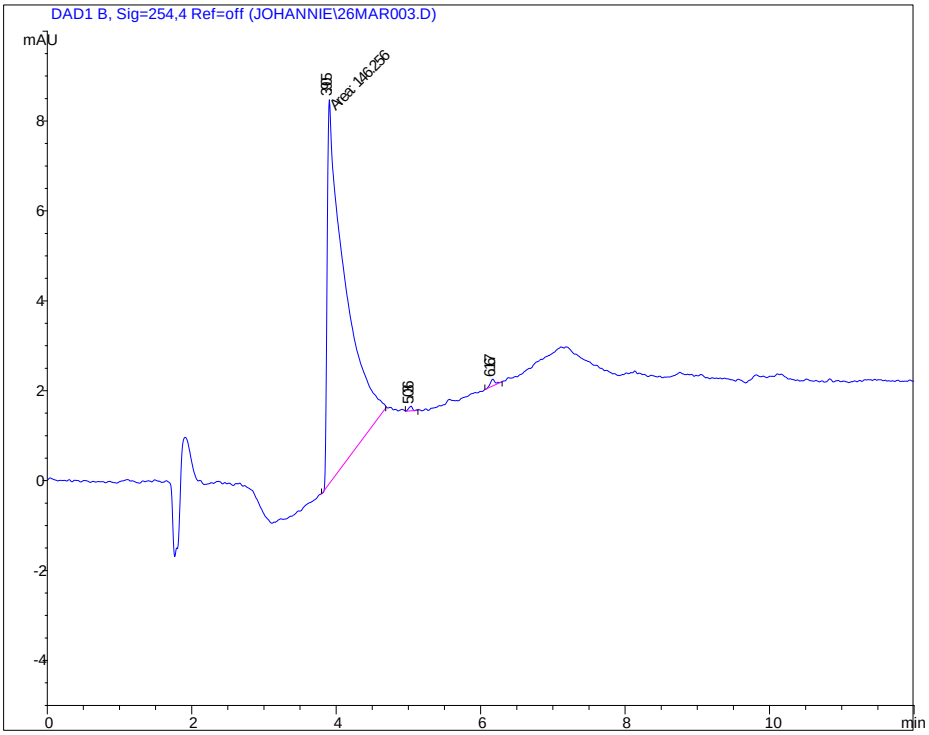

HPLC chromatogram peak properties of JDB1:

Peak #	*Retention time (min)*	*Type*	*Width (min)*	*Area (mAU*s)*	*Height (mAU)*	*Area %*
1	3.905	MM	0.2849	146.25632	8.55714	99.2926
2	5.036	PB	0.0529	$3.77017e^{-1}$	$1.02478e^{-1}$	0.0253
3	6.167	PB	0.0656	$6.65037e^{-1}$	$1.50226e^{-1}$	0.4515

JDB3: 1-Benzyl-3-hydroxy-2-methylpyridin-4-one

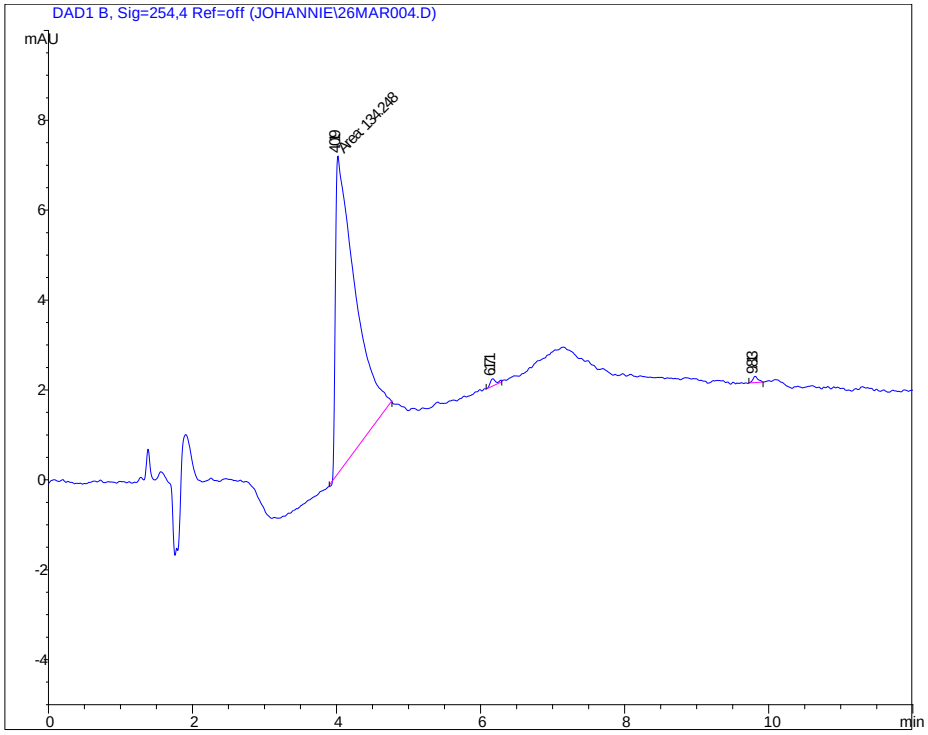

HPLC chromatogram peak properties of JDB3:

Peak #	*Retention time (min)*	*Type*	*Width (min)*	*Area (mAU*s)*	*Height (mAU)*	*Area %*
1	4.019	MM	0.3158	134.24788	7.08614	98.8358
2	6.171	PB	0.0830	$8.95727e^{-1}$	$1.60867e^{-1}$	0.6595
3	9.813	PB	0.0740	$6.85660e^{-1}$	$1.37989e^{-1}$	0.5048

JDB4: 3-Hydroxy-2-methyl-1-(2-phenylethyl)pyridin-4-one

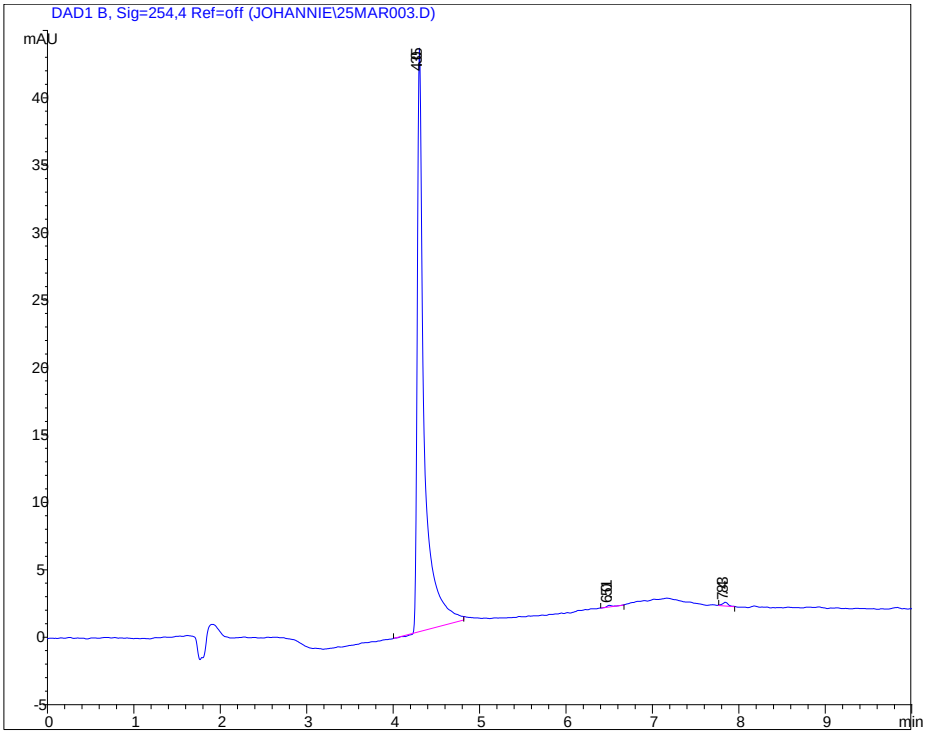

HPLC chromatogram peak properties of JDB4:

Peak #	*Retention time (min)*	*Type*	*Width (min)*	*Area (mAU*s)*	*Height (mAU)*	*Area %*
1	4.305	MM	0.0923	240.59149	43.46284	99.2733
2	6.501	BB	0.0638	$5.31126e^{-1}$	$1.24335e^{-1}$	0.2192
3	7.843	BB	0.0683	1.23008	$2.74216e^{-1}$	0.5076

JDB5: 3-Hydroxy-2-methyl-1-(3-phenylpropyl)pyridin-4-one

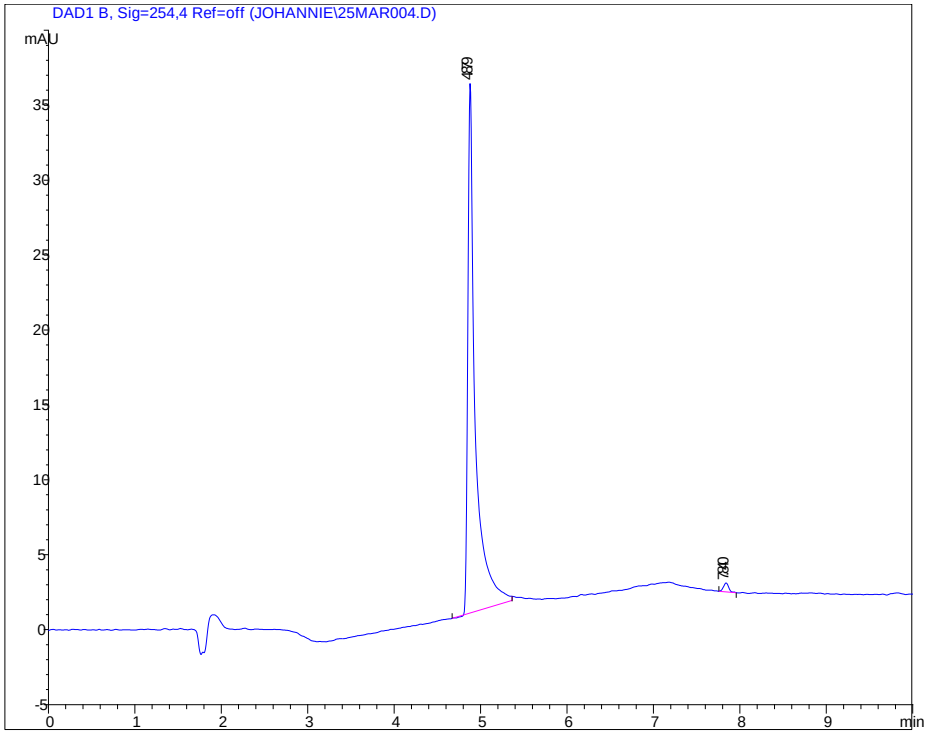

HPLC chromatogram peak properties of JDB5:

Peak #	*Retention time (min)*	*Type*	*Width (min)*	*Area (mAU*s)*	*Height (mAU)*	*Area %*
1	4.879	MM	0.0982	209.29849	35.50786	98.8474
2	7.840	PP	0.0643	2.44041	$5.89440e^{-1}$	1.1526

JDB9: 3-Hydroxy-2-methyl-1-(4-phenylbutyl)pyridin-4-one

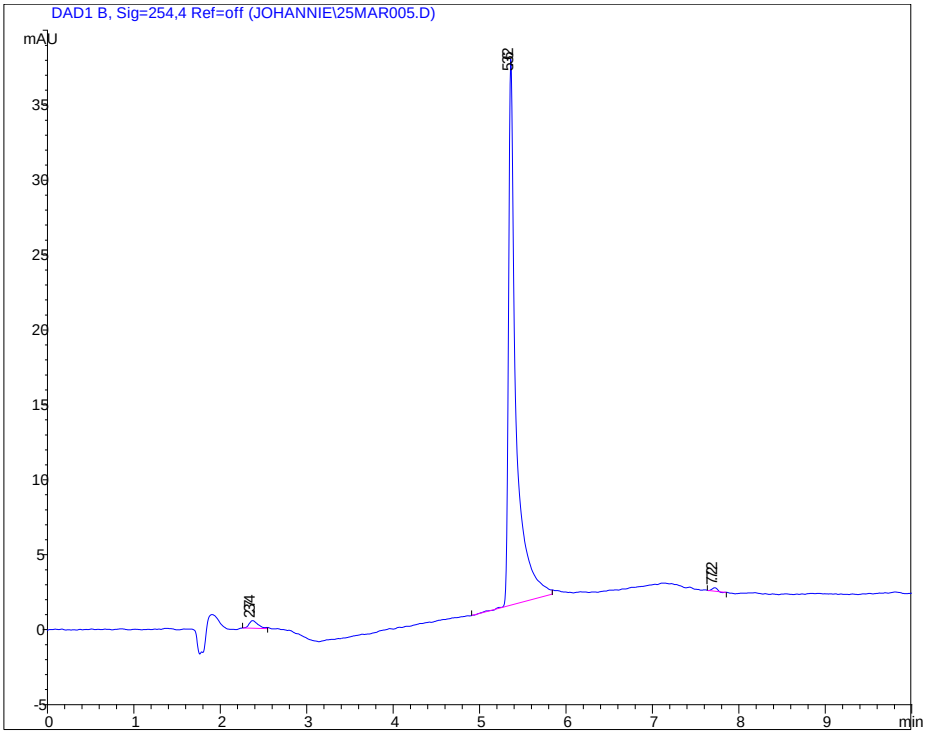

HPLC chromatogram peak properties of JDB9:

Peak #	*Retention time (min)*	*Type*	*Width (min)*	*Area (mAU*s)*	*Height (mAU)*	*Area %*
1	2.374	BB	0.1069	3.71209	$5.10371e^{-1}$	1.6845
2	5.362	MM	0.0985	215.86560	36.50717	97.9550
3	7.722	PB	0.0592	$7.94544e^{-1}$	$2.25182e^{-1}$	0.3605

JDB10: 1-Cyclohexyl-3-hydroxy-2-methylpyridin-4-one

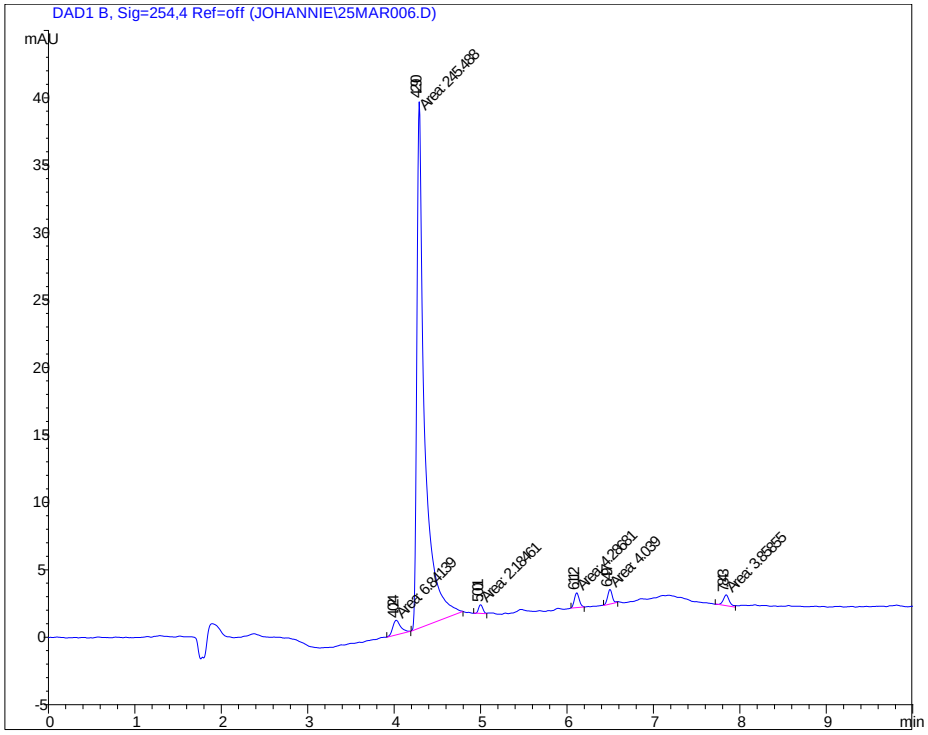

HPLC chromatogram peak properties of JDB10:

Peak #	*Retention time (min)*	*Type*	*Width (min)*	*Area (mAU*s)*	*Height (mAU)*	*Area %*
1	4.024	MM	0.1049	6.84139	1.08648	2.5652
2	4.290	MM	0.1045	245.48792	39.13574	92.0471
3	5.0014	MM	0.0562	2.18461	$6.47861e^{-1}$	0.8191
4	6.112	MM	0.0647	4.28681	1.10349	1.6074
5	6.497	MM	0.0616	4.03900	1.09192	1.5144
6	7.843	MM	0.0805	3.85855	$7.99209e^{-1}$	1.4468

JDB11: 1-Cyclopentyl-3-hydroxy-2-methylpyridin-4-one

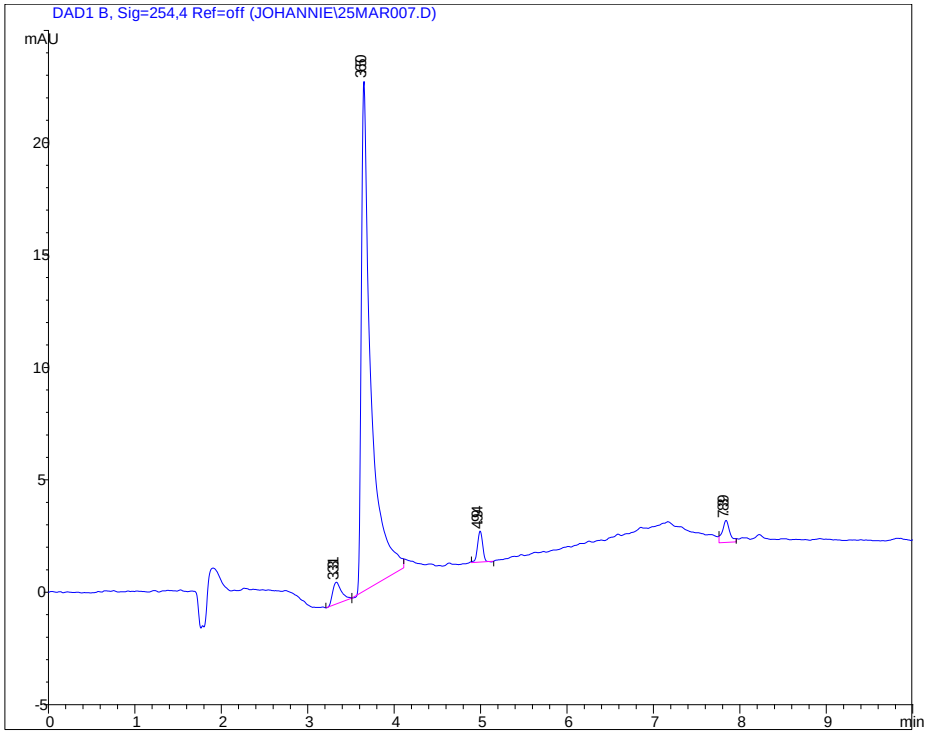

HPLC chromatogram peak properties of JDB11:

Peak #	*Retention time (min)*	*Type*	*Width (min)*	*Area (mAU*s)*	*Height (mAU)*	*Area %*
1	3.331	PP	0.1079	6.80015	$9.68912e^{-1}$	3.5203
2	3.650	VB	0.1059	174.96625	22.70809	90.5776
3	4.994	BP	0.0632	5.58340	1.37991	2.8904
4	7.839	BB	0.0851	5.81751	$9.82594e^{-1}$	3.0116

JDB12: 1-(3-Chlorophenyl)-3-hydroxy-2-methylpyridin-4-one

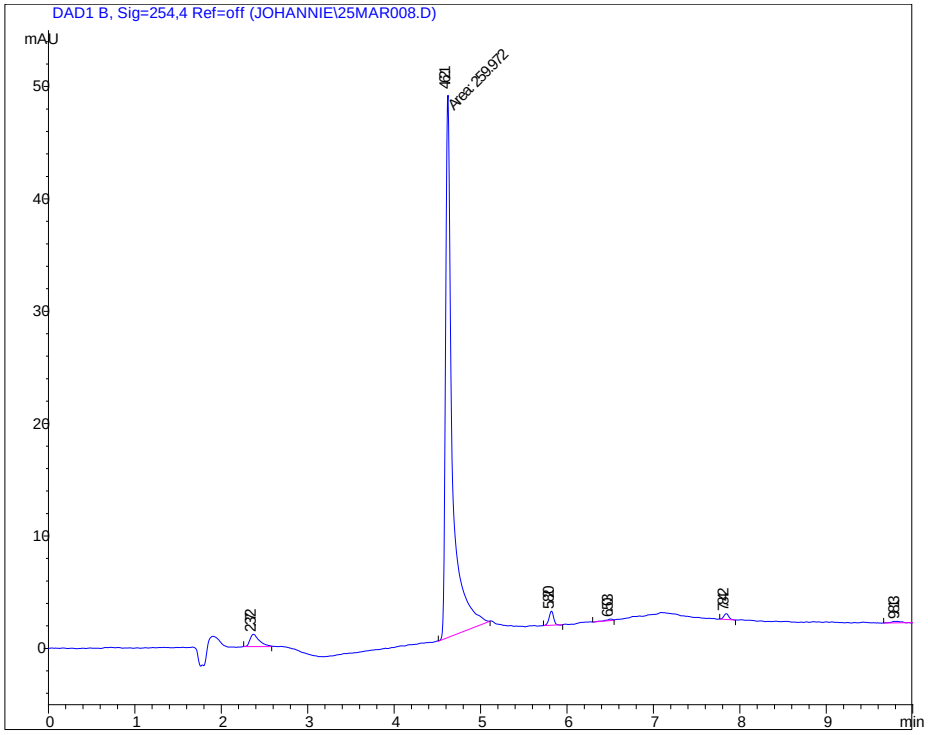

HPLC chromatogram peak properties of JDB12:

Peak #	*Retention time (min)*	*Type*	*Width (min)*	*Area (mAU*s)*	*Height (mAU)*	*Area %*
1	2.372	BB	0.1124	8.30847	1.09657	3.0049
2	4.621	MM	0.0892	259.97232	48.55114	94.0232
3	5.820	PP	0.0558	4.49240	1.25304	1.6247
4	6.503	PV	0.0719	$7.04474e^{-1}$	$1.37162e^{-1}$	0.2548
5	7.842	BP	0.0621	2.04273	$5.17041e^{-1}$	0.7388
6	9.813	PP	0.0986	$9.77612e^{-1}$	$1.31777e^{-1}$	0.3536

JDB13: 1-(4-Chlorophenyl)-3-hydroxy-2-methylpyridin-4-one

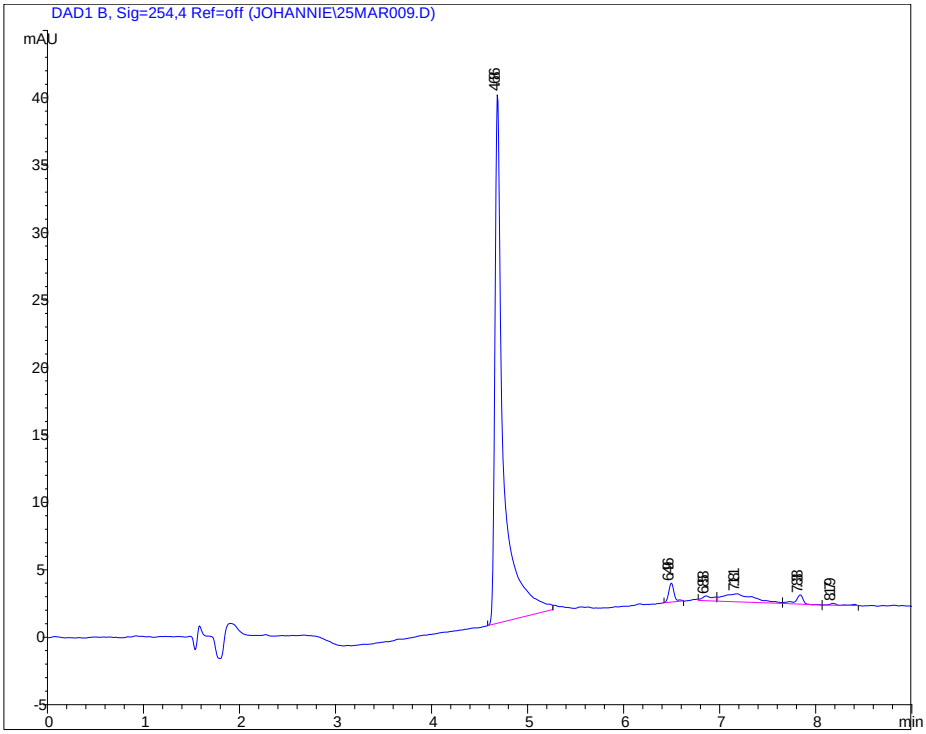

HPLC chromatogram peak properties of JDB14:

Peak #	*Retention time (min)*	*Type*	*Width (min)*	*Area (mAU*s)*	*Height (mAU)*	*Area %*
1	4.686	PB	0.0854	240.62602	39.32584	90.1054
2	6.496	PP	0.0584	5.32407	1.39925	1.9937
3	6.858	BB	0.1110	2.81987	$3.46444e^{-1}$	1.0559
4	7.181	BV	0.2780	13.30511	$5.87997e^{-1}$	4.9823
5	7.838	VP	0.0854	3.97459	$6.88085e^{-1}$	1.4883
6	8.179	VB	0.1098	$9.99838e^{-1}$	$1.27106e^{-1}$	0.3744

JDB14: 3-Hydroxy-2-methyl-1-(4-methylbenzyl)pyridin-4-one

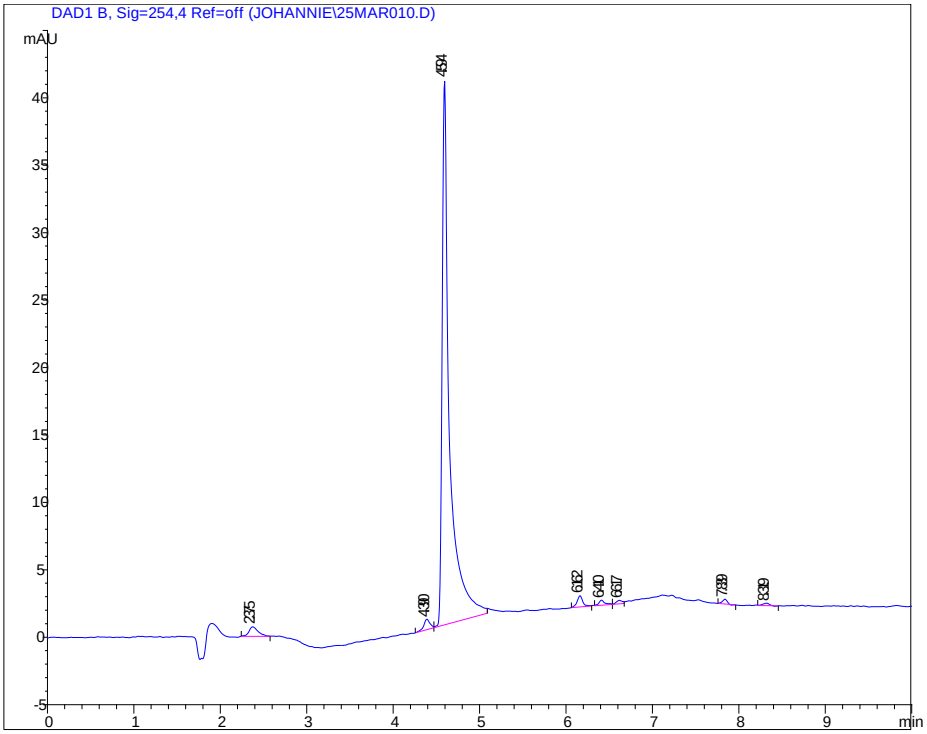

HPLC chromatogram peak properties of JDB14:

Peak #	*Retention time (min)*	*Type*	*Width (min)*	*Area (mAU*s)*	*Height (mAU)*	*Area %*
1	2.375	BB	0.1082	5.36824	$7.10457e^{-1}$	2.0713
2	4.390	PV	0.0723	3.90886	$7.81952e^{-1}$	1.5082
3	4.594	VB	0.0835	240.87749	40.40883	92.9405
4	6.162	PB	0.0673	3.76281	$8.23244e^{-1}$	1.4518
5	6.410	BV	0.0702	1.84919	$3.83878e^{-1}$	0.7135
6	6.617	VV	0.0755	1.28827	$2.61245e^{-1}$	0.4971
7	7.839	PP	0.0555	1.23536	$3.47434e^{-1}$	0.4767
8	8.319	BP	0.0725	$8.83573e^{-1}$	$1.82457e^{-1}$	0.3409